The evolution of antibiotic-resistant bacteria and their treatment using epoxytigliane-based therapeutics

Jingxiang Wu

A thesis submitted for the degree of Doctor of Philosophy

Cardiff University

September 2025

Acknowledgments

First and foremost, I would like to express my deepest gratitude to my supervisors, Professor David Thomas and Dr Katja Hill, for their invaluable guidance and support throughout my PhD journey and the writing of this thesis. Their expertise and insightful feedback have been instrumental in shaping both this work and my growth as a researcher. I would also like to acknowledge the Chinese Scholarship Council and QBiotics Ltd. for their financial support, without which this research would not have been possible.

I would like to extend my heartfelt thanks to my colleagues and friends in the ATG group—Dr Jennifer Adams, Dr Joana Stokniene, and Dr Wenya Xue—for their generous guidance and advice, especially when I initially started in the lab. I'm also thankful to my friends at the School of Dentistry—Abdullah Albarrak, Ghaida Khalid K Almuthri, Priyanka Sharma, Francesca Boardman, Yanni Lu, Jacob Evans and Emma Wright—for the many moments of laughter we shared in the office, which made this journey so much more enjoyable. I would also like to thank the technical team who have contributed to the smooth running of the lab and the success of my experiments.

I would like to sincerely acknowledge the work of all those who assisted me with the experiments presented in this thesis—Dr Jennifer Adams for the growth curve assay (Chapter 2), Dr Manon Pritchard for the motility assay and ATP viability assay (Chapter 2), Dr Lydia Powell for the AFM force curve measurement (Chapter 2) and

CLSM imaging (Chapter 2,3 and 4), Professor Owen B. Spiller, Dr Mei Li, Ian Boostrom and Jordan Mathias for the WGS and bioinformatics analysis (Chapter 3), Carles Tardío Pi and Rafael Peña-Miller for the mathematical modelling of plasmid population dynamics (Chapter 3), Georgina E. Menzies for the MD simulations (Chapter 4), Philip R. Davies and Niklaas J. Buurma for the XPS analysis (Chapter 4), Dr Liana Azizova and Dr Josh Davies-Jones for the PiFM imaging (Chapter 4).

On a personal note, I am profoundly grateful to my family for their unconditional love, patience, and unwavering support throughout this journey. Above all, to Minmin—your love, faith, and constant encouragement have been my greatest source of strength and inspiration. This thesis would not have been possible without you by my side. I can't wait to open this next chapter of our lives together.

Summary

The discovery of plasmid-encoded **m**obile **c**olistin **r**esistance (*mcr*) genes and their rapid dissemination and persistence in humans, animals and the environment represents a significant global health concern. Understanding the fitness costs conferred by *mcr* and how these genes are maintained in bacterial populations is crucial for developing effective containment strategies. Epoxytiglianes such as EBCs, a novel class of lipophilic, plant-derived compounds, may hold promise in overcoming *mcr*-mediated colistin resistance, as previous research has revealed their potential role against antibiotic-resistant, biofilm-associated Gram-negative infections.

The phenotypic effects of *mcr-1* and *mcr-3* carriage on bacterial growth and biofilm assembly were studied. The persistence of both *mcr* plasmids in *E. coli* populations in the presence and absence of colistin selective pressure was studied in an evolutionary bead biofilm model and modelled mathematically. Changes in resistance profiles and plasmid genetics were monitored using minimum inhibitory concentration assays and whole genome sequencing. The direct interaction of EBCs with the Gram-negative bacterial cell membrane was studied using *in silico* simulations, and the induced cell surface chemical changes were characterised *in vivo* using spectroscopy- and microscopy-based surface chemistry analyses. Bacterial membrane and biofilm disruption after EBC treatment was also examined using bacterial membrane permeability assays and microscopic imaging.

Phenotypic characterisation demonstrated that both *mcr-1* and *mcr-3* plasmid carriage were associated with fitness costs, with biofilm-associated characteristics, including formation, mechanics and stress response to colistin, also significantly altered. In the absence of colistin, *mcr-1* was rapidly lost (Day 23), but *mcr-3* persisted (>51 days). At the end of the evolution experiment, colistin resistance rapidly re-emerged in the apparently *mcr-1*-depleted biofilm populations upon re-exposure to colistin (in <48 h). Sequencing confirmed maintenance of *mcr-1* was associated with deletion of other antimicrobial resistance genes from the plasmid multidrug resistance region. Interaction of EBC-1013 with the bacterial cell membrane was evident *in silico* and *in vivo*, with alterations in the membrane lipid and protein compositions, which was reflected in compromised membrane integrity. The marked synergistic effect of EBC-1013 upon colistin activity against *mcr E. coli* was evident in the biofilm disruption assay.

This work highlights the importance of the fitness costs of *mcr* carriage and describes underlying compensatory mechanisms within the biofilm environment which may maintain carriage of colistin resistance. This study also emphasises the potential value of EBC-1013 as a novel antimicrobial agent that can target *mcr*-bearing, colistin-resistant bacteria in human disease through its interaction with the bacterial outer membrane and by potentiating the activity of colistin.

Papers to be published

Published:

Wenya Xue, Manon F. Pritchard, Saira Khan, Lydia C. Powell, Joana Stokniene, **Jingxiang Wu**, Nicholas Claydon, Paul Reddell, David W. Thomas, Katja E. Hill, 2023. Defining *in vitro* topical antimicrobial and antibiofilm activity of epoxy-tigliane structures against oral pathogens. *Journal of oral microbiology*, 15(1), p.2241326.

Under review:

Manon F. Pritchard, Wenya Xue, **Jingxiang Wu**, Francesca Boardman, Mei Li, Yuqing Zhou, Saira Khan, Lydia C. Powell, Joana Stokniene, Josh Davies-Jones, Philip R. Davies, Niklaas J. Buurma, Georgina E. Menzies, Owen B. Spiller, Timothy R. Walsh, Paul Reddell, Katja E. Hill & David W. Thomas, 2025. Epoxytiglianes potentiate the activity of colistin against resistant *Escherichia coli* via modification of the bacterial cell membrane. *mBio*.

Jingxiang Wu, Jennifer Y.M. Adams, Mei Li, Francesca Boardman, Ian Boostrom, Jordan Mathias, Lydia C. Powell, Manon F. Pritchard, Carles Tardío Pi, Rafael Peña-Miller, Timothy R. Walsh, Owen B. Spiller, David W. Thomas, Katja E. Hill, 2025. Plasmid adaptation drives *mcr-1* persistence within *Escherichia coli* biofilms in the absence of colistin selection. *npj Biofilms and Microbiomes*.

Abbreviations

µg	Microgram
µl	Microlitre
µM	Micromolar
µm	Micrometre
A. baumannii	*Acinetobacter baumannii*
AFM	Atomic Force Microscopy
AHLs	Acyl-Homoserine Lactones
AI	Autoinducer
ANOVA	Analysis of Variance
ARG	Antimicrobial Resistance Gene
ATCC	American Type Culture Collection
ATP	Adenosine Triphosphate
ATR	Attenuated Total Reflectance
BE	Binding Energy
CFU	Colony-Forming Units
CL	Cardiolipin
CLSI	Clinical and Laboratory Standards Institute
CLSM	Confocal Laser Scanning Microscopy
cm	Centimetre
CPS	Capsule Polysaccharide
dH_2O	Distilled Water
DHFR	Dihydrofolate Reductase
DNA	Deoxyribonucleic Acid
DNases	Deoxyribonucleases
DPPE	Dipalmitoylphosphatidylethanolamine
dsDNA	Double-stranded DNA
E. aerogenes	*Enterobacter aerogenes*
E. cloacae	*Enterobacter cloacae*

E. coli	*Escherichia coli*
EBC	EcoBiotics Compound
eDNA	Extracellular Deoxyribonucleic Acid
EDTA	Ethylenediaminetetraacetic Acid
EPS	Extracellular Polymeric Substance
eV	Electronvolt
EVs	Extracellular Vesicles
FTIR	Fourier Transform Infrared
FWHM	Full Width at Half Maximum
G. mellonella	*Galleria mellonella*
gDNA	Genomic DNA
h	Hour(s)
HGT	Horizontal Gene Transfer
IL	Interleukin
IM	Inner Membrane
Inc	Incompatibility
IR	Infrared
IRs	Inverted Repeats
IS	Insertion Sequence
K. pneumoniae	*Klebsiella pneumoniae*
kDa	kilodalton
kHz	Kilohertz
KJ	Kilojoule
kV	kilovolt
L-Ara4N	4-amino-4-deoxy-L-arabinose
LB	Luria-Bertani
LPS	Lipopolysaccharide
LTA	Lipoteichoic Acid
mA	Milliampere
MBEC	Minimum Biofilm Eradication Concentration

mcr/MCR	Mobile Colistin Resistance
MD	Molecular Dynamics
MDR	Multidrug-Resistant/Multidrug Resistance
MH	Mueller Hinton
MIC	Minimum Inhibitory Concentration
ml	Millilitre
mm	Millimetre
mM	Millimolar
mRNA	Messenger Ribonucleic Acid
MRSA	Methicillin-Resistant *S. aureus*
MSD	Minimum Significant Difference
nN	Nanonewton
O/N	Overnight
OD	Optical Density
ODEs	Ordinary Differential Equations
OM	Outer Membrane
OMP	Outer Membrane Protein
P. aeruginosa	*Pseudomonas aeruginosa*
PBP	Penicillin-Binding Proteins
PBS	Phosphate Buffered Saline
PCR	Polymerase Chain Reaction
PE	Phosphatidylethanolamine
pEtN/PEA	Phosphoethanolamine
PG	Phosphatidylglycerol
pH	potential of Hydrogen
PiFM	Photo-induced Force Microscopy
PKC	Protein Kinase C
pmol	Picomole
QC	Quality Control
QS	Quorum Sensing

RNA	Ribonucleic Acid
ROS	Reactive Oxygen Species
rpm	Revolutions Per Minute
rRNA	Ribosomal Ribonucleic Acid
RT-qPCR	Real-Time Quantitative Polymerase Chain Reaction
S. aureus	*Staphylococcus aureus*
S. enterica	*Salmonella enterica*
S. pyogenes	*Streptococcus pyogenes*
S. Typhimurium	*Salmonella typhimurium*
SAR	Structure-Activity Relationship
SD	Standard Deviation
Spp.	Species
sRNA	Small Ribonucleic Acid
ST	Sequence Type
TA	Toxin-Antitoxin
TEM	Transmission Electron Microscopy
TER	TAAB Embedding Resin
THF	Tetrahydrofolic Acid
TNF	Tumor Necrosis Factor
TSB	Tryptone Soy Broth
TSDs	Target Site Duplications
v/v	% Volume in Volume
WGS	Whole Genome Sequencing
WHO	World Health Organisation
XPS	X-ray Photoelectron Spectroscopy

Table of Contents

List of Figures

Chapter 1

Chapter 2

Chapter 3

Chapter 4

List of Tables

Chapter 2

Chapter 3

Chapter 4

Chapter 1

General Introduction

1.1 Bacteria

Bacteria are single-celled living microorganisms with a plasma membrane made up of a phospholipid bilayer structure surrounding the cytoplasm. Two major bacterial groups have been characterised, namely Gram-negative and Gram-positive (**Figure 1.1**).

1.1.1 Gram-negative bacteria

The Gram-negative bacterial cell envelope is composed of three principal layers; the outer membrane (OM), the peptidoglycan cell wall, and the cytoplasmic or inner membrane (IM). The OM is an element that is only present in Gram-negative bacteria. It is a lipid bilayer scattered with non-transmembrane lipoproteins and transmembrane proteins (Silhavy et al. 2010). The transmembrane proteins are also termed outer membrane proteins (OMPs), and are believed to function in the passive diffusion of small molecules including mono- and disaccharides, amino acids and ions across the OM (Silhavy et al. 2010). The outer leaflet of the OM consists of glycolipids, mainly lipopolysaccharide (LPS) (Kamio and Nikaido 1976). LPS is a well-studied molecule accountable for endotoxic shock induced by septicemia triggered by Gram-negative bacteria (Raetz and Whitfield 2002). In addition, negatively charged LPS molecules also act as a barrier for hydrophobic molecules by binding one another to form a nonfluid continuum, particularly with the help of divalent cations like Mg^{2+} linking them electrostatically (Vaara 1992; Silhavy et al. 2010). This characteristic in

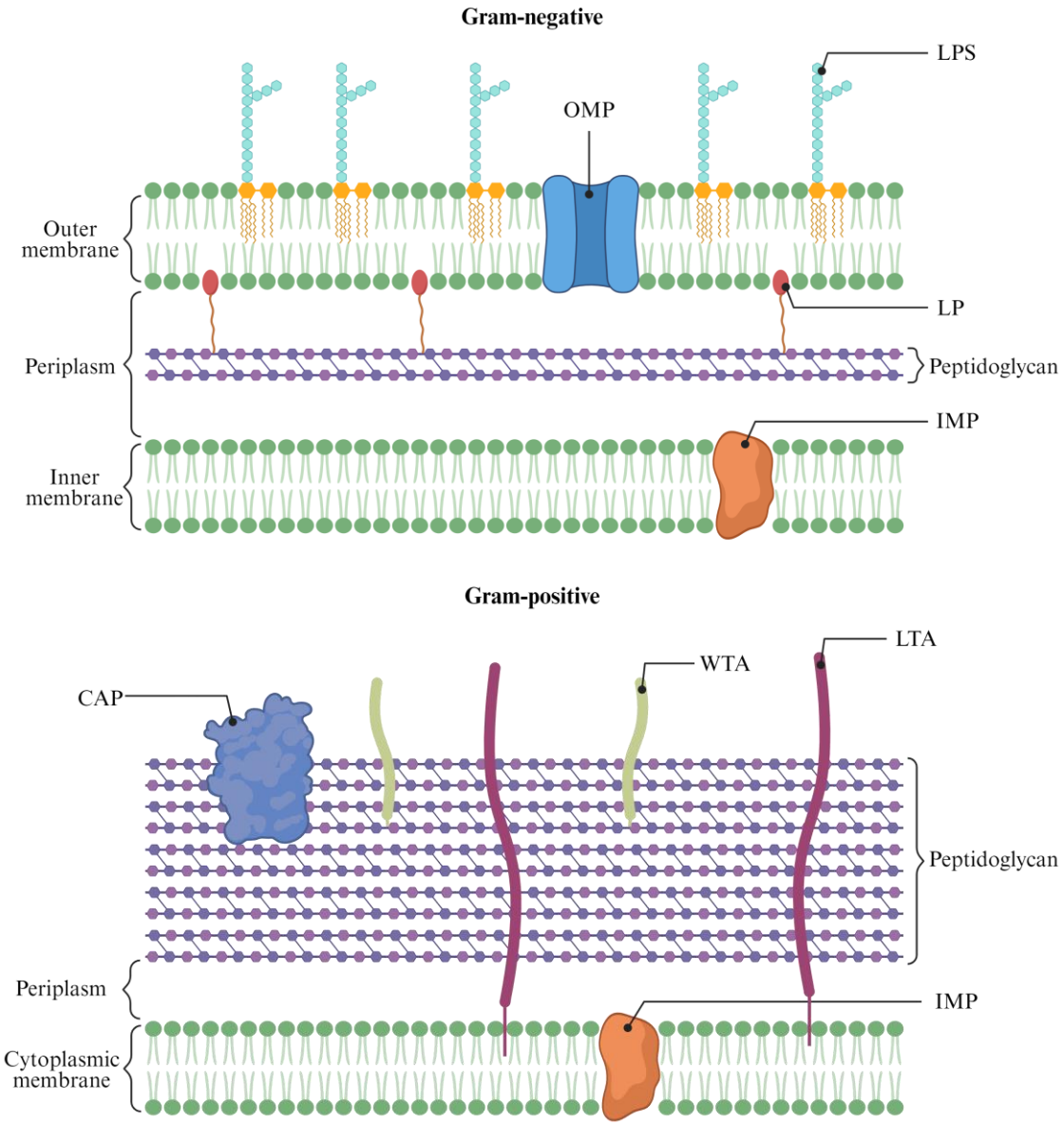

Figure 1.1 Schematic diagram of Gram-positive and Gram-negative cell envelopes. CAP, covalently attached protein; IMP, integral membrane protein; LP, lipoprotein; LPS, lipopolysaccharide; LTA, lipoteichoic acid; OMP, outer membrane protein; WTA, wall teichoic acid. The figure was created with BioRender.com.

conjunction with the functions of OMPs, make the OM a highly selective yet, effective permeability barrier.

The peptidoglycan cell wall is comprised of repeating units of the disaccharide N-acetyl glucosamine-N-actyl muramic acid, which are further cross-linked by pentapeptide side chains (Vollmer et al. 2008). It serves as a substrate on which the OM is firmly anchored by lipoproteins (Braun 1975). Additionally, peptidoglycan imparts rigidity and cell shape to bacteria.

Unlike eukaryotic cells, bacteria lack intracellular organelles. Therefore, most of the essential cellular activity, such as energy production, lipid synthesis, protein transport and secretion, occurs in the periplasm, an aqueous compartment between the OM and the IM.

Escherichia coli is a Gram-negative facultative anaerobic bacterium which mostly inhabits the intestines of warm-blooded organisms. It is rod-shaped and non-sporulating and has been used as a model bacterial species in biological engineering and industrial microbiology (Lee 1996). Although most *E. coli* can be beneficial by competing against other pathogenic bacteria (Paul 1999), pathogenic *E. coli* strains are a major cause of disease, being associated with significant morbidity and mortality. These pathogenic strains are classified into two types: intestinal and extraintestinal *E. coli*. Intestinal *E. coli* are comprised of many toxin-producing strains which have been implicated in intestinal infections such as Crohn's disease, enteric syndromes and

haemorrhage, while extraintestinal *E. coli* predominantly lead to urinary tract infections, neonatal sepsis, meningitis in humans and a number of infections in animals such as mastitis (Vogeleer et al. 2014). Furthermore, *E. coli* has also been found to be the cause of an array of medical device-related infections, as in urethral and intravascular catheters, shunts and prosthetic grafts and joints (Reisner et al. 2014).

1.1.2 Gram-positive bacteria

The Gram-positive bacterial cell envelope is made up of two layers; the peptidoglycan cell wall and the cytoplasmic membrane. While peptidoglycan in Gram-negative microorganisms is only a few nanometers thick, peptidoglycan in Gram-positive counterparts is much thicker (30-100 nm).

Two major classes of teichoic acids (long anionic polymers mainly consisting of glycerol phosphate, or ribitol phosphate repeats) have been identified on the surface of a wide range of Gram-positive bacteria. These include cell wall teichoic acids (WTAs), which are covalently connected to peptidoglycan, and lipoteichoic acids (LTAs), which are inserted into the cytoplasmic membrane through a glycolipid anchor (Neuhaus and Baddiley 2003). Together, the WTAs and LTAs form a continuum of negative charge, and promote cation homeostasis by binding cations (Marquis et al. 1976).

In addition to teichoic acids, there are also a variety of proteins spread over the surface of Gram-positive cells. Without the OM to contain them, these proteins feature either elements that anchor them in the cytoplasmic membrane, or are covalently attached to

peptidoglycan or teichoic acids (Scott and Barnett 2006).

1.2 Biofilm

Biofilms represent architectural aggregates of microorganisms formed on a biotic or abiotic surface (Mishra et al. 2024). Biofilms show differing morphologies, depending on the bacterial component species as well as the local micro-environment (Dhekane et al. 2022; Dong et al. 2023). Most bacteria are able to switch between a planktonic (free-floating) state and biofilm (cellular aggregate) state. The high cell density in a biofilm creates an ideal setting for the occurrence of horizontal gene transfer, e.g., plasmid exchange via conjugation, which may lead to widespread dissemination of antibiotic-resistant genes among individual cells (Hausner and Wuertz 1999).

Bacterial biofilms are often pathogenic and have been found associated with a number of human diseases, for example, cystic fibrosis, dental caries, periodontal disease, wound infections, urinary infections and cardiac valve infections (Rabin et al. 2015). In fact, according to the US National Institutes of Health, biofilm formation occurs in 65% and 80% of all microbial and chronic infections, respectively (Jamal et al. 2018). With these biofilms being difficult to eradicate (reportedly displaying resistance to antibiotics 100 to 1000-fold higher than that of single free-floating cells (Ceri et al. 1999), they are difficult to treat and remain a significant clinical problem.

1.2.1 Biofilm structural assembly

Bacteria within biofilms are encased in a self-secreted extracellular polymeric substance (EPS) matrix, primarily composed of exopolysaccharides, proteins, extracellular DNA (eDNA), lipids and other metabolites (Flemming et al. 2007; Flemming and Wingender 2010). Microorganisms constitute only 5-35% of the total biofilm volume, with the greatest component being the EPS matrix. Water channels running through the biofilm allow for water, oxygen and essential nutrients to be delivered to every part of the system and for waste removal (Zhang et al. 1998).

Within biofilms, exopolysaccharides function as scaffolds to which other biomolecules can attach and therefore provide shape, viscoelasticity and structural support to the biofilm. The synthesis of exopolysaccharides takes place either intracellularly or extracellularly (Nwodo et al. 2012). Three major exopolysaccharides have been identified in the *E. coli* biofilms: β-1,6-N-acetyl-D-glucosamine polymer, cellulose and colanic acid (consisting of glucose, galactose, fucose, glucuronic acid, acetate, and pyruvate), all of which play an important role in *E. coli* biofilm formation (Sharma et al. 2016).

Some extracellular proteins adhere to bacterial surfaces and polysaccharides and, play an important role in stabilising and maintaining biofilm structure (Lynch et al. 2007). In contrast, enzymes (often produced by the biofilm bacteria themselves) play a part in structural degradation within biofilms, and their substrates include a variety of EPS

matrix components. The breakdown of biopolymers by the action of these enzymes is crucial for supplying bacterial cells with carbon and energy sources, particularly during starvation (Zhang and Bishop 2003). Detachment and dispersal of cells in the biofilm life cycle is also initiated by enzymes degrading the EPS matrix, which releases planktonic cells from the biofilm surface (Kaplan et al. 2004).

eDNA in EPS matrix can be derived either endogenously from lysed cells, cellular quorum sensing-mediated secretions (**see Chapter 1 Section 1.2.3** for details about quorum sensing) and outer membrane vesicles, or exogenously from polymorphonuclear leukocytes at infection sites (Allesen‐Holm et al. 2006; Jakubovics et al. 2013). As an anionic macromolecule, eDNA helps to bind substrate receptors to promote bacterial adhesion (underlining its significance in biofilm formation) (Das et al. 2010) and chelates metal cations such as Mg^{2+}; divalent cation-limitation is a trigger for activation of the PhoPQ/PmrAB two-component systems, which leads to resistance to cationic antimicrobial peptides and polymyxin in *Pseudomonas aeruginosa* (Mulcahy et al. 2008; Lewenza 2013). Furthermore, eDNA has also been demonstrated to coordinate cellular twitching motility in *P. aeruginosa* biofilm formation (Gloag et al. 2013).

1.2.2 Stages of biofilm formation

1.2.2.1 Conditioning layer

The first stage of biofilm formation generally involves a conditioning layer. This forms

on the substrate and is composed of a multitude of organic (e.g., proteins/peptides and carbohydrates) and inorganic (e.g., salts of sodium and phosphate-containing precipitates) molecules (Leefmann et al. 2015; Yang et al. 2016; Bhagwat et al. 2021). This layer can potentially alter the surface properties of a substrate, including surface charge, surface potential and surface tension, the changes of which might turn the substrate into a favourable surface for bacteria to adhere to (Donlan 2002; Garrett et al. 2008). In dental plaque, this film is called the acquired pellicle and is composed of different proteins (mainly acidic proline-rich proteins, amylase, cystatin, immunoglobulins, lysozyme, and mucins), as well as fatty acids and carbohydrates (Enax et al. 2023). The dental pellicle can develop within minutes after cleaning of the tooth surface.

1.2.2.2 Initial adhesion

Long-range physical forces play an important role in the initial adhesion of bacterial cells to the conditioning layer. Generally, for the adhesion to occur, attractive forces between the surface and the microorganism should exceed repulsive forces (Garrett et al. 2008). When 10-20 nm away from the surface, bacteria are repelled by negative charges on most substrata because they carry negative charges on their cell surface (Palmer et al. 2007). However, this repulsive electrostatic force can be offset by the attractive van der Waals force between the cells and the surface (Palmer et al. 2007). Bacterial appendages are another key factor in overcoming repulsive forces. In *E. coli*, peritrichous flagella can generate mechanical propulsion to facilitate adhesion. This

active motility increases the interaction between bacteria and the surface, thus contributing substantially to this first cell-to-surface contact. Nonetheless, non-motile bacteria can also attach to the surface, taking advantage of their abundantly expressed adhesion factors (Beloin et al. 2008). The bonds of the initial attachment are weak, as evidenced by the low activation energy for desorption of bacteria (van Merode et al. 2006).

1.2.2.3 Early development of biofilm

At this early stage of biofilm formation, short-range forces become the dominant form of interaction between bacterial cells and surfaces, including hydrophilic-hydrophobic interactions as well as covalent and hydrogen bonding (Palmer et al. 2007). Gene expression for flagella synthesis is repressed as bacteria change from planktonic to an adhered state. In *E. coli*, a few small molecules such as cyclic-diguanylic acid (c-di-GMP) are responsible for the shift to a sessile state. Meanwhile, the expression of adhesive organelles such as type 1 fimbriae and curli fimbriae, induced by initial adhesion, is also of great importance for the strengthening of cellular attachment of *E. coli* to the surface (Beloin et al. 2008; Wood 2009). Throughout this stage, cell aggregation and microcolony formation occur through cell-to-cell interactions as the biofilm develops.

1.2.2.4 Biofilm maturation

After the first layer of biofilm has been formed, bacteria of the same species and/or

other species are constantly recruited to the biofilm from the bulk fluid. Concurrently, the adhered bacteria keep on dividing, making cell clusters expand outwards and upwards. As the cells enter an exponential growth phase, the biofilm grows into a thick mushroom- or tower-like structure, in which the component bacteria are layered according to their metabolic characteristics and oxygen tolerance. During this biofilm maturation process, cellular gene expression for bacterial appendages is downregulated (Hall-Stoodley and Stoodley 2002), whereas gene expression for the production of cell surface proteins and biofilm matrix components (proteins, eDNA, polysaccharides), becomes upregulated (Hancock et al. 1990). Therefore, robust bonds between cells as well as between cells and the surface are established via the EPS matrix (Dunne Jr 2002). Once the biofilm has reached a high cell density, a series of cell-signalling mechanisms come into play to coordinate bacterial behaviour and prevent biofilm overgrowth.

1.2.2.5 Biofilm dispersal

Biofilm dispersal may take place in the whole biofilm or in individual regions of the biofilm. A number of factors are involved including nutrient deficiency, oxygen depletion and cell "competition". The dispersal process can occur as a result of enzymes produced by the entrapped bacteria breaking down the EPS matrix of the biofilm, causing detachment and release of the biofilm surface-associated bacteria into surrounding environments. These bacteria regain their flagella-driven motility (only if they have flagella) and are then available to colonise other surfaces, which is critical

for the formation of new biofilms at other sites (Perni et al. 2014). A schematic representation of biofilm formation can be seen in **Figure 1.2**.

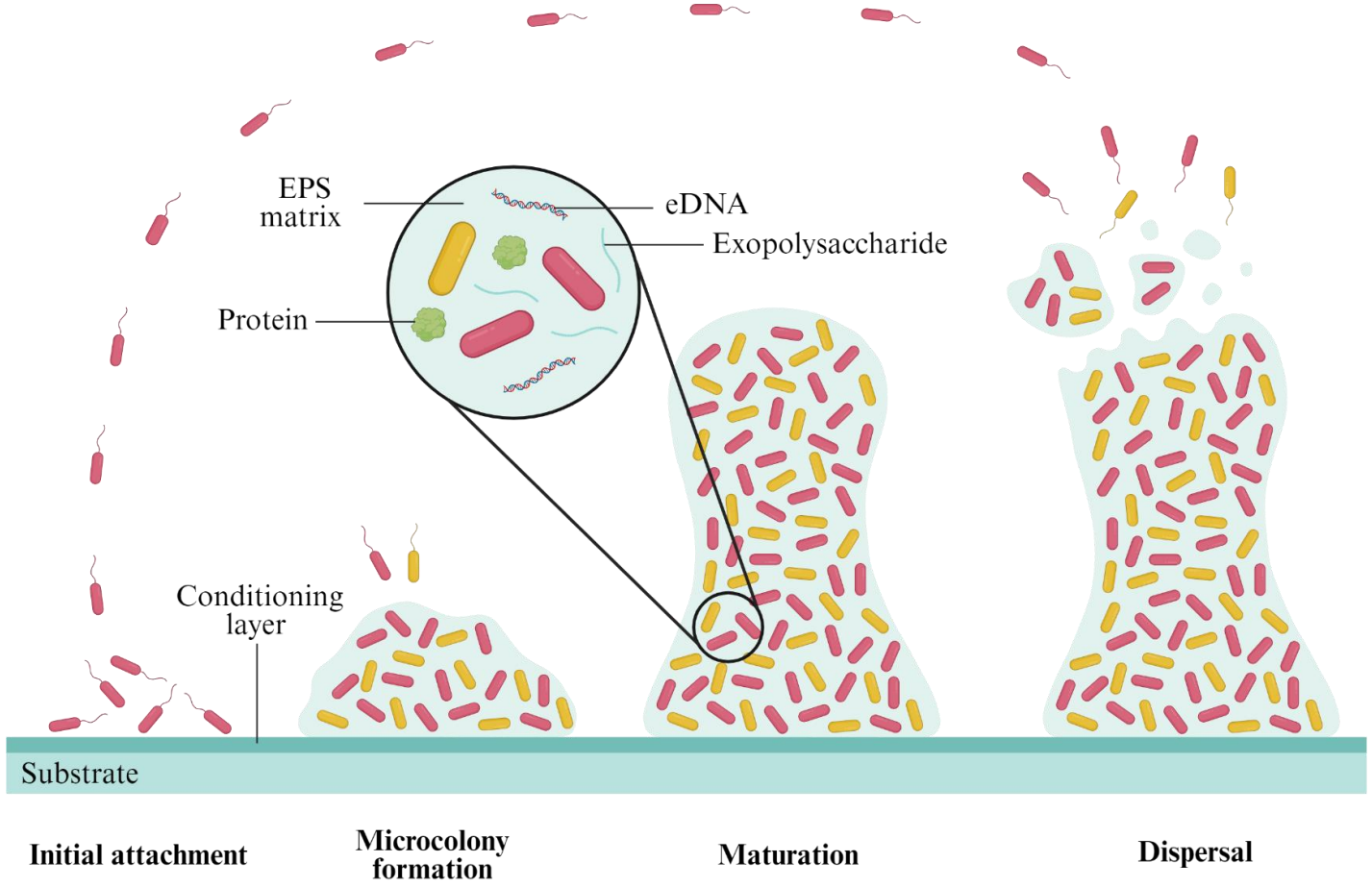

Figure 1.2 Schematic diagram representing the process of biofilm formation including initial attachment, microcolony formation, maturation and dispersal. The figure was created with BioRender.com.

1.2.3 Quorum sensing in biofilms

Quorum sensing (QS) is a cell-cell communication mechanism by which bacteria in a biofilm at high cell density 'talk' to each other to synchronise their gene expression and regulation of physiological activities (Lyon and Muir 2003). This process is mediated by bacteria responding to changes in levels of extracellular signal molecules called quorum sensing molecules, which are secreted by bacteria themselves (Camilli and Bassler 2006). At low cell density, the signal molecule concentration is low and therefore has no impact. However, as cell density increases, the signal molecule concentration reaches a threshold, from which point the molecule activates corresponding intracellular signalling pathways, upregulating or downregulating target genes (Miller and Bassler 2001). The target genes finely regulated by QS are related to diverse bacterial activities, including cell virulence, biofilm formation and maturation, antibiotic resistance and bioluminescence. A number of small QS signal molecules have so far been characterised, which are specific for different species. For instance, acyl-homoserine lactones (AHLs) mediate QS in >50 Gram-negative bacteria including *P. aeruginosa*, whilst autoinducing peptides mediate QS in Gram-positive bacteria such as *Staphylococcus aureus*. *E. coli* itself does not synthesise AHLs, but can sense and react to AHLs secreted by other bacteria, hence enhancing its biofilm formation, motility and virulence (Beloin et al. 2008). The QS systems in *E. coli* include the orphan SdiA regulator, autoinducer-2 (AI-2), autoinducer-3 (AI-3) system, and indole. AI-2 is involved in QS signaling in both Gram-negative and Gram-positive

bacteria (Rezzonico and Duffy 2008).

1.3 Mechanisms of antibiotic resistance and tolerance in biofilms

Antibiotic resistance, in general, refers to a rise in the minimum inhibitory concentration of an antibiotic, resulting from a permanent change in its target bacteria, which might arise via acquisition of resistance genes, or by mutation. Antibiotic tolerance refers to the ability of bacterial cells to survive the action of an antibiotic via temporary and reversible phenotypic change (Mah 2012a). For planktonic bacteria, these definitions are easy to describe, but for biofilms, these arise as a result of the biofilm as a whole. Bacteria in a biofilm are more likely to survive antibiotics and host immune systems than planktonic bacteria, via several mechanisms operating together to increase tolerance/resistance. Furthermore, even in the same biofilm, there exist distinct mechanisms by which different subpopulations of cells are protected from antibiotic treatment (Roberts and Mullany 2010; Mah 2012b).

1.3.1 Limited antibiotic penetration

The penetration of antibiotics into biofilms can be decreased by being bound to or sequestered in the EPS matrix (Mah et al. 2003; Walters III et al. 2003; Chiang et al. 2013). The extent to which this occurs appears to be dependent on the bacterial species or strain, the class of antibiotic, and the age, thickness and heterogeneity of the biofilm. Positively-charged antibiotics like aminoglycosides and polypeptides can be trapped by negatively-charged matrix components such as exopolysaccharides and eDNA, which

bind antibiotics trying to diffuse into the biofilm (Bagge et al. 2004; Doroshenko et al. 2014). In contrast, uncharged antibiotics can be effectively hydrolysed by the enzymes present in the biofilm matrix. For example, *P. aeruginosa* biofilms can accumulate high concentrations of secreted β-lactamase in the matrix, causing degradation of β-lactam antibiotics before they reach their cellular targets (Ciofu and Høiby 2008; Hengzhuang et al. 2013).

1.3.2 Physiological heterogeneity, hypoxia, nutritional limitation and reduced metabolic activity

Physiological heterogeneity refers to the differences in gene expression, metabolism and phenotype of bacteria in different zones of a biofilm (Lenz et al. 2008; Stewart and Franklin 2008; Williamson et al. 2012), caused by an uneven distribution of oxygen and nutrients (Xu et al. 1998; Stewart and Franklin 2008). Typically, oxygen and nutrient concentrations are relatively low in the biofilm interior. This creates hypoxic, acidic and nutrient-deprived areas in biofilms, typified by reduced metabolic activity and cell division rates (de Beer et al. 1997; Walters III et al. 2003; Fux et al. 2004). Since many antibiotics target physiological processes such as replication, transcription, translation and cell wall synthesis in growing bacteria, these "stationary phase-like" bacteria become insensitive to antibiotic treatment (Ciofu et al. 2015). The role of hypoxia in antibiotic tolerance is supported by the fact that anaerobically grown biofilms are more tolerant to antibiotics than aerobically grown counterparts (Borriello et al. 2004). Similarly, the role of nutrient starvation is demonstrated in a study where

E. coli amino acid auxotrophs with mutations in amino acid biosynthetic genes showed augmented biofilm tolerance to ofloxacin and ticarcillin (Bernier et al. 2013).

1.3.3 Oxidative stress responses

In addition to killing bacterial cells via traditionally agreed mechanisms of action, some antibiotics (e.g., norfloxacin, ampicillin, kanamycin) increase their lethality by increasing cellular respiration and promoting the production of high levels of reactive oxygen species (ROS) (Kohanski et al. 2007; Dwyer et al. 2015; Lobritz et al. 2015). Hydroxyl radicals, a byproduct of this process, are able to cause cell death by oxidising critical molecules including deoxyguanosine triphosphate (Foti et al. 2012) and DNA (Kohanski et al. 2007; Imlay 2013). Therefore, in the context of biofilms, approaches to detoxify antibiotic-induced ROS could be important mechanisms by which cells attain a high degree of antibiotic tolerance. For instance, a study found that, compared to wild-type *P. aeruginosa* biofilms, *katA*-knocked-out biofilms generated more ROS and were less tolerant to ciprofloxacin because *katA*-encoded catalase is an antioxidant and can partially detoxify antibiotic-induced ROS (Jensen et al. 2014).

1.3.4 Quorum sensing-associated mechanisms

QS has also been implicated in biofilm tolerance to antibiotics. Biofilms formed by a QS-deficient mutant *P. aeruginosa*, were significantly less tolerant to tobramycin and H_2O_2 than wild-type biofilms and were more easily phagocytosed by polymorphonuclear leukocytes (Bjarnsholt et al. 2005). One explanation for this QS-

driven biofilm recalcitrance to antibiotics is that QS might cause an accumulation of ROS and a reduction in membrane potential, which ultimately leads to autolysis and eDNA release (Hazan et al. 2016).

1.3.5 Persister cells

Cells on the outer layers of a biofilm generally have a rapid turnover. However, in the centre of a biofilm, bacteria termed persister cells, can be dormant or have a growth rate which is extremely low (Keren et al. 2004; Lewis 2007). Typically, persister cells adopt a dormant phenotype in which energy-producing and biosynthetic functions are repressed. Since most antibiotics target growing and dividing bacteria to kill them, these 'hibernating' cells are highly antibiotic tolerant. After antibiotic treatment, persister cells can revive and revert to a normal growth state, thereby re-colonising the infection sites and making biofilm infections extremely difficult to treat (Wood 2017).

1.3.6 Mutation

Interestingly, bacterial cells in a biofilm experience antibiotic resistance-associated mutations at higher rates than planktonic cells. For instance, the mutation frequency of *P. aeruginosa* biofilm cells to ciprofloxacin and rifampicin was shown to be 105-fold higher than for planktonic cells (Driffield et al. 2008). A number of factors are thought to make cells grown in biofilms inherently prone to spontaneous mutations, and these might include nutrient deficiency, excess of waste products, hypoxia, exposure to sub-MIC levels of antibiotics, and oxidative stress. For example, continuous exposure of

cells in *P. aeruginosa* biofilms to sub-inhibitory concentrations of ciprofloxacin resulted in gene mutations conferring high-level ciprofloxacin resistance as well as cross-resistance to β-lactam antibiotics (Jørgensen et al. 2013). Reduced ability to deal with oxidative stress due to downregulated ROS-detoxifying enzymes in *P. aeruginosa* biofilm cells, was also shown to increase mutation frequency (Driffield et al. 2008).

1.3.7 Horizontal gene transfer

Horizontal gene transfer (HGT) is a process that facilitates genetic exchange between bacterial individuals of intra- and inter-species. It is an important means for bacteria to acquire new genetic materials, e.g., antibiotic resistance genes, to promptly adapt to quick-changing environments, particularly in a biofilm setting. Four main pathways for HGT in bacteria have been identified: conjugation, transformation, transduction, and vesiduction (**Figure 1.3**).

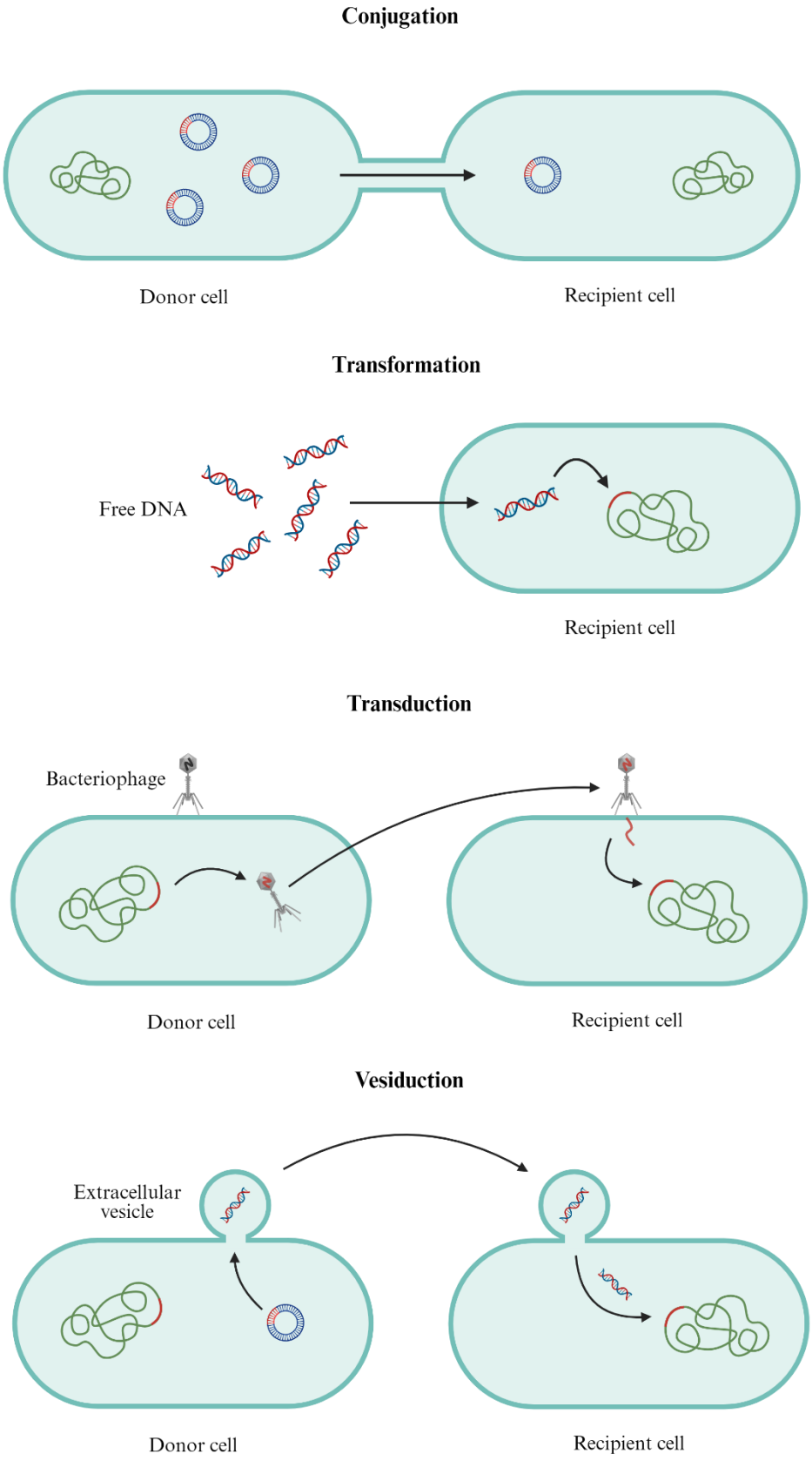

Figure 1.3 Four types of horizontal gene transfer. The figure was created with BioRender.com.

1.3.7.1 Conjugation

Conjugation is generally regarded as the most prevalent pathway in HGT (Cabezón et al. 2015). When genetic materials are transferred by direct cell-to-cell contact via cell surface pilus or adhesion between a donor cell and a recipient cell, conjugation occurs (Juhas et al. 2008; Alvarez-Martinez and Christie 2009; Wozniak and Waldor 2010). The initiation of conjugation requires a DNA-binding complex of proteins (the relaxosome) at the site of transfer and a coupling protein to connect these two complexes together. Plasmids, a common vehicle for resistance genes, are the most often transferred mobile genetic element in HGT and have been widely recognised as a significant factor contributing to the prevalence and dissemination of antibiotic resistance determinants within biofilms. In fact, the conjugal transfer frequency of a multidrug resistance plasmid in biofilms can be 10,000 times higher than that observed in planktonic cultures (Savage et al. 2013). This increased transfer efficiency is likely due to the sessile setting of a biofilm and the close spatial proximity of bacterial cells (Molin and Tolker-Nielsen 2003; Madsen et al. 2012; Król et al. 2013). Usually, these transferred resistance genes become integrated into the genome of the new host and passed onto any progeny.

1.3.7.2 Transformation

Transformation refers to the process by which extracellular DNA fragments from the environment (e.g., from dead bacteria) are taken up by competent recipient cells by

transport across the cell membrane. Any resistance genes they carry will then become incorporated into the genome (Domingues et al. 2012). Only a limited subset of bacteria, such as *Haemophilus* and *Streptococcus* spp., are naturally competent, characterised by their ability to readily take up naked free DNA fragments (Claverys et al. 2009). However, competence can also be induced in other bacterial species, including *E. coli*, through exposure to antibiotics or stimulation with calcium chloride (Johnston et al. 2014; Sturød et al. 2018). The transformation process is highly sophisticated and requires the engagement of type II and type IV secretion systems, type IV pili, and a highly preserved channel in the cytoplasmic membrane, through which the DNA travels (Krüger and Stingl 2011).

1.3.7.3 Transduction

In transduction, genetic material is transferred between bacterial cells via bacteria-infecting viruses termed bacteriophages (Coleman et al. 2006; Novick et al. 2010). Bacteriophages can replicate inside the infected bacteria using either their own or host replication machinery. During this process, potential resistance genes from the donor cell can be integrated into the genome of the bacteriophages or *vice versa* (Modi et al. 2013). As a result, the resistance genes are recombined into host DNA, thus conferring antibiotic resistance. Transduction does not require cell-to-cell contact, safeguarding foreign DNA encapsulated in bacteriophages from potential degradation by DNases in the environment. However, bacteriophage-mediated transduction is not a major player of DNA transfer in natural environments due to its high selectivity for target bacteria.

1.3.7.4 Vesiduction

Alongside the three established mechanisms mentioned above, the transfer of DNA mediated by extracellular vesicles (EVs), referred to as vesiduction, has been suggested as an additional form of HGT (Soler and Forterre 2020), being a common occurrence in both Gram-positive and Gram-negative bacteria (Deatherage and Cookson 2012; Brown et al. 2015; Kim et al. 2015; Schwechheimer and Kuehn 2015). When carrying DNA, EVs can transfer genetic material between bacterial cells, protecting DNA from degradation by outside forces. Although EVs have been observed to facilitate the transfer of endogenous and/or exogenous plasmids between cells (Gaudin et al. 2013; Erdmann et al. 2017), the mechanisms of vesiduction are still not well understood.

1.4 Mechanisms of antibiotic resistance in bacteria

1.4.1 Enzymatic modification or inactivation of antibiotics

Enzymatic modification and enzymatic inactivation can occur in both Gram-positive and Gram-negative bacteria. In enzymatic modification, antibiotics are chemically-modified by bacterial enzymes e.g., by addition of specific chemical groups, thereby disabling antibiotic target site-binding functionality. For example, acetylation, adenylation and phosphorylation by aminoglycoside modifying enzymes can lead to a decreased avidity of aminoglycosides for their targets (Ramirez and Tolmasky 2010).

In enzymatic inactivation, bacterial enzymes directly bind antibiotics and disarm them

via hydrolytic cleavage action. This is exemplified by the inactivation of penicillin and cephalosporin by β-lactamases, an enzyme that destroys the amide bond of the β-lactam ring (Bradford 2001; Bush and Jacoby 2010).

1.4.2 Reduced intracellular accumulation of antibiotics

Reduced accumulation of antibiotics within bacterial cells can be achieved by decreased influx and increased efflux of the relevant antibiotic. The influx of antibiotics into Gram-negative bacteria usually depends on an entry point on the outer membrane, such as porins, which are the major route of entry for hydrophilic antibiotics such as β-lactams, fluoroquinolones, tetracyclines and chloramphenicol (Christaki et al. 2020). Therefore, reduced expression, loss, and structural modification of the porin molecules can lead to decreased antibiotic influx.

The efflux of antibiotics, on the other hand, can be affected by efflux pumps, which are energy-dependent transport systems on the cytoplasmic membrane able to pump toxic substances out of the cell. Hence, upregulated efflux pump expression or enhanced pumping ability due to mutation can bring about acquired antibiotic resistance (Piddock 2006a,b). Although some efflux pumps are drug-specific, most are capable of transporting several unrelated drugs and can, therefore, confer multidrug resistance (Piddock 2006a,b; Nikaido and Pagès 2012). To date, many efflux systems have been found to be associated with antibiotic resistance, such as the resistance-nodulation-cell division (RND) family, major facilitator superfamily (MFS), ATP-binding cassette

(ABC) family and multidrug and toxic-compound extrusion (MATE) family (Putman et al. 2000; Poole 2005; Schwarz et al. 2005).

1.4.3 Target alteration

Antibiotic target alterations include target replacement, target-site mutations, target site enzymatic modifications, and target overproduction. One example of target replacement is the replacement of bacterial penicillin-binding proteins (PBPs), also known as transpeptidases and carboxypeptidases. These enzymes are crucial for building and maintaining the bacterial cell wall by polymerising and cross-linking the peptidoglycan layer and are the targets of β-lactam antibiotics (Zapun et al. 2008; Abushaheen et al. 2020). Methicillin resistance in *S. aureus* is the result of the combination of the *mecA* resistance gene and native chromosomal DNA. The *mecA* gene encodes PBP2a, an analogue of PBP that has an extremely low affinity for most β-lactams. Consequently, *mecA* does not inhibit cell wall synthesis, even in the presence of β-lactams (Chambers 1999; Moellering Jr 2012; Hiramatsu et al. 2013).

Mutations in genes encoding the target sites of antibiotics are a common mechanism for the development of antibiotic resistance. Quinolone resistance usually results from mutations in the genes encoding bacterial gyrase and/or topoisomerase IV, which is important for DNA synthesis (Aldred et al. 2014). Rifampicin resistance is the result of mutational changes in the RNA polymerase β subunit gene (Goldstein 2014). Resistance to macrolide, lincosamide, and streptogramin B, however, are caused by

mutations in the 23S rRNA gene (Leclercq 2002).

Antibiotic target site modifications by enzymes represent another class of resistance mechanism. Methylation of the 23S rRNA by enzymes that are encoded by *erm* (erythromycin ribosome methylase) genes, is responsible for cross-resistance to macrolides, lincosamides, and streptogramin B (Leclercq 2002), while methylation of the 23S rRNA by enzymes encoded by the *cfr* gene has been implicated in resistance to linezolid, chloramphenicol, and clindamycin (Schwarz et al. 2004; Kehrenberg et al. 2005; Morales et al. 2010).

Target overproduction can confer antibiotic resistance by overwhelming the drug with excess target molecules. An example is trimethoprim resistance in *E. coli*, which arises from the overproduction of dihydrofolate reductase (DHFR) (Flensburg and Sköld 1987; Eliopoulos and Huovinen 2001). Trimethoprim inhibits DHFR, an enzyme required for converting dihydrofolic acid to tetrahydrofolic acid (THF), a key precursor for bacterial DNA and protein synthesis. Overproduction of DHFR allows sufficient THF synthesis to continue despite the presence of the antibiotic.

1.5 Colistin

1.5.1 Polymyxin family and colistin

In the last 20 years, the increasing incidence of multidrug-resistant (MDR) bacterial infections and the shortage of new antibiotics entering clinical trials has significantly

affected the ability of clinicians to successfully manage hard-to-treat infections in humans and animals. As a result, recourse to traditional antibiotics such as polymyxins has been a necessity (Nang et al. 2019; Zajac et al. 2019). Polymyxins are a family of antimicrobial cationic polypeptides. The polymyxin family consists of 5 derivatives (polymyxin A, B, C, D and E) (Landman et al. 2008), with each characterised by a cyclic heptapeptide, a linear tripeptide and a hydrophobic fatty acyl chain (**Figure 1.4**). However, due to the high toxicity of polymyxin A, C and D, only polymyxin B and E (colistin) have so far been used in clinical practice (Schwarz and Johnson 2016). Polymyxin B and colistin exhibit identical primary sequences, differing solely at position 6, where polymyxin B is D-Phe and colistin is D-Leu (**Figure 1.4**). Polymyxin B1 and polymyxin B2 are two subdivisions of polymyxin B, and are *N*-terminally acylated at the fatty acyl chain region by 6-methyloctanoic acid and 6-methylheptanoic acid, respectively; similarly, colistin A and colistin B are two subdivisions of colistin, and are acylated by 6-methyloctanoic acid and 6-methylheptanoic acid, respectively (Velkov et al. 2010) (**Figure 1.4**). The conserved chemical structure of polymyxins includes two hydrophobic domains: the *N*-terminal fatty acyl chain and the D-Phe^{6}-L-Leu^{7} segment (polymyxin B) or D-Leu^{6}-L-Leu^{7} segment (colistin); these domains are separated by polar L-Thr and cationic L-Dab residues (**Figure 1.4**). The coexistence of distinct hydrophobic and polar domains in polymyxins determines their amphipathic nature, which is essential for their interaction with the lipid A component of LPS on the bacterial outer membrane, a critical step in initiating their antimicrobial action (Velkov et al. 2010). The narrow spectrum of colistin targets most members of the Gram-

negative *Enterobacteriaceae* family, including *E. coli, Klebsiella, Citrobacter*, *Shigella*, *Enterobacter* and *Salmonella* spp. (Gogry et al. 2021). Colistin also exhibits notable bactericidal activity against common non-fermentative Gram-negative bacteria, such as *P. aeruginosa*, *Acinetobacter baumannii*, and *Stenotrophomonas maltophilia* (Falagas et al. 2005; Lim et al. 2010; Sultan et al. 2020).

However, bacteria such as Morganella morganii, Pseudomonas mallei, Burkholderia cepacia, Serratia marcescens, Vibrio cholera, Proteus spp., Providencia spp., Edwardsiella spp., Chromobacterium spp., Campylobacter, Brucella, and Legionella all exhibit natural resistance to colistin (Gogry et al. 2021). In addition, colistin is ineffective against Gram-positive bacteria, anaerobic bacteria, fungi, and parasites (Poirel et al. 2017a; Mohapatra et al. 2021).

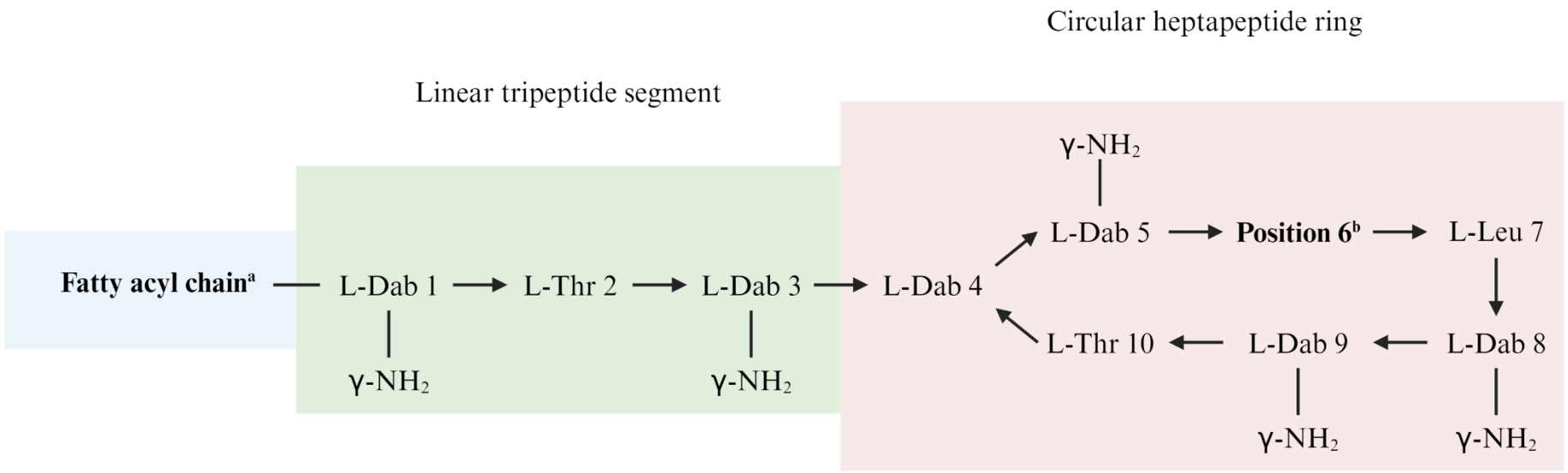

Figure 1.4 Chemical structures of polymyxin B and colistin. The structural segments of polymyxins are coloured as follows: blue, fatty acyl chain; green, linear tripeptide segment; red, circular heptapeptide ring. [a]6-methyloctanoic acid in polymyxin B1 and colistin A, and 6-methylheptanoic acid in polymyxin B2 and colistin B. [b]D-Phe in polymyxin B and D-Leu in colistin. Dab, α, γ-diaminobutyric acid; Thr, threonine; Phe, phenylalanine; Leu, leucine. Arabic numbers represent the positions of amino acid residues. The figure was created with BioRender.com.

1.5.2 Colistin usage history

Colistin was first used clinically in the 1950s in Japan, Europe, and the United States, but was subsequently abandoned in the early 1980s owing to side effects, including nephrotoxicity and neurotoxicity (Yu et al. 2015). However, given the rise in MDR Gram-negative bacteria, many of which resist conventional antibiotics (Yong et al. 2009; Kumarasamy et al. 2010), colistin was later reintroduced into clinical usage in the mid-1990s as a valuable drug and designated a last-resort antibiotic by the WHO (Falagas et al. 2005; World Health Organization 2014). Subsequent reevaluations of the safety of colistin in the treatment of severe infections concluded that colistin is less nephrotoxic than previously assumed, and improved dosage regimens may limit its toxicity (Reed et al. 2001; Li et al. 2006; Honore et al. 2013). Currently, colistin is administered in human medicine as a treatment option for potentially lethal infections caused by MDR and carbapenem-resistant Gram-negative pathogens, namely carbapenem-resistant *P. aeruginosa*, *A. baumannii*, *Klebsiella pneumoniae*, *E. coli*, and other *Enterobacteriaceae* (Paterson and Harris 2016; El-Sayed Ahmed et al. 2020). In veterinary medicine, colistin is commonly used to prevent *E. coli* infections in farm animals (Kempf et al. 2013), and in Asia, colistin has been used as a growth promoter in livestock feed at high dosages (Nguyen et al. 2016; Walsh and Wu 2016; Wongsuvan et al. 2018). All these practices have, together, greatly contributed to the alarmingly rapid spread of colistin resistance worldwide.

1.5.3 Mechanism of action of colistin

The exact mechanism of how colistin kills bacteria is unknown but likely involves three key processes: destabilisation of the outer membrane via colistin-LPS interaction, self-promoted uptake of colistin towards the inner membrane, and finally cell lysis mediated by disruption of the inner membrane (**Figure 1.5**). Therefore, a prerequisite for colistin initiating its bactericidal activity against Gram-negative bacteria is binding of colistin to the LPS of the outer membrane. Lipid A, the lipid element of LPS, is typically composed of a β-1'-6-linked D-glucosamine (GlcN) disaccharide and six attached fatty acyl chains (Velkov et al. 2010). The disaccharide component of lipid A possesses two phosphoryl groups at the 1- and 4'-positions, with both phosphates being able to be further modified by the addition of groups including ethanolamine, glucose, mannose, or 4-amino-4-deoxy-L-arabinose (L-Ara4N) (Erridge et al. 2002; Needham and Trent 2013). It is believed that lipid A imparts a negative charge to the cell surface and contributes to stabilising the structural integrity of the outer membrane, with the closely packed fatty acyl chains serving as a hydrophobic anchor (Nikaido 2003). A classic model of colistin binding to the lipid A of LPS has been established. Briefly, positively charged L-Dab residues of colistin (the polar domain) bind to negatively charged 1- and 4'-phosphate groups of the lipid A moiety on LPS molecules via electrostatic interactions (El-Sayed Ahmed et al. 2020). Initial binding helps to competitively supplant the divalent cations (Mg^{2+} and Ca^{2+}), which act as a bridge to stabilise the LPS, from the phosphate groups of the lipid A (Storm et al. 1977; Yu et al. 2015). In the

meantime, the hydrophobic D-Leu^{6}-L-Leu^{7} segment and the fatty acyl chain of colistin (together as the hydrophobic domain) also interact with the fatty acyl tails of lipid A, weakening the neighbouring lipid A fatty acyl chains. All these dynamics lead to destabilisation and increased permeability of the outer membrane. Following insertion, as colistin permeates through the periplasm, it creates pores in the inner membrane and disrupts the physical integrity of the membrane, followed by the outflow of cytoplasmic contents and ultimately cell death (Wanty et al. 2013).

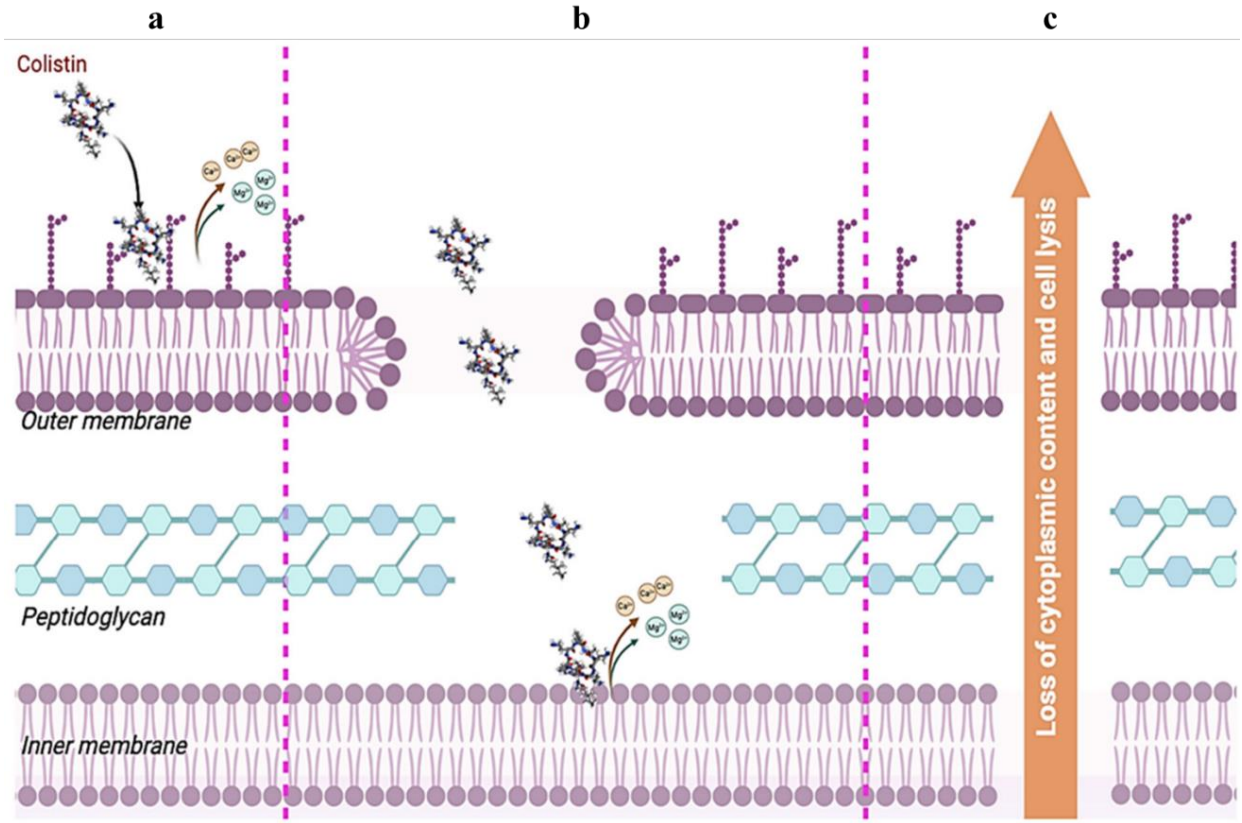

Figure 1.5 Schematic representation of the mechanism of action of colistin against Gram-negative bacteria. **a** Colistin binds to LPS, causing displacement of Ca^{2+} and Mg^{2+} and destabilising the outer membrane. **b** Colistin goes through the periplasm, reaching the inner membrane, where it creates pores and displaces Ca^{2+} and Mg^{2+}. **c** Colistin disrupts the inner membrane, altering the osmotic balance and leading to the outflow of cytoplasmic contents and, ultimately, cell death. The figure was derived from Diani et al. (2024).

1.6 Mechanisms of acquired colistin resistance

The mechanisms for acquired colistin resistance have been reported in many Gram-negative bacteria, for example, the *Enterobacteriaceae* family, including *Escherichia*, *Enterobacter*, *Salmonella*, and *Klebsiella* spp. (Poirel et al. 2017a; Stefaniuk and Tyski 2019). The various known mechanisms of colistin resistance are either plasmid-mediated (**see Chapter 1 Section 1.6.2**) or chromosomally-mediated. In chromosome-mediated colistin resistance mechanisms, covalent modification of LPS at its lipid A phosphate groups by the addition of cationic groups, i.e., phosphoethanolamine (pEtN/PEA) and L-Ara4N occurs. This represents a classic mechanism for acquired colistin resistance in Gram-negative bacteria, as it undermines the net negative charge of lipid A and reduces the initial binding of colistin to LPS (Olaitan et al. 2014b; Simpson and Trent 2019; Zhang et al. 2021a). Notably, LPS alteration can also be achieved by other means at different moieties of LPS, e.g., by deacylation and hydroxylation (Olaitan et al. 2014b). Other chromosome-mediated colistin resistance mechanisms involve the complete loss of LPS, the role of efflux pumps and capsule polysaccharides.

1.6.1 Chromosome-mediated colistin resistance

1.6.1.1 Two-component system-regulated colistin resistance

As previously mentioned in **Chapter 1 Section 1.6**, the addition of pEtN and L-Ara4N

to the lipid A moiety of LPS are the most common mechanisms that lead to resistance to colistin. The enzymes responsible for this lipid A modification are largely transcriptionally regulated by the so-called two-component systems, namely PmrAB and PhoPQ (Gunn 2008; Prost and Miller 2008) (**Figure 1.6**). The PmrAB and PhoPQ systems are highly conserved among pathogenic *Enterobacteriaceae* (Needham and Trent 2013), including in *E. coli* (Olaitan et al. 2015; Nordmann et al. 2016), *K. pneumoniae* (Jayol et al. 2014; Jayol et al. 2015), *Salmonella enterica* (Sun et al. 2009), *Enterobacter cloacae* (Kang et al. 2019), *Enterobacter aerogenes* (Diene et al. 2013), as well as in *A. baumannii* (Adams et al. 2009; Cheah et al. 2016; Lima et al. 2018) and *P. aeruginosa* (Miller et al. 2011; Moskowitz et al. 2012; Lee and Ko 2014). These systems regulate a large panel of downstream genes and operons involved in LPS modification and can be modulated by specific regulators such as the PmrAB-regulating CrrAB system and the PhoPQ-regulating MgrB protein (**see Chapter 1 Section 1.6.1.1.3** for detailed information about these two regulators). The activation of the PmrAB and PhoPQ two-component systems is triggered by environmental stimuli, or certain genetic mutations within the systems that lead to their constitutive activation and subsequent activation of LPS modification-associated genes, thereby ultimately conferring colistin resistance (Gunn and Miller 1996; Gunn et al. 2000; Trent et al. 2001b; Abraham and Kwon 2009; Barrow and Kwon 2009; Miller et al. 2011; Poirel et al. 2017a).

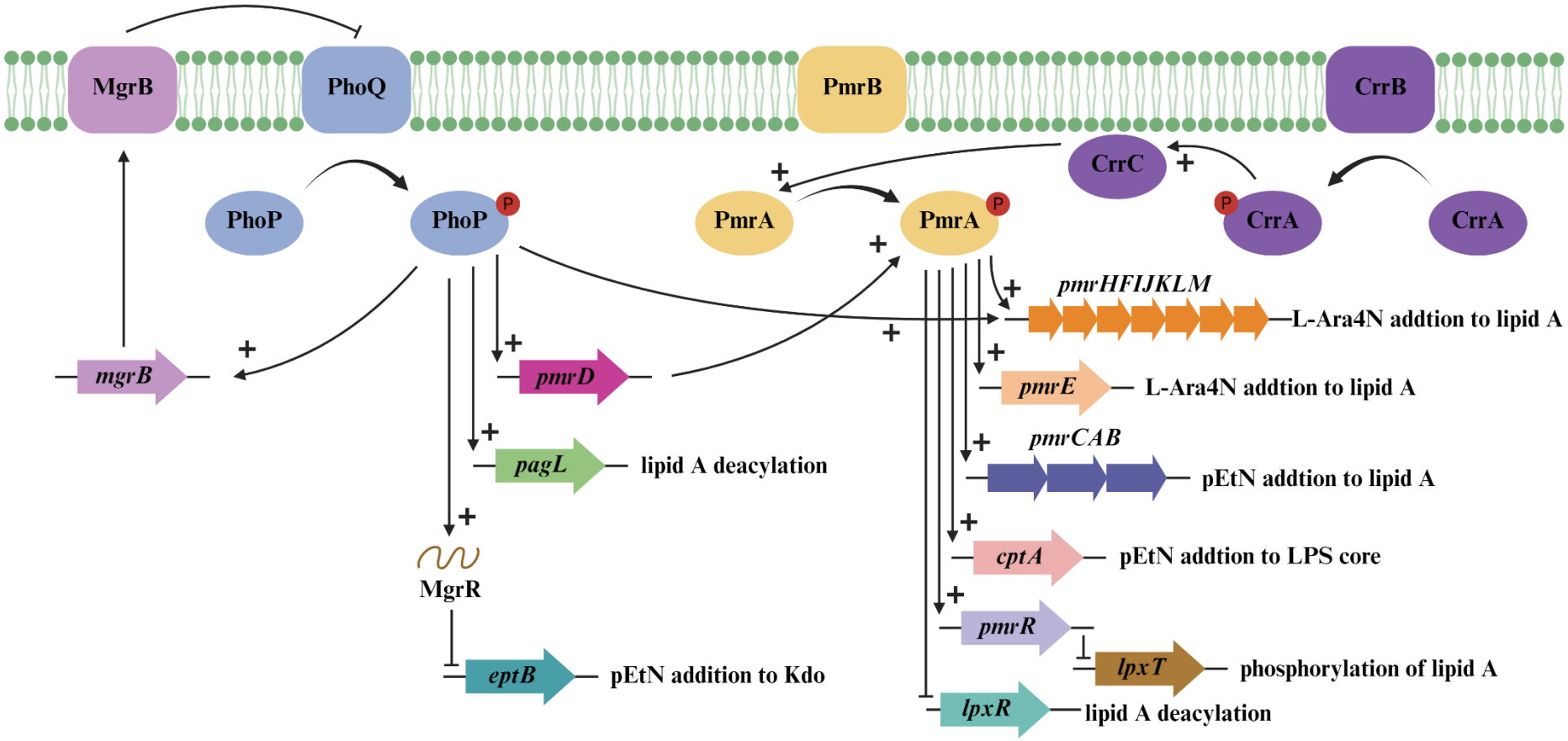

Figure 1.6 Diagram illustrating the main pathways involved in colistin resistance via PmrAB and PhoPQ two-component system-regulated LPS modification in Gram-negative bacteria. The pathways illustrated here are limited to LPS modifications that have been shown to affect resistance to polymyxins. The figure was created with BioRender.com.

1.6.1.1.1 The PmrAB two-component system

In 1993, the PmrAB two-component system was first discovered in a polymyxin B-resistant mutant of *Salmonella typhimurium* (Roland et al. 1993). It is encoded by the *pmrCAB* operon and is comprised of a sensor kinase with tyrosine kinase activity, PmrB, and its corresponding response regulator, PmrA (**Figure 1.6**). The *pmrC* gene (also known as *pagB* or *eptA*) in the *pmrCAB* operon encodes PmrC, a pEtN phosphotransferase that facilitates LPS modification by the addition of cationic pEtN to lipid A (Gunn 2008; Aghapour et al. 2019; Sinha et al. 2019; Hamel et al. 2021). When under environmental conditions of polymyxin pressure, macrophage phagosomes, high levels of Fe^{3+} and Al^{3+}, or low pH, PmrB undergoes autophosphorylation and activates PmrA by phosphorylation (Perez and Groisman 2007; Gunn 2008; Chen and Groisman 2013). As a DNA-binding regulatory molecule, PmrA regulates the expression of several LPS modification-related operons and genes. For example, PmrA activates the *pmrCAB* operon, leading to the transfer of pEtN to lipid A (Gunn 2008). PmrA can also activate the transcription of the *pmrHFIJKLM* operon (also known as *arnBCADTEF* or *pbgPE*) and the *pmrE* gene responsible for the biosynthesis and addition of L-Ara4N to the 1- or 4'-phosphate group of lipid A (Gunn et al. 1998; Yan et al. 2007; Mitrophanov et al. 2008). It has been reported that the modification of LPS by L-Ara4N provides a higher level of resistance compared to pEtN modification (Tamayo et al. 2005a).

Apart from pEtN- and L-Ara4N-mediated LPS modification at the lipid A phosphate groups, the PmrAB system also regulates a few other genes that contribute to LPS modification-associated colistin resistance (**Figure 1.6**). In *Salmonella*, the *cptA* gene is regulated by PmrA and is responsible for the addition of pEtN to the phosphorylated heptose-I residue at the LPS core (Tamayo et al. 2005a; Tamayo et al. 2005b). PmrA activates *pmrR*, which represses the expression of *lpxT*, a gene found to mediate the phosphorylation of the 1-phosphate of lipid A to form 1-diphosphate (1-PP) and impair pEtN modification due to the increased net negative charge of lipid A (Jones et al. 2008; Touzé et al. 2008; Herrera et al. 2010; Kato et al. 2012). In *S. typhimurium* and various other Gram-negative bacteria, *lpxR*, a hydrolase gene that mediates the removal of the 3'-acyloxyacyl residue from lipid A resulting in a decreased number of acyl groups attached to lipid A, is usually repressed by the PmrAB system and has been demonstrated to play a part in polymyxin resistance (Helander et al. 1996; Tran et al. 2005; Reynolds et al. 2006; Clements et al. 2007; Murray et al. 2007). In fact, the number of genes modulated by the PmrAB system is large. In *Salmonella*, this system regulates more than 20 confirmed genes and potentially up to 100 genes, as established through microarray, mutagenesis, and in silico analyses (Tamayo et al. 2002; Marchal et al. 2004; Tamayo et al. 2005a).

1.6.1.1.2 The PhoPQ two-component system

The PhoPQ two-component system was first characterised in *S. typhimurium* in 1989 to regulate several genes involved in bacterial virulence and survival in macrophages

(Miller et al. 1989). It is encoded by the *phoPQ* operon and consists of PhoQ, a sensor protein kinase with tyrosine kinase activity, and its cognate regulator protein, PhoP (**Figure 1.6**). When triggered by environmental stimuli, such as polymyxins, macrophage phagosomes, low Mg^{2+} and Ca^{2+}, and low pH, PhoQ is activated through its periplasmic domain and phosphorylates PhoP (Véscovi et al. 1996; Bader et al. 2005; Gunn and Richards 2007; Gunn 2008; Simpson and Trent 2019). The phosphorylated PhoP regulates LPS modification via two distinct pathways; it directly binds to and activates the transcription of the *pmrHFIJKLM* operon (*arn* operon) to promote the L-Ara4N-mediated LPS modification, or it indirectly controls the PmrAB system-regulated genes by upregulating the expression of PmrD (Winfield et al. 2005; Mitrophanov et al. 2008; Cheng et al. 2010; Johnson et al. 2013; Huang et al. 2020; Huynh and McPhee 2021). PmrD is a small connector protein that acts as a bridge linking the downstream of the PhoPQ system with the upstream of the PmrAB system (Gunn and Miller 1996; Soncini and Groisman 1996; Rubin et al. 2015). Upon activation by phosphorylated PhoP, PmrD binds to phosphorylated PmrA at the N-terminal domain, which helps to stabilise the phosphorylated PmrA and prevent it from being dephosphorylated by PmrB (Gunn 2001; Kato and Groisman 2004; Falagas et al. 2010; Luo et al. 2013; Rubin et al. 2015). This interaction ultimately leads to the constitutive activation of a series of PmrA-regulated genes, including the *pmrCAB* operon, *pmrE*, and *pmrHFIJKLM* operon (Huang et al. 2020), the transcription of which confers colistin resistance by LPS modification with the addition of L-Ara4N and pEtN.

It has been reported that the PhoPQ system regulates genes other than the above-mentioned pathways involved in colistin resistance (**Figure 1.6**). In *Salmonella*, PhoP activates the *pagL* gene, which is involved in the deacylation of lipid A via the removal of the R-3-hydroxymyristate at position 3 of lipid A (Trent et al. 2001a); activation of *pagL* increases polymyxin resistance in those strains unable to perform L-Ara4N and pEtN modifications of lipid A (Kawasaki et al. 2007). In *E. coli*, the PhoPQ system activates *mgrR*, an sRNA known to repress the *eptB* gene, which modifies LPS by adding pEtN to its outer Kdo (3-deoxy-D-manno-octulosonic acid) residue (Reynolds et al. 2005; Raetz et al. 2007). This modification decreases the net negative charge of LPS, eventually leading to polymyxin resistance (Moon and Gottesman 2009).

1.6.1.1.3 Regulators of the PmrAB and PhoPQ two-component systems

In 2015, research into the genetic mechanisms of colistin resistance in two clinical *K. pneumoniae* strains revealed that mutations in a previously uncharacterised histidine kinase gene that is part of a two-component regulatory system were associated with upregulated expression of the *pmrCAB* operon, and this system was designated crrAB (Wright et al. 2015). The crrAB system is encoded by the *crrAB* operon and consists of a histidine sensor kinase, CrrB, and a response regulator protein, CrrA (Wright et al. 2015; McConville et al. 2020) (**Figure 1.6**). The *crrB* mutation-induced elevation of *crrB* expression was also observed to be accompanied by high expression of an adjacent uncharacterised gene encoding a conserved hypothetical membrane protein, which was speculated by the authors to possibly act as a connector protein linking the PmrAB and

CrrAB systems (Wright et al. 2015). This gene was later designated *crrC* and confirmed to mediate *crrB* mutation-induced overexpression of the *pmrHFIJKLM* operon and *pmrC* via the PmrAB two-component system, leading to LPS modification by L-Ara4N and pEtN, respectively, and subsequently colistin resistance (Cheng et al. 2016). The *crrAB* genes were found to lack clear orthologs in *E. coli* or *Salmonella*; however, orthologs of these genes are present in several *Enterobacter* species (Wright et al. 2015).

The PhoPQ two-component system-regulating MgrB was initially discovered in 1999 in *E. coli* as a short lipoprotein responsive to depletion of extracellular Mg^{2+} and regulated by the PhoPQ pathway (Kato et al. 1999). It was later established to be a negative feedback regulator of the PhoPQ system (**Figure 1.6**); knockout of the *mgrB* gene resulted in upregulation of the PhoPQ system in *E. coli*, *S. typhimurium*, *Yersinia pestis* and other related bacteria (Lippa and Goulian 2009). MgrB is a small transmembrane protein composed of 47 amino acids, with its N-terminus in the cytoplasm and C-terminus in the periplasm (Lippa and Goulian 2009). Upon activation by PhoP, the *mgrB* gene is upregulated. The expressed MgrB protein directly interacts with the periplasmic sensor domain of PhoQ and inhibits the kinase activity and/or stimulates the phosphatase activity of PhoQ, which represses the phosphorylation of PhoP, thereby downregulating the PhoP-regulated genes (Lippa and Goulian 2009). Therefore, the inactivation or downregulation of MgrB caused by any genetic changes in *mgrB,* including point mutations, insertions or deletions of nucleotide sequences, can

result in the overexpression of PhoP, leading to the activation of the *pmrHFIJKLM* operon either directly or indirectly via PmrD, and the subsequent acquisition of L-Ara4N-mediated colistin resistance (Mitrophanov et al. 2008; Cheng et al. 2010; Cannatelli et al. 2013; Cannatelli et al. 2014b; Gaibani et al. 2014; Kim et al. 2014; López-Camacho et al. 2014; Olaitan et al. 2014a; Poirel et al. 2015; Andrade et al. 2020).

1.6.1.2 Loss of LPS

A. baumannii lacks the biosynthesis genes for L-Ara4N; however, the *pmrCAB* operon-mediated lipid A modification by the addition of cationic pEtN represents a primary mechanism of colistin resistance in *A. baumannii* and is strictly regulated by the PmrAB two-component system (Adams et al. 2009; Arroyo et al. 2011; Beceiro et al. 2011; Park et al. 2011; Lesho et al. 2013; Choi and Ko 2014). Nevertheless, mutations in the first three lipid A biosynthesis genes, *lpxA*, *lpxC* and *lpxD*, are another important mechanism for acquired colistin resistance in *A. baumannii*. Nucleotide substitution or deletion and insertional inactivation with insertion elements in these genes can lead to the loss of lipid A production and potentially the resultant complete removal of LPS (Moffatt et al. 2010; Moffatt et al. 2011). Since lipid A is the main binding target for colistin, the resistance level generated via lipid A loss can be very high (MIC >128 mg/L) (Moffatt et al. 2010; Andrade et al. 2020). Besides *A. baumannii*, *lpx* gene-associated lipid A deficiency or loss of LPS can also occur in *E. coli*. Moosavian et al. (2020) found that 6 out of 14 colistin-resistant clinical *E. coli* isolates possessed no LPS,

and the *lpx* biosynthetic cluster was disrupted, with the highest MIC reaching >256 mg/L.

1.6.1.3 Efflux pumps

Several studies have indicated that efflux pumps, such as KpnEF, AcrAB, Emr and mexAB-oprM, can contribute to polymyxin resistance. It has been reported that the *kpnEF* mutant strain displayed increased antibiotic susceptibility, including to colistin (a two-fold decrease in MIC) compared with the wild-type strain in *K. pneumoniae* (Srinivasan and Rajamohan 2013). The *K. pneumoniae* strain with the *acrB* knockout from the AcrAB efflux pump showed increased susceptibility to polymyxin B compared with the wild-type strain, and the efflux of polymyxin B from the cell by AcrAB was confirmed to be an energy-dependent process (Padilla et al. 2010). In *A. baumannii*, the Emr pump system has been shown to confer resistance to colistin, as the wild-type strain could tolerate colistin better than the *emrB* mutant (Lin et al. 2017). Similarly, the mexAB-oprM efflux pump was also found to play a significant role in the colistin tolerance development in a metabolically active subpopulation in *P. aeruginosa* biofilms because the mutants defective in *mexAB-oprM*-mediated colistin efflux could not form a tolerant biofilm subpopulation (Pamp et al. 2008).

1.6.1.4 Capsule polysaccharide

Apart from being an important pathogenic factor, bacterial capsule polysaccharide (CPS) has been shown to act as a protective barrier against antimicrobial peptides

(Campos et al. 2004; Spinosa et al. 2007). A *K. pneumoniae* mutant lacking CPS was found to be more sensitive to and more bound by polymyxin B than the wild-type strain (Campos et al. 2004). Additionally, polymyxin B induced upregulation of CPS biosynthesis genes, with polymyxin B resistance levels being significantly correlated with the levels of CPS expression. CPS was found to be released from the bacterial surface of capsulated *K. pneumoniae*, *Streptococcus pneumoniae* and *P. aeruginosa* when treated with polymyxin B, decreasing its bactericidal activity, likely due to the binding of free CPS to antimicrobial peptides, thereby diminishing the quantity of drug reaching the bacterial cell surface (Llobet et al. 2008). Furthermore, CPS architecture might play a role in colistin resistance because monolayered and multilayered CPS has been observed in a colistin-sensitive *K. pneumoniae* strain and its colistin-resistant derivative, respectively (Formosa et al. 2015). This highlights the significance of CPS in resistance to polymyxins via upregulation of capsular biosynthesis genes, which in turn decreases the interaction of colistin with the bacterial surface.

1.6.2 Plasmid-mediated colistin resistance

1.6.2.1 Emergence of mobile colistin resistance genes

Traditionally, bacterial resistance to colistin was exclusively attributed to chromosome-mediated mechanisms, especially involving chromosomal mutations (**see Chapter 1 Section 1.6.1**). Chromosome-mediated processes typically do not enable the rapid spread of colistin resistance. However, in 2015, the first plasmid-mediated mobile

colistin resistance (*mcr*) gene, *mcr-1*, carried on an IncI2 conjugative plasmid, was identified in *E. coli* isolated from food animals, food and humans in China (Liu et al. 2016). This discovery sparked major concerns in the global community, as highly transferable plasmids provide an easy mechanism for colistin resistance to spread, thus posing a significant threat to human health. Unsurprisingly, less than three months after it was first reported, the spread of *mcr-1* was soon confirmed in more than 20 countries around the world, (Baron et al. 2016; Rhouma et al. 2016).

To date, a total of 10 *mcr* variants have been identified (*mcr-1* to *mcr-10*), with the principal bacterial hosts harbouring these genes being *Enterobacteriacae* including *E. coli* (*mcr-1* to *mcr-3*) (Liu et al. 2016), *S. enterica* (*mcr-4*, *mcr-5*, and *mcr-9*) (Carretto et al. 2018; Borowiak et al. 2019; Ling et al. 2020), *K. pneumoniae* (*mcr-7* and *mcr-8*) (Wang et al. 2018b; Yang et al. 2018), *E. cloacae* complex (*mcr-9*) (Xu et al. 2022a; Xu et al. 2022b), and *Enterobacter roggenkampii* (*mcr-10*) (Wang et al. 2020a), as well as *Aeromonas* spp. (*mcr-3*) and *Moraxella* spp. (*mcr-6*) (AbuOun et al. 2017; Shen et al. 2019). Epidemiological data suggests that *mcr-1*, found in 62 countries/regions spanning six continents in animals, humans, and the environment, is the most extensively dispersed of all the *mcr* genes. This is followed by *mcr-9*, *mcr-10*, *mcr-8*, *mcr-3* and *mcr-4*, which have been detected in 53, 27, 24, 23 and 23 countries, respectively, while the other *mcr* variants have so far exhibited a more restricted geographic distribution (Liu et al. 2024a) (**Figure 1.7**).

Genetic studies and sequencing have demonstrated that *mcr* genes might be derived

from *mcr*-like genes present on the chromosomes of bacterial species such as *Moraxella* (*mcr-1* and *mcr-2*), *Aeromonas* (*mcr-3* and *mcr-7*), *Shewanella* (*mcr-4*), *Kosakonia* (*mcr-8*), and *Buttiauxella* (*mcr-9* and *mcr-10*) (Liu et al. 2024a).

A variety of plasmid incompatibility types have been found to carry *mcr* genes, including IncI1, IncI2, IncX1, IncX3, IncX4, IncF, IncFII, IncFIA, IncFIB, IncH1, IncHI1, IncHI2, IncK2, IncP, IncY, IncC, and ColE (Zurfluh et al. 2017; Hammerl et al. 2018; Hadjadj et al. 2019; Sia et al. 2020; Liu et al. 2021), the most common of which are IncI2, IncHI2, IncX4, and IncP (Elbediwi et al. 2019). All of the latter four incompatibility types have been shown to carry *mcr-1*, with IncX4, IncI2, and IncP plasmids also being capable of carrying *mcr-2, mcr-7,* and *mcr-3,* respectively. IncHI2 is linked to the greatest number of *mcr* variations, including *mcr-1*, *mcr-3*, and *mcr-9* (Mmatli et al. 2022).

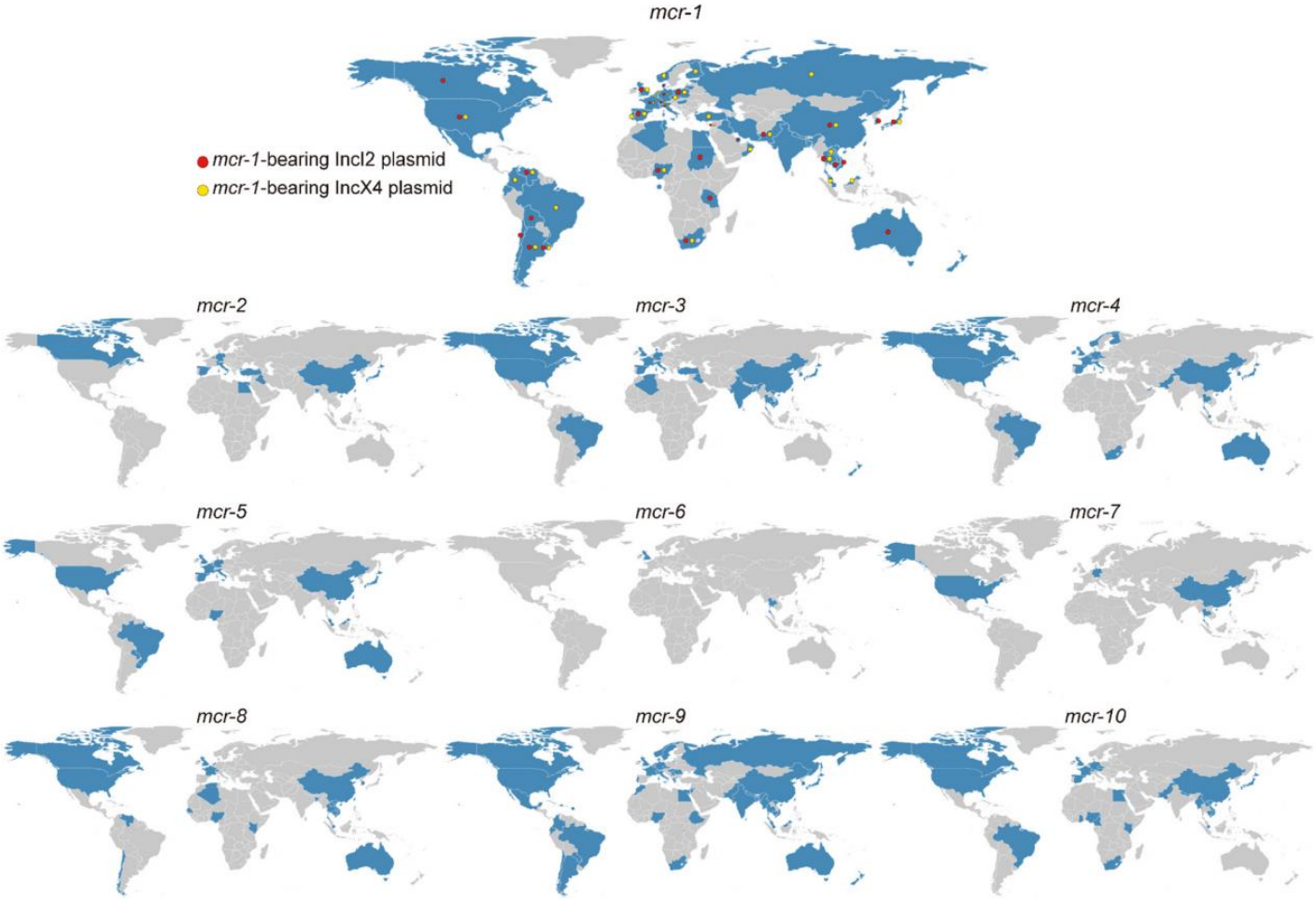

Figure 1.7 Geographical distribution of *mcr-1* to *mcr-10*. The countries/regions where the *mcr* genes have been identified are indicated in blue. *Mcr-1* is currently the most widely distributed *mcr* gene in the world. The figure was derived from Liu et al. (2024a)

Generally, the colistin resistance conferred by *mcr* genes is relatively low (MIC ranging from 2 to 8 mg/L) (Bertelloni et al. 2022). Nonetheless, "silent" *mcr* genes have also been reported. In carbapenem-resistant *Enterobacteriaceae* strains, Teo et al. (2018) identified *mcr-3*-like and *mcr-4*-like genes that did not impart colistin resistance. Zhou et al. (2018) observed that the insertion of an IS*1294b* element generated an inactivated form of *mcr-1* gene, while the loss of this element and the reactivation of *mcr-1* could occur on exposure to increasing concentrations of colistin. Similarly, an inactive version of *mcr-1* blocked by a 22-bp tandem repeat was found in the human pathogen *Shigella sonnei* during selection without antibiotics (Pham Thanh et al. (2016). The *mcr-1* gene, however, was able to regain its activity after exposure to colistin by deleting one copy of the 22-bp repeat, leading to a high degree of colistin resistance (32 mg/L). This possible resurgence of colistin resistance is worth noting, as it may impact clinical treatment of infections (Zhou et al. 2018).

Worryingly, *mcr*-like genes have been shown to coexist with other antibiotic resistance genes, especially the carbapenem resistance gene bla_{NDM} (Shen et al. 2018b; Wang et al. 2018b; Sulian et al. 2020). Of the 43 carbapenemase-producing *E. coli* strains found in a study of 3859 stool specimens from healthy Chinese participants, 14 were shown to coexist with $bla_{\text{NDM-5}}$ and *mcr-1* (Shen et al. 2018b). This finding was in line with a previous investigation by Wang et al. (2017b), who discovered that the percentage of bla_{NDM} and *mcr-1* co-existence in carbapenemase-producing *E. coli* was 23% (37/161). These findings highlight the need to urgently implement measures to address the

dissemination of these pan-drug resistant bacteria (Paveenkittiporn et al. 2021).

1.6.2.2 Mechanism of *mcr*-mediated colistin resistance

All the *mcr* genes share a conserved colistin resistance mechanism. Among the *mcr*-encoded MCR family, MCR-1 is the most representative and extensively studied enzyme. As an *mcr-1*-encoded, PmrC-like pEtN transferase, MCR-1 confers resistance to colistin by catalysing the transfer of a pEtN from the cytomembrane to the lipid A moiety on the LPS of Gram-negative bacteria, thereby reducing the net negative charge of LPS, and consequently, reducing colistin binding (Zhang et al. 2019a; Hussein et al. 2021) (**Figure 1.8**).

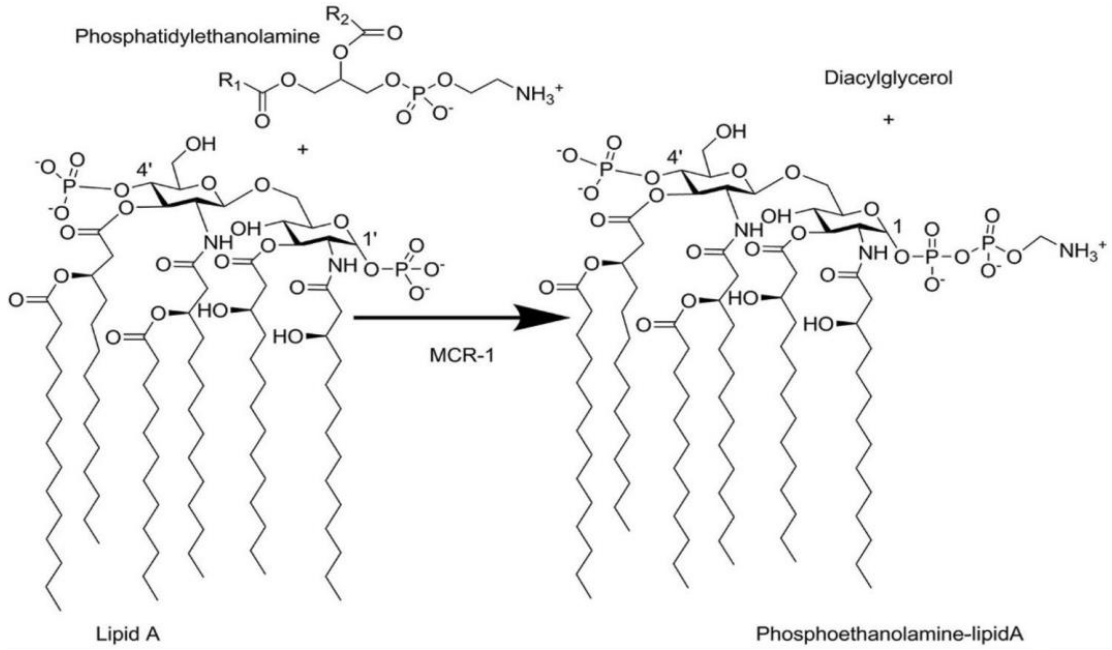

Figure 1.8 The phosphoethanolamine transfer reaction catalysed by MCR-1. MCR-1 transfers phosphoethanolamine from a phosphatidylethanolamine to the 1- or 4'-phosphate group of lipid A, forming a phosphoethanolamine-lipid A structure, with diacylglycerol also being one end product (Hussein et al. 2021).

Structural analysis has revealed that MCR-1 is a membrane-anchored protein consisting of 541 amino acid residues. It features an N-terminal transmembrane domain, which comprises five hydrophobic membrane-spanning α-helices, a C-terminal periplasmic catalytic domain, and a periplasmic loop and a bridging helix that connect these two domains (Anandan et al. 2017; Hinchliffe et al. 2017; Xu et al. 2018a). The transmembrane domain is necessary for the MCR-1 enzyme to localise appropriately in the membrane and to orient substrate binding, while the catalytic domain contains a core hydrophilic fold-containing catalytic motif, which is essential for the transfer of pEtN (Wanty et al. 2013; Gao et al. 2016). The active centre of the catalytic domain houses a membrane interaction surface pocket formed by 12 essential residues that facilitate the accommodation of the phosphatidylethanolamine (PE) lipid substrate molecule (Xu et al. 2018b). The conserved nucleophilic threonine residue Thr285 within the active centre is believed to be phosphorylated by pEtN (Hinchliffe et al. 2017). Moreover, the active site contains metal-binding residues that chelate zinc ions, thereby stabilising the alkoxide form of Thr285 (Stojanoski et al. 2016; Wei et al. 2018). This allows Thr285 to perform a nucleophilic attack on the phosphate group of PE, leading to the production of a diacylglycerol product and an intermediate known as the Thr285-pEtN complex (Hu et al. 2016; Stojanoski et al. 2016). This complex transfers pEtN to the 1- or 4'-phosphate position of lipid A, thereby undermining the net negative charge of lipid A and conferring colistin resistance (Xu et al. 2018a). It has been demonstrated that removing the transmembrane domain from the MCR-1 protein may reinstate colistin susceptibility in recombinant *E. coli* (Gao et al. 2016). Similarly,

substitutions of five putatively conserved locations in the catalytic domain of the MCR-1 protein (E246, T285, H395, D465, and H466) result in considerable decreases in the colistin MIC (Gao et al. 2016; Hinchliffe et al. 2017). These findings suggest that both transmembrane and catalytic domains are indispensable for the proper functioning of MCR-1.

In addition to MCR-1, nine other homologs (MCR-2 to MCR-10), have also been identified as pEtN transferases that possess both transmembrane and catalytic domains. Phylogenetic tree analysis indicated that MCR-1 exhibits significant amino acid sequence similarity with MCR-2 (81%) and MCR-6 (83%), categorising them within the same subgroup (Shen et al. 2020; Liu et al. 2024a) (**Figure 1.9**). Nonetheless, MCR-3 (32%), MCR-4 (34%), MCR-7 (35%), MCR-8 (31%), MCR-9 (36%), and MCR-10 (36%) constitute a distinct subgroup based on their amino acid homology. MCR-5 (36%) is classified into a third subgroup owing to its reduced amino acid homology relative to other members.

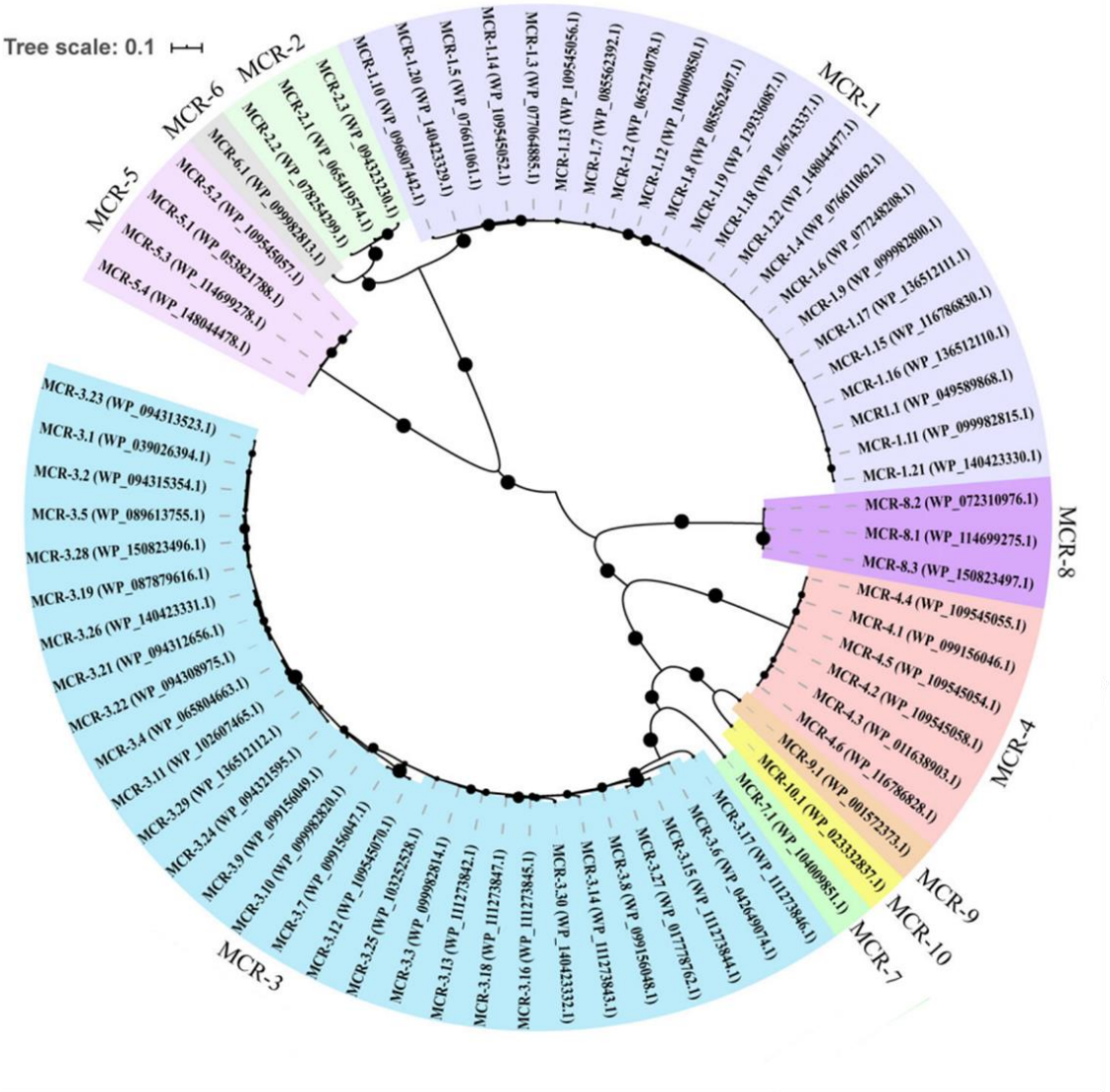

Figure 1.9 Topology tree of all *mcr* variants. Ten MCR proteins were coloured with different background. All MCR proteins can be categorised into three subgroups: first subgroup contains MCR-1, MCR-2 and MCR-6; second subgroup contains MCR-3, MCR-4, MCR-7, MCR-8, MCR-9 and MCR-10; third subgroup contains MCR-5. The figure was derived from Shen et al. (2020).

1.7 Fitness cost of antibiotic resistance and compensatory evolution

1.7.1 Fitness cost of antibiotic resistance acquisition

In general, the acquisition of antibiotic resistance is expected to confer a fitness cost, regardless of whether the resistance is gained via chromosomal mutations or by uptake of exogenous resistance genes through HGT. In chromosome-mediated antibiotic resistance, mutations usually occur in genes associated with antibiotic targets that are intrinsically linked to cellular physiology, e.g., DNA replication/transcription, RNA translation, and cell wall synthesis (Andersson and Hughes 2010; Hernando-Amado et al. 2017). These are mutations which may impair bacterial fitness and lower competitiveness in comparison to sensitive parental strains (Björkman and Andersson 2000; Melnyk et al. 2015). In the case of acquiring resistance determinants via mobile genetic elements, e.g., plasmids, a physiological burden results from extra resources and energy required for their replication, transcription, and protein synthesis (Hernando-Amado et al. 2017). In addition, plasmids can interfere with cellular pathways and regulatory mechanisms, resulting in a metabolic burden on the host cell (Harrison et al. 2016). It is worth noting that the acquisition of antibiotic resistance is not always associated with a fitness cost; some resistance mutations are cost-free (Hernando-Amado et al. 2017). Melnyk et al. (2015) demonstrated that mutations confer resistance to fusidanes and dihydrofolate reductase inhibitors failed to incur a fitness cost. The notion of fitness cost is important, as resistant bacteria may, in the

long term, be outcompeted in the absence of selective antibiotic pressure by their sensitive counterparts, thereby ultimately restricting the spread of resistance (Andersson and Hughes 2010; Christaki et al. 2020). Therefore, determination of the fitness cost conferred by acquisition of antibiotic resistance is a key factor in estimating the rate and maintenance of resistance and plays an essential role in predicting population-based evolution of antimicrobial resistance (Melnyk et al. 2015).

Fitness cost usually involves changes in bacterial growth/survival rates and virulence/pathogenesis. Basically, three methods exist to measure the fitness cost of antibiotic resistance. The easiest technique is to use growth parameters as an indicator, e.g., comparing susceptible and resistant isolates *in vitro* over time (Melnyk et al. 2015). Competition modelling may also compare sensitive strains and resistant mutants to examine the physiological strength of each, where fitness is represented as the proportion of susceptible to resistant strains in the mixture after antibiotic-free serial passage (Melnyk et al. 2015). *In vivo* assays using a range of host organisms, including *Galleria mellonella* and *Caenorhabditis elegans* models are also important and have been used to evaluate changes in bacterial virulence and fitness after acquisition of resistance (Paulander et al. 2007; Jiang et al. 2021). Besides, competition assays between sensitive and resistant cultures can also be conducted in *in vivo* models by monitoring the change in population ratios over time (Pope et al. 2010).

1.7.2 Compensatory evolution compensates for plasmid fitness cost

Acquisition of plasmids carrying resistance genes through HGT represents a major way of acquiring antibiotic resistance. Although plasmid-conferred fitness cost contributes to restricting the dissemination of antibiotic resistance, a growing body of research has demonstrated that the effects of the fitness cost in antibiotic-resistant bacteria may be offset by compensatory evolution. In other words, compensatory evolution ameliorates the plasmid fitness cost and enables resistant bacteria to persist in antibiotic-free conditions without losing antibiotic resistance by partly or fully restoring their fitness to the level of their ancestral sensitive clones (Andersson and Hughes 2010). The presence of compensatory evolution can enhance the overall permissiveness of MDR plasmids, providing an effective approach for the maintenance of costly MDR plasmids. It has been considered a significant factor contributing to the high prevalence of certain plasmids and pathogens (Benz and Hall 2023), and it also affects the evolutionary trajectory of bacterial populations harbouring MDR plasmids (San Millan 2018).

Compensatory evolution occurs when genetic mutations emerge that mitigate or negate fitness costs, thereby enabling the plasmid to persist within the bacterial population (Bouma and Lenski 1988; Millan et al. 2014; Harrison et al. 2016; Durão et al. 2018; Zhang et al. 2022), and these evolutionary mutations can occur on bacterial chromosomes, plasmids, or both (Brockhurst and Harrison 2022). Compensatory evolution on chromosomes primarily results from mutations in transcriptional regulatory factors (Liu et al. 2024c). However, plasmid-located compensatory

evolution generally has a more significant impact than chromosomal compensation, owing to its capacity for both vertical and horizontal inheritance. There are three main compensatory evolution patterns on plasmids: fragment deletion, fragment acquisition, and plasmid-borne point mutations.

1.7.2.1 Deletion of fragments on plasmids

Compensatory evolution involving deletion of costly fragments is a common evolutionary mechanism for plasmids, which is frequently associated with beneficial outcomes, including a decrease in plasmid fitness costs and an improvement in plasmid stability. Fragment deletion often occurs in the plasmid conjugation transfer region and the MDR region, likely due to the "energy cost" of expression of the conjugation genes and the antimicrobial resistance genes (Zahrl et al. 2006; Yang et al. 2017; Rajer and Sandegren 2022). Nonetheless, a "trade-off" is present, as physiological function of plasmids may also be compromised, with decreased conjugation frequency and resistance levels (Porse et al. 2016; Dorado-Morales et al. 2021; Zhang et al. 2022). An MDR IncHI2 plasmid, pJXP9, underwent a deletion event that eliminated both the MDR regions and the conjugation transfer region I, thereby compensating for the fitness cost linked to plasmid carriage; this improved plasmid maintenance and vertical transmission but negatively affected plasmid horizontal transfer ability and bacterial physiology (Zhang et al. 2022). Similarly, adaptive evolution of a large cointegrate plasmid pL53T led to a large-scale DNA fragment loss, and the evolved plasmid imposed minimal fitness cost on the host bacteria but exhibited a greatly reduced

conjugation frequency due to the loss of the *psiB* gene (Liu et al. 2024b).

1.7.2.2 Acquisition of fragments on plasmids

In addition to the deletion of certain fragments, the acquisition of foreign DNA fragments represents an alternative strategy for compensating for plasmid fitness cost and enhancing plasmid persistence, particularly through acquisition of sequences encoding toxin-antitoxin (TA) systems and resolvases (Loftie-Eaton et al. 2016; Stalder et al. 2017). TA systems contribute to plasmid maintenance in proliferating bacterial populations through a mechanism known as addiction, which results in the targeted elimination of plasmid-free daughter bacteria, thereby enhancing the prevalence of plasmids within the bacterial population (Goeders and Van Melderen 2014). Transposon-encoded resolvases help to resolve cointegrates, including plasmid multimers that are often formed before cell division, thus decreasing plasmid loss frequency (Grindley 2007; Field and Summers 2011). However, it is worth noting that the occurrence of plasmid compensatory evolution via additional fragment acquisition is less frequent than fragment deletion, likely due to the increased metabolic burden imposed on host bacteria.

1.7.2.3 Plasmid-borne point mutations

Compensatory evolution can also be achieved by point mutations, which frequently occur in genes associated with plasmid replication and conjugation, leading to enhanced plasmid maintenance (Porse et al. 2016; Stalder et al. 2017; Ares-Arroyo et al. 2022;

Metzger et al. 2022; Yang et al. 2023). DNA replication-related mutations compensate for plasmid fitness costs, e.g., by regulating plasmid copy number (Sota et al. 2010; San Millan et al. 2015; Yano et al. 2016), whereas mutations in conjugation genes reduce plasmid fitness costs by affecting horizontal transmission capability (Yang et al. 2023).

1.8 Plant-derived antimicrobials and epoxytiglianes

1.8.1 Antimicrobial phytochemicals and terpenes

The excessive use of antibiotics in recent decades has resulted in the emergence of numerous MDR bacteria, or superbugs, complicating infection treatment in clinical settings. This rapid rise in antimicrobial resistance has necessitated ongoing research for novel antimicrobial agents to combat this escalating issue, even as the availability of new drugs diminishes. Recently, the emphasis on antimicrobial discovery and development has transitioned towards plants, fungi, lichens, endophytes, and diverse marine sources, including seaweeds, corals, and other microorganisms, owing to their promise in addressing antibiotic resistance in bacterial pathogens (Angelini 2024). Among these natural sources, plant-derived secondary metabolites as antimicrobial agents have shown desirable antibacterial and antifungal effects. Although significant independent antibacterial activity may not be evident, their use along with other antibiotics can significantly enhance their antimicrobial efficacy against resistant pathogens (Upadhyay et al. 2014; Bribi 2018). These naturally occurring products encompass a variety of phytochemicals, including terpenoids, alkaloids, polyphenols,

and sulfur-containing compounds, among which the terpene-based terpenoids are the most diverse and extensively distributed category across the plant kingdom (Angelini 2024; Arzani et al. 2025).

Terpenes, also known as isoprenoids, represent one of the most diverse families of natural compounds found in nature. They are present in nearly all life-forms and serve multiple functions, including involvement in the primary structure of cells (e.g., steroids and cholesterol in cell membranes) and in cellular processes (e.g., carotenoids and quinones in photosynthesis and electron transport, respectively) (Khameneh et al. 2021; Toffolatti et al. 2021). In plants, terpenes are extensively found in the leaves, stems, flowers, fruits, buds and wood, with more than 80,000 identified terpenes/terpenoids present in the wild. They are the primary natural components of herbal resins and are responsible for the characteristic aromas of various plants (Zhou and Pichersky 2020; Al Musayeib et al. 2022). Terpenes are basic hydrocarbons composed of five-carbon isoprene units (CH_2=C(CH_3)CH=CH_2, C_5H_8), which are the building-blocks of all types of terpenes, whereas terpenoids are a modified class of terpenes, characterised by specific functional groups and the repositioning or removal of oxidised methyl groups at various sites (Perveen et al. 2021). These terms are often used interchangeably. Terpenes are classified based on the number and structure of the isoprene units (**Figure 1.10**); these include hemiterpenes (C_5H_8), monoterpenes ($C_{10}H_{16}$), sesquiterpenes ($C_{15}H_{24}$), diterpenes ($C_{20}H_{32}$), sesterterpenes ($C_{25}H_{40}$), triterpenes ($C_{30}H_{48}$), tetraterpenes ($C_{40}H_{64}$), and polyterpenes (>8 isoprene units)

(Arzani et al. 2025). A range of plant-derived terpenes/terpenoids, including farnesol, nerolidol, carvone, thymol, carvacrol, ursolic acid, α-amyrin, eugenol and cinnamaldehyde, have been found to exhibit antimicrobial effects against numerous microorganisms, including *S. aureus*, *Campylobacter jejuni*, *Enterococcus faecium*, *E. coli*, *E. aerogenes*, *P. aeruginosa*, *Salmonella*, *Listeria monocytogenes*, *Helicobacter pylori*, *Candida albicans*, *Candida glabrata* and *Candida krusei* (Amaral et al. 2015; Yadav et al. 2015; Zhang et al. 2015; Althunibat et al. 2016; Rathinam et al. 2017; Catteau et al. 2018; Marinelli et al. 2018; Cox-Georgian et al. 2019; Godlewska et al. 2021; Zhang et al. 2021b; Han et al. 2022; Ben Miri et al. 2023; El Fannassi et al. 2023). Gram-positive bacteria usually display greater susceptibility to terpenes compared to Gram-negative bacteria, attributable to the lipophilic characteristics of terpenes (Angelini 2024). In addition, it has been shown that oxygenated terpenes (phenolic terpenoids), including carvacrol, ρ-cymene, and thymol, exhibit greater antimicrobial activity compared to hydrocarbon terpenes, such as camphene, R-(–)-limonene, terpinene, and (+)-α-pinene (Guimarães et al. 2019). Apart from their antimicrobial activity, some terpenes/terpenoids have also been utilised in medicine as pharmaceutical agents exhibiting anti-inflammatory (Gallily et al. 2018), anti-tumor (Salminen et al. 2008; Cör et al. 2018), and antioxidant properties (Guimarães et al. 2019; Wang et al. 2019a).

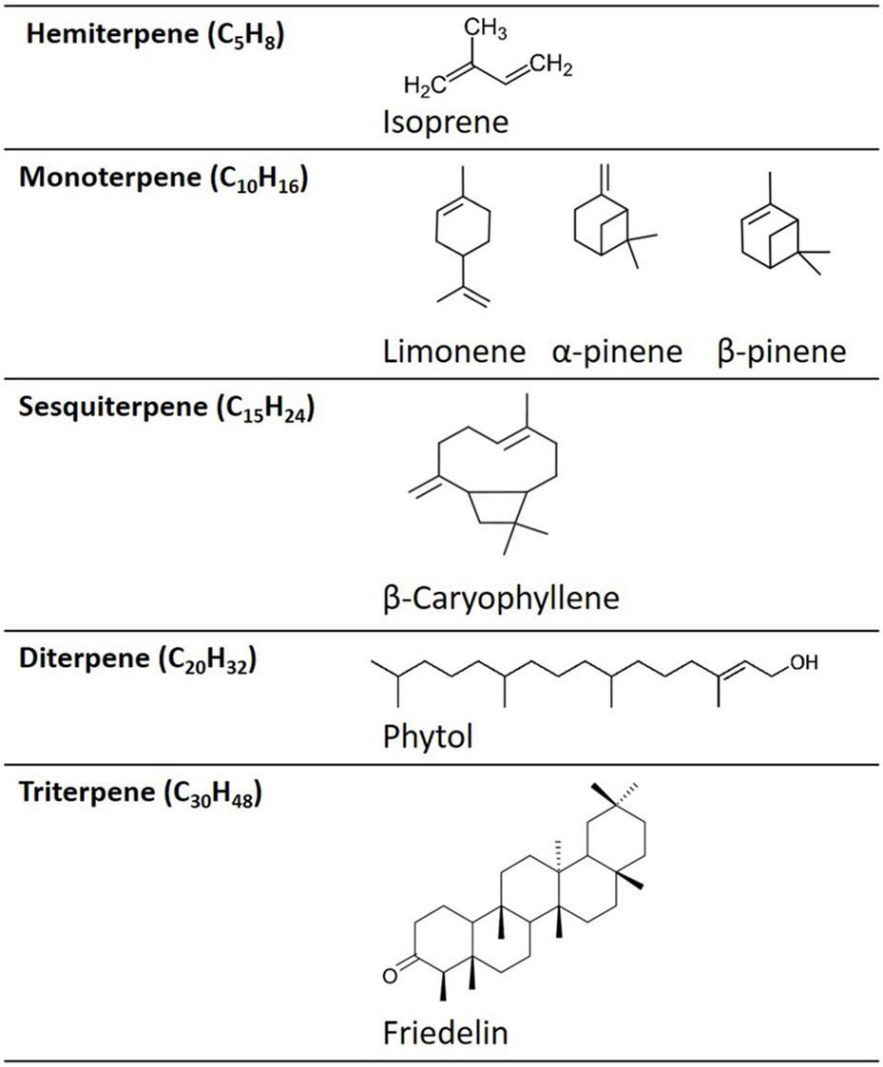

Figure 1.10 Examples of the chemical structures of different terpene categories. The figure was derived from Weston-Green et al. (2021).

1.8.2 Epoxytiglianes

1.8.2.1 EBC-46

Epoxytiglianes such as EcoBiotics Compounds (EBCs; named after the biotechnology company EcoBiotics), are a novel group of diterpene esters discovered and extracted from the seed of a blushwood tree, *Fontainea picrosperma* (*Euphorbiaceae*), a plant

endemic to the Australian rainforest (Grant et al. 2017; Moses et al. 2023). EBC-46 (12-tigloyl-13-(2-methylbutanoyl)-6,7-epoxy-4,5,9,12,13,20-hexahydroxy-1-tigliaen-3-one), also known as tigilanol tiglate, is the naturally-occurring prototypical epoxytigliane, and was initially studied for its potent anti-cancer effects in humans and companion animals (**Figure 1.11a)** (Boyle et al. 2014; Barnett et al. 2019; Panizza et al. 2019). Intra-tumoral injection of EBC-46 induced a rapid inflammatory response *in situ* and damage to the tumor vasculature, causing significant haemorrhagic necrosis and subsequent tumor ablation in melanoma, squamous cell carcinoma and other mouse tumor models (Boyle et al. 2014; Barnett et al. 2019). These changes are, in part, attributable to the activation of the protein kinase C (PKC) signaling pathway (Boyle et al. 2014). This PKC-activating activity of EBCs is structurally dependent, with the 6,7-epoxide structural motif and position critical to PKC activation *in vitro*, and the alkyl branching features of the C12-ester influencing their potency (Cullen et al. 2021). Currently, EBC-46 is under Phase II human clinical trials as a local therapeutic agent for various cancers and has recently received approval as a veterinary pharmaceutical for the treatment of non-metastatic canine mast cell tumours, marketed under the

tradename STELFONTA® (De Ridder et al. 2021; Jones et al. 2021; Moses et al. 2023).

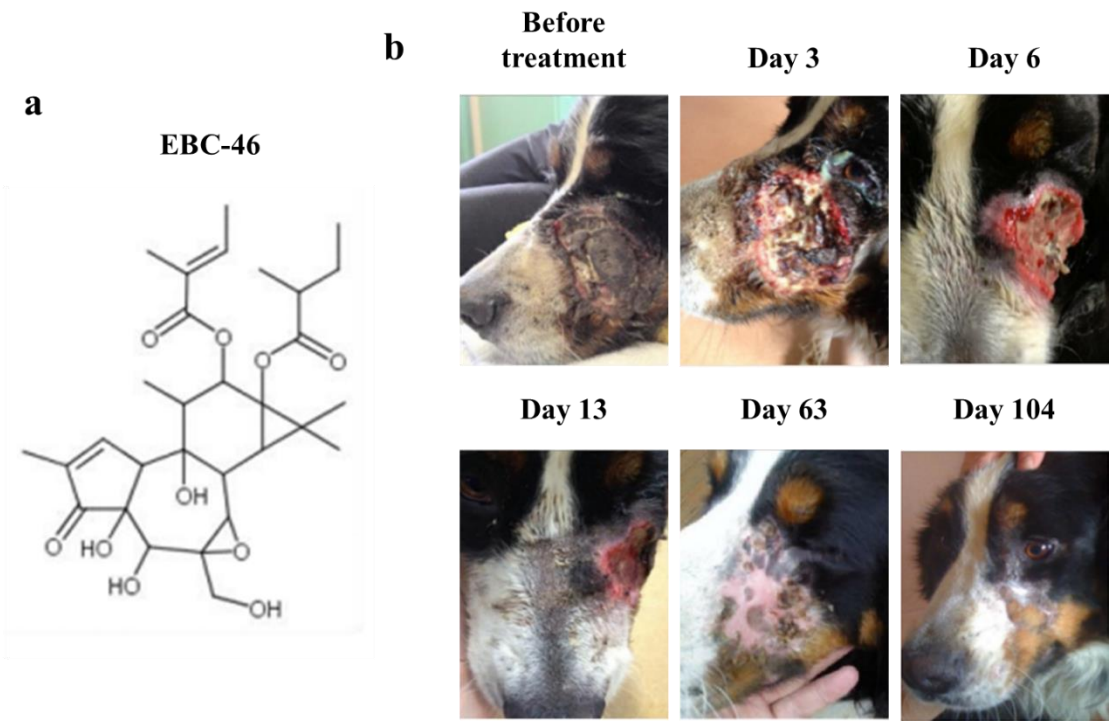

Figure 1.11 Chemical structure of EBC-46 and the resolution of chronic wound infection by EBC-46. **a** EBC-46 molecular structure. **b** Images depicting the resolution of a chronic (3-month) necrosing ulcer in a canine model, which did not respond to conventional antibiotic and anti-inflammatory treatments, following administration of EBC-46. Images courtesy of Powell et al. (2022).

In addition to its anti-cancer properties, EBC-46 also induces remarkable dermal wound healing responses at sites of tumor destruction *in vivo*, with accelerated wound re-epithelialisation and closure observed following treatment (Reddell et al. 2021). Such enhanced wound healing is, in part, due to the fact that epoxytiglianes stimulate keratinocyte wound healing responses by expediting cell proliferation, promoting cell

migration and wound repopulation, and facilitating regulation of downstream gene expression in favour of enhanced wound healing, via PKC activation (Moses et al. 2020). Recently, EBC-46 and its selected analogues demonstrated exceptional PKC affinities, distinct PKC isoform selectivities, and are potential lead compounds as latency reversing agents for "kick and kill" strategies aimed at HIV eradication (Gentry et al. 2025).

Apart from healing benefits in tumors, EBC-46 has also demonstrated utility in resolving infected, non-healing chronic wounds unresponsive to routine antibiotic and anti-inflammatory therapy in veterinary studies (**Figure 1.11b)** (Powell et al. 2022). As the chronicity of these infected skin wounds is highly associated with the existence of bacterial biofilms with decreased susceptibility to antimicrobial treatment (van Hoek et al. 2011; Mah 2012a; Percival et al. 2012), the observed ability of EBC-46 to resolve infection and induce wound healing could be related to its antibacterial/antibiofilm effects. This has led to the exploration and screening of numerous natural, semisynthetic and synthetic EBCs for antimicrobial activity.

1.9 Aims

The aims of this thesis were, first, to investigate the phenotypic effects associated with carriage of *mcr* plasmids in *E. coli*, with a particular focus on the fitness cost of *mcr* carriage; second, to characterise the stability of *mcr* plasmid carriage during long-term evolution of *E. coli* biofilms and the associated genotypic changes occurring over

evolutionary time; and finally, to investigate the antimicrobial effects of novel epoxytiglianes against *mcr*-negative or -positive *E. coli* and to elucidate their mechanism of action on the bacterial membrane.

Chapter 2

Phenotypic characterisation of plasmid-mediated colistin resistant *Escherichia coli*

2.1 Introduction

2.1.1 The *mcr-1* gene

Since its first discovery in 2015, plasmid-borne *mcr-1* from an *E. coli* farm isolate has become so widespread that it has been detected in a variety of bacterial species including *E. cloacae, E. coli, K. pneumoniae* and *Salmonella* species, in humans, animals and the environment in numerous countries across the world (Arcilla et al. 2016; Liu et al. 2016; Quan et al. 2017; Hussein et al. 2021). Interestingly, a retrospective study showed that the incidence of *mcr-1* could be traced back to the 1980s, when colistin was first introduced in veterinary medicine in China as a food additive and a therapeutic treatment in animal husbandry (Shen et al. 2016), suggesting that the emergence of *mcr-1* is highly likely to be linked with selective pressure caused by excessive antibiotic exposure. Moreover, the authors monitored the occurrence of *mcr-1*-carrying *E. coli* of chicken origin over an extended period from 1970 to 2014 and found that the outbreak of *mcr-1*-positive *E. coli* began as early as 2009. The incidence of *mcr-1*-positive isolates increased from 5.2% (6/115) in 2009 to 30.0% (15/50) in 2014 (Shen et al. 2016).

Following the discovery of *mcr-1*, and to control colistin consumption in agriculture, in 2017 China declared the prohibition of the use of colistin in food-producing animals. This policy was likewise also quickly taken up by Thailand, Malaysia, Brazil, and India (Wang et al. 2020b). The discontinued large-scale use of colistin in agriculture, has

appeared to significantly decrease (although not completely eliminate) colistin resistance in China, as evidenced by a considerable reduction in the mean colistin residue concentration, the median relative abundance of *mcr-1*, and the percentage of colistin resistant *E. coli* isolates from pigs, chickens and humans (Wang et al. 2020b).

The *mcr-1* gene is 1626 bp in size and, when carried on conjugative plasmids, is highly transferable in nature. It has been found on various plasmid Inc types including IncX4, IncI2, IncHI2, IncP, IncX and IncFII, with IncI2 being the most predominant (Li et al. 2017a; Zhang et al. 2021a). Previous conjugation experiments have confirmed that *mcr-1* could be efficiently transferred between *E. coli* strains at high frequencies (10^{-3} to 10^{-1} transconjugant cells per recipient cell by conjugation), as shown by dramatically elevated colistin MICs (8-16 times) in the transconjugants (Liu et al. 2016). Furthermore, *mcr-1* is also able to integrate into the chromosomal genome in *E. coli*, confirming its highly mobile characteristics (Lin et al. 2020). To date, several new variations of *mcr-1* have been identified from different sources and in various countries, such as *mcr-1.1* (on IncX4 plasmids in MDR *E. coli* isolated from rainbow trout) (Hassan et al. 2020a), *mcr-1.2* (on IncX4 plasmids in a carbapenemase-producing *K. pneumoniae* from a surveillance rectal swab from a leukemic child) (Di Pilato et al. 2016), and *mcr-1.6* (on IncP plasmids in a colistin resistant *S. enterica* serovar typhimurium isolated from a healthy individual) (Lu et al. 2017).

E. coli plays an essential role in *mcr-1* transmission and, appears to be the primary host of *mcr-1,* having been isolated in *E. coli* from human bloodstream infections and

imported chicken (Hasman et al. 2015). Moreover, *mcr-1* has also been detected in *E. coli* isolates from human wound infections that produce extended-spectrum beta-lactamases and carbapenemases (Falgenhauer et al. 2016). The findings of *mcr-1* in MDR infections in patients, and possible co-existence with other antibiotic resistance genes, emphasises the critical need for alternate antibiotic therapies, as well as the requirement for continued active worldwide monitoring of clinical antibiotic-resistant pathogens.

2.1.2 The *mcr-3* gene

The *mcr-3* gene was discovered in China in 2017 in *E. coli* obtained from a healthy porcine faecal sample, carried on the 261 kb IncHI2 plasmid pWJ1, where it was found to coexist with 18 other resistance determinants (Yin et al. 2017). The *mcr-3* gene is 1626 bp in size and, exhibits 45.0% nucleotide sequence identity to *mcr-1*. MCR-3 encoded by *mcr-3* shows 32.5% amino acid sequence similarity to that of MCR-1, and 99.8 to 100% identity to pEtN transferases of other *Enterobacteriaceae* origins. Similar to MCR-1, the MCR-3 protein structure is also thought to possess a trans-membrane domain and a pEtN transferase catalytic domain. As with *mcr-1*, *mcr-3* is found to have been widely disseminated, as it has been identified in *E. coli*, *Aeromonas* and *Proteus* spp. isolated from animals and humans in Europe, South America and Asia (Carattoli et al. 2017). Intriguingly, a 801-bp fragment upstream of *mcr-3* shares 87% of its nucleotide sequence with the truncated transposon Tn*As2*, which has only been discovered in *Aeromonas salmonicida*, suggesting that it may have formerly originated

from an *Aeromonas* species (Yin et al. 2017). This speculation is further supported by epidemiological evidence, which indicates that *Aeromonas* spp. possess a high prevalence of *mcr-3* and *mcr-3*-like genes (Ling et al. 2017; Shen et al. 2018a).

2.1.3 Fitness cost in colistin resistance

As previously mentioned (**see Chapter 1 Section 1.6**), there are essentially three LPS-associated colistin resistance mechanisms identified so far: 1) LPS loss mediated by mutations in *lpxACD* genes; 2) LPS modification mediated by mutations in the PmrAB or PhoPQ two-component systems and, 3) LPS modification mediated by acquisition of *mcr* genes. Evidence exists regarding the fitness cost associated with all three colistin resistance mechanisms.

In *A. baumannii*, the acquisition of colistin resistance through *lpxACD* mutation was concomitant with a significant decrease in bacterial fitness (as manifested in *in vitro* growth rate and *in vitro* and *in vivo* competitive-growth experiments) and virulence, as well as a high-level resistance to colistin (MIC > 128 mg/L). While *pmrAB* mutation-associated colistin resistance also conferred a reduction in fitness, no significant decrease in virulence was detected and the colistin resistance level was moderate (MIC 16-64 mg/L) (Beceiro et al. 2014). This result suggests that the biological burden of *lpxACD* mutants is higher than that of *pmrAB* mutants, which is consistent with the clinical observation that isolates of LPS loss are less frequently reported than those of LPS modification. Although most studies have observed a fitness cost in *pmrAB*

mutation-dependent colistin resistance, this is not always the case. A previous study demonstrated that a P233S substitution in the PmrB sensor kinase led to colistin resistance, but it did not cause any decrease in bacterial fitness or virulence (Durante-Mangoni et al. 2015). Findings like this could imply that the cost in fitness or virulence brought on by *pmrAB* mutations varies depending on their location, type, and quantity.

In *K. pneumoniae*, few studies have reported on the fitness cost of colistin resistance resulting from mutations in *pmrAB* and/or *phoPQ*. Choi and Ko (2015) developed colistin resistant mutants from colistin-susceptible hypervirulent hypermucoviscous *K. pneumoniae* ST23 strains. The authors found that the acquisition of colistin resistance by changes in *pmrAB* and *phoPQ* was accompanied by reduced hypermucoviscosity, decreased formation of capsular polysaccharides, decreased survival rates in the presence of normal human serum, and impaired competitiveness compared to the parental strains, indicating a significant fitness cost. However, opposite results were reported by Cannatelli et al. (2014a), whose investigation on sequential colistin-sensitive and colistin-resistant isolates of carbapenemase-producing *K. pneumoniae* from the same patient before and after low-dose colistin treatment, respectively, showed that colistin resistance mediated by PmrB mutations was not associated with a significant fitness cost and that this resistant phenotype could be stable for up to 50 generations without antibiotic selection. As *K. pneumoniae* is an important pathogen, the possible lack of fitness cost in some resistant isolates could worryingly facilitate a wider spread of colistin resistance.

In *E. coli*, the fitness cost of *mcr*-mediated colistin resistance has also been explored. Tietgen et al. (2018) demonstrated that *mcr-1* carried on a TOPO expression vector in *E. coli* J53 displayed significantly reduced growth rates compared with the parental *E. coli* J53, while in contrast, similar growth rates were obtained between *E. coli* J53(pKP2442) (a natural IncHI2 plasmid containing *mcr-1*) and the parental strain. These findings indicate that *mcr-1* expression may reduce fitness, although acquisition of the natural plasmid-carrying *mcr-1* appeared to have a much lower fitness cost in *E. coli* J53. In another study, Choi et al. (2020) evaluated the fitness and virulence of both *mcr-1*-mediated and chromosome-mediated (mutations in *pmrAB*, *phoPQ*, or *eptA*) colistin resistant *E. coli* strains, by comparing them with colistin susceptible strains. Their findings indicated that although the resistant strains showed no reduction in growth rates, chromosome-mediated resistant strains were less competitive than susceptible strains, while the *mcr-1*-mediated strains showed no reduction in competitiveness. In addition, chromosome-mediated strains had relatively decreased survival rates in human serum, macrophages, and fruit flies, whereas *mcr-1*-mediated strains exhibited similar survival rates (in human serum and fruit flies) to susceptible strains (Choi et al. 2020), suggesting that chromosome-mediated colistin resistance in *E. coli* is associated with a greater fitness cost, than conferred by *mcr-1*. Since the usage of colistin is widespread, the fitness cost of carriage of colistin resistance may be important in the dissemination of colistin resistance, with *mcr-1*-positive strains having a significant competitive advantage.

2.1.4 Aims and objectives

Despite the few studies in the literature addressing the fitness effects of *mcr-1* plasmid carriage in *E. coli*, evidence regarding other phenotypic effects associated with *mcr-1* plasmids in planktonic and biofilm states remains scarce. In addition, direct comparisons of the effects of *mcr-1* carriage with those of other *mcr* genes, such as *mcr-3*, have rarely been investigated. Therefore, studies addressing these questions are urgently needed to achieve a more comprehensive understanding of the effects of *mcr* carriage. The objective of this chapter was to characterise and compare the phenotypic changes induced by *mcr-1* and *mcr-3* plasmid carriage in *E. coli* strains, specifically of *E. coli* strains J53, J53(pE30) and J53(pWJ1).

The specific aims for this chapter were:

1. To characterise *mcr* plasmid-carrying *E. coli* strains J53(pE30) and J53(pWJ1) using minimum inhibitory concentration and growth curves assays by comparison to the plasmid free J53 host.

2. To determine the effect of plasmid carriage on bacterial motility profiles of *mcr* and plasmid-free *E. coli* strains using motility assays.

3. To examine the viability of biofilms formed by *mcr* and plasmid-free *E. coli* strains under colistin stress using an ATP cell viability assay.

4. To investigate the effects of *mcr* plasmid carriage on *E. coli* biofilm formation using

confocal laser scanning microscopy (CLSM) with COMSTAT image analysis, and on biofilm architecture using atomic force microscopy (AFM) force curve measurements.

2.2 Materials and methods

2.2.1 Preparation of colistin solutions

Colistin sulphate was purchased from Sigma-Aldrich Ltd., Dorset, U.K. Stock solutions of colistin were prepared in sterile distilled water (dH_2O) at 1 mg/ml. All stock solutions were sterilised using 0.2 μm hydrophilic polyethersulfone membrane filters (Sigma-Aldrich Company Ltd., Dorset, U.K.) and stored at -20°C before being diluted to appropriate working concentrations prior to use.

2.2.2 Bacterial strains and growth conditions

The bacterial strains used in this chapter are shown in **Table 2.1**. All strains were provided by the Department of Medical Microbiology and Infectious Disease at Cardiff University and were stored on Microbank beads (Pro-Lab Diagnostics) at -80°C. *E. coli* J53 is a well-characterised laboratory mutant of *E. coli* K12 resistant to sodium azide. *E. coli* J53(pE30) and *E. coli* J53(pWJ1) are transconjugants derived from transferring *mcr-1*- and *mcr-3*-carrying IncHI2 plasmids from the donor strains *E. coli* E30 and *E. coli* WJ1, respectively, into the same recipient host strain, *E. coli* J53. When required, strains on beads were cultured aerobically at 37°C on Luria-Bertani (LB) agar plates (Sigma-Aldrich Company Ltd., Dorset, U.K.). For overnight (O/N) broth cultures, single colonies were inoculated into 10 ml LB broth and cultured aerobically at 37°C under shaking (120 rpm) for 16-18 h, with colistin (1 μg/ml) for *mcr*-positive strains to ensure maintenance of the plasmid, or without for the control lab strain J53.

Table 2.1 Characteristics of colistin-sensitive and colistin-resistant *E. coli* used in this study.

Strain	Country of Origin	Source	*mcr* type	MLST[a] group	Phylogenetic type	Plasmid incompatibility group [sequence type] / Size (bp)	Reference
J53[b]		Lab strain		10	A		(Jacoby and Han 1996)
E30[c]	China	Swine	*mcr-1.1*	48	A	IncHI2 [ST3] / 252 729	(Li 2023)
WJ1[c]	China	Swine faeces	*mcr-3.1*	1642	B1	IncHI2 [ST3] / 247 821	(Yin et al. 2017)
J53(pE30)[d]			*mcr-1.1*	10	A	IncHI2 [ST3] / 252 729	(Yang et al. 2020)
J53(pWJ1)[d]			*mcr-3.1*	10	A	IncHI2 [ST3] / 247 821	(Yang et al. 2020)

[a]MLST, multi-locus sequence type

[b]Laboratory strain resistant to sodium azide

[c]Wild-type strains

[d]Transconjugants derived from transfer of *mcr*-harbouring plasmids from the original wild-type strains into the laboratory strain *E. coli* J53

2.2.3 Minimum inhibitory concentration (MIC) assays

Bacterial susceptibility to colistin was performed by MIC assays using the broth microdilution method in accordance with Clinical and Laboratory Standards Institute (CLSI) guidelines (2012). Colistin was prepared in Mueller Hinton (MH) broth, at a starting concentration of 32 μg/ml. Two-fold serial dilutions of colistin were then performed in sterile, flat-bottom 96-well microtitre plates. O/N bacterial cultures of *E. coli* J53, J53(pE30) and J53(pWJ1) (n=3) were adjusted to an optical density (OD) between 0.08 and 0.10, equivalent to 0.5 McFarland (ca. 10^8 colony-forming units/ml; CFU/ml) at OD_{600nm} in phosphate buffered saline (PBS; 137 mM NaCl, 3 mM KCl, 8 mM Na_2HPO_4, 1.5 mM KH_2PO_4, pH 7.3; Oxoid, BR0014G). The adjusted bacterial cultures were diluted 1 in 10 in MH broth, followed by a further 1 in 20 dilution in the wells of the microtiter plates containing the colistin serial dilutions. Plates were wrapped with parafilm and incubated aerobically at 37°C for 16-20 h before being analysed for results. MIC values were determined as the lowest concentration where there was no visible growth. To visually aid the MIC assessment, 30 μl of resazurin (Sigma-Aldrich Company Ltd., Dorset, U.K.; 0.01% in dH_2O) solution was added into each well to confirm bacterial growth. Each MIC assay was performed in triplicate (n=3 biological repeats), with n=3 technical replicates included as well. The MIC result for each strain was recorded as the mode value from n=3 biological replicates.

2.2.4 Minimum biofilm eradication concentration (MBEC) assay

MBEC assays were performed as adapted from Cruz et al. (2018). Briefly, O/N cultures were adjusted to an optical density between 0.08 and 0.10 at OD_{600nm}, equivalent to 0.5 McFarland in MH broth. Then, 100 µl of the adjusted cultures was placed in the wells of a 96-well microtitre plate, before sealing it with parafilm and incubating it aerobically at 37°C at 30 rpm to establish biofilms in the wells. After 24 h of incubation, the supernatants were removed with care, and the biofilms were gently washed with 100 µl of PBS, which was then removed. To create colistin treatment with the intended concentration range, two-fold serial dilutions of colistin were prepared in MH broth in a fresh, 96-well microtitre plate, with a starting concentration of 4096 µg/ml before adding this to the biofilm plate (100 µl of the serially diluted colistin per well) and then incubated at 37°C for 24 h at 30 rpm. After incubation, the supernatants were carefully removed from each well and replaced with 100 µl of fresh MH broth. Plates were then again incubated at 37°C for another 24 h at 30 rpm before being read. The visual evaluation of bacterial re-growth was conducted subsequent to the addition of resazurin solution per well (0.01% in dH_2O). Each MBEC assay for all three strains was performed in triplicate (n=3 biological repeats), as well as with (n=3) technical replicates. The MBEC result for each strain was recorded as the mode value from n=3 biological replicates.

2.2.5 Growth curve assay

O/N broth cultures of the five *E. coli* strains (*E. coli* J53, J53[pE30], J53[pWJ1], E30, WJ1) were adjusted to an optical density between 0.08 and 0.10 at OD_{600nm} in LB broth, equivalent to 0.5 McFarland. Then, 5 µl of the adjusted cultures was diluted 1 in 40 in a sterile, flat-bottomed, 96-well microtitre plate in LB ± 1 µg/ml colistin. Plates were placed in a FLUOstar® Omega multi-mode microplate reader (BMG Labtech), and absorbance was monitored aerobically at 37°C for 96 h. Measurements were recorded hourly at OD_{600nm} after shaking at 200 rpm for 20 s. Each growth curve assay for all strains was performed in three biological repeats (n=3) and three technical replicates, and results are presented as mean values. The Tukey-Kramer method was employed to determine the minimum significant difference (MSD) in Minitab 17.2.1 (Minitab Inc, State College, PA, USA). With thanks to Dr Jennifer Adams for the help with setting up the growth curve assay.

2.2.6 Motility assay

E. coli J53, J53(pE30), and J53(pWJ1) O/N cultures were adjusted in LB broth to OD_{600nm} between 0.08 and 0.1, equivalent to 10^8 CFU/ml. Bacterial motility was tested qualitatively by inoculating MAST ID™ Motility Test Agar (Mast Group Ltd., Bootle, UK) with the adjusted bacterial suspensions using a sterile toothpick. The inoculated samples were incubated aerobically for 24 h at 37°C statically before recording growth and colour development in the medium. A positive result was indicated by a diffuse

pink cloud throughout the medium, which is missing for non-motile bacterial strains which form a bright red line along the track of the inoculation stab. With thanks to Dr Manon Pritchard for providing the motility data.

2.2.7 ATP biofilm cell viability assay

O/N cultures of *E. coli* J53, J53(pE30), and J53(pWJ1) were adjusted to 1×10^8 CFU/ml and were further diluted (1 in 10) in LB broth. The resultant cultures (1×10^7 CFU/ml) were added in LB in 96-well glass-bottomed plates (Grenier, UK), in a 1:10 ratio (100 µl/well), and grown for 24 h statically at 37°C. After incubation, half of the supernatant was then removed and replaced with fresh LB ± colistin (2, 4, 8, 16, 32, 64, 128, 256 or 512 µg/mL), followed by a further 24 h static incubation at 37°C wrapped in parafilm. To assess biofilm viability after colistin treatment, the BacTiter-Glo™ Microbial Cell Viability Assay (Promega) was used to quantify adenosine triphosphate (ATP) production according to the manufacturer's instructions. The plates were read for luminescence (relative light units) on a FLUOstar® Omega multi-mode microplate reader (n=3). With thanks to Dr Manon Pritchard for the setup of the ATP biofilm viability assay.

2.2.8 Biofilm formation assay and COMSTAT analysis

E. coli J53, J53(pE30), and J53(pWJ1) cultures grown for 16-18 h were standardised to OD_{600nm} of 0.05 in LB prior to being inoculated (1:10 v/v in LB broth) into a sterile black 96-well glass-bottomed plate (Grenier, UK) and incubated for 24 h on a rocker

(37°C; 30 rpm) to establish biofilms. After biofilm formation, the supernatant in each well was gently removed, and biofilms were stained with 6 µl of LIVE/DEAD® stain in PBS (BacLight Bacterial Viability Kit, Invitrogen, Paisley, UK; SYTO 9 : propidium iodide : PBS; 1 : 1 : 200). The green SYTO 9 (excitation/emission; 480/500 nm) was used to visualise live cells, and the red propidium iodide (excitation/emission; 490/635 nm) was used to visualise dead/dying cells. The plate was wrapped in foil and incubated in the dark for 5 mins, and a further 44 µl of PBS was then added in each well to keep the biofilms hydrated before imaging. CLSM imaging was performed in triplicate on a Zeiss LSM980 with Airyscan2, with five technical Z-stack images taken of each sample. Settings used for CLSM imaging were as follows: zoom, ×1; lens, ×63 oil immersion; line averaging, 1; resolution, 1584×1584; step size, 0.69 µm; and slice number, 60. With thanks to Dr Lydia Powell for performing the CLSM imaging.

ImageJ (National Institutes of Health, USA) software was used for exporting and processing the images in tagged image file format. COMSTAT2 image analysis software (Heydorn et al. 2000; Vorregaard 2008) was used to quantify the CLSM Z-stack images to achieve the biofilm parameters, i.e., biomass, biofilm thickness, roughness coefficient, and Dead/Live bacterial ratio.

2.2.9 Atomic Force Microscopy

E. coli J53, J53(pE30), and J53(pWJ1) were cultured in LB broth (120 rpm; 37°C) for 17 h and subsequently adjusted to 10^6 CFU/ml in LB broth. The adjusted cultures (1

ml) were then placed in a 35 mm polystyrene petri dish (Fisher Scientific; UK) and incubated on a rocker (20 rpm; 37°C) for 4 h. After incubation, the supernatant was removed and replaced with fresh LB broth before being incubated for a further 20 h on rocker (20 rpm; 37°C). The supernatant was removed, and the established biofilms were washed in PBS (x2) and covered by 1 ml PBS for imaging. All experiments were performed in triplicate.

To investigate whether *mcr* carriage alters biofilm biomechanics, the mechanical properties of the *E. coli* biofilms were examined by AFM using a Nanowizard 4 BioAFM (Bruker Instruments; Berlin, Germany). Young's modulus, indentation depth, adhesion force, and work of adhesion of the biofilms were measured using a borosilicate colloidal AFM probe with a sphere diameter of 20 µm and a spring constant of 0.06 N/m (NovaScan). Prior to each measurement, the deflection sensitivity and spring constant of each probe were calibrated on a glass slide. Over approximately 600 force curves were obtained per sample (three biological repeats). A ramp size of 9 µm, tip speed of 35 µm/s, and an applied force of 1 nN were used. The force curves were fitted to the Hertz model and analysed using JPK Data Processing software (V 7.1). Kruskal-Wallis and Dunn's multiple comparison tests were used for statistical analyses. With thanks to Dr Lydia Powell for performing the AFM force curve measurement.

2.3 Results

2.3.1 *mcr* carriage increases resistance of planktonic and biofilm bacteria to colistin

MIC and MBEC assays were employed to evaluate changes in colistin resistance in planktonic and biofilm culture, respectively, in the host strain J53 after acquisition of *mcr* genes (**Table 2.2**). In planktonic culture, the MIC to colistin for J53 was 0.25 μg/ml, while carriage of *mcr-1* or *mcr-3* in their respective transconjugants exhibited an MIC of 8 μg/ml. In biofilm culture, colistin resistance for J53(pE30) *mcr-1* and J53(pWJ1) *mcr-3* was 128 μg/ml and 64 μg/ml, as determined by MBEC, being four-fold and two-fold higher respectively than the MBEC value of 32 μg/ml for the plasmid-free J53.

Table 2.2 Minimum inhibitory concentration and minimum biofilm eradication concentration determinations for *E. coli* J53, J53(pE30) and J53(pWJ1) (μg/ml) (n=3). Both *mcr* transconjugants have elevated MIC and MBEC values compared to their host strain J53.

Strain	*mcr* type	MIC	MBEC
J53		0.25	32
J53(pE30)	*mcr-1.1*	8	128
J53(pWJ1)	*mcr-3.1*	8	64

2.3.2 Growth kinetics of *mcr*-carrying *E. coli* strains

To investigate the effects of *mcr* carriage on bacterial growth kinetics, J53 and the colistin-resistant strains were monitored for their growth over 96 h, with or without the presence of 1 μg/ml colistin (**Figure 2.1**). The *mcr-1* and *mcr-3* originating wild-type strains E30 and WJ1 were also tested. It was demonstrated that, when compared to J53, both J53(pE30) *mcr-1* and J53(pWJ1) *mcr-3* (with colistin or without) showed lower growth rates in the exponential phase and stabilised at a lower cell density in the stationary phase, indicating a fitness cost of *mcr* carriage, although this did not reach significance (MSD=0.268). There was also no visible difference between the two *mcr* strains. However, in the two wild-type strains, *mcr-1* carriage in E30 displayed significantly impaired growth compared to *mcr-3* carriage in WJ1, both in the presence and absence of colistin, while growth of WJ1 was similar to the plasmid-carrying J53 strains.

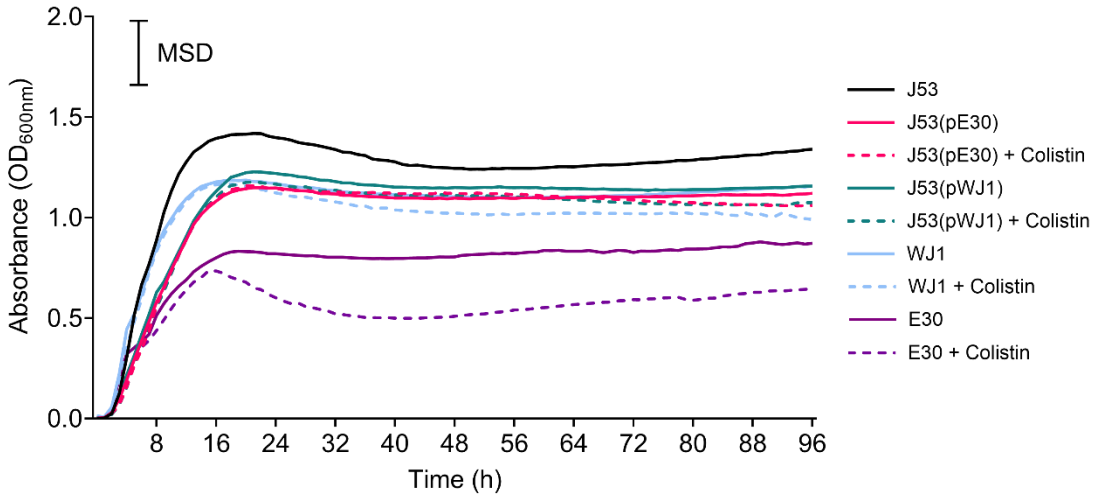

Figure 2.1 Growth curves (96 h) of *mcr*-positive and negative *E. coli* strains in LB broth ± colistin (1 µg/ml); n=3. Both transconjugants *E. coli* J53(pE30) *mcr-1* and J53(pWJ1) *mcr-3* showed lower growth rates compared to their host strain *E. coli* J53, indicating a fitness cost of *mcr* carriage, although this did not reach significance (MSD = 0.268).

2.3.3 *mcr* carriage does not affect bacterial motility

mcr-1 and *mcr-3* carriage was tested for their effects on bacterial motility (**Figure 2.2**). The motility assay was conducted on a semi-solid medium that is capable of supporting the growth of *Enterobacterales*. All the three strains tested, *E. coli* J53, J53(pE30), and J53(pWJ1), demonstrated a pink diffuse growth spread throughout the medium, indicating the motility of these strains.

E. coli J53

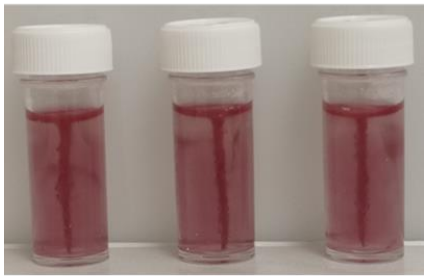

E. coli J53(pE30)

E. coli J53(pWJ1)

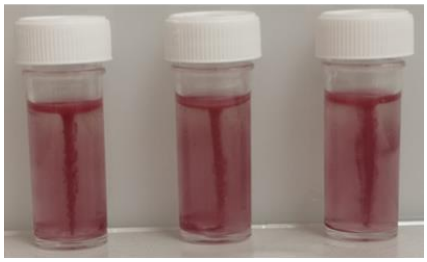

Figure 2.2 24 h Motility assay of *E. coli* J53, J53(pE30), and J53(pWJ1). All three strains are motile as the pink pigmentation throughout the stab and the medium represents a positive growth pattern. The three tubes for each tested strain are biological repeats (n=3).

2.3.4 *mcr* carriage mitigates biofilm defensive response to colistin stress

The ATP biofilm viability assay revealed that when subjected to colistin treatment at

increasing concentrations (0-16 µg/ml), both pre-established biofilms of J53(pE30) *mcr-1* and J53(pWJ1) *mcr-3* exhibited similarly stable cell viability. In contrast, after initial linear ATP production (between 0 and 2 µg/ml) J53 showed a steady surprising increase in biofilm viability with increasing colistin concentration, indicating its defensive response to colistin stress. Viability of the biofilms of all three strains sharply decreased as the colistin concentration approached their respective MBEC values (>16 µg/ml) (**Figure 2.3**). Furthermore, comparison between the two *mcr* strains demonstrated that *mcr-1* carriage in J53(pE30) led to significantly higher biofilm viability than *mcr-3* carriage in J53(pWJ1) when under sub-inhibitory colistin pressure (0-16 µg/ml), indicating a more metabolically active nature of the former biofilm within this concentration range (**Figure 2.3**; MSD=22754).

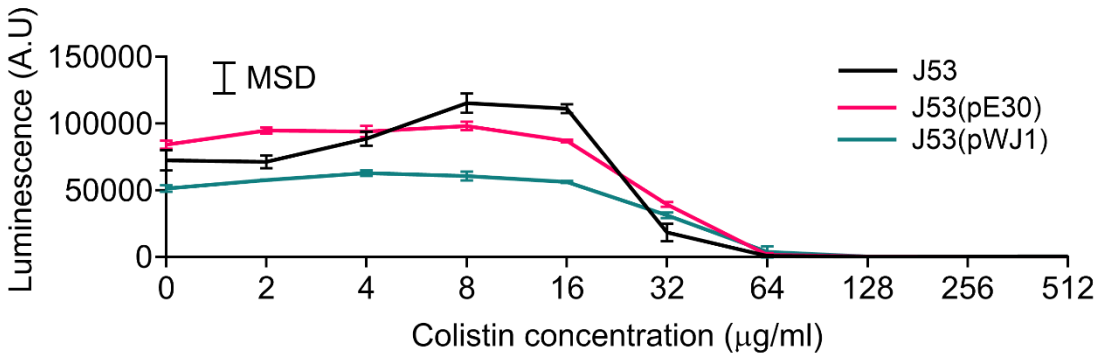

Figure 2.3 ATP biofilm viability assay showing the effects of *mcr* carriage on *E. coli* biofilm defensive response to increasing concentrations of colistin. *E. coli* J53, J53(pE30) and J53(pWJ1) biofilms were grown for 24 h before being treated with colistin (2-512 µg/ml) for a further 24 h; n=3. *Mcr* carriage in the two *E. coli* transconjugants helped to reduce biofilm defensive response to colistin stress under sub-MBEC concentrations (2-16 µg/ml) when compared to the host strain *E. coli* J53. Results are expressed as mean ± SD; (MSD=22754).

2.3.5 *mcr* carriage is associated with altered biofilm formation

To understand the effects of *mcr* carriage on biofilm-forming ability, 24 h-grown biofilms of the control *E. coli* J53, J53(pE30) and J53(pWJ1), were compared by CLSM in a biofilm formation assay. CLSM demonstrated that *mcr* carriage produced biofilms with altered biofilm assembly, which was particularly evident for J53(pE30), which produced a denser biofilm and with more dead cells compared to J53 (**Figure 2.4a**). This was also reflected in the COMSTAT analysis; *mcr-1* carriage in J53(pE30) resulting in an increase in biofilm biomass and biofilm thickness (although these did not reach significance) and a significant increase in Dead/Live bacterial ratio compared to J53 (**Figure 2.4b**). Furthermore, a significant difference in all parameters (biomass, roughness coefficient, biofilm thickness, and Dead/Live cell ratio) was observed between *mcr-1* and *mcr-3* carriage, with all (except roughness coefficient) significantly higher for J53(pE30) biofilms than J53(pWJ1) biofilms (**Figure 2.4b**).

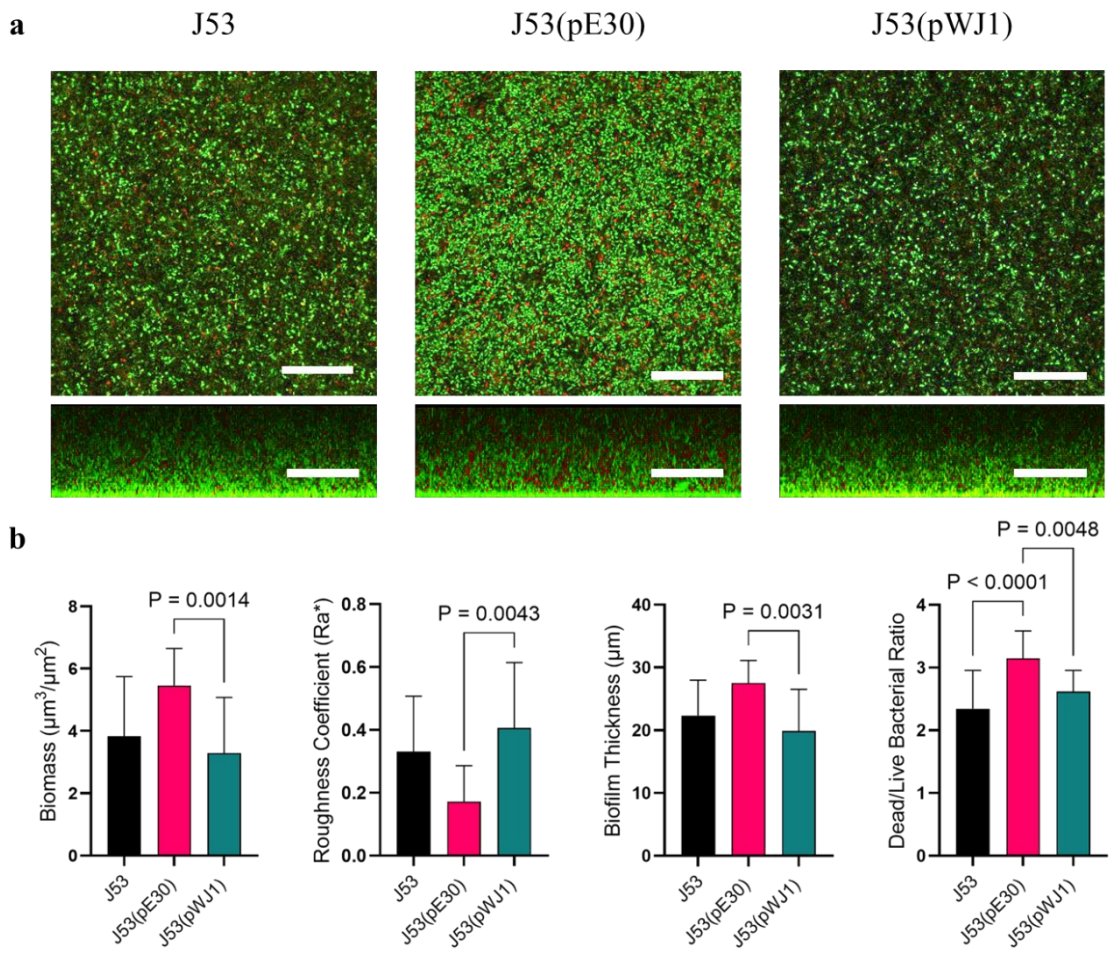

Figure 2.4 Biofilm formation assay showing effects of *mcr* carriage on *E. coli* biofilm establishment. **a** CLSM imaging of 24 h-grown biofilms of *E. coli* J53, J53(pE30), and J53(pWJ1) with LIVE/DEAD® staining; (n=3). scale bar, 30 μm. **b** Corresponding COMSTAT image analysis showing biomass, roughness coefficient, biofilm thickness, and Dead/Live bacterial ratio. *Mcr* carriage in the two *E. coli* transconjugants induced altered biofilm formation compared to the host strain *E. coli* J53, with significant differences also observed between *mcr-1* and *mcr-3* biofilms. Results are expressed as mean ± SD. A *P*-value cutoff of 0.05 was used.

2.3.6 *mcr* carriage is associated with altered biofilm biomechanics

The biomechanical properties of the biofilms from *E. coli* J53, J53(pE30), and J53(pWJ1) were compared using AFM. Quantification of the four biomechanical parameters from the obtained force curves showed that *mcr* carriage incurred specific changes in biofilm biomechanics (**Figure 2.5**). *mcr-1* carriage in J53(pE30) biofilms significantly reduced Young's modulus, indentation, and adhesion when compared to J53, indicating the "softer" and less "sticky" nature of this biofilm. In contrast, *mcr-3* carriage caused a significant increase in all three parameters in J53(pWJ1) biofilms, suggesting these biofilms were more mechanically robust and stickier than J53 biofilms. None of the examined biofilms showed any differences in work-of-adhesion values.

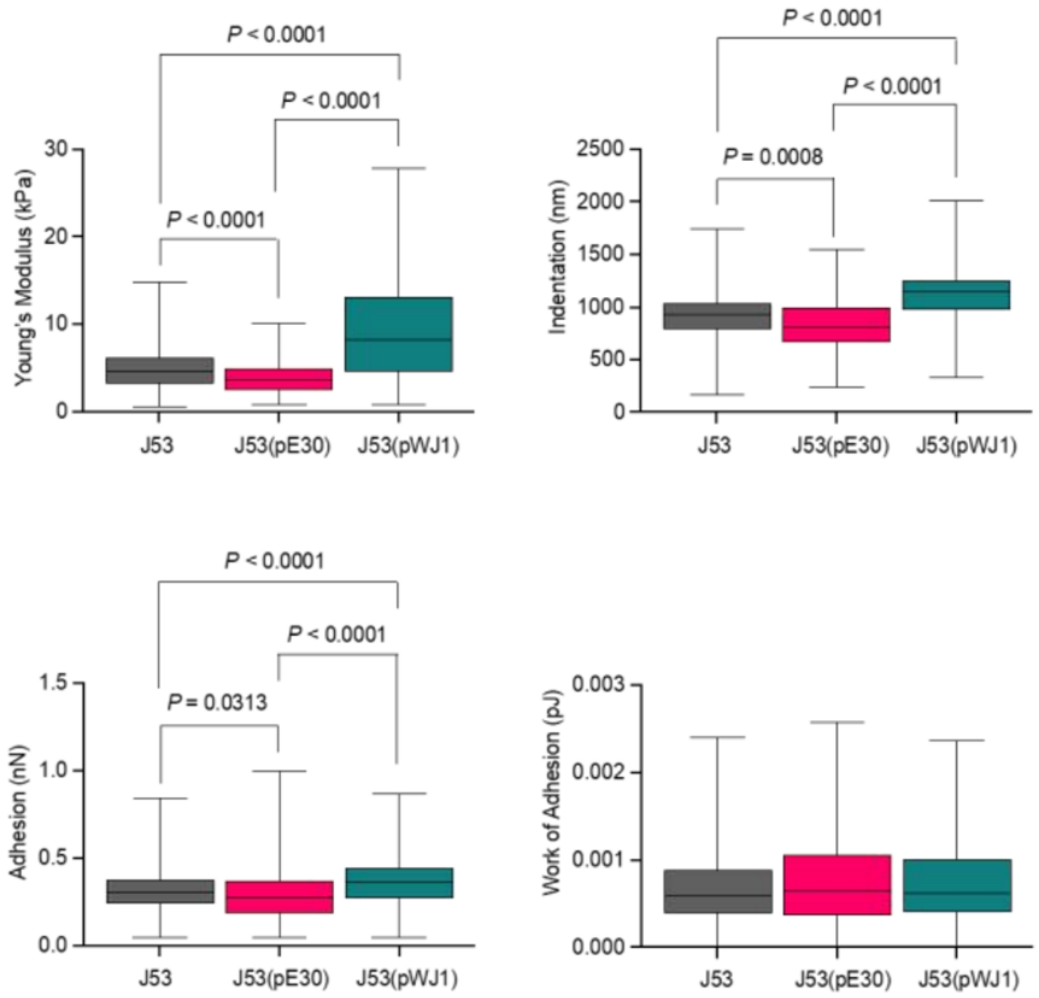

Figure 2.5 Atomic force microscopy to determine the effects of *mcr* carriage on the biomechanical properties of *E. coli* biofilms. *E. coli* J53, J53(pE30), and J53(pWJ1) biofilms were grown for 24 h, followed by force curve measurements showing Young's modulus, indentation, adhesion, and work of adhesion; n=3. *Mcr* carriage in the two *E. coli* transconjugants induced significant altered biofilm biomechanics compared to the host strain *E. coli* J53. Results are expressed as mean ± SD. A *P*-value cutoff of 0.05 was used.

2.4 Discussion

The widespread overuse of colistin in food-producing animals has led to the emergence of plasmid-mediated colistin resistance in *E. coli*. The *mcr-1* gene and the *mcr-3* gene following their discovery have attracted extensive attention due to their rapid dissemination worldwide, threatening global health by increasing bacterial resistance to colistin, the last-resort antibiotic treatment for MDR pathogens (Liu et al. 2016; Yin et al. 2017). Hence, further research is needed to thoroughly characterise the phenotype of carrying these two *mcr* genes in bacteria in both planktonic and biofilm states. It is vital to improve our understanding of the biological cost imposed by *mcr*-plasmids to better understand their spread and transmission in the environment.

Previous studies have established that carriage of *mcr* genes usually confers low-level resistance to colistin (MICs; 4-8 μg/ml) in planktonic cells, as opposed to a relatively high level of colistin MICs (≥16 μg/ml) caused by chromosomal mutations (Smelikova et al. 2022). This is exemplified by a study where the authors screened *mcr*-carrying *E. coli* isolates from clinical patients and found that the majority of the recovered strains demonstrated MICs of 4-8 μg/ml (Li et al. 2022). Similarly, in a study targeting clinically-healthy animals, all the *mcr-1* and *mcr-3*-positive *E. coli* isolates recovered from faecal samples displayed MIC values ranging from 4-8 μg/ml (Belaynehe et al. 2018). Moreover, all the *mcr* genes in these isolates were capable of being transferred to a recipient *E. coli* J53 strain by conjugation via broth mating, and the resultant

transconjugants possessed an identical colistin resistance level, suggesting that *mcr*-derived colistin resistance is specific and not influenced by other mechanisms in the donor strains (Belaynehe et al. 2018). However, to the best of our knowledge, no published data is currently available on colistin MBEC values for *mcr*-harbouring *E. coli*, although in a survey of poultry-associated *E. coli* isolates derived from retail meat, Noreen et al. (2022) reported a 32-64-fold increase in colistin resistance for colistin-sensitive strains when grown in biofilm culture (MBECs of 64-128 μg/ml) compared with planktonic culture (MICs of 2 μg/ml). In my study, the *mcr-1* and *mcr-3* J53 strains grown in biofilm culture had similar MBECs to those of the Noreen study (64-128 μg/ml), even though their planktonic MICs were considerably higher (8 μg/ml).

The carriage of *mcr* is associated with a fitness cost (Ma et al. 2018; Li et al. 2021; Wu et al. 2021b), and this is often reflected by the slower growth of the bacterial host. Lima et al. (2022) evaluated the growth rates of *E. coli* J53 in comparison to 14 J53 transconjugants carrying *mcr-1*-bearing IncHI2, IncHI1, IncP, IncN, $IncI_1$, or FIB plasmids by monitoring the optical density for 30 h. The authors found that the growth rates of all transconjugants decreased to varying degrees when compared to the plasmid-free host strain J53, with five showing significant reductions, highlighting the fitness cost of *mcr-1* plasmid carriage. In addition, a significantly higher mean growth rate was observed for transconjugants grown in colistin-free medium compared to 4 μg/ml colistin-containing LB broth, showing that expression of colistin resistance impairs the *in vitro* growth of *mcr-1*-carrying bacteria, thereby also resulting in a

significant fitness cost. These results partly align with my study, where I show reduced (but not significantly different) growth rates for J53(pE30) *mcr-1* and J53(pWJ1) *mcr-3* when compared to J53, reflecting the fitness cost of both *mcr-1* and *mcr-3* plasmid carriage. In addition, the maximum growth density was lower when grown in 1 μg/ml colistin than in colistin-free medium for the wildtype strains, especially for strain E30, even though this effect was less obvious in the transconjugant strains. However, when directly comparing *mcr-1* and *mcr-3* plasmid carriage, I observed no significant difference between the growth kinetics of the two transconjugants. This is in contrast to a study by Li et al. (2021), who cloned individual *mcr* genes (*mcr-1 to 5*) into an arabinose-inducible pBAD/His expression vector, and demonstrated that bacterial growth of the MCR-3-expressing strain was inhibited in the log phase compared with that of the MCR-1-expressing strain, both in the presence or absence of colistin, highlighting the fitness advantage of MCR-1 expression over MCR-3 expression. This differs considerably with my findings but likely reflects overexpression of *mcr* in the expression vector, showing that fitness is related to all aspects of the environment that a plasmid finds itself in, not only plasmids and host bacterial strains used.

Flagellum-mediated motility is a key factor in driving initial cell adhesion and early biofilm formation in some Gram-negative bacteria (Mahajan et al. 2009; Haiko and Westerlund-Wikström 2013; Coloma-Rivero et al. 2021; Benyoussef et al. 2022). The correlation between bacterial motility and the acquisition of certain plasmids has been previously explored. For instance, carriage of the conjugative IncP-7 carbazole-

degradative plasmid pCAR1 was found to cause a reduction in swimming motility in three different *Pseudomonas* host strains under various agar concentration conditions, suggesting that pCAR1 carriage may affect flagella assembly or induce a shortage of energy for its motor (Takahashi et al. 2015). However, few studies in the existing literature have addressed the effects of *mcr*-harbouring plasmids on bacterial motility. An examination of the swarming motility of the recombinant *E. coli* DH10*β*(pUC19) *mcr-1* with the empty pUC19 vector demonstrated a significantly impaired motility for the MCR-1-expressing strain (Frantz et al. 2023). Similar results were found in another study, in which significantly reduced swimming motility was demonstrated for *E. coli* ATCC 43894 carrying *mcr-1*-harbouring pFORC82_3 (an IncI2 plasmid) compared to the corresponding *mcr-1* knockout mutant strain (Kim et al. 2019; Ahn 2021). These findings indicated that *mcr-1* carriage may interfere with bacterial motility, potentially compromising their dissemination in the environment. In my study, I reported the motility profile of all three strains tested, *E. coli* J53 and its *mcr-1* and *mcr-3* transconjugants. However, since our motility assay was only qualitative, quantitative comparisons between the strains were not possible. Future quantitative studies could shed light on whether differences in motility are present between *mcr*-positive and negative strains, as well as between *mcr-1*-and *mcr*-3-carrying strains.

ATP is a major biological energy source existing in all living microbes, and therefore, quantification of ATP via the bioluminescence-based ATP assay represents an effective, real-time method to reflect cell viability and metabolic changes (Eed et al. 2016). The

ATP assay has been widely applied in microbiology. For example, it has been used to monitor the treatment effects of various β-lactam antibiotics at different concentrations on *E. coli* regrowth (Hanberger et al. 1990), and to quantify *S. aureus* biofilms on the surface of various different materials (Herten et al. 2017). In the present study, the ATP assay-determined biofilm viability was relatively constant for the two transconjugants carrying *mcr-1* and *mcr-3* when treated with increasing sub-MBEC colistin concentrations, while the *mcr*-free colistin-sensitive strain showed an increase in ATP production, indicating that *mcr* carriage can stabilise ATP-related energy metabolism in biofilms. To date, current research appears to have focused solely on the effects of *mcr* carriage on bacterial metabolism in planktonic culture. Specifically, MCR-1 overexpression (8 h) in planktonically grown *E. coli* TOP10 carrying the recombinant plasmid pBAD-*mcr-1* was found to induce global metabolic perturbations as determined by metabolomics. This included: a dramatic increase in lipid metabolites affecting cell wall synthesis (e.g., fatty acids, glycerophospholipids and lysophosphatidylethanolamines); a significant decrease in intermediate metabolite levels (peptides, amino sugars, carbohydrates and nucleotides metabolism); a significant reduction in metabolites associated with the pentose phosphate pathway and pantothenate and CoA biosynthesis and, finally, significantly depleted levels of key energy-associated metabolites (ATP, ADP, $NADP^+$) (Liu et al. 2020). Transcriptomics further showed that MCR-1 overexpression led to extensive transcriptomic changes, including dysregulation of multiple genes involved in LPS biosynthesis and modification, and gene expression associated with carbohydrate metabolism and

intracellular stress responses to oxidative and nucleic acid damage (Lu et al. 2022). These metabolomic and transcriptomic findings induced by *mcr-1* expression provide insights into the molecular mechanisms underpinning the fitness cost of *mcr-1* carriage in planktonic bacterial cells. However, similar characterisation of *mcr-1* expression in biofilms has yet to be investigated.

To compare the biofilm-forming ability of *E. coli* J53 and the two transconjugants after acquisition of *mcr-1* and *mcr-3* plasmids, I performed CLSM to quantify the biofilm formation. The biofilms of J53(pE30) *mcr-1* were significantly thicker and denser than the biofilms of both J53 and J53(pWJ1) *mcr-3*, despite a higher dead/live bacterial ratio, suggesting that the acquisition of *mcr-1* may enhance the biofilm-forming ability of the host cell. Interestingly, this is consistent with epidemiological studies, which established *E. coli* harbouring *mcr-1* as a good biofilm former. For example, 41% (7/17) of *mcr-1*-positive *E. coli* isolated from poultry and 60% (6/10) of *mcr-1*-positive *E. coli* obtained from chickens with colibacillosis were identified by crystal violet assay as moderate and strong biofilm producers, respectively (Ćwiek et al. 2021; Dhaouadi et al. 2023). A further study noted that 50% (28/56) of *mcr-1*-positive *E. coli* porcine isolates exhibited significantly increased biofilm forming ability compared to the plasmid-free control *E. coli* ATCC 25922 strain (Cheng et al. 2021). This may suggest a possible correlation between *mcr-1* plasmid carriage and increased bacterial biofilm formation. However, since many studies have reported a reduced cell growth rate for *mcr-1*-expressing *E. coli* (Yang et al. 2017; Tietgen et al. 2018; Li et al. 2020a; Liu et

al. 2020; Lima et al. 2022), the underlying reason for the increased biomass of biofilms formed by *mcr-1*-positive *E. coli* remains challenging to elucidate.

As previously mentioned (**see Chapter 1 Section 1.6.2.2**), *mcr* genes impart colistin resistance by encoding a pEtN transferase enzyme (e.g., MCR-1) that facilitates the addition of pEtN to a phosphate at the N-acetylglucosamine headgroup of lipid A in the outer membrane (Gao et al. 2016; Hinchliffe et al. 2017). However, the consequent biophysical impacts following this biological event on the bacterium are still not fully understood. Two independent studies using transmission electron microscopy both demonstrated that *mcr-1* overexpression (8 h) in *E. coli* TOP10 (pBAD-*mcr-1*) significantly affected cellular morphology in comparison with the *mcr*-negative *E. coli* TOP10 (pBAD), with the former showing damaged membrane structure integrity and cytoplasmic changes including granular degeneration and vacuolation, and the latter showing an intact, well-defined inner and outer membrane, as well as a highly homogeneous electron density in the cytoplasm region (Yang et al. 2017; Liu et al. 2020). A further mechanistic study, using coarse-grained molecular dynamics simulations with quantitative lipidomics models, suggested that pEtN modification of lipid A would substantially alter the morphology and physicochemical properties of the outer membrane, providing a mechanistic link between *mcr-1* expression and the observed membrane disruption (Ma et al. 2021). Specifically, the lipid A-pEtN modification produced an abnormally twisted conformation and a closer packing state as a result of enhanced inter-lipid electrostatic attraction, leading to a lipid A-pEtN

accumulation-driven negative curvature of the outer membrane. Subsequent changes in the physical properties of the outer membrane included altered surface tension, and possibly increased elasticity/fluidity and decreased rigidity (Ma et al. 2021). Nevertheless, current understanding of the biophysical effects of *mcr* carriage is limited to the cellular level. Given that biofilms are complex 3-dimensional structures consisting of bacteria and extracellular matrix, their biophysical properties as a whole should be studied rather than those of individual cells. In the present study, we compared, for the first time, the biofilms formed by *mcr*-free J53, J53(pE30) *mcr-1* and J53(pWJ1) *mcr-3*. I found that carriage of *mcr-1* plasmid produced softer, less sticky biofilms, whereas carriage of *mcr-3* plasmid was associated with more rigid, sticky biofilms. It is possible that these distinct mechanical properties observed for *mcr-1* and *mcr-3* biofilms were caused by potentially different biofilm extracellular matrices produced, as the mechanical behaviour of *E. coli* biofilms has been linked to the composition and organisation of their secreted extracellular matrix (Hung et al. 2013; Horvat et al. 2019; Serra and Hengge 2021; Siri et al. 2024).

2.5 Conclusion

This chapter demonstrated the specific phenotypic effects caused by the carriage of *mcr-1* and *mcr-3* plasmids in planktonic and biofilm growth. Both *mcr-1* and *mcr-3* plasmid carriage was associated with a fitness cost, as evidenced by reduced planktonic bacterial growth, although this cost also appeared to be host strain-dependent. Both colistin-resistant strains showed distinct differences to one another with *mcr-1* biofilms being more metabolically active than *mcr-3* biofilms which was translated into biofilms of greater biomass, thickness, and higher dead/live bacterial ratio. Hence, it is particularly important to look at colistin resistance on an individual basis taking into account both the specific plasmids present, but also the plasmid host bacterial strains that carry them.

Chapter 3

Experimental evolution of bacterial populations in plasmid-mediated colistin resistant *Escherichia coli*

3.1 Introduction

3.1.1 Genomic context of *mcr-1*

The plasmid-encoded colistin resistance gene, *mcr-1*, typically exists as a part of a conserved ~ 2.6 kb cassette, with the open-reading frame typically being a *pap2* gene encoding a putative PAP family transmembrane protein (Li et al. 2016; Poirel et al. 2016; Li et al. 2017b; Poirel et al. 2017c). Previous research suggests that *mcr-1* may have originated from *Moraxella* species, which is known to possess the intrinsic chromosome-encoded *mcr*-like genes and the *pap2* membrane-associated lipid phosphatase (Kieffer et al. 2017; Poirel et al. 2017b). Additional evidence that supports this speculation is the identification of the IS*Apl1* element in *Moraxella bovoculi* and *Moraxella porci*; an insertion sequence (IS) that frequently accompanies the *mcr-1-pap2* unit in *mcr-1*-positive bacteria (Poirel et al. 2017b; Li et al. 2018). It has been proposed that IS*Apl1* first integrated into *M. bovoculi* and subsequently evolved in conjunction with the *mcr*-like genes (Li et al. 2018).

IS*Apl1* is an insertion sequence 1,070 bp in size and was first identified in *Actinobacillus pleuropneumoniae*, belonging to the IS*30* family (Tegetmeyer et al. 2008). It contains a 924 bp open-reading frame encoding a 307 amino acid (36 kDa) transposase, which is flanked by a pair of 27 bp terminal inverted repeats (IRs) at both ends of IS*Apl1* with six mismatches (Tegetmeyer et al. 2008). Similar to IS*30* family members, IS*Apl1* is transposed via formation of a double-strand IS circle transposition

intermediate. Here, the covalently closed double-stranded DNA carries a dinucleotide of host flanking DNA between the abutted transposon ends and, once integrated into the target sequence, generates 2-bp target site duplications (TSDs), the process of which represents a transposition mechanism known as 'copy out and paste in' (Kiss et al. 2007; Szabó et al. 2008; Tegetmeyer et al. 2008; Chandler et al. 2015). Furthermore, the IS*30* family has a high affinity for an insertion site of an imperfect palindrome sequence rich in AT with a slight central CG bias (Kiss et al. 2007).

In general, four varied structures of *mcr-1* cassettes have been identified with differing IS*Apl1* flanking elements as seen in **Figure 3.1** (Snesrud et al. 2016; Snesrud et al. 2018). The complete composite transposon (the fourth type) was later designated Tn*6330* (Li et al. 2017b). The consistently noted close association between IS*Apl1* and the core *mcr-1* gene may indicate that IS*Apl1* plays a pivotal role in the dissemination of *mcr-1*. Analysis of the structure of Tn*6330* revealed a conserved IR-abutting AT dinucleotide between the right IR (IRR) of the upstream IS*Apl1* and the *mcr-1-pap2* segment, and a CG dinucleotide between the left IR (IRL) of the downstream IS*Apl1* and the *mcr-1-pap2* segment (Snesrud et al. 2016). These conserved internal AT and CG TSDs have been suggested to represent two former independent insertion events of IS*Apl1* into the TA-rich region of the *mcr-1-pap2* unit, thereby generating Tn*6330* (Snesrud et al. 2018).

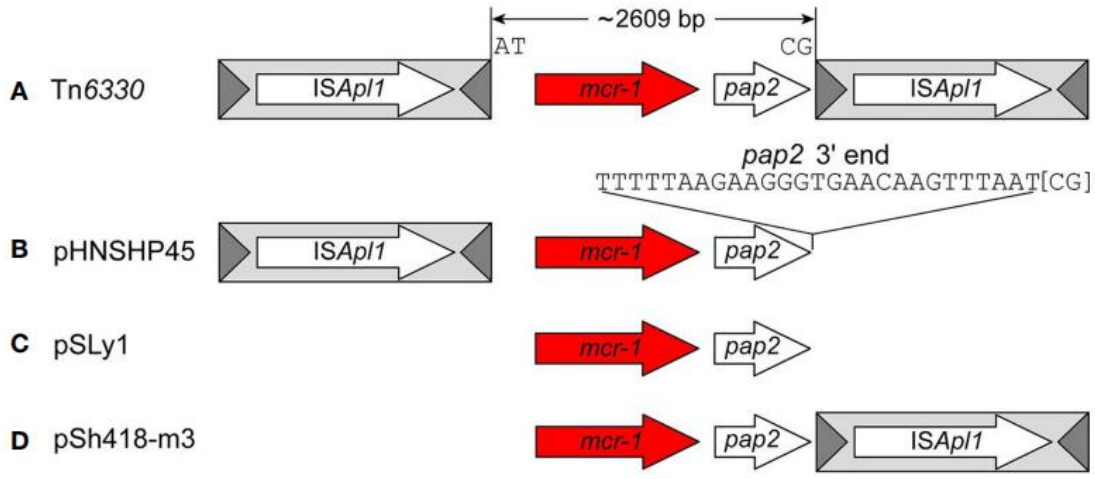

Figure 3.1 Schematic diagram illustrating the four types of *mcr-1* cassettes with differing IS*Apl1* flanking elements identified to date. **A** The complete composite transposon with both copies of IS*Apl1* elements flanking *mcr-1-pap2* (Tn*6330*) (Li et al. 2017b). **B** *mcr-1-pap2* with a single copy of IS*Apl1* located upstream (pHNSHP45). **C** *mcr-1-pap2* (pSLy1). **D** *mcr-1-pap2* with a single copy of IS*Apl1* located downstream (pSh418-m3). The ~2,609 bp *mcr-1-pap2* segment is flanked by the conserved, ancestral target site duplication dinucleotides AT and CG. The last 27 bp that comprise the 3' end of the putative *pap2* gene are indicated for clarity. IS*Apl1*, light grey box; transposase, long white arrows; terminal inverted repeats, IRs (IRR and IRL), dark grey triangles; *mcr-1*, red arrows; *pap2*, short white arrows. The figure was derived from Snesrud et al. (2018).

There is expanding evidence that IS*Apl1*-mediated Tn*6330* could be a key element in the transposition of *mcr-1* (Snesrud et al. 2016; Zurfluh et al. 2016; Li et al. 2017b). On the one hand, IS*Apl1* has played an important role in transposing the *mcr-1* gene into a variety of plasmids and host chromosomes (Li et al. 2017b; Poirel et al. 2017c; Zhao et al. 2017; Li et al. 2018). On the other hand, IS*Apl1* can mobilise independently

of *mcr-1* across different genetic sites in the host (Snesrud et al. 2017; Li et al. 2019). A study by Snesrud et al. (2018) analysing the *mcr-1* genetic context demonstrated that Tn*6330* exhibits a strong tendency to undergo IS*Apl1* deletion(s), most likely through a process of illegitimate recombination, thereby transfixing *mcr-1* into a target plasmid, a finding that is consistent with many observations of *mcr-1* cassette structures lacking one or both copies of IS*Apl1* (Snesrud et al. 2016; Poirel et al. 2017c). This property of IS*Apl1* loss (decay) may facilitate its self-deletion from the cassette and the transfixation of the *mcr-1* gene into a target sequence. This loss of transposability driven by the loss of IS*Apl1* increases the stability of the *mcr-1* cassette in plasmids, promoting the spread of colistin resistance (Snesrud et al. 2016; Ji et al. 2019; Tarabai et al. 2019). However, it should be noted that single-ended IS*Apl1* structures (e.g., IS*Apl1-mcr-1-pap2*) are still able to mobilise even without a complete Tn*6330* when the IRR of the deleted downstream IS*Apl1* is kept intact, as the transposase encoded by the upstream IS*Apl1* can still identify the residual IRR (Snesrud et al. 2016).

3.1.2 Fitness costs and plasmid stability of *mcr-1*

The acquisition of plasmids carrying *mcr-1* has a proven benefit for the host, increasing bacterial survival when exposed to colistin (Nang et al. 2018; Mmatli et al. 2022). However, concurrently, a fitness burden may also be conferred by *mcr-1* plasmid carriage, although contrasting results have been reported (Tietgen et al. 2018). Acquisition of a *mcr-1*-bearing plasmid in one study in *K. pneumoniae* resulted in a substantial fitness cost for the host (Nang et al. 2018), while acquisition of an IncI2

plasmid, in a range of sizes, carrying *mcr-1*, did not appear to confer a significant fitness cost at all (Zheng et al. 2017; Wang et al. 2018a). This suggests that the fitness costs associated with acquisition of *mcr-1*-harbouring plasmids is dependent on a range of factors including the bacterial species, the plasmid incompatibility type, and whether compensatory mutations have occurred in the acquired plasmid.

Several studies have revealed that the expression of *mcr-1* imposes a fitness cost on the host by generating a series of costly impacts. Overexpression of *mcr-1* in a pBAD vector was seen to result in an impaired growth rate, and reduced cell viability and competitive ability in *E. coli* TOP10 (. Simultaneously, profound alterations in the cell outer membrane architecture and significant disruption of the membrane structural integrity were also observed in the cellular morphology analysis, causing efflux of cytoplasmic contents and cell death. Additionally, the authors developed high-level colistin-resistant mutants from wild-type *mcr-1* positive *E. coli* strains by serial passage over 14-days in increasing concentrations of colistin (Yang et al. 2017). Compared to the parental strains, the mutants exhibited decreased fitness, significantly diminished virulence in a *G. mellonella* infection model, and higher susceptibility to most other antibiotics. Therefore, the authors reasonably inferred that the expression of *mcr-1* is delicately regulated in host bacteria to achieve an equilibrium between colistin resistance and fitness costs. Similar results were further seen in another study by Yang et al. (2020) for *mcr-3* expression, where the expression of two *mcr-3* variants in *E. coli* TOP10, *mcr-3.1* and *mcr-3.5*, significantly decreased bacterial growth rates *in vitro*,

indicating an impact on fitness. Interestingly however, both *mcr-3* variants appeared to impose less of a fitness cost than *mcr-1*.

Plasmid stability assays have been conducted for *mcr-1* in *K. pneumoniae* using conventional plate count methods. Nang et al. (2018) serially passaged *K. pneumoniae* B5055 harbouring either an *mcr-1* recombinant plasmid or the vector plasmid for 10 consecutive days without colistin selective pressure. The control vector plasmid showed high stability across the passages, whereas a gradual loss of the *mcr-1* recombinant plasmid was detected, with roughly only 30% of the population maintaining the *mcr-1* recombinant plasmid at day10. This again corroborates the significant fitness cost of *mcr-1*-bearing plasmids in *K. pneumoniae*, showing how *mcr-1* plasmid carriage decreases over time in the absence of colistin selection (Nang et al. 2018).

3.1.3 Biofilm evolution and the bead transfer model

Biofilms represent an important form of microbial existence, wherein one or more bacterial species congregate to form densely populated communities, usually enveloped within a polymer-based extracellular matrix. Biofilms are ubiquitous in nature and can inhabit a wide range of biotic and abiotic surfaces. Limited diffusion within biofilms results in the formation of specific gradients, (e.g. pH, oxygen etc) which subsequently gives rise to a heterogeneous environment characterised by unique spatial structures (Nadell et al. 2008; Stewart and Franklin 2008). Bacteria that reside in biofilms exhibit

greater resilience to physical and chemical disturbances compared to their planktonic counterparts, and this can have significant economic implications for both industry and medicine (Davies 2003; Ciofu et al. 2015).

Natural biofilm evolution is a complex process and is influenced by numerous factors. To more fully understand the dynamics of prolonged evolutionary processes, evolutionary experiments can be designed to study changes that occur in a biofilm under conditions set by the researcher. Biofilm evolutionary studies have been previously conducted to, for example, illuminate biofilm evolution in cystic fibrosis chronic infections (Traverse et al. 2013), and investigate fundamental evolutionary principles (Rainey and Travisano 1998; Kassen 2009; Spiers 2014). A number of environmental and experimental factors may affect the outcome of experimental evolution, such as nutrient levels, bacterial strains under study and their evolutionary history, inoculation size, flow rate, substrate area, physical disturbance, experiment duration, etc. (Steenackers et al. 2016).

Several models have been utilised to study evolution in biofilms, among which the bead transfer model developed by Poltak and Cooper (2011) is an ideal *in vitro* batch model suitable for studying long-term evolution and diversification of biofilms. In this model, the first test tube containing a plastic bead is inoculated with planktonic bacterial cells to grow biofilms on the bead. After 24-hour incubation, the colonised bead is transferred to a new tube containing a new sterile bead, allowing bacteria to disperse from the old bead to colonise the new bead. This transfer cycle can be repeated for a

prolonged duration and thus, biofilm evolution over time can be monitored. During the experiment, the plates are slowly shaken, to mimic the sheer conditions biofilms may be exposed to in real life.

The bead transfer model is useful in that it simulates a real biofilm formation cycle, including attachment to new surfaces, biofilm maturation and biofilm dispersion, allowing variables to be easily changed to meet the needs of different experiments. For instance, the total length of time of the experiment and the number of transfer cycles, etc., can be adjusted. This bead transfer model has been successfully employed in long-term evolutionary studies (spanning approximately 1500 generations) to elucidate the fundamental ecological and genetic mechanisms that underlie the process of phenotypic diversification in *Burkholderia cenocepacia* biofilms (Poltak and Cooper 2011; Traverse et al. 2013; Ellis et al. 2015; O'Rourke et al. 2015). In addition, in a more recent study, this model was adapted to investigate the experimental evolution of *P. aeruginosa* in response to the antimicrobial OligoG CF-5/20, a low-molecular-weight inhaled alginate oligomer therapy, with continuous passage of 45 days (~245 generations) in 24-well microtiter plates instead of test tubes (Oakley et al. 2021).

3.1.4 Aims and objectives

The evolutionary stability of an acquired antibiotic-resistant plasmid is a key indicator of its fitness costs and determines whether it can be stably maintained in the environment. Previous evolutionary studies examining the stability of *mcr* plasmids have been conducted only in planktonic culture and are largely limited to short-term timeframes. Therefore, understanding how *mcr* plasmid-carrying bacteria evolve in biofilm culture over prolonged periods, along with the associated phenotypic and genotypic changes, is crucial for the design of effective strategies to contain *mcr* dissemination. The objectives of this chapter were first to compare the stability of *mcr-1* and *mcr-3* plasmid carriage in *E. coli* transconjugants after prolonged evolution in biofilms, and second to characterise the phenotypic and genotypic changes in *mcr-1 E. coli* biofilm populations before and after evolution as a result of the fitness cost of *mcr-1* plasmid carriage.

The specific aims for this chapter were:

1. To characterise the evolutionary fitness costs of *mcr-1* and *mcr-3* plasmid carriage in a bead biofilm model.

2. To characterise changes in colistin resistance and biofilm-forming phenotypes of *mcr-1 E. coli* biofilm populations during evolution by minimum inhibitory concentration assay and biofilm formation assay.

3. To describe the genotypic changes in *mcr-1 E. coli* biofilm populations associated with long-term evolution by whole genome sequencing (WGS).

4. To test the observed persistence of *mcr-1* gene in the bead biofilm model in the absence of colistin and its re-emergence following colistin re-exposure by investigating plasmid dynamics via mathematical modelling.

5. To characterise the virulence of the strain mutants isolated from the *mcr-1 E. coli* biofilm populations at the end of evolution via a *G. mellonella* infection model.

3.2 Materials and Methods

3.2.1 Preparation of colistin solutions

Colistin stock solutions were prepared and sterilised as described in **Chapter 2 Section 2.2.1**. Prior to use, stock solutions were diluted as appropriate to achieve the intended working concentrations in each experiment.

3.2.2 Bacterial strains and growth conditions

The bacterial strains used to inoculate a bead biofilm model described in this chapter were *E. coli* J53, J53(pE30), and J53(pWJ1); see **Chapter 2 Section 2.2.2** for detailed information about the strains and their growth conditions.

The collected samples from the bead biofilm model were stored as -80°C bead stocks, and when required, were cultured aerobically (37°C; 120 rpm) in 10 ml LB broth ± colistin (0.125 or 1 μg/ml) to grow for cultures of 16-18 h depending on the colistin concentration the originating sample was exposed to during evolution.

All J53(pE30) mutant strains isolated from the bead biofilm model were stored as frozen stocks at -80°C. When required, the mutant strains were cultured on LB agar or grown in 10 ml LB broth (37°C; 120 rpm) for O/N cultures ± 1 μg/ml colistin, depending on the presence or absence of *mcr-1*.

3.2.3 Bead biofilm evolution model

The bead biofilm evolution model was adapted from Poltak and Cooper (2011) (**Figure 3.2**). Briefly, O/N cultures of *E. coli* J53, J53(pE30) and J53(pWJ1) were adjusted to an optical density between 0.08 and 0.10 at OD_{600nm} in LB broth, equivalent to a 0.5 McFarland index. The adjusted cultures were then used as inocula for the biofilm bead model by dilution in 1.5 ml LB broth ± colistin (0.125 or 1 μg/ml) in a 24-well microtitre plate to achieve a final concentration of 5×10^4 CFU/ml. Two sterile borosilicate glass beads (7 mm diameter; with red and blue colours used for alternate transfer and sampling) were placed in each well of the model (n=4 biological replicates). A sterile LB broth control was included in all plates. Plates were incubated for 48 h (37°C; 20 rpm) per passage cycle for 51 days. On passage days (every 48 h), one bead from each well of the old plate was transferred into fresh medium in a new plate using sterile forceps. The established biofilm population on the remaining bead was harvested by transferring the bead into 1.5 ml LB ± corresponding colistin concentration (0.125 or 1 μg/ml) and vortex mixed for 2 mins. The planktonic bacterial population in the entire supernatant from the same well was also harvested. All the collected biofilm (bead) and planktonic (supernatant) samples from bead biofilm model were stored at -80°C for later RT-qPCR analysis (**see Chapter 3 Section 3.2.4**), whereas for later phenotypic characterisation experiments (MICs and biofilm formation assay), only biofilm samples from the middle timepoint Day 23 and the end timepoint Day51 were tested to reflect the overall trend during evolution while minimising the

sample size to a manageable level. Purity tests were performed weekly on each well over the course of the experiment by streaking on Urinary Tract Infection ChromoSelect Agar (NutriSelect® Plus, Millipore) to check for any signs of contamination.

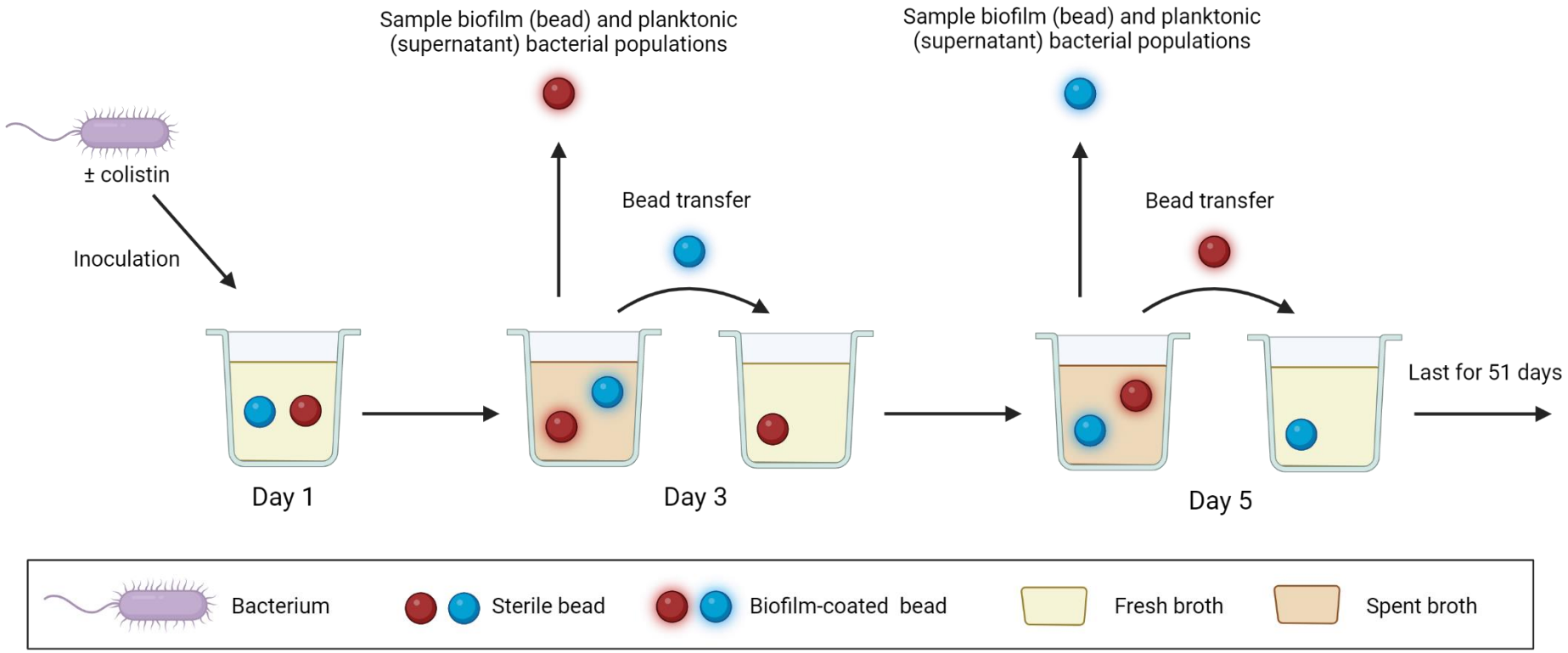

Figure 3.2 Schematic diagram showing the bead biofilm evolution model and experimental strategy used. Biofilms of *E. coli* J53, J53(pE30) *mcr-1* or J53(pWJ1) *mcr-3* were grown in LB broth in 24-well microtitre plates ± colistin (0.125 or 1 μg/ml) on sterile 7 mm-diameter borosilicate glass beads and, passaged into fresh medium (bead transfer) and sampled (bead and supernatant) every 2 days (51 days; n=4). Red and blue beads were used for alternate transfer and sampling on passage days. The figure was created with BioRender.com.

3.2.4 Multiplex real-time quantitative polymerase chain reaction (RT-qPCR)

To monitor persistence of *mcr* genes throughout the evolution experiment, a multiplex RT-qPCR assay was conducted on the collected biofilm (bead) and planktonic (supernatant) samples to quantify levels of both *mcr-1* and *mcr-3* in all the bead biofilm model samples. For this, RT-qPCR was performed in 96-well plates, using a Bio-Rad CFX384 system (Corbett Research, Sydney, AUS) with the addition of specific primers and probes shown in **Table 3.1**. Each reaction in RT-qPCR contained 5 µl template (the collected sample), 4 µl SsoAdvanced Universal Probes Supermix (Bio-Rad Laboratories, Inc., US), 0.15 µl (10 pmol/µl) of each primer and 0.15 µl (10 pmol/µl) of each probe, with sterile Milli-Q water being added to reach a total reaction volume of 20 µl. The parameters employed for RT-qPCR amplification were 5 min denaturing at 95°C, followed by 44 cycles of 15s denaturing at 95°C and 15s annealing/elongation at 60°C. Standard curves for *mcr-1*, *mcr-3* and the house keeping gene *rpoB* were generated using serial dilutions of a copy number standard (provided by Dr Mei Li) in which all three genes had been cloned (695 bp insertion) into the 2686 bp cloning vector pUC57 (GenScript Biotech, Netherlands) producing a single copy of each gene per cell (i.e. 36.8 pg of DNA corresponding to 10^7 copies, as calculated on the website: http://cels.uri.edu/gsc/cndna.html). The abundance of each *mcr* gene in each test sample was then calculated as a ratio of the absolute copy number of each *mcr* to that of *rpoB*, and therefore designated as copy number per cell.

Table 3.1 Primer and probe sequences used for RT-qPCR, and primer sequences used for PCR.

RT-qPCR /PCR	Primer/Probe	Sequence (5' - 3')	Size (bp)	Tm (°C)	Reference
RT-qPCR	*mcr-1* qF	TGGCGTTCAGCAGTCATTAT	120	60	Adapted from (Irrgang et al. 2016)
	mcr-1 qR	AGCTTACCCACCGAGTAGAT			
	mcr-1 probe	FAM[a]-AGTTTCTTTCGCGTGCATAAGCCG-BHQ1[a]			
	mcr-3 qF	CGTGTTCCTATGCAGGTGTG	150	60	Adapted from (Yang et al. 2020)
	mcr-3 qR	CGAGTATCAGCGGCTTTCTG			
	mcr-3 probe	ROX[a]-TGCAAACACGCCATATCAACGCCT-BHQ2[a]			
	rpoB-qF	AAGCTGCTTTCCGTTCCGTA	200	60	(Yang et al. 2017)
	rpoB-qR	CGCCACGGATTTGACATTCC			
	rpoB probe	HEX-ATACGTCAGCTACCGCCTTG-BHQ1			
PCR	*mcr-1* F	GCTACTGATCACCACGCTGT	953	60	(Yang et al. 2017)
	mcr-1 R	TGGCAGCGACAAAGTCATCT			

[a]The indicated fluorophores on the original probes have been adapted as shown for this study.

3.2.5 Minimum inhibitory concentration assays

MIC assays were performed on Day 23 and 51 biofilm (bead) samples of *E. coli* J53, J53(pE30) and J53(pWJ1) as previously described in **Chapter 2 Section 2.2.3**. Briefly, stock colistin was prepared in MH broth, with a starting concentration of 64 μg/ml. Two-fold serial dilutions of colistin were performed in a sterile, flat-bottom 96-well microtitre plate. O/N bacterial cultures of Day 23 and 51 biofilm samples were adjusted to an optical density between 0.08 and 0.10 at OD_{600nm} in PBS and were then diluted 1 in 10 in MH broth, followed by a further 1 in 20 dilution in the wells of the microtiter plates containing the colistin serial dilutions. Plates were incubated aerobically at 37°C for 20 h before recording the results. MIC plates for Day 51 biofilm samples of *E. coli* J53(pE30) (evolved under no colistin in the bead biofilm model) were incubated for a further 28 h prior to recording MIC values a second time. Each MIC assay was performed in 3 biological repeats. The MIC result for each replicate sample was recorded as the mode value from n=3 biological repeats.

3.2.6 Polymerase chain reaction (PCR) and agarose gel electrophoresis

PCR was performed on well supernatant obtained from the MIC assay (n=3) for each replicate (n=4) of Day 51 *E. coli* J53(pE30) biofilm samples (no colistin). Supernatant from the first well that showed turbidity in each row at both 20 and 48 h incubation in the MIC assay was used as the template for PCR. PCR was carried out using a Thermocycler High Fidelity PCR system (ThermoFisher, UK) with *mcr-1* primers

(**Table 3.1**). A total volume of 12 µl was used in the reaction system, which contained 5µl 1 × PCR master mix, 0.5 µl forward primer (10 pmol/µl), 0.5 µl reverse primer (10 pmol/µl), 1 µl template and 5 µl molecular water. The parameters adopted for PCR amplification were denaturation at 94°C for 5 min, 30 cycles of denaturation at 94°C for 30s, annealing at 60°C for 30s and extension at 72°C for 30 s, with a final extension at 72°C for 10 min.

The amplified products obtained from the PCR reaction were loaded onto an agarose gel to visualise the target DNA fragments. For this, 2% Hi-Res Standard Agarose (Cambridge Reagents Ltd, UK) was prepared in 1 × Tris-Borate-EDTA buffer (TBE) with 0.1 mg/L of ethidium bromide (Invitrogen, UK). The SmartLadder of 200-10000 bp (Eurogentec, UK) was utilised to verify the size of the DNA fragments. Gels were visualised and recorded by a G:BOX Chemi XX6 gel imaging system (Syngene, Bangalore, IND).

3.2.7 Biofilm formation assay and COMSTAT analysis

All evolved *E. coli* J53(pE30) biofilm populations at Day 23 and 51 (replicates 1, 2 and 3) were tested in a biofilm formation assay as described in **Chapter 2 Section 2.2.8**. Cultures grown for 16-18 h were adjusted to OD_{600nm} equal to 0.05 in LB broth before being further diluted 1 in 10 in LB in a Greiner 96-well glass-bottomed plate. Plates were incubated on a rocker (30 rpm) at 37°C for 24 h. After biofilm formation, the supernatant was gently removed, and 6 µl of LIVE/DEAD® stain in PBS was added

into each well. The stained biofilms were incubated wrapped in foil for 5 mins, and then hydrated with addition of 44 µl of PBS. Five Z-stack images were taken for each sample using a Zeiss LSM980 with Airyscan2 (n=3). Settings used for CLSM imaging were: zoom, ×1; lens, ×63 oil immersion; line averaging, 1; resolution, 1584×1584; step size, 0.69 µm; and slice number, 60. With thanks to Dr Lydia Powell for performing the CLSM imaging.

ImageJ software was used for exporting and processing the images in tagged image file format. COMSTAT2 image analysis software (Heydorn et al. 2000; Vorregaard 2008) was used to quantify the CLSM Z-stack images to achieve the biofilm parameters, i.e., biomass, biofilm thickness, roughness coefficient, and Dead/Live bacterial ratio.

3.2.8 Isolation of J53(pE30) strain mutants for sequence analysis

Seven strain mutants were purified from the evolved Day 51 biofilm populations of *E. coli* J53(pE30) (no colistin). The three *mcr-1*-positive mutants were numbered 2, 3 and 4, and were isolated from the well one dilution below MIC for a given replicate in the MIC assay (from replicates 1, 3, 4 in the bead biofilm evolution experiment, respectively) and purified on LB agar + colistin (1 µg/ml). The four *mcr-1*-negative mutants were numbered 5, 6, 7 and 8, and were isolated from the colistin-free control well for the same given replicate in the MIC assay (from replicates 1, 2, 3, 4, respectively) and purified on LB agar.

3.2.9 Whole genome sequencing

Briefly, gDNA was extracted from a 2 ml culture grown for 16-18 h using the QIAcube automated system (Qiagen, Germany), and quantified using the Qubit 3.0 (ThermoFisher Scientific) through the dsDNA high sensitivity assay. With thanks to Professor Owen B. Spiller, Ian Boostrom and Jordan Mathias for performing the WGS.

3.2.9.1 Illumina sequencing

WGS of gDNA was carried out using the Illumina MiSeq platform (Illumina Inc., CA). DNA libraries were prepared for paired-end sequencing (2 × 301 cycles) using Nextera XT (Illumina). Quality control (QC) of raw sequence reads included fastqc 0.11.2, and quality and adaptor trimming were performed using Trim galore 0.4.3. For each *E. coli* isolate, at least 80 × coverage was generated. Reads were assembled in contigs using the de novo assembler SPAdes 3.9.0 (.fasta) and were aligned to the original fastq reads using BWA aligner 0.7.15. Any assembly mapping errors in the contigs were corrected using Pilon 1.22. Assembly metrics were evaluated using Quast 2.1.

3.2.9.2 Nanopore sequencing

Sequencing libraries from gDNA were prepared using the Rapid Barcoding Kit (SQK-RBK004) following the manufacturers' instructions. Following a QC check of the Nanopore flow cell (R9.4) just before use, over 1200 active pores were detected. The flow cell was primed according to the manufacturer's guidelines, and the library was

gently mixed using a pipette tip and loaded onto the Nanopore flow cell (R9.4). WGS was performed for 48 hours using a MinION (Oxford Nanopore, UK) and associated MinKNOW software. Raw fastq sequences were concatenated, and the strains were de-barcoded using Porechop. Unicycler (Wick et al. 2017) was used to create a hybrid assembly with a combination of MiSeq short reads and MinION long reads. The resulting hybrid assembly was visualised using Bandage to confirm complete genome assembly of the plasmids.

3.2.10 Bioinformatics and sequence analysis

MLST loci (by MLST 2.0), acquired resistance genes (by ResFinder 4.1, with minimum 95% identity and 80% coverage), plasmid replicon typing (by PlasmidFinder 2.1, using *Enterobacteriaceae* database with minimum 95% identity and 80% query coverage), plasmid multiLocus sequence typing (pMLST) (by pMLST 2.0) for IncHI2 and IncF plasmids, and virulence genes (by VirulenceFinder 2.0, with minimum 95% identity and 80% coverage) were retrieved from the online databases (CGE platform: http://www.genomicepidemiology.org/services/).

Geneious 10.2.6 was used to annotate genes from the closest homologues in the NCBI Genome database. IS elements were further annotated from ISfinder database (service available at: https://isfinder.biotoul.fr/). For plasmid analysis, alignment of plasmids from the parental strain and Day 51 mutants was performed using BLAST Ring Image Generator (BRIG v0.95). Visualisation of deletion areas identified on day 51 mutants

was performed by Easyfig 2.2.5. With thanks to Professor Owen B. Spiller and Dr Mei Li for performing the sequence analysis.

3.2.11 Growth curve assay

Growth curve assays were performed on the original *E. coli* J53(pE30) and the seven mutants isolated from Day 51 biofilm populations (no colistin) as previously described in **Chapter 2 Section 2.2.5**. Briefly, adjusted O/N cultures were diluted in a ratio of 1 to 40 in LB broth. Growth curves were performed in triplicate in a sterile, flat-bottomed 96-well microtitre plate (200 µl/well). Absorbance measurements were taken hourly at OD_{600nm} over 96 h at 37°C using a FLUOstar® Omega multi-mode microplate reader. The results are presented as mean values.

3.2.12 Plasmid population dynamics model

A mathematical model was developed based on ordinary differential equations (ODEs) to investigate the dynamics of plasmid-bearing bacterial populations. The model tracks three distinct subpopulations: plasmid-bearing (B_p), plasmid-free ($B_ø$), and plasmid-adapted (B_a) cells, all competing for a single limiting resource (R). The growth of each subpopulation followed Monod kinetics, a widely used approach in microbial population dynamics (Hernández-Beltrán et al. 2021; Dewan and Uecker 2023), with strain-specific parameters defining their resource utilisation and conversion efficiency. I assumed a homogeneous environment where resource availability was the primary constraint on bacterial growth.

The model incorporated three key plasmid-related processes, namely replication (modeled as a constant segregation rate, λ), where plasmid-bearing cells can lose plasmids during replication; conjugation (modeled as a conjugation rate, γ, using mass-action kinetics), where plasmid-bearing and plasmid-adapted cells can transfer plasmids to plasmid-free cells through conjugation; compensatory mutation (modeled as a mutation rate, χ). Additionally, plasmid-bearing cells can acquire compensatory mutations that mitigate the fitness cost of plasmid carriage, leading to the emergence of a plasmid-adapted subpopulation. A resistance coefficient, κ, was also considered to account for antibiotic-induced killing, where a larger κ implies greater susceptibility to the antibiotic. The system's dynamics are described by the following equations:

$$\frac{dR}{dt} = -\left(U\left(R;\psi_{\varnothing}\right)\cdot B_{\varnothing} + U\left(R;\psi_{p}\right)\cdot B_{p} + U\left(R;\psi_{a}\right)\cdot B_{a}\right),$$

$$\frac{dA}{dt} = -A\cdot\left(\alpha_{\varnothing}B_{\varnothing} + \alpha_{p}B_{p} + \alpha_{a}B_{a}\right),$$

$$\frac{dB_{\varnothing}}{dt} = \left(G\left(R;\psi_{\varnothing}\right) - \kappa_{\varnothing}A\right)\cdot B_{\varnothing} + \lambda\left(G\left(R;\psi_{p}\right)\cdot B_{p} + G\left(R;\psi_{a}\right)\cdot B_{a}\right) - \gamma\left(B_{\varnothing}B_{p} + B_{\varnothing}B_{a}\right),$$

$$\frac{dB_{p}}{dt} = \left(1-\lambda\right)G\left(R;\psi_{p}\right)\cdot B_{p} - \kappa_{p}A\cdot B_{p} + \gamma\left(B_{\varnothing}B_{p} + B_{\varnothing}B_{a}\right) - \chi G\left(R;\psi_{p}\right)\cdot B_{p},$$

$$\frac{dB_{a}}{dt} = \left(1-\lambda\right)G\left(R;\psi_{a}\right)\cdot B_{a} - \kappa_{a}A\cdot B_{a} + \chi G\left(R;\psi_{p}\right)\cdot B_{p},$$

where $U(R; \psi)$ is the resource uptake rate (following Monod kinetics), $G(R; \psi)$ is the

growth rate (calculated as $\rho \cdot U(R; \psi)$), A is the antibiotic concentration, α represents antibiotic degradation rate, and κ represents antibiotic susceptibility (subscripts denote strain-specific values). These ODEs were solved numerically using the SciPy and standard scientific libraries to simulate the temporal dynamics of the bacterial populations and the resource under various conditions (**Appendix Figure 1**). The initial resource concentration is $R(0)$, and the initial antibiotic concentration $A(0)$, as well as the initial densities of the three bacterial subpopulations $B_{\emptyset}(0)$, $B_p(0)$, and $B_a(0)$, are determined by the specific experimental setup being simulated.

To parameterise the mathematical model, strain-specific parameters related to bacterial growth were first determined and antibiotic susceptibility were estimated from experimental data. First, strain-specific growth rate (ρ) and the ratio of the maximum growth rate to the half-saturation constant (V_{max}/K_m, also referred to as μ/K) were determined by fitting the Monod growth model to time-course OD measurements of each strain obtained from growth curve assays (**Appendix Figure 2a**). Non-linear least squares optimization was employed to estimate these parameters, ensuring they remained within biologically plausible ranges. The goodness-of-fit was assessed by calculating the R^2 value for the fitted curves, with all strains achieving $R^2 > 0.95$, indicating agreement between the model and the experimental data. Next, the antibiotic susceptibility coefficient (κ) for each strain was estimated by fitting our model to experimental MIC data (**Appendix Figure 2b**). Specifically, we simulated dose-response curves over a range of antibiotic concentrations and optimized κ values using

the L-BFGS-B algorithm implemented in Python, constraining the fitted values to biologically realistic bounds. In this context, a larger κ implies greater susceptibility to the antibiotic. Parameters used for the simulations are described in **Table 3.2**. The data and code used for this analysis, along with a more detailed description of the model, are publicly available as Jupyter Notebooks (https://github.com/ccg-esb-lab/mcr). With thanks to Carles Tardío Pi and Rafael Peña-Miller for the setup of the mathematical modelling and data analysis.

Table 3.2 Parameters used in the numerical simulations.

Parameter	Description	B_p	$B_ø$	B_a	Units
T	Duration of experimental season				24 hours
S0	Initial concentration of limiting resource				1 μg/ml
d	Transfer dilution rate				0.1
B0	Initial bacterial density	1×10^{6}	0	0	cells/ml
V/Km	Specific affinity for resource	3.7932×10^{-10}	3.85495×10^{-10}	6.42797×10^{-10}	ml/cells
ρ	Maximum growth rate	1.22365×10^{9}	1.68465×10^{9}	1.14193×10^{9}	cells/hour
κ	Antibiotic susceptibility	0.03156	0.47272	0.04026	μg/ml
χ	Mutation rate	-	-	1×10^{-8}	locus/allele/generation
γ	Conjugation permissiveness	1×10^{-12}	-	1×10^{-12}	ml/cells/hour
λ	Segregation rate	0.02	0.02	0.02	per division
α	Antibiotic degradation rate	1×10^{-12}	1×10^{-11}	1×10^{-12}	ml/cells/hour

B_p, plasmid-bearing subpopulation; $B_ø$, plasmid-free subpopulation; B_a, plasmid-adapted subpopulation.

3.2.13 *Galleria mellonella* infection model

In vivo virulence of the seven strain mutants isolated from the Day 51 J53(pE30) biofilm populations (no colistin) was compared with the parental Day 0 J53(pE30) and evaluated using a *G. mellonella* infection model. The wax moth *G. mellonella* larvae (Live Foods UK Ltd., http://www.livefood.co.uk) were stored in the dark in the fridge and used within 5 days. All bacteria were sub-cultured on fresh LB agar plates ± colistin (1 µg/ml) and grown overnight at 37°C. A loopful of growth was taken from the plate, washed in sterile 0.85% saline, and then adjusted to an OD_{600nm} between 0.65 and 0.75 to generate a bacterial suspension of ~ 10^9 CFU/ml. Using a 300 µl insulin syringe, a 10 µl aliquot of the diluted test cell concentration (10^8 or 10^7 CFU/ml) was injected into the haemocoel of each larva through the rear left proleg. For each cell concentration, 10 randomly chosen larvae were selected for injection (n=3). In all experiments, controls included 10 larvae injected with sterile 0.85% saline and 10 larvae receiving mock injections. Larvae were incubated at 37°C, and survival was monitored every 24 h for 3 consecutive days. Death was denoted when larvae no longer responded to touch. Results were analysed by Kaplan-Meier survival curves and comparison of survival curves was achieved by performing Log-rank (Mantel-Cox) tests (GraphPad Prism statistics software).

3.3 Results

3.3.1 Carriage of *mcr-1* imposes a higher fitness cost than *mcr-3* in the bead biofilm model

mcr-1 persistence in *E. coli* J53(pE30) and *mcr-3* persistence in *E. coli* J53(pWJ1), in both biofilm (bead) and planktonic (supernatant) bacterial populations in the presence or absence of colistin selection (0.125 or 1 μg/ml), was monitored in a bead biofilm model by RT-qPCR for 51 days (**Figure 3.3**; **Appendix Figure 3**). The general trend in *mcr* dynamics between biofilm and planktonic populations closely mimicked each other, despite the fact that the planktonic populations showed a higher level of day-to-day variability than the biofilm populations in the frequency plots (**Figure 3.3a and b**). As the biofilm and supernatant populations were shown to effectively resemble one another closely, only biofilm samples were analysed in further experiments to limit sample numbers to manageable levels.

When under no colistin selection, *mcr-1* abundance in J53(pE30) biofilm and planktonic populations underwent a continuous reduction from Day 7, which became virtually undetectable by RT-qPCR by Day 23; its copies/cell being 0.004 (biofilm) and 0.01 (planktonic) at this time point (**Figure 3.3a**). In contrast, *mcr-3* abundance in J53(pWJ1) biofilm and planktonic populations exhibited relative stability until Day 35, after which it steadily declined but remained detectable until Day 51, with copies/cell being 0.16 (biofilm) and 0.17 (planktonic) (**Figure 3.3b**). For both *E. coli* strains, the

presence of colistin selection at subinhibitory concentrations (0.125 or 1 μg/ml) aided maintenance of *mcr* genes throughout the 51 days, with no apparent differences observed in *mcr* levels between the two colistin concentrations, in both biofilm and planktonic populations (**Figure 3.3a and b**). Taken together, the distinct evolutionary patterns in *mcr* genes observed in the absence of colistin indicate a higher fitness cost of *mcr-1* than *mcr-3* carriage.

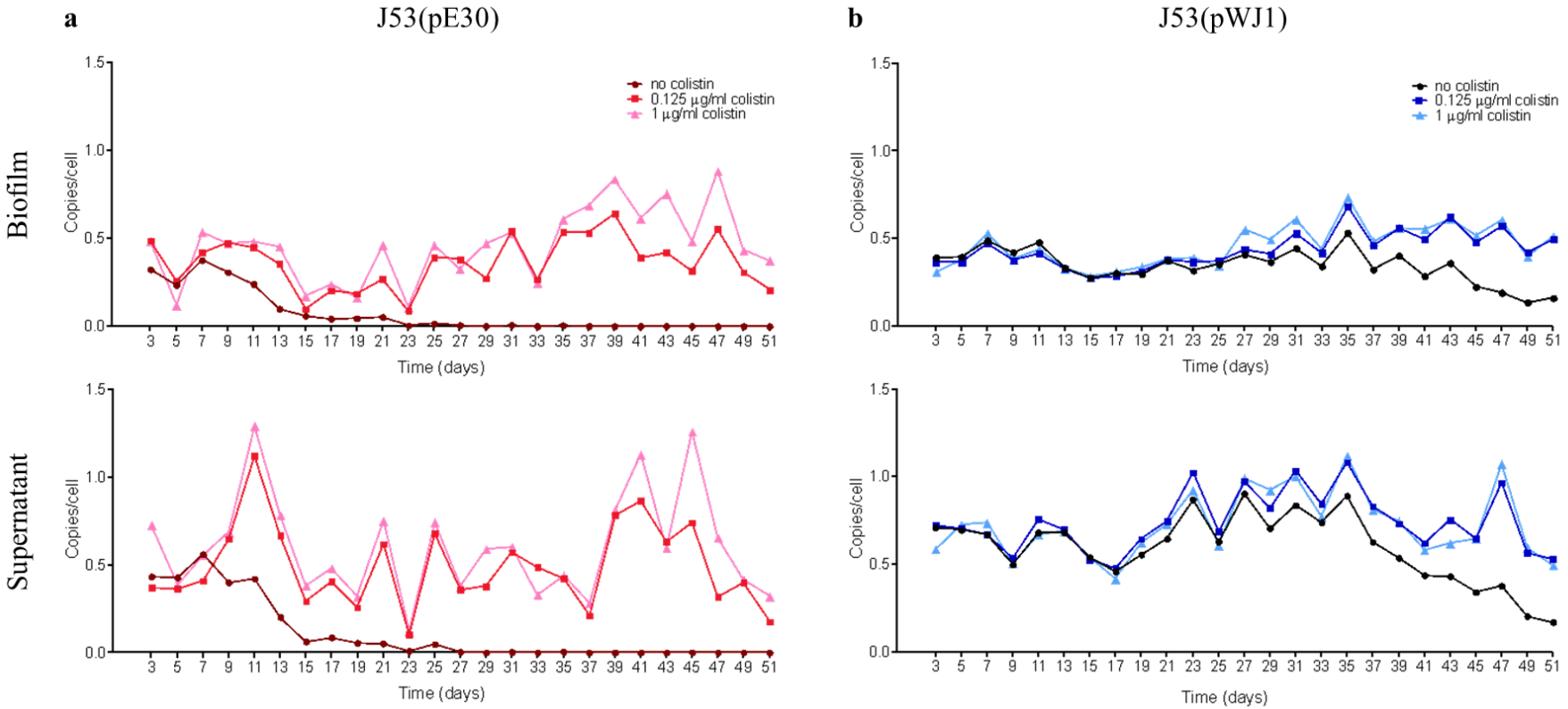

Figure 3.3 RT-qPCR monitoring of *mcr-1* and *mcr-3* persistence in *E. coli* J53(pE30) and J53(pWJ1), respectively, in a bead biofilm evolution model over 51 days ± colistin selective pressure (0.125 or 1 µg/ml). RT-qPCR was conducted on both bead and supernatant samples to monitor *mcr* gene levels in biofilm and planktonic bacterial populations, respectively. **a** J53(pE30) *mcr-1*. **b** J53(pWJ1) *mcr-3*. Abundance of *mcr-1* and *mcr-3* was calculated as the absolute copy number of the *gene* relative to *rpoB* (representing copies/cell). Without colistin selection, *mcr-1* in J53(pE30) biofilm and planktonic populations became undetectable by Day 23, whereas *mcr-3* was still maintained in J53(pWJ1) biofilm and planktonic populations by Day 51, indicating a higher fitness cost of *mcr-1* carriage. Each data point is a mean of four biological repeats (n=4). (Error bars not shown).

3.3.2 Colistin susceptibility of evolved *E. coli* biofilm populations at days 23 and 51

Changes in susceptibility to colistin for all evolved *E. coli* J53, J53(pE30) and J53(pWJ1) biofilm populations in the bead biofilm model (4 replicates for each control/condition) was monitored by performing standard MIC assays (20 h incubation) on Day 23 and 51 samples (**Table 3.3**). MIC values of all biofilm populations at Day 23 demonstrated no real change in colistin resistance when compared to their respective originating strain at Day 0 (**see Chapter 2 Table 2.2** for Day 0 MICs). At Day 51, the MIC values for the J53 and J53(pWJ1) biofilm populations were also comparable to those at Day23 (maximum one-fold change) regardless of the presence or absence of colistin, as did those of J53(pE30) grown under colistin selection (0.125 and 1 µg/ml). However, for J53(pE30) biofilm populations evolved in the absence of colistin, 3/4 biological replicates showed a 16-fold decrease in MIC from 8 µg/ml (at Day 23) to 0.5 µg/ml (at Day 51), with the remaining biological replicate still being colistin resistant at Day 51 (4 µg/ml). This was consistent with the corresponding PCR findings, where replicates 2, 3 and 4 were *mcr-1* negative, and replicate 1 was *mcr-1* positive (**Figure 3.4**).

3.3.3 Rapid *mcr-1* resurgence in long-term evolved biofilm populations following re-exposure to colistin

The MIC plates for Day 51 *E. coli* J53(pE30) biofilm populations (no colistin) were incubated until 48 h, and the MIC and PCR results were compared with those obtained at 20 h incubation to monitor any changes in colistin resistance profile (**Figure 3.4**). At 48 h, replicate 1 showed an MIC of 4 μg/ml and tested positive for *mcr-1*, i.e., unchanged from the 20 h incubation result. However, this increase in incubation time resulted in a full return of detectable *mcr-1* in 2/3 of the remaining replicates that had been *mcr-1* negative at 20 h (as determined by PCR). This was also corroborated phenotypically by a return of colistin resistance in these two replicates, with the modal MIC values demonstrating an 8-fold increase following further incubation.

Table 3.3 Minimum inhibitory concentrations for evolved *E. coli* J53, *mcr-1* J53(pE30) and *mcr-3* J53(pWJ1) biofilm populations at days 23 and 51 in the bead biofilm model (µg/ml; n=3).

Biofilm population (strain)	Colistin (µg/ml)	Replicate	Day 23	Day 51
J53	0	1	0.25	0.25
		2	0.25	0.125
		3	0.25	0.5
		4	0.5	0.5
J53(pE30)	0	1	8	4
		2	8	**0.5**
		3	8	**0.5**
		4	8	**0.5**
J53(pE30)	0.125	1	8	8
		2	8	8
		3	8	8
		4	16	8
J53(pE30)	1	1	16	8
		2	16	8
		3	16	16
		4	16	16
J53(pWJ1)	0	1	8	4
		2	8	8
		3	8	8
		4	8	8
J53(pWJ1)	0.125	1	8	8
		2	8	4
		3	8	8
		4	8	8
J53(pWJ1)	1	1	8	8
		2	8	8
		3	8	8
		4	8	8

Values in bold represent significant decreases in colistin MIC for the three J53(pE30) biofilm replicates evolved under no colistin, corresponding to the apparent loss of *mcr-1* in these biofilm populations. Day 0 MICs for *E. coli* J53, J53(pE30) *mcr-1* and J53(pWJ1) *mcr-3* are 0.25, 8 and 8 µg/ml respectively.

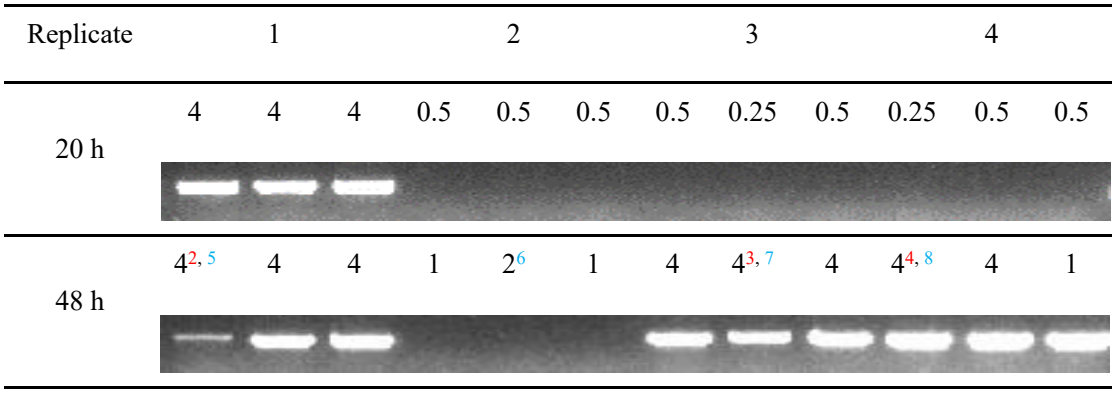

Figure 3.4 Rapid resurgence of colistin resistance in evolved Day 51 *E. coli* J53(pE30) biofilm populations (no colistin) after re-exposure to colistin. Colistin resistance for all 4 replicates of Day 51 *E. coli* J53(pE30) biofilm populations (no colistin) was assessed at both 20 and 48 h incubation in MIC assays (μg/ml; n=3). PCR and agarose gel electrophoresis were performed in parallel to verify the presence of *mcr-1* in each MIC replicate (n=3) for each respective replicate in the bead biofilm evolution experiment (n=4). Superscript numbers in red indicate source of *mcr-1*-positive mutants (2, 3, 4), purified from the well at the dilution just below MIC for the given MIC replicate at 48 h incubation; superscript numbers in blue indicate source of *mcr-1*-negative mutants (5, 6, 7, 8), purified from the no colistin control well for the same MIC replicate at 48 h incubation.

3.3.4 Adaptation of *mcr-1* biofilm populations in the bead biofilm model is associated with time-dependent reduction of fitness cost in the biofilm environment

Longitudinal changes in the biofilm-forming phenotype of three replicate biofilm populations of J53(pE30) *mcr-1* evolved in the bead biofilm model at Days 23 and 51 were studied in a biofilm formation assay. CLSM imaging revealed that the biofilms

grown from replicate 1 demonstrated a marked reduction in cell viability from Day 23 to Day 51 (**Figure 3.5a**), shown by increasing dead/live bacterial ratio ($P < 0.0001$) and a corresponding reduction in biofilm biomass ($P < 0.001$) (**Figure 3.5b**), irrespective of the presence/absence of previous colistin selection in the bead biofilm model (0.125 or 1 μg/ml).

In contrast, in replicates 2 and 3, the biofilms grown from Day 51 biofilm populations were generally thicker and healthier than those grown from Day 23 (**Figure 3.5a**). This was confirmed by COMSTAT analysis, where a significant decrease in dead/live bacterial ratio between Day 23 and Day 51 in the presence/absence of colistin ($P < 0.05$) and a significant increase in biofilm biomass between Day 23 and Day 51 in the absence and presence of 1 μg/ml colistin ($P < 0.05$) were noted (**Figure 3.5b**). The observed increasing biofilm-forming ability in evolved replicate 2 and 3 biofilm populations indicates longitudinal adaptation and amelioration of the fitness cost of *mcr-1* in a biofilm environment.

Interestingly, when comparing directly between the replicate biofilm populations at Day 51 with no colistin selection, replicate 1 generated biofilm with significantly increased dead/live bacterial ratio ($P < 0.0001$; **Appendix Table 1**) and significantly decreased biofilm biomass ($P \leq 0.0005$; **Appendix Table 2**) when compared to both replicates 2 and 3. This result, along with the finding in **Figure 3.4** that this was the only replicate to be *mcr-1*-positive by PCR at 20 h, indicates that maintenance of the *mcr-1* gene in this Day 51 biofilm population had an adverse effect on both cell viability

and biomass of the generated J53(pE30) biofilm structure.

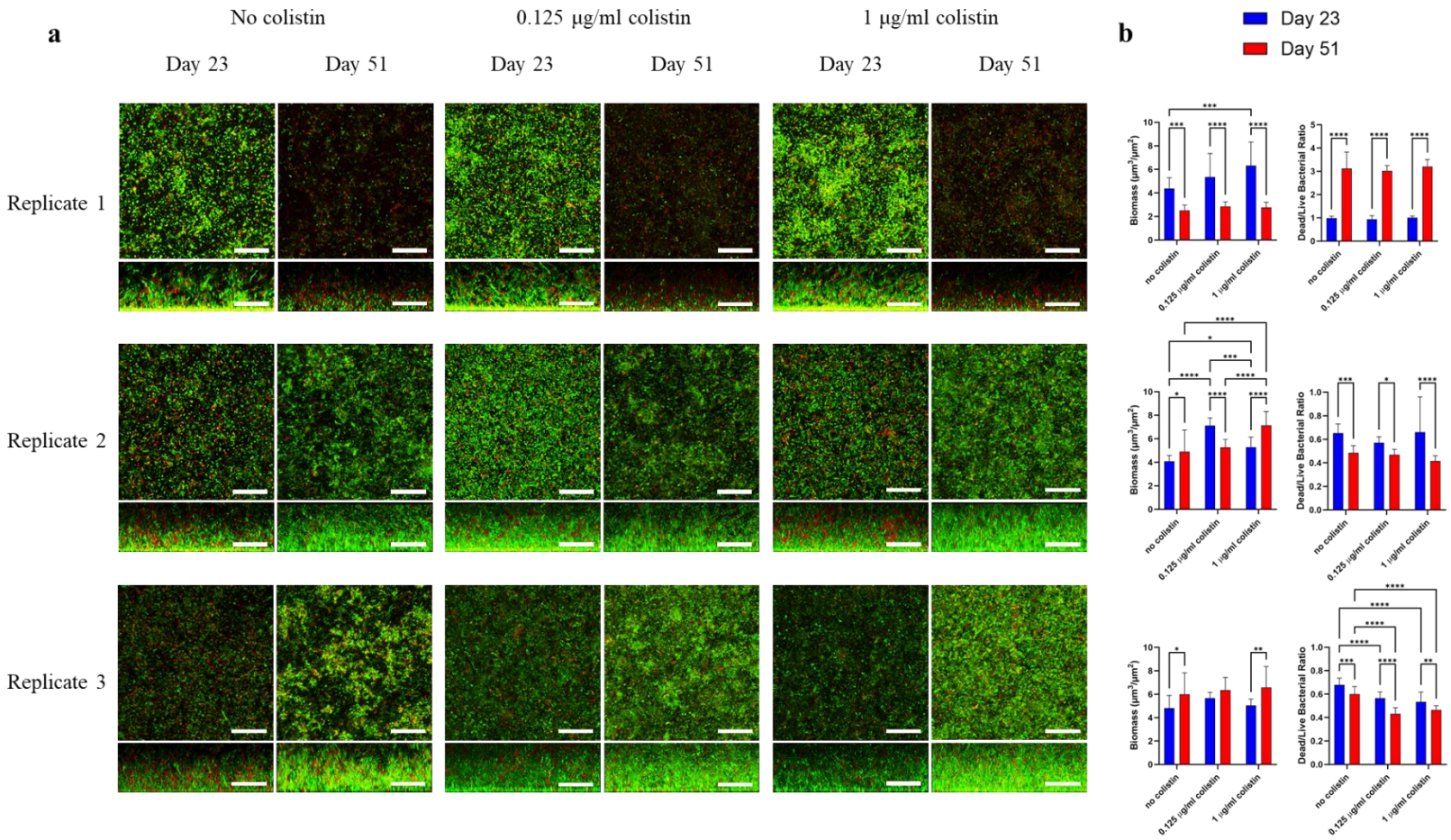

Figure 3.5 Biofilm formation assay of Day 23 and Day 51 *E. coli* J53(pE30) *mcr-1* biofilm populations evolved ± colistin (0.125 or 1 µg/ml) in the bead biofilm model (replicates 1-3). **a** CLSM imaging with live/dead staining of 24 h established biofilms (n=3); Scale bar = 30 µm. **b** Corresponding COMSTAT image analysis (Biomass and Dead/Live Bacterial Ratio). Statistical analyses were made using ordinary two-way ANOVA with Tukey multiple comparisons test. *P < 0.05, **P < 0.01, ***P < 0.001, ****P < 0.0001

3.3.5 Analysis of *mcr-1* carrying pE30 at Day 0 reveals a MDR nature of the plasmid

Analysis of the original E30 plasmid in J53 at Day 0 showed that it belonged to IncHI2 plasmid family with a size of 252,712 bp (**Figure 3.6**). *mcr-1* was located within a complete composite transposon, Tn*6330* (IS*Apl1*-*mcr-1*-*pap2*-IS*Apl1*). The plasmid was found to contain various other resistance genes that are resistant to diverse antibiotics. These include aminoglycosides (*aadA2*, *aadA1*, *aac(3)-IV*, *bleO*), fosfomycin (*fos*), sulfamethoxazole (*sul2*), tetracycline (*tetA*), β-lactams ($bla_{\text{CTX-M-14}}$), chloramphenicol (*cmlA1*, *floR*), and *oqxAB* that encodes MDR efflux pumps resistant to chloramphenicol, benzylkonium chloride, cetylpyridinium chloride, nalidixic acid, ciprofloxacin, and trimethoprim. Alignment of pE30 with 9 other *mcr-1*-harbouring IncHI2 plasmids from diverse origins (retrieved from GenBank) showed conserved homology for the majority of the plasmid (including *mcr-1*), but high variability was found in the MDR region, consistent with the high density of IS and transposon elements in this region.

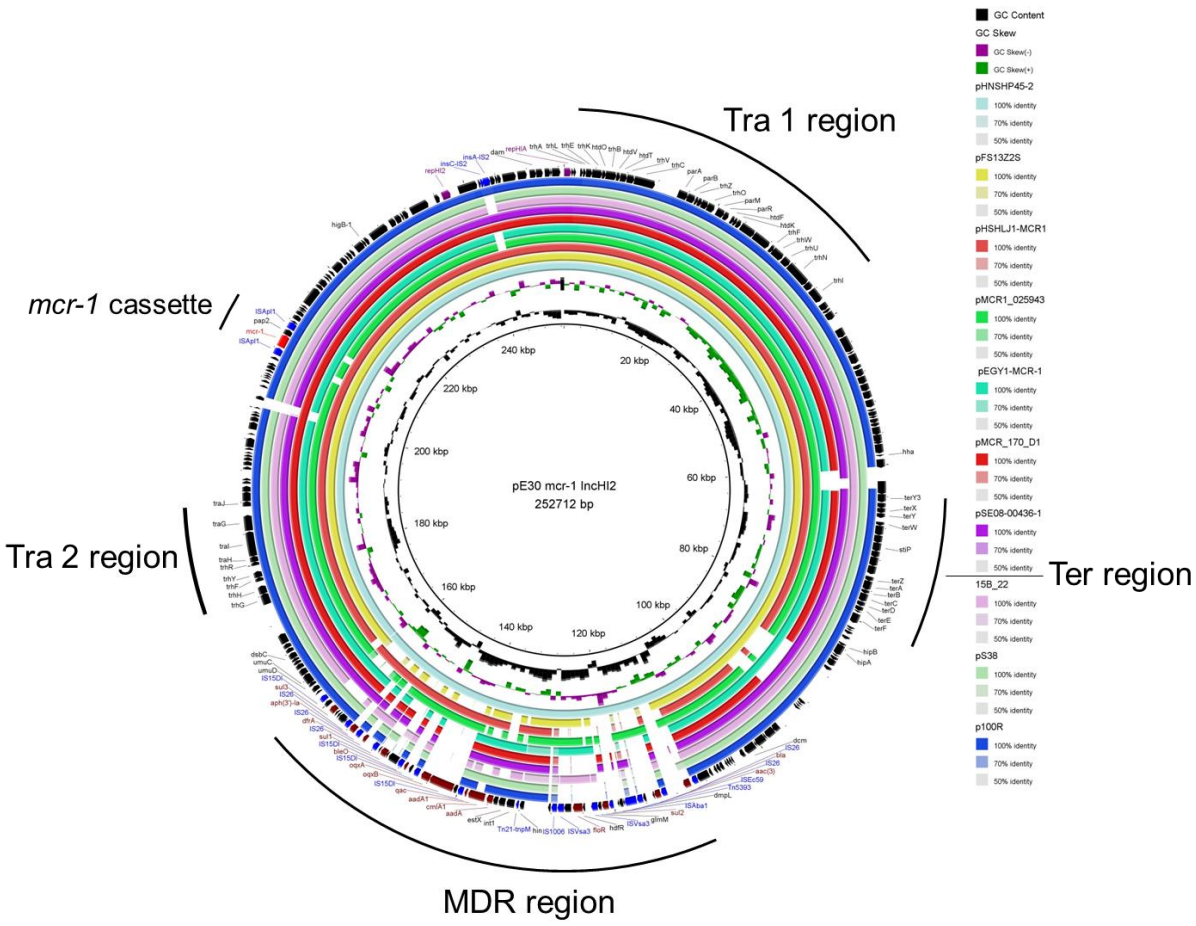

Figure 3.6 BRIG comparison of pE30 with nine other *mcr-1*-harbouring IncHI2 plasmids. Different gene types in pE30 are highlighted as follows: *mcr-1* gene (red), other antibiotic resistance genes (maroon), mobile elements (blue), and plasmid *rep* genes (purple) with arrows indicating the position and direction of these genes. The coloured rings represent different levels of identity of the IncHI2 plasmids to pE30. The pE30 backbone, comprised of transfer regions (*tra1* and *tra2*), DNA replication terminus region (*ter*), multidrug resistance (MDR) region and *mcr-1* cassette (Tn*6330*), is indicated by black curves on the outer ring.

3.3.6 Analysis of evolved Day 51 mutants reveals distinct evolutionary patterns for *mcr-1* positive and negative pE30

WGS was performed on the seven Day 51 *E. coli* J53(pE30) mutants (**Figure 3.4**) to monitor the genetic changes that had occurred in pE30 during evolution in the bead biofilm model and compared them to the original pE30 at Day 0 (**Figure 3.7**; **Table 3.4**). Unsurprisingly, WGS confirmed the intactness of *mcr-1* cassette on pE30 in all three *mcr-1*-positive mutants (mutants 2, 3 and 4). However, remarkably, the evolved pE30 plasmids in these mutants were found to have undergone an identical deletion event (28,197 bp) in part of the MDR region resulting in 9/13 of the antimicrobial resistance genes being lost, and this despite all the 3 mutants originating from completely independent replicates. For *mcr-1* negative mutants, WGS revealed a complete loss of pE30 in mutants 5, 6 and 7. Mutant 8 though, was found to have retained a remnant of pE30 (including IncHI2 determinants) but had lost 101,199 bp, including the entire MDR cassette and the downstream *mcr-1* cassette (except the downstream flanking IS*Apl1*). These distinct genetic changes in pE30 observed in the seven Day 51 J53(pE30) mutants suggest the distinct adaptive evolution pathways for pE30 within an *E. coli mcr-1* biofilm population in the absence of colistin selection.

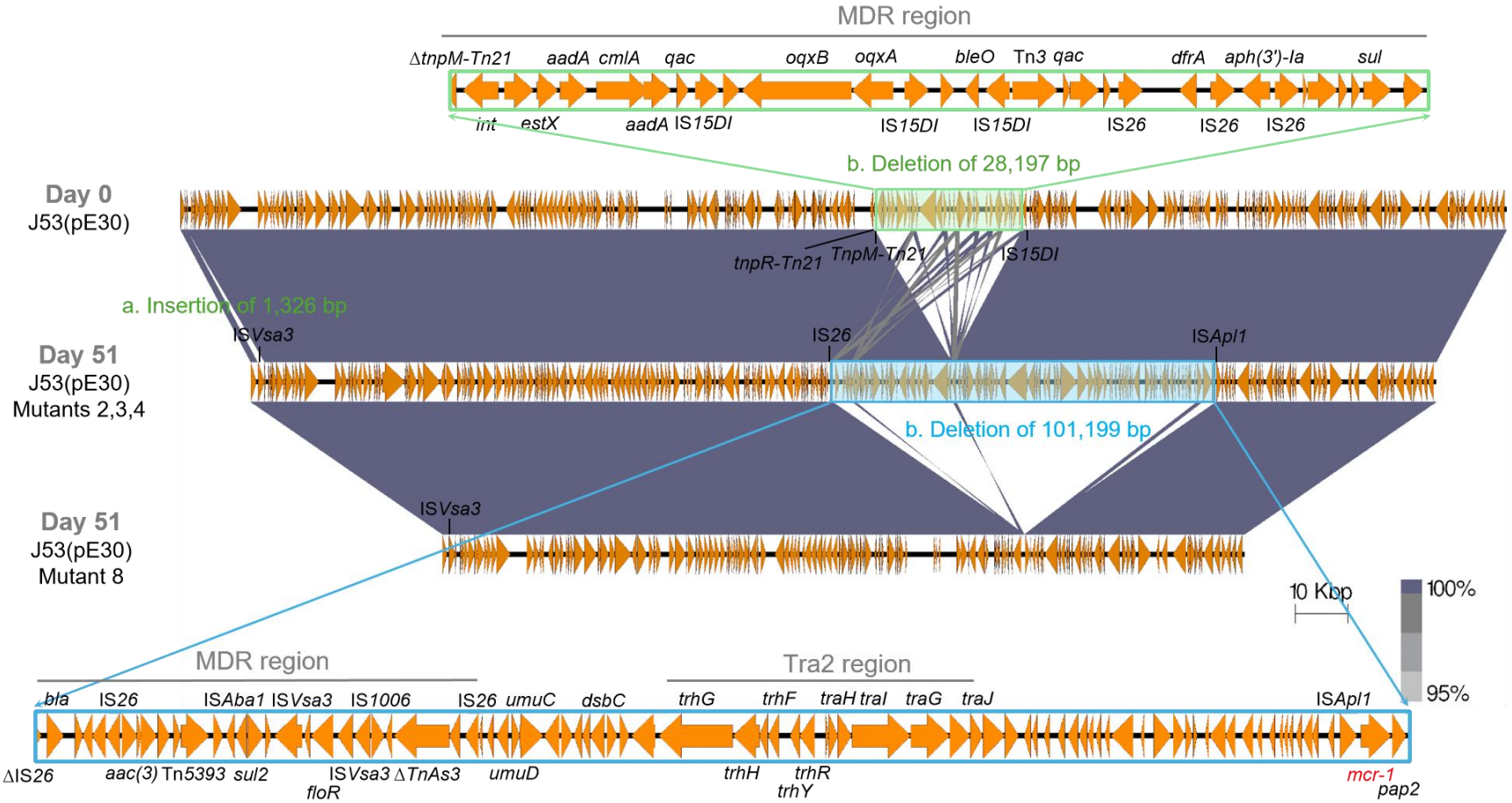

Figure 3.7 A linear depiction of genetic changes in pE30 following prolonged evolution by comparison of the original pE30 in Day 0 J53(pE30) with the evolved pE30 in strain mutants isolated from Day 51 J53(pE30) biofilm populations (no colistin). Insertion/deletion regions shown in green (a and b, mutants 2, 3, 4 vs Day 0 J53[pE30]) and blue (b, mutant 8 vs mutants 2, 3, 4), are amplified in the figure. **a** 1,326 bp insertion (IS*Vsa3*). **b** 28,197 bp deletion (partial MDR region). **b** 101,199 bp deletion (whole MDR and Tra2 regions, as well as part of the *mcr-1* cassette). Δ indicates truncated genes. The map was generated with Easyfig.

Table 3.4 Sequencing summary table showing comparison of the original Day 0 pE30 and the 7 evolved pE30 in respective strain mutants (2-8) isolated from Day 51 J53(pE30) biofilm populations (no colistin) in the bead biofilm model.

Mutants	Colistin resistance	Deletions (insertions) compared to original pE30 (bp)	Size of remaining plasmid (bp)	Comments
pE30	+		252,712	Day 0 J53(pE30)
2	+	28,197 (1,326)	225,841	Deletion in MDR region (9/13 ARGs lost); *mcr-1* & both flanking IS*Apl1* elements intact; insertion of IS*Vsa3*
3	+	28,197 (1,326)	225,841	Deletion in MDR region (9/13 ARGs lost); *mcr-1* & both flanking IS*Apl1* elements intact; insertion of IS*Vsa3*
4	+	28,196 (1,326)	225,842	Deletion in MDR region (9/13 ARGs lost); *mcr-1* & both flanking IS*Apl1* elements intact; insertion of IS*Vsa3*
5	−	252,712	0	Complete plasmid loss
6	−	252,712	0	Complete plasmid loss
7	−	252,712	0	Complete plasmid loss
8	−	101,199 (1,326)	152,839	Complete MDR region deleted along with *mcr-1* and upstream flanking IS*Apl1*; downstream flanking IS*Apl1* intact; insertion of IS*Vsa3*

The three *mcr-1*-positive mutants (2, 3 and 4) had undergone partial deletion in the MDR region, whereas the four *mcr-1*-negative mutants had either lost the whole plasmid (mutants 5, 6 and 7) or had a substantial fragment deleted including the complete MDR region (mutant 8). MDR, multidrug resistance; ARG, antimicrobial resistance gene.

3.3.7 Mathematical modelling of pE30 dynamics in the bead biofilm model

To further explore the mechanisms driving persistence (and loss) of *mcr-1* carrying pE30 observed in the bead biofilm model, a mathematical model was developed to uncover how ecological and evolutionary forces shape plasmid dynamics in J53(pE30) populations. First, environments without antibiotic selective pressure were employed, providing insights into the conditions that favour plasmid-bearing (B_p) and plasmid-free cells ($B_ø$), both competing for a single limiting resource (R). To capture the growth parameters of each subpopulation required for numerical simulations, Monod kinetics was applied, where subpopulation-specific growth rates for B_p, $B_ø$ and B_a were determined from growth curves of each strain (Day 0 J53[pE30] and seven Day 51 mutants) grown in isolation (**Figure 3.8a**). By plotting out specific affinity (V_{max}/K_m) as a function of antibiotic susceptibility (κ) (**Figure 3.8b**), uptake rate ($u[R]$) as a function of resource concentration (R) (**Figure 3.8c**), and death rate ($\kappa \cdot A$) as a function of antibiotic concentration (A) (**Figure 3.8d**) for each of these eight strains, mean values were calculated for each subpopulation (B_p, $B_ø$ and B_a) and were used as parameters required in the numerical simulations.

Numerical simulations with only B_p and $B_ø$ subpopulations included in the model were first performed to examine the stability of B_p and $B_ø$ cells under varying levels of antibiotic selection using a serial transfer protocol. By systematically varying antibiotic

concentrations, I evaluated how selection pressure influences plasmid stability. In the absence of colistin, B_p cells rapidly lost their plasmids, while higher colistin levels progressively stabilised the plasmid-carrying population (**Figure 3.9a**). Following a 51-day phase of evolution without antibiotic selection, **Figure 3.9b** shows the final densities of the evolved subpopulations after a subsequent 1-day exposure to increasing antibiotic concentrations. As the antibiotic concentration increases, the model predicted that B_p would recover from low densities and increase in prevalence.

To gain further insights into plasmid adaptation in long-term dynamics, the model was extended to include a plasmid-adapted (B_a) subpopulation, which represents cells that have acquired compensatory mutations mitigating the fitness cost of plasmid carriage. The interactions between $B_ø$, B_p, and B_a subpopulations are illustrated in the model diagram (**Figure 3.9d**), with the formation of B_a cells determined by a fixed mutation rate χ. In the absence of antibiotic selection pressure, the numerical simulations showed that B_a would rapidly outcompete both B_p and $B_ø$ cells, dominating the population over time (**Figure 3.9c**). In keeping with our experimental observations in the bead biofilm model, the mathematical model predicted the persistence of B_p cells (albeit at low densities) at the end of the experiment (**Figure 3.9c**). This suggests that segregation events maintain a small subpopulation of B_p cells, despite the apparent competitive advantage of the B_a cells (**Figure 3.10**).

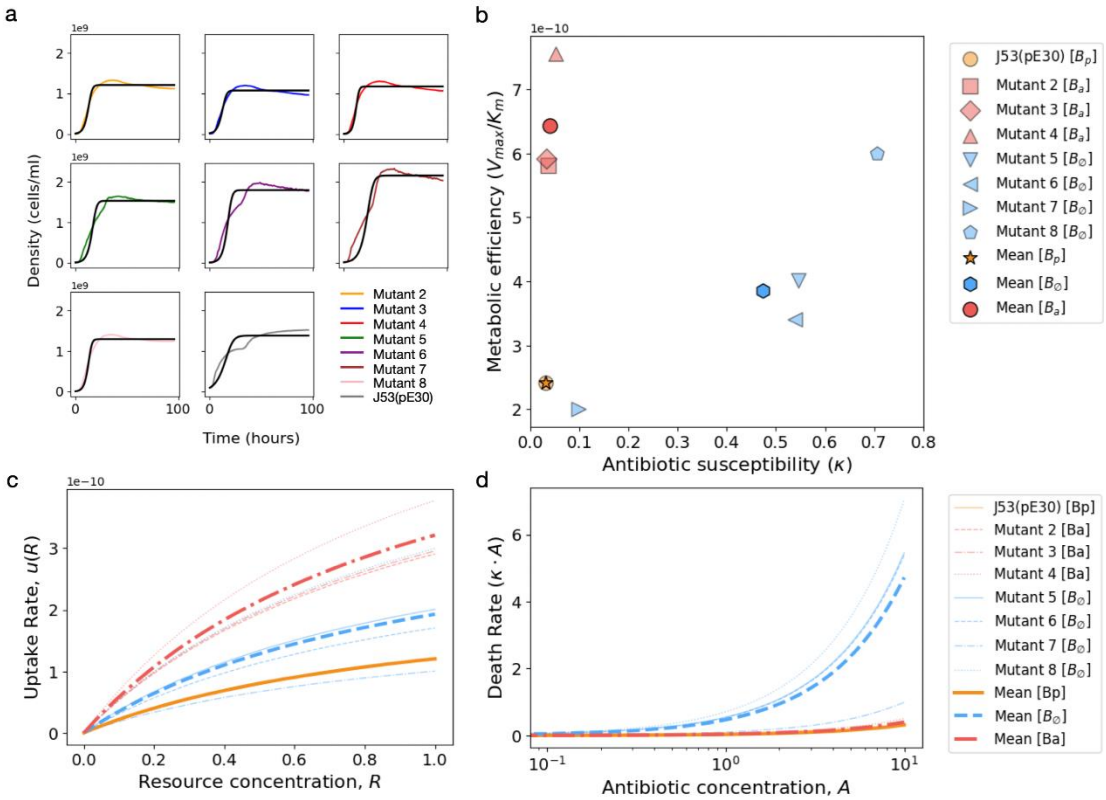

Figure 3.8 Model parametrisation. **a** Growth curves (OD measurements) for different strains grown in isolation. The black lines represent numerical model solutions using best-fit Monod parameters ($\psi = (V_{\max}/K_m, \rho)$) for each strain in the absence of selection. **b** Scatter plot showing the growth parameters ($V_{\max}/K_m$, specific affinity) on the y-axis and antibiotic susceptibility (κ) on the x-axis for calibrated strains: B_p (orange), B_a (red), and $B_\varnothing$ (blue). Mean values for each subpopulation, used in the numerical experiments, are highlighted with increased opacity. **c** Plot of uptake rate $u(R)$ vs resource concentration (R) for B_p, B_a, and $B_\varnothing$ strains. Lines with increased opacity represent the mean values used in simulations. B_a has a higher uptake rate than both B_p and $B_\varnothing$, while $B_\varnothing$ has a slightly higher uptake rate than B_p, reflecting the fitness cost of plasmid carriage. **d** Plot showing the death rate ($\kappa \cdot A$) as a function of antibiotic concentration (A, log scale) for all $B_\varnothing$, B_p, and B_a strains. Lines represent response of each strain to increasing antibiotic concentrations, with $B_\varnothing$ exhibiting a higher death rate than both B_p and B_a strains.

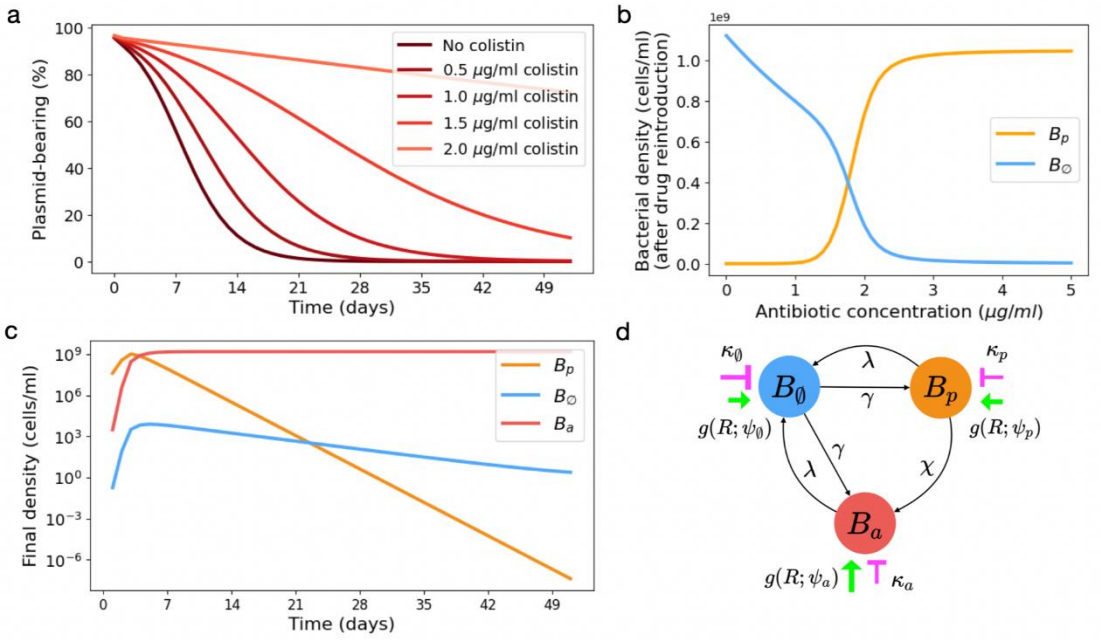

Figure 3.9 Theoretical model of J53(pE30) subpopulation dynamics. **a** Percentage of plasmid-bearing (B_p) cells over time at varying antibiotic concentrations (A) in a numerical model where B_p and $B_ø$ subpopulations compete for a single limiting resource, recorded daily for 51 days. Lines represent different A values, with red colour intensity decreasing as antibiotic concentration rises. The frequency of B_p cells, calculated as a proportion of the total bacterial population, is plotted at the end of each day. **b** Final densities after 1 day of exposure to increasing antibiotic concentrations in subpopulations previously evolved without selection for 51 days. As the antibiotic concentration increases, B_p cells recover from low initial density and becomes more prevalent. **c** Densities of B_p, $B_ø$, and B_a cells at the end of each day in the absence of selection ($A = 0$). B_a outcompetes the other strains, but both $B_ø$ and B_p persist at low densities by the end of the experiment. **d** Diagram illustrating the key processes in the dynamics of bacterial subpopulations under antibiotic selection. The orange node represents B_p cells, the blue node represents $B_ø$ cells, and the red node represents B_a cells. The resource concentration (R) is included. Growth rates (g), depending on (R) and strain-specific Monod parameters ($\psi = [V_{max}/K_m, \rho]$), are indicated by green arrows. Plasmid loss at rate λ is represented by curved arrows from B_p to $B_ø$ and B_a to $B_ø$. Plasmid transfer (conjugation) from $B_ø$ to B_p and B_a at rate γ is shown by directional arrows. Compensatory mutations, converting B_p to B_a at rate χ, are represented by a directional curved arrow. Antibiotic-induced death rates (κ) are shown as magenta blunt arrows targeting all bacterial subpopulations, with higher κ values indicating increased susceptibility.

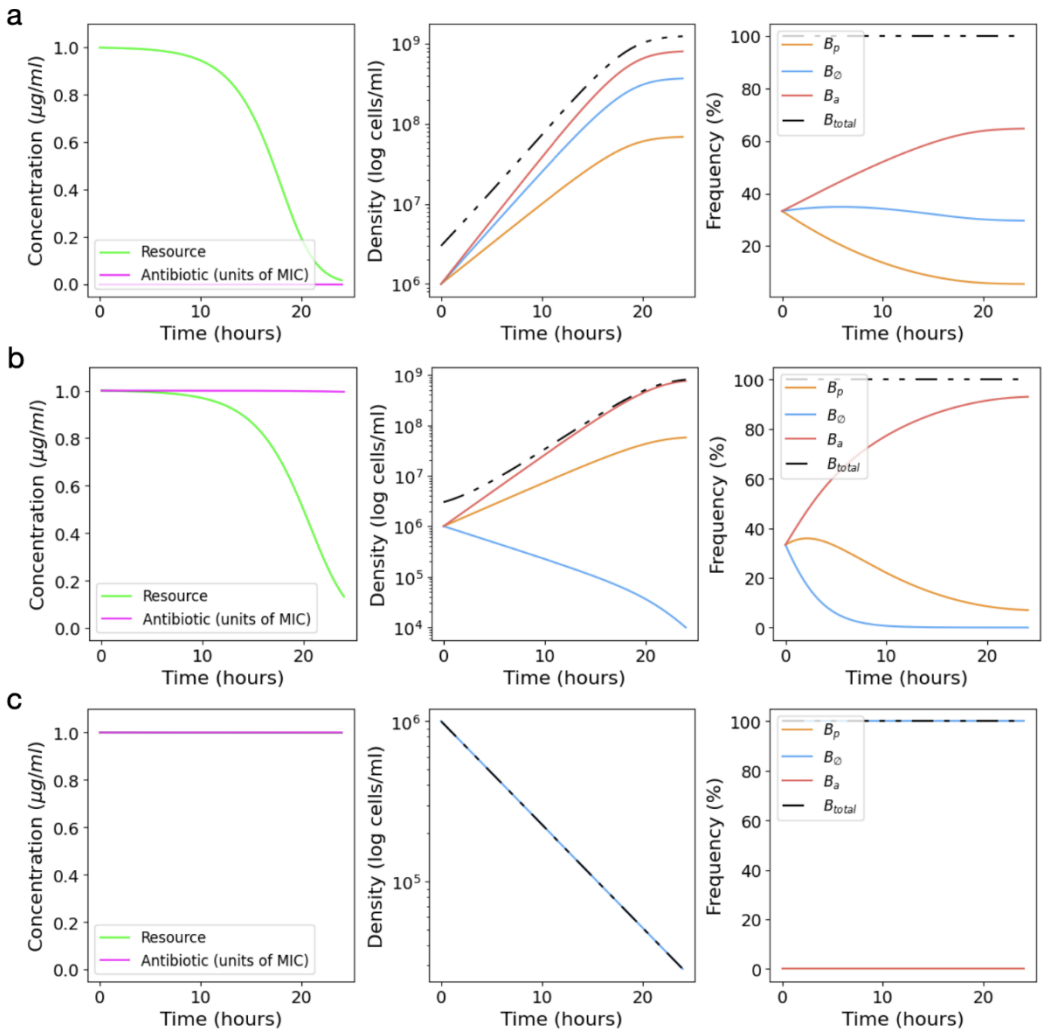

Figure 3.10 Numerical simulations showing J53(pE30) subpopulation dynamics over 24 hours under varying resource and antibiotic conditions. Each plot contains three subplots: (left) resource concentration (green) and antibiotic concentration (magenta, in MIC units); (middle) bacterial density (log scale) for plasmid-bearing (B_p, orange), plasmid-free ($B_ø$, blue) and plasmid-adapted (B_a, red) subpopulations, with total bacterial density shown as a dashed black line; (right) frequency of each subpopulation in corresponding colours. **a** No antibiotic (A = 0), with equal initial densities of B_a, B_p, and $B_ø$. **b** Antibiotic (A = 1), with equal initial densities of B_a, B_p, and $B_ø$. **c** Antibiotic (A = 1), with only $B_ø$ subpopulation included in the simulation. Initial densities for each subpopulation were set at 10^6 cells.

3.3.8 Low virulence in the evolved Day 51 strain mutants

A *G. mellonella* infection model was employed to study the virulence of the seven strain mutants isolated from Day 51 J53(pE30) biofilm populations (no colistin) post-evolution and compare them to the original J53(pE30) strain at Day 0 (**Figure 3.11**). With an inoculum of 10^8 CFU/ml, only *G. mellonella* infected with mutant 2 and 7 showed a significantly reduced survival rate after 72 h when compared to J53(pE30) (P = 0.0013 and 0.0117, respectively), indicating these two evolved mutants had increased virulence than their parent strain. However, when *G. mellonella* was infected with an inoculum of 10^7 CFU/ml, no significant differences in survival rate were observed for any of the seven mutants when compared to J53(pE30).

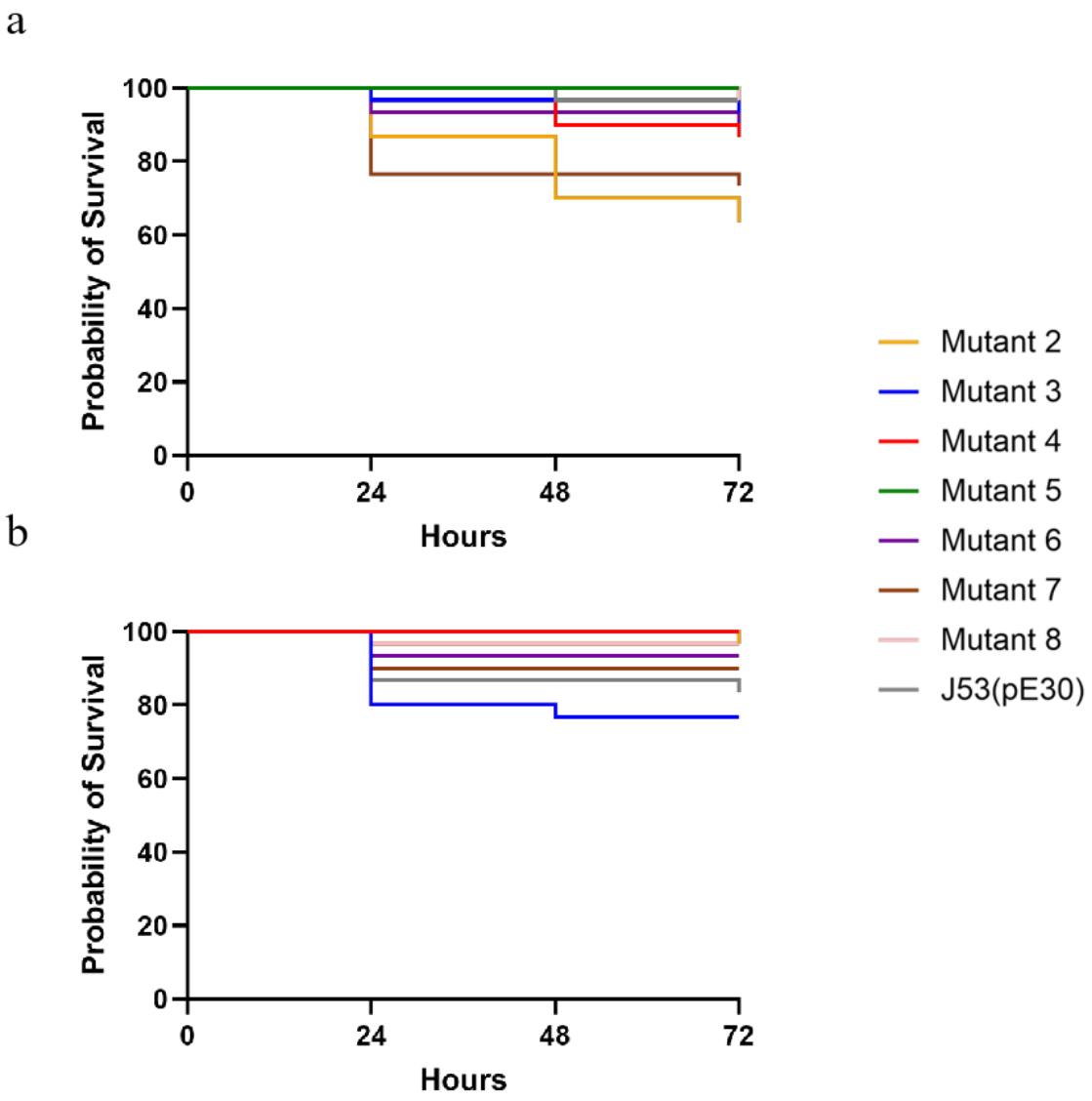

Figure 3.11 Kaplan-Meier survival curves of *G. mellonella* larvae infected with J53(pE30) or strain mutants 2, 3, 4, 5, 6, 7 or 8 isolated from Day 51 J53(pE30) biofilm populations (no colistin). Bacterial inocula were prepared in 0.85% saline at two different concentrations: **a** 10^8 and **b** 10^7 CFU/ml; n=3. Pairwise comparison between survival curves was achieved by using Log-rank (Mantel-Cox) tests (*P* value cutoff was set at 0.05). The majority of the strain mutants tested at both inoculation concentrations showed no significant differences in *G. mellonella* survival rate when compared to the Day 0 J53(pE30) (except mutant 2 and 7 at 10^8 CFU/ml), indicating low virulence in the evolved Day 51 J53(pE30) mutants.

3.4 Discussion

Competition experiments and plasmid stability testing represent an effective and reliable experimental method to investigate the fitness effects associated with *mcr*-carrying plasmids. To date, diverse plasmids have been reported to carry the *mcr-1* gene, including IncI2, IncX4, IncHI1, IncHI2, IncFI, IncFII, IncP and IncK (Donà et al. 2017; Poirel et al. 2017a; Wang et al. 2017a). Studies on *mcr-1* carried on plasmids from different incompatibility groups has generated evidence that *mcr-1* confers a fitness cost on the host strain. Competition of *E. coli* EC600 transconjugants of *mcr-1*-harbouring plasmids of various replicon types against the plasmid-free recipient strain EC600 in a 24 h competition experiment showed that the relative fitness of all the *mcr-1* transconjugants was < 1, indicative of a fitness cost, although the plasmids could still be stably maintained in the host strain in a 10-day passage assay (in the absence of antibiotic selection) (Cheng et al. 2021). Similarly, Wu et al. (2018) compared the stability of five *mcr-1*-harbouring plasmids, from IncX4, IncHI2, IncI2, IncY, and IncFII incompatibility groups, by serial passage of *E. coli* DH5α transformants of each in an antibiotic-free environment for 14 days. All plasmid types remained stable in *E. coli* up to Day 14 except for the IncFII plasmid, which showed a sharp decline from Day 5 onwards. In a further 96 h competition assay, the five *mcr-1* plasmid-harbouring *E. coli* transformants were each made to compete against the plasmid-free *E. coli* DH5α. The authors found that the strains carrying IncI2 and IncX4 showed increased fitness, while carriage of IncHI2, IncY and IncFII plasmids imposed a fitness cost on the host,

with IncHI2, although maintained stable in the passage assay, being the most disadvantageous. These findings also suggest that the *mcr-1* gene, when carried on different plasmids, may show different fitness effects on the host bacterium.

IncHI2 is a common plasmid replicon type among various *mcr-1*-carrying plasmids (Matamoros et al. 2017; Poirel et al. 2017a). IncHI2 plasmids are usually large in size, exceeding 200 kb. Such large plasmids, when carrying *mcr-1*, might be assumed to impose a considerable metabolic cost on bacterial hosts and may be lost during bacterial cell division. However, studies that have specifically focused on the stability and fitness costs of *mcr-1*-bearing IncHI2 plasmids have suggested that this might not always be the case. In an *E. coli* J53 transconjugant, pMCR1_1943, an *mcr-1*-harbouring 265.5-kb IncHI2 plasmid, was monitored over 14 days in a plasmid stability test (Ma et al. 2018). pMCR1_1943 was stably maintained in the host strain after 880 generations in nutrient-rich LB and for 220 generations in nutrient-restricted M9 broth. Furthermore, the initial fitness costs imposed by pMCR1_1943 (in both broths) were largely compensated for after a 14-day passage, as determined by 24 h head-to-head competition assays. The authors argued that the stable maintenance and the significantly reduced cost after passage may contribute to the widespread prevalence of *mcr-1*-carrying IncHI2 plasmids. Similar findings were seen in another study with the 236.3-kb IncHI2 plasmid pFS13Z2S carrying *mcr-1*, which was stably maintained in the parental *E. coli* strain for over 200 generations after passage in LB broth without antibiotic selection (Sun et al. 2018).

In contrast to the evidence described above, other studies have reported a rapid plasmid loss and significant fitness costs associated with carriage of *mcr-1*-positive IncHI2 plasmids. In a 10-day serial transfer assay in the absence of colistin, two out of three *mcr-1*-bearing IncHI2 plasmids demonstrated high retention (>85%) in their respective parental strains, but an almost complete loss (<5%) in the transconjugant *E. coli* J53, with the remaining IncHI2 plasmid showing a comparable partial loss (~30-40%) in both the parental and transconjugant strains (Lima et al. 2022). Similarly, Tietgen et al. (2018) conducted 72-h pairwise competition experiments between transconjugants harbouring the clinical 217-kb IncHI2 *mcr-1* plasmid pKP2442 and their respective isogenic recipient strains (*E. coli* J53 or *K. pneumoniae* PRZ). Plasmid carriage did not alter the fitness in J53 (plasmid-carrying and plasmid-free hosts having similar growth patterns), but did impose a significant competitive disadvantage in *K. pneumoniae* PRZ, indicating a clear difference in fitness costs in these different host species. Findings like these may suggest that the stability profile and fitness costs of *mcr-1*-carrying IncHI2 plasmids are actually bacterial host-dependent.

Few studies to date have directly compared plasmid stability and competitiveness between different *mcr* genes. A pioneering study by Yang et al. (2020) developed two competition models, comparing *mcr-1* and *mcr-3* plasmid stability in planktonic bacterial populations using qPCR. In the first model, three wild-type *E. coli* strains, PN4, PN24 and PN42, with co-existence of both *mcr-1* and *mcr-3.1* plasmids, were independently passaged over 14 days, with or without the presence of colistin (Yang et

al. 2020). In all cases, slow loss of *mcr-1* was observed, while the abundance of *mcr-3.1* plasmids (after a brief initial drop) rebounded, with the overall ratio of *mcr-3.1*/*mcr-1* increasing over the time of the experiment. In the second model, *E. coli* J53 transconjugants harbouring either *mcr-1* plasmids (IncX4) or *mcr-3.5* plasmids (IncF) were produced; and were grown either in monoculture or co-cultured over the course of 14 days, in the absence and presence of colistin (Yang et al. 2020). Here, a decreased abundance of both *mcr-1* and *mcr-3.5* plasmids was evident in both mono-cultures and co-cultures, suggesting that the *mcr* plasmids in this host also induced a fitness cost. However, again, the ratio of *mcr-3.5*/*mcr-1* plasmids gradually increased under direct competition in co-culture, a finding indicative of the higher stability (less fitness cost) of *mcr-3* plasmid carriage compared to that of *mcr-1*. Although successfully shedding light on the stability differences between *mcr-1* and *mcr-3* plasmids, these studies were only performed on planktonic cells.

I developed a bead biofilm model to examine the stability of *mcr-1* and *mcr-3* plasmids separately in monoculture biofilm populations, following serial passage over 51 days. IncHI2 plasmids of similar size were utilised to carry *mcr-1* and *mcr-3* to minimise potential 'incompatibility group' effects on plasmid stability caused by plasmid features, and the same host *E. coli* J53 was used to ensure an equivalent genetic background. Both *mcr* plasmids were found to be stably maintained throughout the experiment under colistin selection (at 0.125 and 1 μg/ml). Conversely, in the absence of colistin, the *mcr-1* plasmid was lost after 23 days, whereas the *mcr-3* plasmid, although in decline,

persisted until Day 51, thereby further supporting the hypothesis that *mcr-1* plasmid carriage has a greater instability/fitness cost in *E. coli* than *mcr-3* plasmid carriage.

In the present study, all 4 replicates from the Day 51 *E. coli* J53(pE30) *mcr-1* biofilm populations (evolved without colistin selection) in the bead biofilm model tested negative for *mcr-1* by RT-qPCR, and 3/4 replicates (replicates 2, 3 and 4) were *mcr-1* missing by PCR and tested susceptible to colistin with the MIC being only 0.5 µg/ml compared to the initial MIC of 8 µg/ml, indicating a nearly complete loss of the *mcr-1* plasmids and significant colistin resistance reduction in the *E. coli* biofilms after evolution. Loss of *mcr-1* colistin resistance in the bead biofilm model without selection described here is in keeping with another recent biofilm study, which also showed partial loss of *mcr-1*-carrying plasmids in *E. coli* isolated from poultry (Al Mana et al. 2022). In this case, biofilm growth was considerably shorter, only being studied at Days 3 and 6, and all the isolates harboured between 4 and 9 different plasmids. Replicate 1 in this study was the exception, demonstrating rapid resurgence of resistance (within 20 h) after reinstatement of colistin selection. I hypothesised that this could be due to the low-level persistence of small numbers of *mcr-1*-carrying cells (outside the levels of RT-qPCR detection) within the biofilm. To test this conjecture, the MIC plates were incubated for a further 28 h. Surprisingly, this showed that low-level persistence of *mcr-1* was also present in replicates 3 and 4 (which had initially tested *mcr-1* negative), as confirmed by PCR and so could be a more widespread phenomenon than originally thought. Similar findings have been described by Lima et

al. (2022) in the absence of colistin selection over a 10-day experimental period for 6 different *mcr-1* plasmids. Here, *mcr-1* loss from the microbial population was shown to be highly variable, ranging between complete retention or loss. The authors went on to suggest that *mcr-1* may be more stably maintained in IncHI2 plasmids (where they are often found) compared to, for example, IncP plasmids, which rarely carry *mcr* genes. In contrast to these short-term evolutionary experiments by other authors, my results provide clear evidence that long cessation of colistin use (>50 days) from veterinary and clinical settings may not effectively help to eliminate *mcr*-associated colistin resistance, because a small proportion of *mcr*-positive bacteria will persist in an apparently colistin-susceptible biofilm population, only to rapidly re-emerge when re-exposed to colistin.

To monitor the longitudinal changes in the biofilm-forming ability of the evolving *E. coli* J53(pE30) biofilm populations in the bead biofilm model, which might be a useful indicator of the overall fitness dynamics for individual biofilm populations, I compared the biofilms grown from Day 23 and 51 biofilm populations for three replicates. Here, I found that replicates 2 and 3 showed an increase in overall biofilm fitness during evolution, with the biofilm-forming phenotype changing from apparently 'unhealthy' (poor and weak growth) at Day 23 to more 'healthy' (vigorous growth) at Day 51, regardless of the presence or absence of colistin exposure. This contrasted with replicate 1, where the exact opposite was found. It is known that the evolution of a biofilm population of a single strain can give rise to strain variants of differential

biofilm-forming phenotypes due to diversification in unique niches within the biofilm (Steenackers et al. 2016; Oakley et al. 2021; Henriksen et al. 2022). Thus, the dynamics of the overall biofilm-forming capacity of a population during evolution is closely linked to and shaped by the biofilm-forming capacity of its individual diversified subpopulations at a certain particular timepoint, which is a complex and unpredictable process. This might explain the differences seen between the biofilm replicates of J53(pE30) in our biofilm formation assay, as replicate 1 and replicates 2 and 3 may have undergone different diversification processes and generated subpopulations of varied biofilm-forming phenotypes. However, my study emphasises the possibility that a *mcr-1* biofilm population of *E. coli* can evolve with increasing biofilm fitness, as manifested in the enhanced biofilm-forming ability of replicates 2 and 3. Another interesting observation in this assay is that when horizontally comparing between the three replicate biofilm populations at Day 51 with no colistin selection, replicate 1 generated biofilms of reduced viability and biomass when compared to replicates 2 and 3. I hypothesised that this could be associated with a relatively higher number of the remaining *mcr-1*-positive cells persisting in the replicate 1 biofilm population at Day 51, with replicate 1 being quickest to react to colistin re-exposure. Similar effects of *mcr-1* in biofilm assembly have been reported before, with *mcr-1* overexpressing *E. coli* TOP10 (*mcr-1*/pBAD) biofilms showing a marked decrease in cell viability compared to the *mcr-1*-free *E. coli* TOP10 (pBAD) biofilms (Yang et al. 2017).

Plasmid genetic adaptation is a critical factor that contributes to improved fitness costs

and prolonged persistence of large conjugative plasmids in *E. coli* hosts (Porse et al. 2016). To investigate the adaptive compensation that occurred in the *mcr-1*-bearing IncHI2 plasmid pE30 during long-term evolution in *E. coli* biofilm without colistin selection, I isolated *mcr-1*-positive or negative isolates from the four replicates of the evolved Day 51 J53(pE30) biofilm populations and performed WGS. I identified three distinct evolutionary trajectories in pE30 by comparison with the original Day 0 J53(pE30). For those plasmids that had retained *mcr-1*, an intact Tn*6330* and an identical partial deletion of the MDR region were detected for all three independently evolved isolates (9/13 ARGs were lost), whereas for those plasmids that had lost *mcr-1*, the plasmids were either completely eliminated from the host or had a deletion of a substantial DNA segment, including the whole MDR region and a truncated Tn*6330* (the IS*Apl1* element downstream of *mcr-1-pap2* remained in the plasmid). Interestingly, similar deletion patterns for *mcr-1* on plasmids after passage in planktonic culture have been reported in the literature. Zhang et al. (2019b) characterised the stability of a ~232 kb MDR plasmid harbouring both *mcr-1* and *mcr-3.19* in *E. coli* CP53 by serial passage in LB broth for 28 days without colistin exposure. Samples were taken at 7, 14, 21 and 28 days with three deletion mechanisms found to account for the loss of *mcr-1*. Similar to my study, one clone had lost the whole plasmid, two clones underwent excision of the IS*Apl1-mcr-1-pap2* segment from Tn*6330* leaving only the downstream IS*Apl1* in the plasmid, and two clones were found to have large DNA deletions (44 kb and 63 kb, respectively) containing a large part of the MDR region and *mcr-1*, with the downstream excision boundary again being within Tn*6330* between *mcr-1-pap2* and

the downstream IS*Apl1* element (Zhang et al. 2019b).

A similar WGS study performed on two colistin-susceptible isolates following a 20-day passage of *E. coli* W5-6 carrying an *mcr-1* MDR IncHI2 plasmid under colistin-free conditions (normal or static) again revealed either total plasmid loss, or DNA deletion of a 37 kb fragment containing functional genes and a truncated *mcr-1*-bearing Tn*6330* (the excision site being exactly between *mcr-1-pap2* and the downstream IS*Apl1*) (Wu et al. 2021b). Similarly in *E. coli* HS30-1, although *mcr-1*-encoding Tn*6330* carried by the hybrid (IncFIB and a phage-like replicon) pHS30-1 plasmid was found to be very stable in bacterial populations after a 15-day passage without colistin selective pressure, Tn*6330* could be reduced in size to a single IS*Apl1* element, indicating an IS*Apl1*-mediated *mcr-1* deletion (Li et al. 2019). These phenomena of DNA rearrangements and/or *mcr-1* deletion seen in these previous studies may be a reflection of a universal route for *mcr-1*-bearing plasmids to compensate their fitness costs during evolution in planktonic bacterial populations. My study highlights, for the first time, the possibility of reducing fitness cost of *mcr-1*-bearing plasmids in an evolved biofilm population by deleting only antibiotic resistance genes from a MDR region, thus preserving colistin resistance in the biofilm.

Mathematical modelling provides a framework to explore how compensatory mutations and plasmid dynamics contribute to the persistence of resistance in the absence of antibiotic selection in the bead biofilm model. My simulations enabled us to explore scenarios where plasmid carriage either imposed fitness costs or provided a competitive

advantage under a range of environmental conditions. Building on previous studies (Zwanzig et al. 2019; Alonso-del Valle et al. 2023), the model integrated key biological processes governing plasmid dynamics including plasmid loss, conjugation and the emergence of plasmid-adapted cells via compensatory mutations. The numerical simulations predicted that compensatory mutations may effectively mitigate the fitness cost of plasmid carriage (San Millan and MacLean 2017), enabling resistance determinants (such as *mcr-1*) to persist under non-selective conditions. Furthermore, the simulations anticipated that the plasmid-bearing populations would re-emerge following re-exposure to antibiotics, emphasising the role of adaptive evolution in shaping resistance dynamics in bacterial populations (Wein et al. 2019; Rodríguez-Beltrán et al. 2021). These findings complement previous studies on the small non-conjugative plasmid pNUK73 where compensatory adaptation and selective pressures were shown to act together to stabilize the plasmid over time (Millan et al. 2014). These theoretical results emphasise the role of compensatory mutations in plasmid persistence, highlighting the evolutionary dynamics which shape bacterial populations under the different environmental conditions that exist within biofilms *in vivo* (Santos-Lopez et al. 2019).

Virulence is characterised as "the relative capacity of a microorganism to cause damage in a host" (Casadevall and Pirofski 2003). LPS serves as an important virulence factor in Gram-negative bacteria, having been associated with the induction of robust immune responses in animals, and the lipid A component of LPS is pivotal in mediating immune

and inflammatory responses, primarily through the initial secretion of cytokines (Baeuerlein et al. 2009; Kabanov and Prokhorenko 2010). Therefore, alterations of lipid A caused by *mcr-1* carriage for example, may correlate with alterations in virulence. Several studies have evaluated the impact of *mcr-1*-conferred colistin resistance on bacterial virulence but have yielded conflicting findings. Li et al. (2021) compared an *mcr-1*-expressing *E. coli* TOP10 (*mcr-1*/pBAD) to an empty vector control and found that it exhibited significantly increased capacity to penetrate the epithelial barrier formed by Caco-2 cell monolayer in a trans-well model *in vitro.* In addition, in an *in vivo G. mellonella* infection model, rapidly decreased larvae movement and increased melanisation within 1 h after injection were observed, with the concentration of released LPS detected in the corresponding larval fluid also being significantly higher, indicating enhanced virulence associated with *mcr-1* expression. However, the study by Yang et al. (2017) found exactly the opposite, namely that the modified LPS extracted from *mcr-1*-expressing *E. coli* TOP10 (*mcr-1*/pBAD) was shown to induce lower production of cytokines (IL-6 and TNF-α) in human macrophages (THP-1) compared to the unmodified LPS extracted from *E. coli* TOP10 (pBAD). Furthermore, the authors demonstrated significantly reduced *G. mellonella* survival rates when infected by four *mcr-1*-free clinical *E. coli* strains compared to their respective *mcr-1* transformants, suggesting a reduction in virulence when acquiring *mcr-1* (Yang et al. 2017). Inconclusive results were reported in yet another study, where acquisition of *mcr-1* carried on a natural IncHI2-type plasmid pKP2442 or a constructed TOPO expression vector plasmid did not significantly influence bacterial

virulence in both the parental strains *E. coli* J53 and *K. pneumoniae* PRZ, with no substantial effects noted in *G. mellonella* survival and cytotoxicity towards A549 human lung epithelial cells (Tietgen et al. 2018). In the *G. mellonella* infection experiment conducted in my study, I found the majority of the mutants (having either lost or retained *mcr-1*) isolated from Day 51 J53(pE30) biofilm populations evolved under no colistin in the bead biofilm model showed comparable virulence with the original *mcr-1*-bearing J53(pE30) strain at Day 0. This may suggest that carriage of *mcr-1* alone may not be a critical factor in determining virulence in *E. coli* J53(pE30).

3.5 Conclusion

In line with previous literature, *mcr-1* plasmid carriage in *E. coli* biofilms was found to impose a higher fitness cost than *mcr-3* plasmid carriage, as evidenced by rapid loss of *mcr-1* (Day 23) and persistence of *mcr-3* (for >51 days) in the absence of colistin selection in the bead biofilm model. Interestingly, comparing evolved populations from Day 23 and Day 51 in the absence of colistin, distinct increases in biofilm-forming ability were noted with time alongside loss of colistin resistance, only to be quickly reversed on re-exposure to colistin (<48 h). WGS demonstrated that one of three apparent compensatory adaptations occurred to counter the fitness cost of *mcr-1* carriage in *E. coli* biofilms, taking the form of either complete plasmid loss, loss of *mcr-1* alongside complete deletion of the MDR region, or partial loss of the MDR region but continued maintenance of an intact *mcr-1*. Mathematical modelling of plasmid dynamics incorporating compensatory mutations supports the observed persistence of *mcr-1* in the absence of selection and its re-emergence following renewed colistin exposure. The mutant strains (with or without *mcr-1*) isolated from Day 51 *mcr-1 E. coli* biofilm populations showed no significant differences in bacterial virulence compared to the parental strain at Day 0 in a *G. mellonella* infection model.

Chapter 4

Escherichia coli bacterial membrane interactions with epoxytiglianes and colistin

4.1 Introduction

4.1.1 EBC-1013 and its analogues

Although natural EBCs show promise as antimicrobial agents, availability is limited due to their low yield from plants. Therefore, a range of semi-synthetic and synthetic derivatives have been developed, including EBC-1013, a semi-synthetic EBC with a similar structure to EBC-46, but with the C12 and C13 ester linkages modified to hexanoate ester chains (**Figure 4.1a)** (Powell et al. 2022; Xue et al. 2023).

The direct antibacterial effects of EBC-1013 have been previously shown against planktonic bacteria and were largely limited to Gram-positive bacteria, as demonstrated by the inhibition of planktonic growth of methicillin-resistant *S. aureus* (MRSA) and *Streptococcus pyogenes* at MIC values of 512 and 256 µg/ml, respectively (Powell et al. 2022). Although EBC-1013 did not inhibit or reduce Gram-negative bacterial planktonic growth and cell viability (*P. aeruginosa* and *E. coli*), it significantly inhibited swarming motility, and reduced the production of extracellular virulence factors, e.g., pyocyanin and rhamnolipid, of *P. aeruginosa* (Powell et al. 2022). EBC-1013 also induced a significant increase in cell membrane permeability in *P. aeruginosa, S. aureus* and *E. coli* (Powell et al. 2022), which is a key mechanism of action mediating the antibacterial activity of some previously reported terpenoids (Di Pasqua et al. 2007; Mulyaningsih et al. 2010; Nazzaro et al. 2013).

The direct antibiofilm effects of EBC-1013 have also been studied. *E. coli* and *S.*

aureus biofilm formation in the presence of EBC-1013 significantly decreased the viability of the cells within the biofilms, and EBC-1013 treatment disrupted pre-established bacterial biofilms (*S. pyogenes*, *A. baumannii*, *E. coli*, and *P. aeruginosa*), with the resulting biofilms showing significantly decreased biofilm biovolume and thickness (Powell et al. 2022). Furthermore, EBC-1013 induced significant changes in the EPS matrix of *E. coli* biofilms, leading to altered biofilm mechanics such as increased creep compliance, as determined by a multiple-particle tracking assay (Powell et al. 2022). This antibiofilm activity of EBC-1013, along with its innate immune induction effects (e.g., cytokine/chemokine production and inflammatory cell recruitment), represents the underlying mechanism for the observed rapid *in vivo* healing of infected, chronic, non-healing skin wounds (Powell et al. 2022).

Recently, two semi-synthetic EBC-1013 analogues, a deuterated EBC-1013 and an alkyne EBC-1013, have been synthesised, with their molecular structures resembling that of EBC-1013 but with modifications in the C12 and C13 ester chains. Both deuterated EBC-1013 and alkyne EBC-1013 have identical C12 and C13 chain lengths to EBC-1013; however, the former contains 22 atoms of deuterium (**Figure 4.1b**) and the latter possesses two terminal triple bonds (**Figure 4.1c**). To aid identification of the antimicrobial agents by specific deuterium atom or triple bond signatures, the two analogues were used alongside EBC-1013 in certain experiments. In addition, a naturally occurring epoxytigliane EBC-147 with a short C12 propanoate ester and C13 methylbutyrate ester (**Figure 4.1d**) was included in a molecular dynamics simulation

study as negative control, as it was known to display minimal antimicrobial activity (Powell et al. 2022).

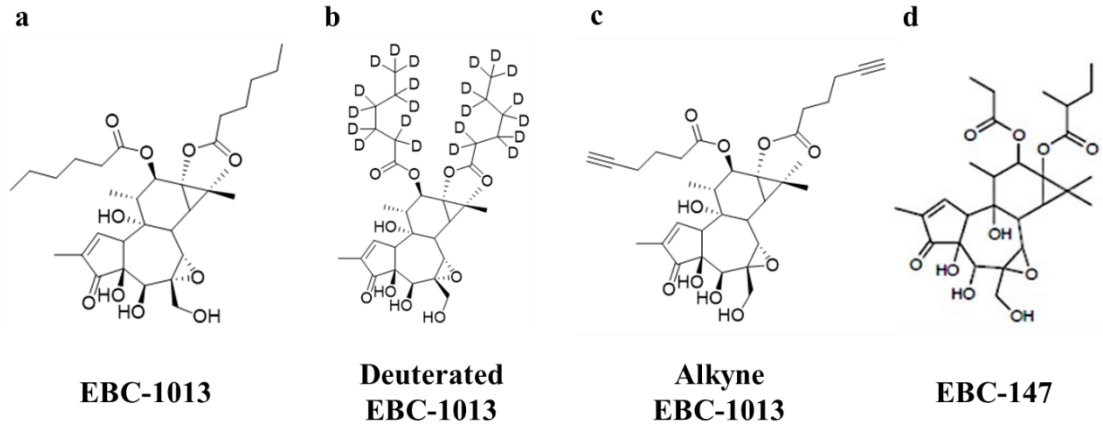

Figure 4.1 Molecular structures of epoxytiglianes used in this chapter. **a** EBC-1013; **b** Deuterated EBC-1013; **c** Alkyne EBC-1013; **d** EBC-147. (Courtesy of Qbiotics Group Ltd).

4.1.2 Molecular dynamics simulation

Molecular dynamics (MD) simulation is a computational technique that simulates and analyses the physical movements and interactions of atoms/molecules in a modelled system for a fixed duration of time, thereby giving insights about the dynamic evolution of the system at femtosecond temporal resolution (Badar et al. 2022). MD simulation has a diverse range of applications across various fields, including biology, physics, chemistry, materials science, meteorology, etc., and when applied in biological science, it represents a powerful tool to thoroughly study the structure and dynamic behaviour

of biomolecules and their complexes during biological processes. Although the first introduction of MD simulation was as early as in the late 1950s (Alder and Wainwright 1957), it was not until 1977 that the biological application, like protein MD simulation, was first performed (McCammon et al. 1977). In the past two decades, MD simulations have gained significant popularity and visibility with biologists. They have been employed in the following applications: to observe and study the conformational changes, movement, and interactions of biomolecules (e.g., proteins); to assess and refine the accuracy of modelled structures; to explore how a biosystem responds to introduced perturbation; to facilitate drug discovery by designing or screening for drug molecules with desired target binding; and to monitor the dynamic evolution and behaviour of a biosystem on a relatively long timescale.

The principle behind an MD simulation is simple. For a given modelled biomolecular system with the positions of all the atoms known, one can compute the force applied to each atom by all of the other atoms based on the chosen physical model of force field governing interatomic interactions. Thereafter, Newton's laws of motion can be used to calculate the spatial position and velocity of each atom as a function of time (Hollingsworth and Dror 2018). By repeating this process at each time step throughout the simulation time, a three-dimensional (3D) motion trajectory of the system is generated at an atomic level by applying algorithms that integrate the equations of motion using the finite difference method. A force field is an empirical set of energy functions that describe the energy associated with atomic interactions (Mayo et al. 1990)

and typically incorporates terms such as bond stretching, bond angle bending, bond torsion, electrostatic (Coulombic) interactions, Van der Waals interactions, hydrogen bond interactions, etc. (Badar et al. 2022). AMBER, CHARMM, and OPLS are some of the most common force field options used in MD simulations (Harder et al. 2016; Huang et al. 2017; Robustelli et al. 2018). A series of steps are involved in performing a typical MD simulation, and these include system preparation (i.e., model selection, choosing a force field, creating a simulation box, solvating the system, and adding counterions), energy minimisation, equilibration, production run, and data analysis. Software used for MD simulations includes GROMACS, NAMD, AMBER, CHARMM, Desmond, and OpenMM (Phillips et al. 2005; Bowers et al. 2006; Brooks et al. 2009; Abraham et al. 2015; Eastman et al. 2017).

MD simulations have been widely employed to investigate biological membranes, including the bacterial cell envelope. Molecular modelling of the bacterial cell envelope in Gram-negative bacteria has progressed from simple outer membrane models of smooth LPS monolayers (Kotra et al. 1999) to complex models that encompass the outer membrane, peptidoglycan, inner membrane, and associated proteins (Boags et al. 2019). However, as the outer membrane is the first barrier that antimicrobials encounter and interact with before initiating their (bacteriostatic or bactericidal) activity, mechanistic studies using MD simulations usually commence with outer membrane models, although more accurate and advanced models are being developed.

The Gram-negative bacterial outer membrane is an asymmetric bilayer, with the lower leaflet primarily made up of phospholipids, including phosphatidylethanolamine (PE), phosphatidylglycerol (PG), and cardiolipin (CL), while the upper leaflet is mainly comprised of LPS molecules (Sharma et al. 2024). The lipid composition of the lower leaflet differs among bacterial strains. For example, *E. coli* exhibits a PE:PG:CL molar ratio of 90:5:5, whereas *P. aeruginosa* demonstrates a constitution of 60:27:13 (Sharma et al. 2024). The LPS molecules in the upper leaflet are composed of lipid A connected to a sequential extension of core oligosaccharide (composed of inner core and outer core sugars) and O-antigen polysaccharide (Pogozheva et al. 2022). Similarly, the sugars making up the core oligosaccharide and O-antigens vary across bacterial strains, making LPS structures highly diverse. Despite this, the integration of the LPS modeller into the CHARMM-GUI web server has significantly expanded the LPS database and advanced the construction of increasingly realistic bacterial outer membrane models.

4.1.3 X-ray photoelectron spectroscopy

X-ray photoelectron spectroscopy (XPS) is a surface-sensitive analytical technique used to obtain information about the elemental composition and chemical states of material surfaces (Ramstedt et al. 2011). The sample should be free of any contaminants or oxides that could potentially interfere with the analysis and should be placed in a vacuum chamber to eliminate contamination from air molecules. The analysis depth of XPS is determined by the escape depth of electrons and depends on the sample nature. For biological materials, this probing depth is typically restricted to

the top ~10 nm of the sample (Ramstedt et al. 2011).

The XPS technique relies on the photoelectric effect as its underlying mechanism. When an X-ray beam irradiates the surface of a sample, interacting with the local atoms, photoelectrons from these atoms are emitted. The kinetic energy of an emitted photoelectron is determined by the energy of the incident X-ray and its binding energy to the atom from which it originates. The binding energy of an electron is not only characteristic of its parent element and the electronic orbit it occupies, but also reflects the chemical environment of the atom (e.g., in different functional groups). Therefore, by knowing the energy of the incoming X-ray beam and measuring the kinetic energies of the released photoelectrons, XPS generates a binding energy spectrum that carries information about the chemical composition of the sample. A typical XPS spectrum shows the number of electrons emitted at each binding energy level, and the peaks in the spectrum correspond to the binding energies of electrons from specific elements and their chemical states present in the sample.

XPS as a method to characterise the elemental composition of microbial cell surfaces has been used for decades. Microbial samples can be freeze-dried before XPS analysis, a process allowing for the creation of powders that are appropriate for insertion into the high vacuum environment required (Wei et al. 2021). Despite the complexity of the biomolecules present in microbial cell surfaces, XPS is still able to quantitatively detect carbon, nitrogen, oxygen, and phosphorus as the main elements within the outermost portion of microbial cells (Wei et al. 2021). Interpretative models exist to convert these

elemental compositions into microbial surface biological components such as proteins, polysaccharides, chitin, glucan, teichoic acid, peptidoglycan, and hydrocarbon-like compounds (Wei et al. 2021). XPS has previously been used for studies of the bacterial cell surface and has identified organic components based on the concentration fractions of various functional groups and the elemental concentration ratios with respect to total carbon. For example, XPS data has been successfully converted to peptide, polysaccharide, and hydrocarbon-like compound concentrations and used to determine the surface chemical composition of Gram-positive bacteria, including *Bacillus brevis* and coryneform bacteria (Dufrêne et al. 1997) and Gram-negative bacteria such as *Aquabacterium commune* (Ojeda et al. 2008).

The primary limitation of XPS is the limited depth at which it can effectively penetrate the cell surface. Consequently, this technique is only suitable for extracellular analysis (Sprenger and Anderson 1991). Other limitations of XPS include the inability to detect hydrogen and the necessity for a high level of vacuum, which leads to a lengthy characterisation process. Finally, it is crucial to exercise caution when performing the deconvolution of XPS peaks, as this can produce misleading results (Sprenger and Anderson 1991). Despite these limitations, XPS is still a valuable tool for analysing bacterial cell surface chemistry due to its ability to provide quantitative measurements and identify chemical bonds based on elemental characterisation (Leone et al. 2006; Hamadi et al. 2008).

4.1.4 Fourier transform infrared spectroscopy

Infrared (IR) spectroscopy-based broad spectrum molecular analysis instruments were first introduced in the 1950s (Levine et al. 1953; Riddle et al. 1956; Kenner et al. 1958). Following a number of enhancements to IR tools, scientists in the 1970s created Fourier transform infrared (FTIR) spectroscopy, and subsequently this technique was introduced to *in situ* investigation of bacteria by Naumann (1991) and Helm (1991).

FTIR can identify changes in the overall chemical composition of bacteria by detecting functional groups within molecules. It has been applied to identify bacteria (Levine et al. 1953; Riddle et al. 1956; Kenner et al. 1958; Whittaker et al. 2003), classify bacterial strains (Helm et al. 1991; Mariey et al. 2001), and differentiate between intact and damaged cells under stress conditions (Lin et al. 2004; Lorin-Latxague and Melin 2005; Al-Qadiri et al. 2008a; Al-Qadiri et al. 2008b; Alvarez-Ordóñez et al. 2010; Liu et al. 2011). Furthermore, FTIR has been employed to characterise structural changes in bacteria following treatment with various nanomaterials, including organic nanoparticles (Riding et al. 2012), quantum dots (Fang et al. 2012), and oxides (Kiwi and Nadtochenko 2005; Nadtochenko et al. 2005; Hu et al. 2007; Jiang et al. 2010; Wang et al. 2011). FTIR is generally a non-destructive analytical tool and offers several benefits, such as easy sample preparation (Carlos et al. 2011), quick spectrum analysis time (Davis and Mauer 2010), and the ability to analyse samples in various states (liquid or solid).

The radiation produced by an IR source travels through an interferometer consisting of a beam splitter, a stationary mirror, and a moving mirror (**Figure 4.2a**). The interferometer determines the wavelength of the emitted IR light so that the sample receives IR light of a specified range of frequencies. When the IR light interacts with the sample, specified frequencies are absorbed by the sample's molecules. This absorption occurs because the energy of the IR light at a specific wavelength matches the energy required to excite the various vibrational modes of the chemical bonds in the molecules, such as stretching (Picquart et al. 2000; Nydegger et al. 2011), bending (Nydegger et al. 2011; Podstawka-Proniewicz et al. 2011), scissoring (Picquart et al. 2000; Podstawka-Proniewicz et al. 2011), and twisting (Picquart et al. 2000; Nydegger et al. 2011). The transmitted IR light signal is then received by a detector and undergoes computational processing involving Fourier transform mathematical principles, which are responsible for separating the individual absorption frequencies from an interferogram (Neves et al. 2024). The final displayed result is a plot called an IR spectrum, where the x-axis represents wavenumber, while the y-axis represents absorbance or transmittance (Kiwi and Nadtochenko 2005; Nadtochenko et al. 2005; Corte et al. 2010). Each peak in the spectrum corresponds to a specific wavelength of IR light that has been absorbed by the chemical bonds in the sample. By analysing the peaks in the spectrum and comparing them to known spectra of different compounds, researchers can identify the chemical composition of the sample, and this may encompass the presence of functional groups, chemical bonding, and molecular structure.

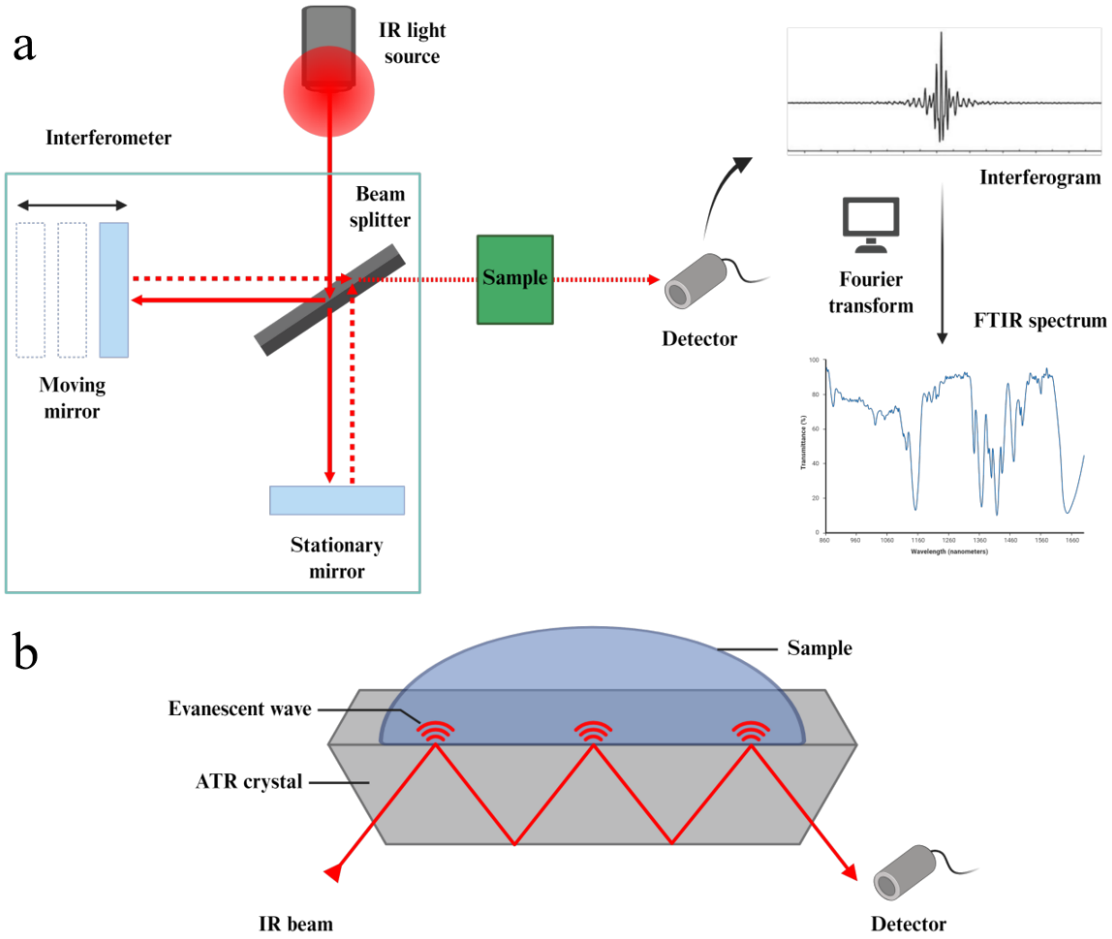

Figure 4.2 Schematic diagram of FTIR spectroscopy and attenuated total reflectance FTIR (ATR-FTIR) sampling technique. **a** The IR source generates radiation that passes through the sample via the interferometer and reaches the IR detector to produce an IR spectrum. **b** Principle of the ATR sampling method in FTIR spectroscopy. The figure was created with BioRender.com.

Attenuated total reflectance FTIR (ATR-FTIR) spectroscopy is a specific sampling method within FTIR that exploits the phenomenon of attenuated total reflectance. Unlike the traditional transmittance FTIR in which the IR beam passes through the

entire thickness of the sample, ATR-FTIR is a surface-sensitive technique, providing information primarily about the composition of the sample surface layer and the near-surface region (**Figure 4.2b**). In ATR-FTIR, the sample is dried onto a crystal surface (Winder and Goodacre 2004; Burgula et al. 2006), which can be fabricated from a variety of materials, usually with a higher refractive index in relation to the sample (Naumann 2000; Burgula et al. 2006). The IR light is sent through the ATR crystal and undergoes multiple internal reflections within it. As the light interacts with the sample at the crystal-sample interface, it generates an evanescent wave. The depth of this penetration into the sample (typically between 0.5 and 2 micrometres) depends on factors such as the refractive index of the ATR crystal, the angle of incidence, and the wavelength of the IR light. The IR spectrum is obtained by detecting changes in the evanescent light intensity resulting from the interaction of the light with the sample. ATR-FTIR has been used to investigate changes in cell membrane on *E. coli*. Wang and colleagues (2011) used ATR-FTIR to characterise the impact of nanowire photocatalysis on *E. coli*, and showed that the treated cells underwent structural changes, resulting in enhanced cell permeability.

4.1.5 Photo-induced force microscopy (PiFM)

PiFM is an emerging technique that has been developed in the last decade (Rajapaksa et al. 2010). It has now become a new-frontier nanoscale chemical imaging technique that integrates atomic force microscopy with infrared spectroscopy, enabling the concurrent collection of 3D topographical data alongside local surface chemistry

information, achieving high spatial resolution of approximately 5 nm, low depth penetration of ≤30 nm and spectral resolution of about 1 cm^{-1} (Otter et al. 2021). PiFM instruments were first made commercially available in 2016, and have since been applied to chemical imaging across various scientific fields including physics, material science, chemistry and biology. The advantages of PiFM includes its non-destructive imaging, no requirement for extensive sample preparation, easy measurement at ambient conditions and high signal-to-noise ratios due to near-field excitation and detection. Among the group of near-field AFM-based spectroscopic techniques currently in use, which include photo-thermal infrared spectroscopy (PTIR or AFM-IR) (Hammiche et al. 1999; Anderson 2000; Dazzi and Prater 2017), scattering-scanning near-field optical microscopy (s-SNOM) (Knoll and Keilmann 1999) and tip-enhanced Raman spectroscopy (TERS) (Stöckle et al. 2000; Pozzi et al. 2013), PiFM demonstrates notable robustness, user-friendliness, and broad applicability across various organic and inorganic sample types.

As the name suggests, the working principle behind PiFM imaging involves detecting the photo-induced force generated between the sample surface and the AFM cantilever tip. The physical origin of this force is very complicated and is mainly a dipole-dipole electromagnetic gradient force between a photo-induced dipole at the sample surface and a mirror dipole in the metal-coated AFM cantilever tip as a result of molecular or atomic polarisation during photo-induced excitation by the PiFM laser. The polarisability of heterogeneous samples differs based on laser wavenumber and

chemical composition, hence offering distinctive absorption regions that reliably identify various molecules within the sample matrix (Murdick et al. 2017). However, depending on the wavelength range setting, material properties and the details of the experiment, thermally modulated van der Waals forces arising from sample thermal expansion due to laser illumination may also contribute to this signature (Jahng et al. 2018; Wang et al. 2019b). For example, this can occur in organic samples with large thermal expansion coefficients; whereas in the case of inorganic materials (usually with lower thermal expansion coefficients), the dipole-dipole interaction force will be the dominant force (Rajapaksa et al. 2010; Tamagnone et al. 2018). Both components of the photo-induced force are in the order of tens of piconewtons, making them detectable with a conventional AFM (Potma et al. 2015; Jahng et al. 2019). Nevertheless, it should be noted that other mechanisms, such as thermally induced photo-acoustic force and photo-induced damping of the cantilever, may play a role as well in the physics at the illuminated tip-sample nanojunction (Sifat et al. 2022). In PiFM, the generated photo-induced forces between tip and sample surface are primarily limited to the near field, exhibiting rapid decay beyond approximately 20 nm. The near-field excitation and detection abilities of PiFM result in diminished noise levels relative to other infrared-based approaches (Rajapaksa et al. 2010; Jahng et al. 2014; Jahng et al. 2015).

The key components of the PiFM microscope are an oscillating AFM tip-cantilever system and a tunable laser that is focused onto the sample surface (**Figure 4.3**). The AFM tip is typically made of silicon coated with a conductive layer of gold or a

platinum-iridium alloy to increase the polarisability of the tip, and usually has a radius of 20 to 30 nm to minimise the number of interacting molecules (Otter et al. 2021). The cantilever beam is externally driven by a dithering piezoelectric element to force an oscillatory motion, and its movement is tracked with high precision by illuminating its surface with a laser beam (feedback laser), which reflects off and is detected by a quadrant photodiode (Sifat et al. 2022). The sample is mounted on glass, mica or silicon, and is laser-illuminated from the side with the use of an off-axis parabolic mirror (illumination from below in an inverted microscope is also common). Unlike traditional FTIR spectroscopy which utilises a polychromatic light source for the instantaneous detection of sample absorption characteristics, PiFM employs a monochromatic tunable laser that sequentially scans across a broad range of wavenumbers (Wickramasinghe and Park 2015). At specific wavelengths, the sample absorbs the irradiated IR light, polarises, and produces photo-induced forces (the PiFM signal) that are manifest in the changes in the cantilever oscillation dynamics and detected by analysing the signal of the quadrant photodiode. Since this process taps into the distinct, fingerprint-like IR absorption characteristics of molecules, peak positions in PiFM spectra align closely with those in traditional far-field FTIR spectra (Nowak et al. 2016; Jahng et al. 2018). For optimal imaging, PiFM is generally conducted in sideband detection mode using a dynamic amplitude modulation method (Jahng et al. 2016). Under this setting, the driving frequency of the cantilever is chosen to coincide with its second mechanical resonance at frequency f_2 for recording the topographic signal, while the PiFM signal is derived from the oscillation amplitude of

the cantilever at its first mechanical resonance frequency f_1, which is driven by modulating or pulsing the infrared laser at the sum or difference frequency of f_2 and f_1. By utilising two lock-in amplifiers, both topography and PiFM images are acquired simultaneously.

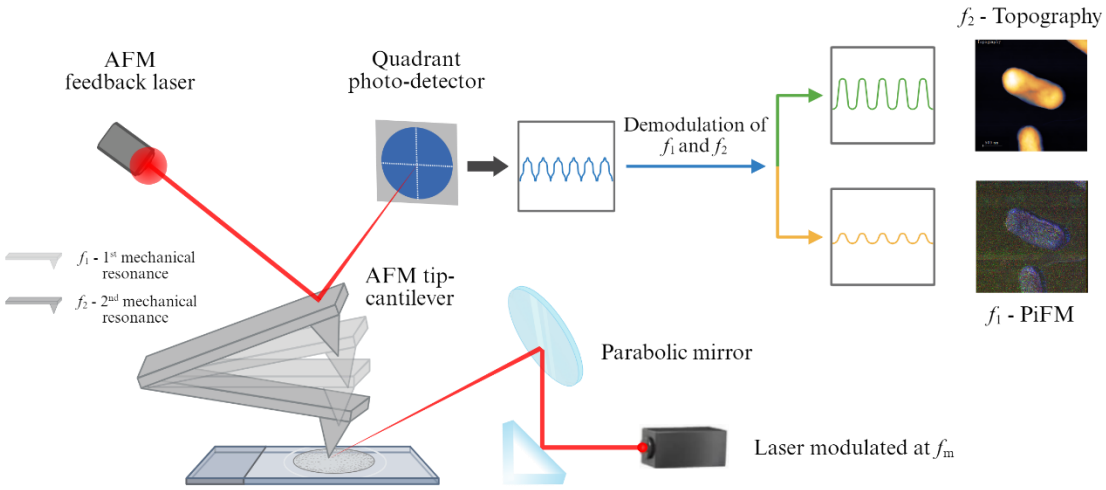

Figure 4.3 Simplified schematic diagram of PiFM. The excitation mid-IR laser is pulsed following the equation $f_m = f_2 - f_1$, where f_1 and f_2 represent the first and second mechanical eigenmode resonances of the AFM cantilever, and are employed to concurrently obtain sample's PiFM signal and topography, respectively. The sample is raster-scanned under the AFM cantilever tip to generate topographic and PiFM maps. The figure was created with BioRender.com.

4.1.6 Aims and objectives

The rapid global dissemination of *mcr* genes has compromised the clinical efficacy of colistin, one of the last-resort antibiotics for treating infections caused by MDR Gram-negative bacteria. Consequently, there is an urgent need to identify effective alternative therapies or adjuvants to colistin. The epoxytigliane compound EBC-1013 has recently been reported to exhibit membrane-active properties and anti-biofilm activity against certain Gram-negative bacteria (Powell et al. 2022). However, its mechanism of action and its effectiveness against *mcr*-positive bacteria, either alone or in combination with colistin, have not yet been systematically investigated. Therefore, the objective of this chapter was to understand the mechanisms and effects of epoxytigliane treatments against the Gram-negative outer membrane using *mcr*-negative or -positive *E. coli* strains, with or without combination use of colistin. By addressing these research gaps, this chapter will clarify the potential of epoxytiglianes, alone or in combination therapy, as effective countermeasures against *mcr* Gram-negative pathogens.

The specific aims for this chapter were:

1. To visualise the interaction of EBC-1013 with the *E. coli* cell membrane in the presence or absence of colistin using molecular dynamics simulations.

2. To examine the changes induced in cell surface chemical composition and membrane morphology following EBC-1013 treatment in the presence or absence

of colistin in *mcr*-negative or -positive *E. coli* by XPS and transmission electron microscopy (TEM), respectively.

3. To investigate the disruptive effects of EBC-1013 in the presence or absence of colistin on established biofilms of *mcr*-negative or -positive *E. coli* using CLSM with COMSTAT image analysis.

4. To characterise the antimicrobial effects and membrane permeabilisation ability of deuterated EBC-1013 and alkyne EBC-1013 against *mcr*-negative or -positive *E. coli* using minimum inhibitory concentration and bacterial membrane permeability assays.

5. To describe the cell membrane chemical changes in colistin-sensitive *mcr*-free *E. coli* after treatment with deuterated EBC-1013 and alkyne EBC-1013 using FTIR spectroscopy and photo-induced force microscopy (PiFM).

4.2 Materials and Methods

4.2.1 Preparation of epoxytiglianes and colistin solutions

The naturally occurring epoxytigliane EBC-147, the semi-synthetic epoxytigliane EBC-1013 and its two structurally modified analogues, deuterated EBC-1013 and alkyne EBC-1013, were provided by QBiotics Group Ltd. (Queensland, Australia) as a lyophilised, white flock powder. These powder-form EBCs were protected from light and stored at 4°C. When required, the EBCs were solubilised in ethanol (Sigma-Aldrich Ltd., Dorset, U.K; >99.8%) in order to make stock solutions at a nominal concentration of 20 mg/ml. All stock solutions were aliquoted into 1.5 ml microcentrifuge tubes and stored at -20°C in a freezer. Before each experiment, the EBC stocks were appropriately diluted to the desired working concentrations. To exclude the potential effects from ethanol in assays where EBC compounds were used, ethanol equivalent controls at the same concentrations as EBCs used in all experiments were tested. Colistin stock solutions were prepared as previously described (**Chapter 2 Section 2.2.1**).

4.2.2 Bacterial strains and growth conditions

The *E. coli* strains used in this chapter were: colistin sensitive J53 and CX-17, colistin resistant J53(pE30), J53(pWJ1), CX-17(pPN16) and HRS.18 (**Table 4.1)**. All *E. coli* strains were kindly provided by the Department of Medical Microbiology and Infectious Disease in Cardiff University. Growth media and growth conditions were as

previously described (**Chapter 2 Section 2.2.2**).

Table 4.1 Characteristics of colistin-sensitive and colistin-resistant *E. coli* used in this chapter.

Strain	Country of origin	Source	Plasmid origin	*mcr* type	MLST[a] group	Plasmid incompatibility group	Reference
J53		Lab strain			10		(Jacoby and Han 1996)
J53(pE30)[b]			E30	*mcr-1.1*		IncHI2	(Yang et al. 2020)
J53(pWJ1)[b]			WJ1	*mcr-3.1*		IncHI2	(Yang et al. 2020)
CX-17	China	Animal			1193		(Zhou et al. 2022)
CX-17(pPN16)[b]	Thailand	Chicken meat	PN16	*mcr-1.1*		IncI2	(Li 2023)
HRS.18	Laos	Human rectal swab		*mcr-1.1*	1081		(Xue 2022)

[a]MLST, multi-locus sequence type.

[b]Transconjugants derived from transfer of *mcr*-harbouring plasmid from the original wild-type strain into the corresponding *E. coli* host.

4.2.3 Molecular dynamics simulations

The membrane built for MD simulations represents the *E. coli* K12 laboratory strain with an upper membrane containing R1 core-Lipid A (ECLPA) molecules with branching K12 core sugars and no O-antigen units and was created based on previously published reference membranes (Pogozheva et al. 2022) using the CHARMM-GUI web interface (Jo et al. 2008). The simulation was then run in a box with epoxytiglianes and colistin added in various combinations (**Table 4.2**). The simulations were performed in triplicate, with each repeat being taken from a new minimised structure with a unique randomly generated starting set of velocities. Each repeat first underwent steepest decent minimisation with a tolerance of 1000 KJ/nm. The membrane then underwent six stages of equilibrium prior to the production run. For all equilibrium simulations, Berendsen temperature coupling thermostat was applied with Nose-Hoover used for the production run. Particle-mesh Ewald (PME) was applied to long range electrostatics and the simulations were run in NPT ensemble (constant number of particles, pressure, and temperature) at a temperature of 310.15K. The production run was for a total of 300 ns. Images were produced using PyMOL. With thanks to Georgina E. Menzies for the running of the MD simulations.

Table 4.2 Molecular dynamics simulations were run in a box with epoxytiglianes and colistin added in various combinations as shown below; (n=3).

Compound	Time	Repeats
Colistin (3 molecules)	300 ns	3
EBC-147 (3 molecules)	300 ns	3
EBC -1013 (3 molecules)	300 ns	3
Colistin + EBC 147 (3 + 2 molecules)	300 ns	3
Colistin + EBC 1013 (3 + 2 molecules)	300 ns	3

4.2.4 X-ray photoelectron spectroscopy

E. coli HRS.18 and CX-17 O/N cultures were cultivated in 150 ml LB broth with or without 1 μg/ml colistin at 37°C for 17 h at 120 rpm shaking. The O/N culture of each strain was aliquoted into five Universal tubes with 20 ml in each and cells were collected by centrifugation at 4000 rpm for 10 min at 4°C, followed by two washes in PBS. The optical densities were then all adjusted to OD_{600} 1.1 in PBS. Subsequently, 10 ml of the adjusted bacterial suspension was transferred to a new Universal tube, centrifuged at 4000 rpm for 10 min at 4°C, and resuspended and incubated in colistin, EBC-1013 or a combined treatment of the two at 37°C for 1 h. For strain HRS.18, colistin and EBC-1013 were used at 2 and 128 μg/ml respectively, while for CX-17,

they were used at 0.5 and 128 μg/ml. The concentrations and treatment duration used in this experiment were selected based on conditions employed in previous cell permeabilisation assays with these two *E. coli* strains (Xue 2022). After incubation, treated cells were harvested by centrifugation at 4000 rpm at 4°C for 10 min, and washed once using PBS. They were then dropped directly onto the cooling stage of the spectrometer and cooled in the load lock to below 250 K before exposure to vacuum.

XPS data was acquired on a Kratos Axis SUPRA using monochromated Al Kα (1486.69 eV) X-rays at 15 mA emission and 12 kV HT (180 W) and a spot size/analysis area of 700 × 300 μm. The instrument was calibrated to gold metal Au $4f_{7/2}$ (83.95 eV), and dispersion was adjusted to give a binding energy (BE) of 932.6 eV for the Cu $2p_{3/2}$ line of metallic copper. The full width at half maximum (FWHM) of Ag $3d_{5/2}$ line at 10 eV pass energy was 0.544 eV. Instrument resolution with the charge compensation system enabled was <1.33 eV FWHM on polytetrafluoroethylene (PTFE). High resolution spectra were obtained using a pass energy of 20 eV, step size of 0.1 eV and sweep time of 60 s, resulting in a line width of 0.696 eV for Au $4f_{7/2}$. Survey spectra were obtained using a pass energy of 160 eV. Charge neutralisation was achieved using an electron flood gun with filament current = 0.4 A, charge balance = 2 V, filament bias = 4.2 V. Successful neutralisation was adjudged by analysing the C(1s) region wherein a sharp peak (with no lower BE structure caused by overcompensation) was obtained. Spectra were charge corrected to the main line of the C(1s) spectrum (adventitious carbon) set to 284.8 eV. Sample cooling was achieved using a ceramic

contact cooled using flowing nitrogen submerged in liquid nitrogen and controlled using a Eurotherm temperature controller. All data was recorded at a base pressure of below 9×10^{-9} Torr and a room temperature of 294 K. Data was analysed using CasaXPS v2.3.19PR1.0 (Fairley et al. 2021). Peaks were fit with a Shirley background prior to component analysis. Comparison of the carbon spectra for colistin and EBC-1013 with the combined protein and lipid signals reported by the UMEÅ group (Ramstedt et al. 2011; Shchukarev et al. 2020) revealed sufficient differences to permit deconvolution. Analysis of the carbon spectra was employed to deconvolute the carbon signals as lipid, polysaccharide and protein. Models for colistin and EBC-1013 were derived from spectra of these molecules adsorbed on inert silica. A summary of all the models implemented in CASAXPS for fitting the XPS spectra is shown in **Table 4.3**. With thanks to Philip R. Davies and Niklaas J. Buurma for performing the XPS data analysis.

Table 4.3 Summary of the peak parameters used to create the models for the peptides, lipids, polysaccharides, colistin and EBC-1013 for fitting the XPS spectra.

Model name	Component name	Position / eV	Relative conc.
Peptide	C1	284.99*	1
	C1	286.2	0.5
	C1	288.25	0.5
Lipid	C2	284.99*	1
	C2	285.83	0.14
	C2	287.1	0.07
	C2	289	0.07
Polysaccharide	C3	284.81*	0.04
	C3	286.65	1
	C3	287.88	0.24
	C3	289	0.03
Colistin	CHx	284.79*	1
	Colistin-OH/NH	286.2	0.44
	Colistin CON	288.06	0.23
	Colistin NH	399.89	N
	Colistin NH2	401.48	0.48*N
	Colistin C=O	531.16	O
	Colistin OH	533.21	0.24*O
	Silica from support	532.12	Variable
EBC-1013	CHx	284.78*	1
	EBC C-OH	286.58	0.17
	EBC CO2	289.13	0.03
	EBC-C=O/OH	532.24	O
	EBC-CO2	533.24	0.18*O

*Main peak constrained to within +/- 0.25 eV of 285 eV. All other C(1s) peaks constrained to fixed positions relative to main peak.

4.2.5 Transmission Electron Microscopy

E. coli HRS.18 cultures were grown in 50 ml LB broth with 1 μg/ml colistin in a flask for 16-18 h and incubated at 37°C under continuous agitation on an orbital shaker at 120 rpm. To avoid any potential damage caused to cell membrane by centrifugation, cell collection was performed by filtration. For this, the O/N cultures were filtered through a sterile polyvinylidene difluoride membrane filter (PVDF; Durapore® Membrane Filter, hydrophilic) of 0.22 μm pore size (Sigma-Aldrich Ltd., Dorset, UK) under negative pressure (20 mm Hg). The filtered cells were washed from the membrane filter in PBS. The resultant bacterial suspension was adjusted to 1.5 at OD_{600nm} in PBS, and aliquots were treated with 2 μg/ml colistin, 128 μg/ml EBC-1013, or a combination of 2 μg/ml colistin and 128 μg/ml EBC-1013 at 37°C for 1 h (The concentrations and treatment duration used in this experiment were kept in line with the conditions employed in the XPS study). An ethanol equivalent (v/v) at 128 μg/ml was also tested as a negative control. Thereafter, cells were fixed in 2.5% glutaraldehyde for 2 h at room temperature. Fixed cells were collected by filtration onto 0.45 μm nucleopore membrane filters (Camlab, Cambridge, UK), gently scraped off, resuspended in an equal volume of 4% low melting point agarose (ThermoFisher Scientific, Newport, Wales, UK) at 50°C, allowed to cool, and cut into 1 mm^3 blocks. Blocks were post-fixed in 2% aqueous osmium tetroxide for 2 h, thoroughly washed in deionised water, and block-stained with 2% aqueous uranium acetate for 2 h. Following thorough washing in deionised water, samples were dehydrated through graded

isopropanol (50%, and 70% for 10 minutes each, 100% for 2 × 15 minutes), infiltrated with hard grade TAAB embedding resin (TER) (TAAB Laboratories Equipment Ltd. UK) (50% in isopropanol for 30 mins, and 4 × 1 h in pure resin) and embedded in TER at 60°C for 24 h.

Thick sections of 0.35 μm were cut on an Ultracut E ultramicrotome, dried onto glass slides, stained with 1% toluidine blue in 1% sodium tetraborate, mounted in Gurr's neutral mountant, and examined with an Olympus BX51 research light microscope (Olympus Optical Co. Ltd, London, UK). Suitable areas were identified for subsequent ultrathin sectioning, and 80-100 nm thick sections cut, collected onto 300 mesh copper grids, and stained with Reynolds lead citrate (Reynolds 1963). Samples were examined using a Hitachi HT7800 TEM (Hitachi High Tech Ltd., UK) at 100 kV and images captured with Radius software (EMSIS GmbH, Germany). With thanks to Christopher Von Ruhland for the preparation of sample sections.

4.2.6 Biofilm disruption assay and COMSTAT analysis

Colistin-sensitive *E. coli* CX-17 and colistin-resistant *mcr-1*-positive *E. coli* CX-17(pPN16) were employed in biofilm disruption assays using CLSM. Bacterial O/N cultures were adjusted to 0.05 at OD_{600nm} in MH broth before being diluted (1:10 v/v in MH broth; total volume 200 μl per well) in a sterile black 96-well glass-bottomed plate (Grenier, UK) and incubated for 18 h at 37°C under shaking (20 rpm) to establish biofilms. After biofilm formation, half the supernatant in each well was gently removed,

replaced with fresh MH broth with or without colistin (8 μg/ml for CX-17 and 32 μg/ml for CX-17[pPN16]), EBC-1013 (128 μg/ml), the combination treatment, or ethanol equivalent control (128 μg/ml), and biofilms were treated for a further 24 h (37°C; 20 rpm). The concentrations and treatment duration used here were selected based on conditions employed in previous CLSM experiments with these two *E. coli* strains (Xue 2022) and were slightly adapted for better image quality. All the supernatant was then removed from each well, and biofilms were stained with 7 μl of LIVE/DEAD® stain in PBS (BacLight Bacterial Viability Kit, Invitrogen, Paisley, UK; SYTO 9 : propidium iodide : PBS; 1 : 1 : 57). The plate was wrapped in foil to avoid light exposure and incubated for 4 mins. A further 43 μl of PBS was finally added to each well to keep the biofilms hydrated before CLSM imaging.

CLSM imaging was performed in triplicate on a Zeiss LSM980 with Airyscan2. Five technical Z-stack images were taken for each sample. Settings used for CLSM imaging were as follows: zoom, ×1; lens, ×63 oil immersion; line averaging, 1; resolution, 1584×1584; step size, 0.69 μm; and slice number, 60. ImageJ (National Institutes of Health, USA) software was used for exporting and processing the images in tagged image file format. COMSTAT2 image analysis software (Heydorn et al. 2000; Vorregaard 2008) was used to quantify the CLSM Z-stack images to produce biofilm measurements of biomass, biofilm thickness, roughness coefficient, and Dead/Live bacterial ratio. With thanks to Dr Lydia Powell for performing the CLSM imaging.

4.2.7 Minimum inhibitory concentration assays

MIC assays were conducted using the technique as previously outlined (**Chapter 2 Section 2.2.3**). The bacterial strains tested were *E. coli* J53, *mcr-1* J53(pE30) and *mcr-3* J53(pWJ1). Stock solutions of the two EBC-1013 analogues (deuterated EBC-1013 and alkyne EBC-1013) were prepared in MH broth, with a starting concentration of 1024 μg/ml. Ethanol equivalent controls (v/v) were also performed alongside EBCs to validate the test results. Two-fold serial dilutions of each EBC compound were made in a sterile 96-well microtitre plate. Plates were incubated aerobically at 37°C for 16-20 h before recording the results. Each MIC assay consisted of three biological repeats and three technical replicates.

4.2.8 Attenuated total reflectance Fourier transform infrared spectroscopy

E. coli CX-17 cultures (n=3) were cultivated in 150 ml LB broth in a 200 ml flask at 37°C for 17 h at 120 rpm shaking. The resultant cultures were well mixed by shaking, and cells (20 ml aliquots) collected by centrifugation at 4000 rpm for 10 min at 4°C, followed by two washes in PBS. The optical densities were then adjusted to OD_{600} 1.1 in PBS. Subsequently, 10 ml of the adjusted bacterial suspension was transferred to a new universal tube, centrifuged at 4000 rpm for 10 min at 4°C, and resuspended and incubated in treatments at 37°C for 1 h. The treatments used were 128 μg/ml EBC-1013, 128 μg/ml deuterated EBC-1013 or 128 μg/ml alkyne EBC-1013. The EBC

concentrations and treatment duration used in this experiment were kept consistent with the conditions employed in the XPS study of *E. coli* CX17. Untreated (PBS) and ethanol equivalent controls (128 μg/ml) were also included. After incubation, treated cells were harvested by centrifugation at 4000 rpm for 10 min at 4°C and resuspended in 10 ml PBS before being equally divided into two groups (5 ml each), which were subjected to either a no wash step or three washes in PBS. Then, 5 μl of the resultant sample was pipetted onto the ATR sampling module of a Nicolet 380 Fourier Transform IR Instrument (ThermoFisher Scientific) and allowed to air dry completely before recording the FTIR spectra at room temperature. The samples were scanned at a wavenumber range between 400 cm^{-1} and 4000 cm^{-1} at a resolution of 2 cm^{-1}, with 64 scans taken to create a mean. Each sample was scanned in triplicate. In addition to the bacterial samples, the stock solutions of EBC-1013, deuterated EBC-1013 and alkyne EBC-1013 were also measured for their FTIR spectra. The obtained spectra were normalised, baseline corrected, and then visualised using GraphPad Prism® statistics software. Spectral analysis and peak assignment were achieved by referring to published literature and an infrared spectroscopy absorption table at (https://chem.libretexts.org/Ancillary_Materials/Reference/Reference_Tables/Spectroscopic_Reference_Tables/Infrared_Spectroscopy_Absorption_Table).

4.2.9 Bacterial membrane permeability assay

The ability of EBC compounds to permeabilise *E. coli* cell membrane was evaluated by use of the SYTOX™ Green Nucleic Acid Stain (Thermo Fisher Scientific), which has

a strong attraction to nucleic acids and is able to enter cells with damaged plasma membranes. The method adopted here was adapted from McLean et al. (2013). Briefly, O/N cultures (n=3) of *E. coli* J53, J53(pE30) and J53(pWJ1) in tryptone soy broth (TSB) were diluted (1 in 200) into 20 ml fresh TSB in triplicate and incubated statically at 37°C aerobically for 3 h to achieve mid-logarithmic phase cultures. Cells were collected after centrifugation at 3200 rpm at 4°C for 10 mins and the supernatant was discarded. Cells were further washed twice in 5% TSB before being resuspended in 1 ml 5% TSB (triplicates were pooled together). The resultant cultures were adjusted to 0.78 – 0.82 at OD_{600nm} in 5% TSB. For the positive control, 1 ml was taken out from the adjusted culture and cells were collected by centrifugation at 8800 g at 4°C for 3 min, followed by resuspension in 1 ml 70% isopropanol and kept at 37°C for 1 h. Isopropanol treated cells were collected by centrifugation at 8,800 g at 4°C for 3 min, washed twice in 5% TSB and re-suspended in 1 ml 5% TSB.

Adjusted cells were added directly (1:1 v/v) to a black-bottomed 96-well microtitre plate (Thermo Fisher Scientific) with prepared treatments at double the tested final concentration. Each strain was tested for EBC-1013, deuterated EBC-1013 and alkyne EBC-1013 at three final concentrations (128, 256 and 512 μg/ml). Equivalent ethanol controls (v/v) (at 128, 256 and 512 μg/ml) were also included. The 96-well plate was incubated at 37°C for 1 h. The EBC concentrations and treatment duration used in this experiment were determined according to the conditions employed in earlier cell permeabilisation assays involving a range of *mcr*-positive and *mcr*-negative *E. coli*

strains (Xue 2022). SYTOX™ Green was diluted to 100 µM in 5%TSB and then diluted 1 in 20 in each well so that a final concentration of 5 µM was achieved. The plates were then wrapped in foil and incubated at 37°C for 90 min before measuring fluorescence intensity in a FLUOstar® Omega multi-mode microplate reader (BMG LABTECH) at excitation 485 nm and emission 550 nm. Results were recorded as mean values ± SD.

4.2.10 Photo-induced force microscopy

E. coli J53 O/N cultures (n=3) were grown in LB broth at 37°C for 17 h at 200 rpm. Cells were collected by centrifugation at 3600 g for 5 min at 4°C, and were subsequently washed twice in PBS. The bacterial suspensions were adjusted to OD_{600} 0.4 in PBS, and 1 ml aliquots from the adjusted culture were treated with EBC-1013, deuterated EBC-1013 and alkyne EBC-1013 at the same concentration of 128 µg/ml at 37°C for 20 min. The EBC concentrations used here were kept consistent with those employed in ATR-FTIR analysis of *mcr*-negative *E. coli*, while a shorter treatment duration was applied to evaluate the sensitivity of PiFM in detecting changes in cell-surface chemical composition. An ethanol equivalent (v/v) at 128 µg/ml was also tested as a negative control. After treatment, cells were centrifuged at 3600 g for 5 min at 4°C and resuspended in 2.5% (v/v) glutaraldehyde (Agar scientific) in PBS for 2 h at room temperature for fixation. Cells were then washed twice with Milli-Q water, resuspended in 500 µl Milli-Q water, before the cell suspensions were placed onto freshly cleaved mica (Agar Scientific) pre-coated with poly-L-lysine (Sigma-Aldrich)

with 7 µl droplets (×5) in a dice layout. The samples on the mica surface were left to air dry at room temperature in sterile conditions before PiFM measurements.

The dried samples were supported on 300 lines per inch mesh copper grids. Imaging and spectral data were acquired using a Vista One nano-IR microscope & spectrometer (Molecular Vista Inc., USA) equipped with a Bloc 780-1930 cm^{-1} quantum-cascade laser (QCL) and Vistascan Version 28 (Molecular Vista Inc., USA). Measurements were performed using non-contact high-resolution PtIr-coated (NCHR) cantilevers with a spring constant of 45 Nm^{-1} and a resonance frequency of 335 kHz. All measurements were conducted on *E. coli* in triplicate using sideband mode, providing a penetration depth of approximately 20 nm and a spectral resolution of 1 cm^{-1}. Bacterial cells were selected randomly for analysis. Both spectral and imaging data were processed and analysed using Surfaceworks 3.0 Release 32 (Molecular Vista Inc., USA). For visualisation and comparison, final spectral plots were generated using GraphPad Prism® statistics software. With thanks to Dr Liana Azizova and Dr Josh Davies-Jones for performing the PiFM imaging and spectral data acquisition.

4.3 Results

4.3.1 EBC-1013 and colistin interact with the *E. coli* outer membrane

The interaction of colistin and epoxytiglianes alone and in combination with the *E. coli* outer membrane were studied using MD simulations. It was revealed that when applied alone, colistin consistently integrated into the outer membrane (**Figure 4.4a**), leading to surface disruption and the formation of multiple hydrogen (H) bonds with neighbouring sugar molecules across all repeat simulations (**Figure 4.4b**). All colistin molecules eventually became embedded within the membrane in the simulation timeframe of 300 ns (**Appendix Figure 4**). In contrast, EBC-1013 alone exhibited unstable interactions with the *E. coli* outer membrane, characterised by transient H-bond formation and rapid attachment and detachment of EBC-1013 from the cell surface (**Figure 4.4c**). Notably, when EBC-1013 and colistin were included in the same simulation, periodic co-localisation at the outer membrane occurred (**Figure 4.4d**), with intermolecular interactions such as H-bonding also establishing between the two molecules. By the end of the simulation however, only colistin remained embedded in the outer membrane (**Appendix Figure 4**). Although EBC-147 alone treatment demonstrated that it was also able to attach to the *E. coli* outer membrane and form unsustained H-bonds (**Figure 4.4e**), it remained away from the outer membrane for most of the simulation. Interactions between EBC-147 and colistin were also observed (**Figure 4.4f**), albeit to a lesser degree compared to those between EBC-1013 and colistin, with colistin molecules embedding in the outer membrane in 2/3 simulations

(**Appendix Figure 4**).

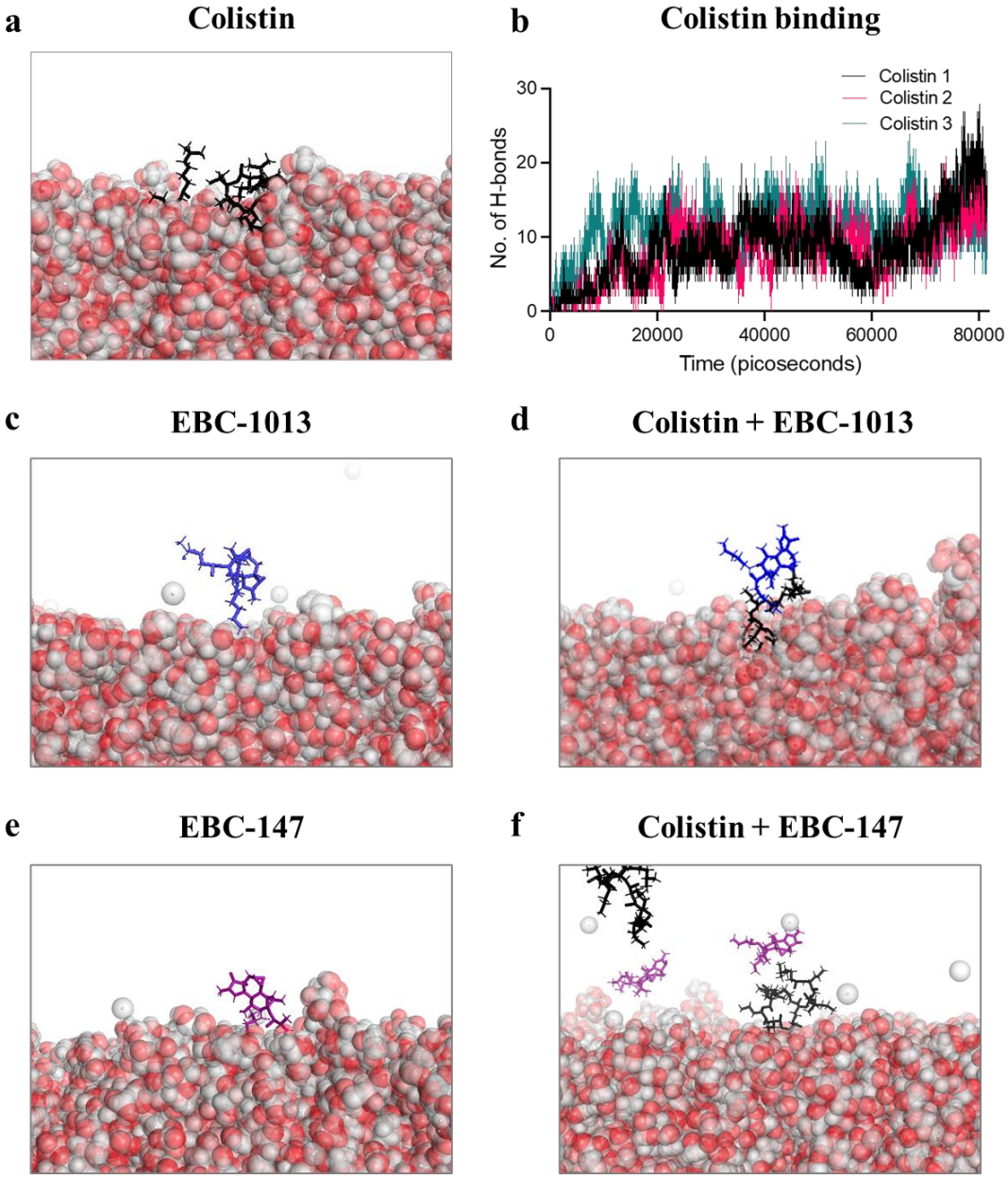

Figure 4.4 Molecular dynamics simulations showing the interaction of colistin or epoxytiglianes or their combinations with a simulated *E. coli* membrane (n=3). (**a**) colistin (black) and (**b**) the number of hydrogen bonds formed between colistin and adjacent sugar molecules on *E. coli* membrane over time (different line colours represent different colistin molecules; n=3). (**c**) EBC-1013 (blue) (**d**) with colistin. (**e**) EBC-147 (purple) (**f**) with colistin. Images were produced using PyMol and are snapshots taken from the first 50 ns of the simulation time. These images showed the ability of EBCs to directly interact with both the *E. coli* membrane and colistin, especially of EBC-1013.

4.3.2 EBC-1013 binding induces changes in the surface chemical composition of the *E. coli* outer membrane

The potential alterations in bacterial outer membrane chemical composition induced by colistin and/or EBC-1013 interacting with the cell surface were studied by performing XPS on colistin-sensitive *E. coli* CX-17 and colistin-resistant, *mcr-1*-positive *E. coli* HRS.18, both treated for 1 h (**Figure 4.5**). The XPS survey spectra provide a quantitative description of the cell surface (up to an approximate depth of 10 nm) in terms of the relative presence of different elements with distinct binding energies. Deconvoluted fine spectra in the C(1s) region reflect contributions from lipids, peptides and polysaccharides with additional terms for colistin and EBC-1013. While the XPS data are quantitative, deconvoluted data in terms of these five components provides a qualitative description of changes in chemical composition of the outer membrane of the two *E. coli* strains tested.

The XPS spectra of both untreated strains were very similar, save for the presence in HRS.18 of an additional C(1s) peak at 289.3 eV (**Figure 4.5a**), a N(1s) peak at 402.3 eV which is typical of NH_4^+, a P(2p) peak at ~135 eV, and an additional O(1s) peak at ~535 eV. These four additional peaks reflect the known addition of pEtN to the lipid A in the resistant strain. The deconvoluted C(1s) XPS spectra of CX-17 and HRS.18 following colistin-only treatment demonstrated clear differences in colistin binding; colistin becoming clearly bound to the CX-17 cell surface, while this was less prominent in the *mcr-1*-harbouring HRS.18 (**Figure 4.5b**). The treatment of 128 μg/ml

EBC-1013 alone, induced a marked increase in the lipid signal at the cell surface of *mcr-1* HRS.18, whilst a relative reduction was seen in CX-17 (**Figure 4.5c**). The opposite effects on lipid composition were observed when the combination treatment of colistin and EBC-1013 was used, with CX-17 showing a higher induced lipid signal than *mcr-1* HRS.18 (**Figure 4.5d**). However, in all cases, the presence of EBC-1013 markedly increased the visibility of the lipid fraction relative to the untreated control and the colistin-only treatment in both strains (**Figure 4.5e**). The incorporation or attachment of both colistin and EBC-1013 to the bacterial outer membrane was evident in both CX-17 and *mcr-1* HRS.18 through suppression of the relative P(2p) signal by both compounds and the general suppression of N(1s), P(2p) and S(2p) signals by EBC-1013 (**Table 4.4**). The additional features present in the N(1s), O(1s) and P(2p) regions of the untreated *mcr-1* HRS.18 (attributed to the pEtN modification of the lipid A), were not apparent upon treatment with either colistin or EBC-1013 or in combination.

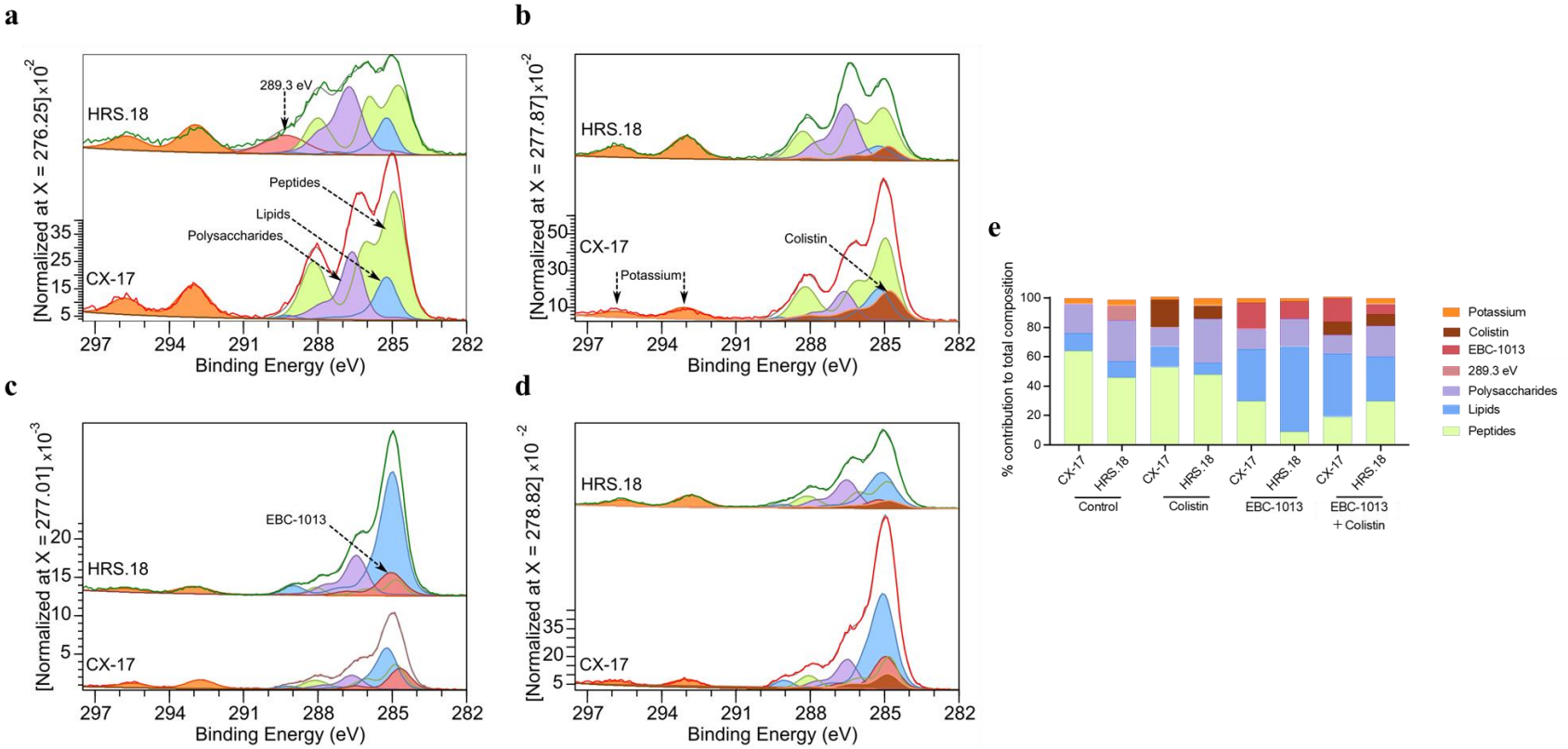

Figure 4.5 X-ray photoelectron spectroscopy showing the cell surface chemical composition of *E. coli* HRS.18 (*mcr-1* positive) and *E. coli* CX-17 (*mcr-1* negative) treated with colistin (2 and 0.5 µg/ml for HRS.18 and CX-17 respectively) and/or EBC-1013 (128 µg/ml) for 1 h; (n=3). The C1s region of the obtained XPS spectra was deconvoluted to identify different cell surface chemical components. **a** untreated control, **b** colistin only, **c** EBC-1013 only, **d** combination of colistin and EBC-1013. **e** Calculated percentage contribution of each surface component to the total chemical composition in each sample. The untreated HRS.18 demonstrated an extra carbon species at 289.3 eV comprising ~ 10% of the total composition. These results demonstrated that EBC-1013 treatment can induce changes in the chemical composition of the *E. coli* outer membrane, especially an increase in the lipid signal.

Table 4.4 X-ray photoelectron spectroscopy showing the effects of the incorporation or attachment of both colistin and EBC-1013 to the bacterial outer membrane of colistin-sensitive *E. coli* CX-17 and *mcr-1*-positive *E. coli* HRS.18 by region expressed as % of C (carbon) signal.

Strain	Sample	% of C (carbon) signal						
		C	N	O	P	S	Cl	Na(1s)
CX-17	Untreated	100	13.8	42.9	5.6	0.5	2.4	2.2
	Colistin	100	15.0	31.6	2.7	0.8	1.9	1.3
	EBC-1013	100	7.2	24.9	1.9	0.3	4.0	1.3
	Colistin + EBC-1013	100	5.4	27.6	2.8	0.0	0.9	1.1
HRS.18	Untreated	100	13.1	35.4	3.3	0.5	3.6	1.6
	Colistin	100	11.6	41.6	2.9	0.7	3.2	2.1
	EBC-1013	100	4.4	24.0	2.6	0.1	1.2	0.6
	Colistin + EBC-1013	100	8.2	27.4	1.4	0.2	3.6	0.9
	Colistin measured	100	59.1	32.5				
	Colistin expected	100	30.8	25.0				
	EBC-1013 measured	100	0.0	35.3				
	EBC-1013 expected	100		31.0				

The incorporation or attachment of colistin to the bacterial outer membrane was demonstrated by the suppression of the P(2p) signal in both *E. coli* strains, and the incorporation or attachment of EBC-1013 to the bacterial outer membrane was evident in suppression of the N(1s), P(2p) and S(2p) signals in both *E. coli* strains.

4.3.3 EBC-1013 induces changes in *mcr E. coli* cell membrane morphology

The potential effects on bacterial cell membrane morphology as a consequence of colistin and/or EBC-1013 treatment were studied and visualised by TEM on *mcr-1*-positive *E. coli* HRS.18 treated for 1 h (**Figure 4.6**). TEM micrographs of untreated cells revealed a slightly wavy membrane morphology, with a clear delineation of the layered membrane ultrastructure, including the outer and inner membranes along with the peptidoglycan layer, characteristic of Gram-negative bacteria (**Figure 4.6a and b**). For cells exposed to colistin at 2 μg/ml, a less wavy but equally intact and distinguishable cell membrane structure to the untreated control was observed (**Figure 4.6c and d**). In contrast, treatment with EBC-1013 at 128 μg/ml, either alone or in combination with colistin, resulted in a compromised membrane morphology, as evidenced by a regionally blurred or fuzzy appearance of the cell envelope and a corresponding loss of clearly defined layered architecture, suggesting compromised membrane integrity or membrane destabilisation (**Figure 4.6e, f, g and h**). Notably, such morphological changes were absent in cells treated with the vehicle control (ethanol) at equivalent concentrations (**Figure 4.6i and j**).

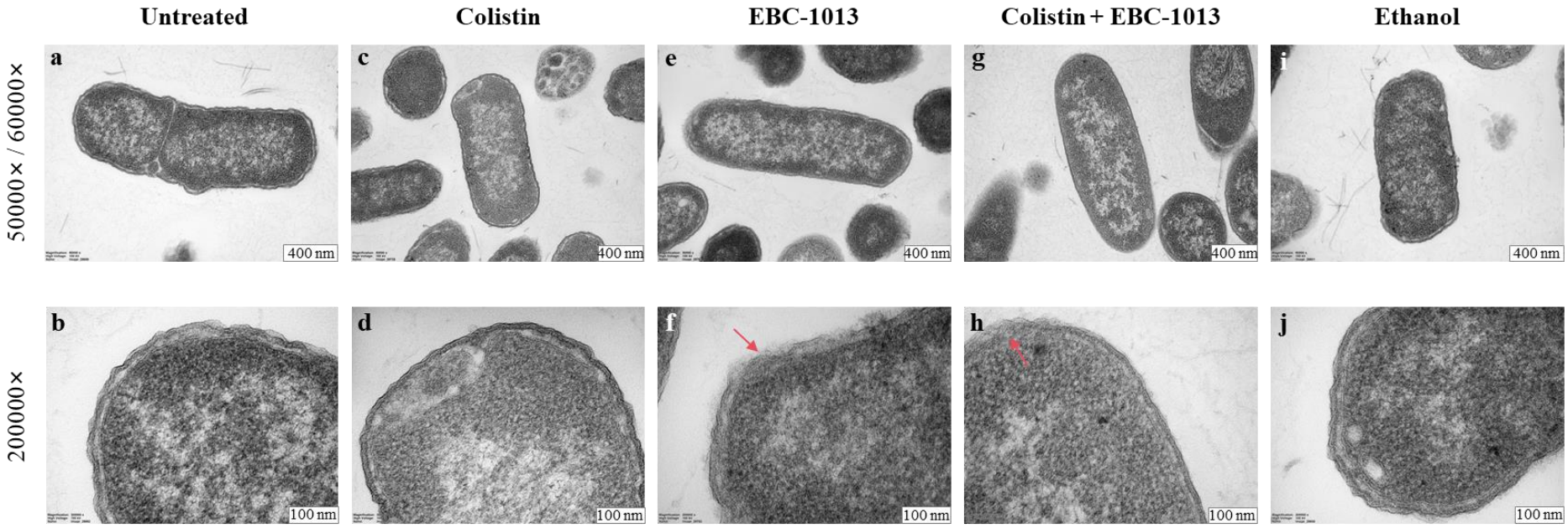

Figure 4.6 Transmission electron microscopy of *E. coli* HRS.18 (*mcr-1* positive) treated with colistin (2 µg/ml) and/or EBC-1013 (128 µg/ml) alongside untreated and ethanol vehicle (128 µg/ml) controls for 1 h; (n=3). Magnification of 50000× or 60000× was used for capturing whole cell TEM micrographs and magnification of 200000× was used to visualise cell membrane structure. Red arrows indicate that the layered membrane ultrastructure exhibited regional disruption or became indistinct following treatment with EBC-1013 alone or in combination with colistin.

4.3.4 EBC-1013 improves the efficacy of colistin in disrupting established biofilms of *mcr E. coli*.

The effects of colistin, EBC-1013, and the combination treatment on established biofilms (18 h) of colistin-sensitive *E. coli* CX-17 and colistin-resistant *mcr-1*-positive *E. coli* CX-17(pPN16) were evaluated using CLSM (**Figure 4.7**; **Appendix Table 3**). COMSTAT image analysis of CX-17 biofilms treated with colistin alone at 8 μg/ml demonstrated significantly reduced biofilm biomass ($P < 0.0001$) and increased Dead/Live bacterial ratio ($P < 0.05$) when compared with the untreated control (**Figure 4.7c**), which was consistent with the reduced biofilm thickness and obviously increased number of dead cells observed in CLSM images (**Figure 4.7a**). Treatment of EBC-1013 alone at 128 μg/ml also exhibited a disruption effect against CX-17 biofilms, as shown by the decreased biofilm biomass in comparison to the untreated control ($P < 0.05$), although to a much lesser extent compared to colistin-only treatment. However, this effect was not significantly different from the ethanol vehicle control ($P > 0.9999$) (**Figure 4.7c**). Combined use of colistin and EBC-1013 showed comparable anti-biofilm effects on CX-17 to the colistin-only treatment, with no significant differences in biomass and Dead/Live bacterial ratio noted ($P > 0.05$) (**Figure 4.7a and c**).

In contrast to the colistin-sensitive strain, both individual colistin (32 μg/ml) and EBC-1013 (128 μg/ml) treatments failed to significantly reduce the *mcr-1* CX-17(pPN16) biofilm biomass ($P > 0.05$) or increase the Dead/Live bacterial ratio ($P > 0.05$)

compared to the untreated control (**Figure 4.7d**). Nevertheless, the combination treatment of colistin and EBC-1013 resulted in a significant reduction in biomass of *mcr-1* CX-17(pPN16) biofilms in comparison to both the untreated control and colistin-only treatment ($P < 0.01$) (**Figure 4.7d**), with the corresponding CLSM images demonstrating thinner and sparser biofilms (**Figure 4.7b**), indicating the ability of EBC-1013 to potentiate the effects of colistin in disrupting established *mcr-1 E. coli* biofilms.

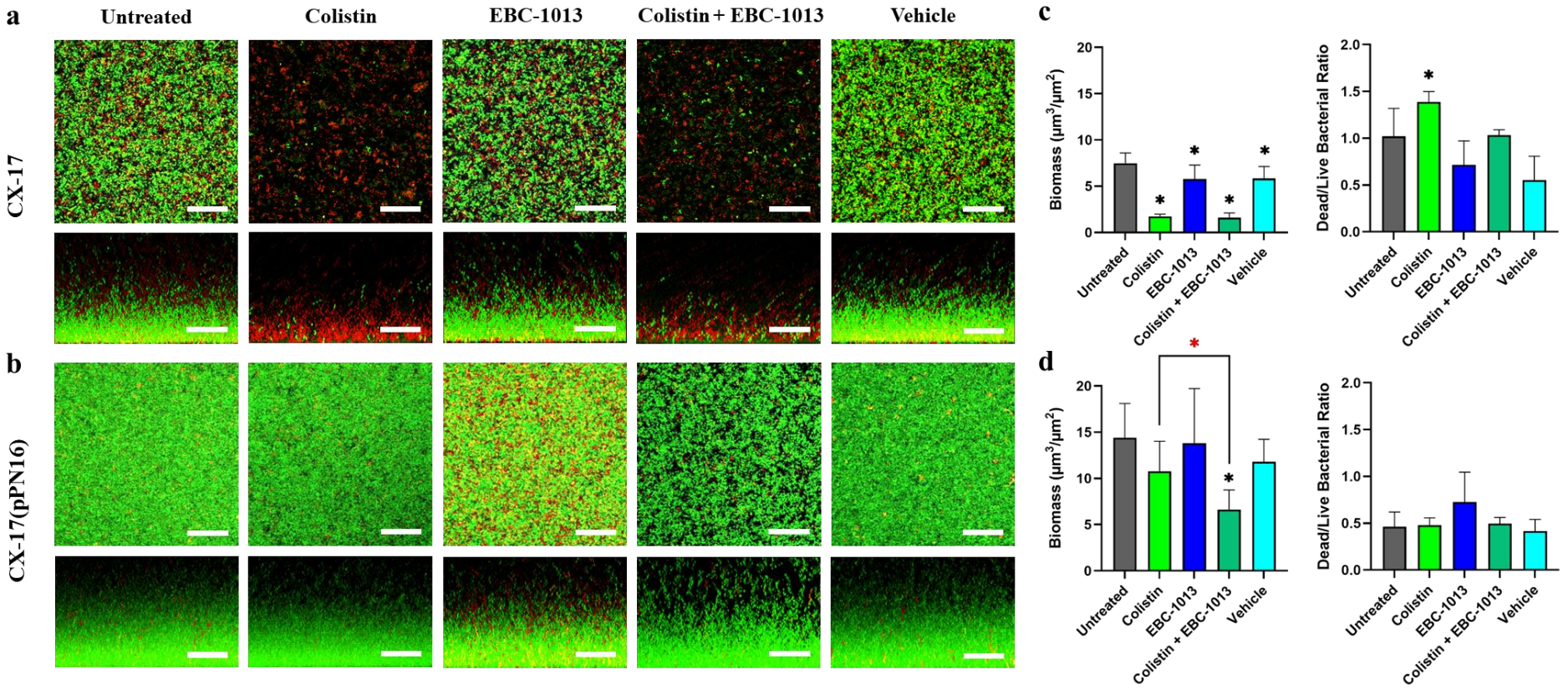

Figure 4.7 Confocal laser scanning microscopy with LIVE/DEAD® staining (aerial and side views) showing disruption of 18 h established biofilms treated (24 h) with colistin (8 μg/ml for *E. coli* CX-17 and 32 μg/ml for *E. coli* CX-17[pPN16]), EBC-1013 (128 μg/ml) or combined therapy, alongside untreated and ethanol vehicle (128 μg/ml) controls (n=3). **a** Colistin-sensitive CX-17. **b** Colistin-resistant *mcr-1*-positive CX-17(pPN16). (Scale bar = 30 μm). **c** and **d** Corresponding COMSTAT image analysis of biofilm CLSM z-stack images. *represents significantly different compared to the untreated control; *represents significant difference between colistin and the combination of colistin and EBC-1013 therapy ($P < 0.05$). These results demonstrated the ability of EBC-1013 to potentiate colistin in the treatment of *mcr E. coli* biofilms.

4.3.5 ATR-FTIR confirms successful synthesis of EBC-1013 derivatives

EBC-1013 and its derivatives, the deuterated EBC-1013 and alkyne EBC-1013, were subjected to ATR-FTIR analysis to identify and confirm the potential differences in their molecular structure (**Figure 4.8**). When compared to EBC-1013, alkyne EBC-1013 demonstrated an additional strong absorbance peak at 3292 cm^{-1} and a weak peak at 2116 cm^{-1}, which correspond to the stretching vibration of C–H and C≡C bonds associated with the terminal monosubstituted alkyne groups within its C12/C13 ester chains, respectively. The emerging peak at 631 cm^{-1}, however, was characteristic of the C–H bending vibration of the terminal alkyne group. Furthermore, the peak intensity of the absorbance band around 2830-3000 cm^{-1} (alkane C–H stretching) was reduced for the alkyne EBC-1013, attributable to a lower number of C–H bonds due to the introduction of the alkyne group.

When directly comparing deuterated EBC-1013 and EBC-1013, a decreased peak intensity of the alkane C–H stretching vibration (2830-3000 cm^{-1}) was observed in the spectrum of deuterated EBC-1013. This decrease was concomitantly accompanied by the emergence of new peaks in the 2050-2250 cm^{-1} range, a phenomenon likely caused by peaks shifting to lower energy upon deuteration (from C–H to C–D) (Shaner and Stone 2023). Additionally, deuterated EBC-1013 displayed reduced peak intensities at both 1716 cm^{-1} (corresponding to the C=O stretching vibration) and 1169 cm^{-1} (an

absorbance position belonging to the C–O stretching vibration). All these ATR-FTIR spectra features confirmed the successful introduction of deuterium or alkyne group(s) into the molecular structure of EBC-1013.

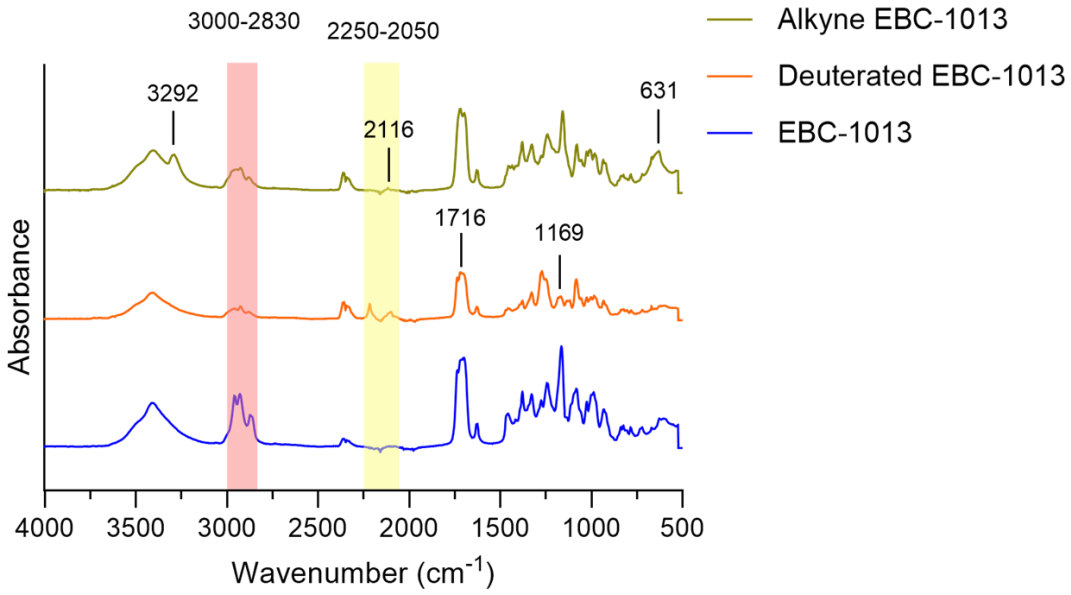

Figure 4.8 Attenuated total reflectance Fourier transform infrared (ATR-FTIR) absorbance spectra of EBC-1013, deuterated EBC-1013 and alkyne EBC-1013 (n=3). Highlighted peaks indicate distinct differences in spectra, potentially representing differences in their molecular structure. These distinct spectra indicated successful synthesis of EBC-1013 derivatives.

4.3.6 Antimicrobial activity of EBC-1013 derivatives

MIC assays were conducted for EBC-1013 derivatives (deuterated EBC-1013 and alkyne EBC-1013) against *E. coli* J53, *mcr-1* J53(pE30) and *mcr-3* J53(pWJ1). Previous studies have shown that extended exposure to 70% ethanol for 16 hours can effectively eliminate microorganisms (Chambers et al. 2006). To ensure that the

potential antimicrobial effects were attributable to EBCs rather than the ethanol solvent, the antimicrobial activity of ethanol at equivalent concentrations was also tested in the MIC assays. Deuterated EBC-1013 exhibited no antimicrobial activity against all three *E. coli* strains within the tested concentration range of 0-1024 μg/ml (MICs > 1024 μg/ml). The same results were found for alkyne EBC-1013 (MICs > 1024 μg/ml). The MIC values obtained for ethanol equivalent controls were all higher than 1024 μg/ml.

4.3.7 ATR-FTIR was unable to detect epoxytigliane interactions with the *E. coli* cell membrane

ATR-FTIR was conducted to identify potential changes in cell membrane chemical composition of colistin-sensitive *E. coli* CX-17 associated with treatment of epoxytiglianes (**Figure 4.9**). Bacterial cells treated with all three EBC candidates at 128 μg/ml and their ethanol equivalent control showed a similar IR spectra to that of untreated cells regardless of the presence or absence of the washing step following treatment. The only exception to this was absorbance peaks with varying intensity at around 2360 cm^{-1} and 669 cm^{-1} in some of the IR spectra. These anomalous peaks were thought to be caused by CO_2 contamination, as the typical CO_2 spectrum is dominated by the asymmetrical stretching mode at 2349 cm^{-1}, and the bending vibration centred at 667 cm^{-1} (Hammel et al. 2024). The overall lack of difference in the spectra of all the test samples suggests that treatment with EBCs for 1 h at 128 μg/ml was insufficient to induce significant alterations in the surface chemistry of the *E. coli* cell membrane that could be detected by ATR-FTIR.

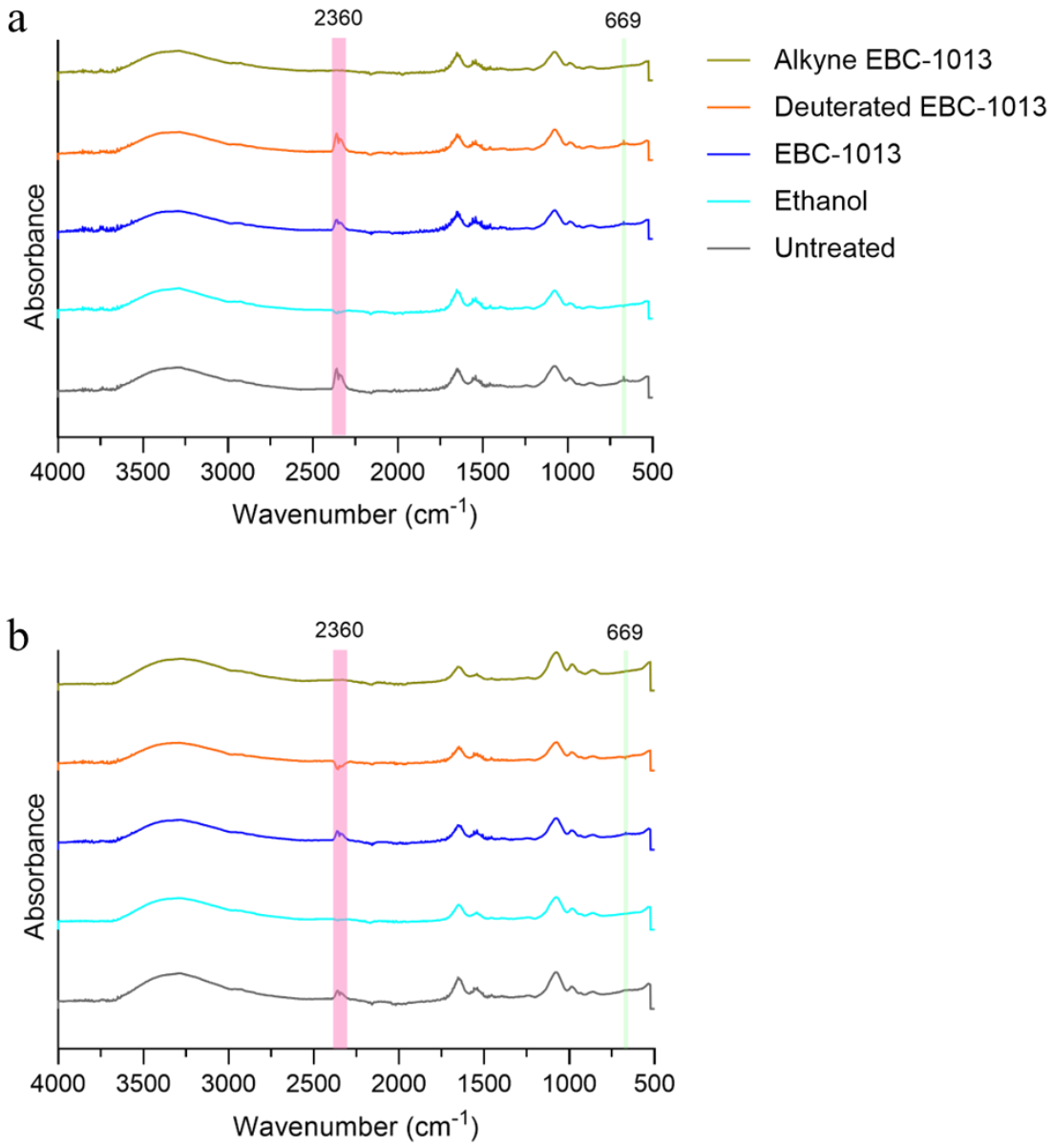

Figure 4.9 Attenuated total reflectance Fourier transform infrared (ATR-FTIR) spectroscopy showing the potential membrane interaction effects of epoxytiglianes on *mcr*-negative *E. coli* CX-17 (n=3). Bacterial cells were treated with epoxytiglianes (128 µg/ml) and ethanol equivalent control (128 µg/ml) for 1 h at 37°C, before being subjected to (**a**) no wash and (**b**) three washes in PBS. The lack of differences observed in the spectra between treatments suggested that ATR-FTIR might not be able to detect interactions between EBC and the *E. coli* cell membrane at the concentration and treatment time used.

4.3.8 Epoxytigliane treatment increases *E. coli* cell membrane permeability

A bacterial membrane permeability assay was conducted to investigate whether treatment of the three EBC candidates (EBC-1013, deuterated EBC-1013 and alkyne EBC-1013) could compromise the cell membrane integrity of both colistin-sensitive *E. coli* J53 and colistin-resistant *E. coli* J53(pE30) *mcr-1* and *E. coli* J53(pWJ1) *mcr-3* (**Figure 4.10**). Both EBC-1013 and deuterated EBC-1013 at all three concentrations tested (128, 256 and 512 μg/ml) exhibited significant, dose-dependent cell membrane permeabilisation effects in all three *E. coli* strains when compared to the untreated control ($P < 0.05$). For alkyne EBC-1013 however, permeabilisation only occurred at the slightly higher concentration of ≥ 256 μg/ml compared to EBC-1013 and deuterated EBC-1013 (≥ 128 μg/ml) ($P < 0.05$). Treatment with the ethanol vehicle control only induced significant cell permeability for all the strains used at 512 μg/ml ($P < 0.0001$). The 70% isopropanol positive control gave a high fluorescence intensity value in every assay, indicative of highly damaged cell membranes.

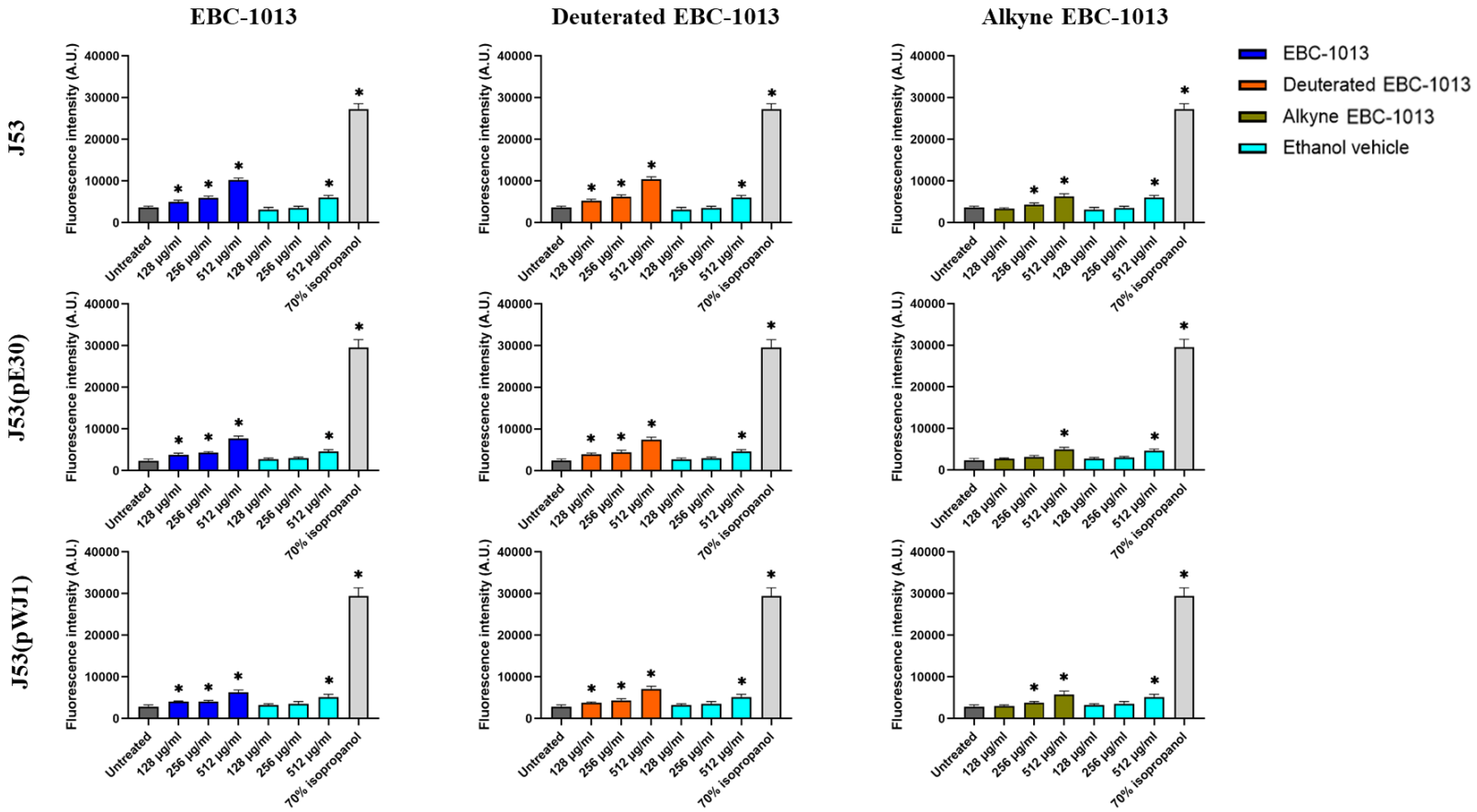

Figure 4.10 Bacterial membrane permeabilisation assay showing the effects of epoxytigliane treatment (1 h) on colistin-sensitive *E. coli* J53 and colistin-resistant *E. coli* J53(pE30) *mcr-1* and *E. coli* J53(pWJ1) *mcr-3*. EBC-1013, deuterated EBC-1013, alkyne EBC-1013 and the vehicle equivalent control (ethanol) were tested at three concentrations (128, 256 and 512 µg/ml). 70% isopropanol was included as a positive control. Results are expressed as fluorescence intensity (A.U.). *represents significantly different compared to the untreated control (n=3; $P < 0.05$). All 3 EBCs were able to permeabilise *E. coli* cell membrane; alkyne EBC-1013 permeabilises at higher concentrations than the other two.

4.3.9 Epoxytiglianes induce changes in *E. coli* membrane lipids and proteins

The potential interactive effects of EBC-1013 and its deuterated and alkyne derivatives on the cell membrane of colistin-sensitive *E. coli* J53 were investigated using PiFM. As shown in the 3D PiFM spectral images (**Figure 4.11**), bacterial cells treated with the three EBC compounds at 128 μg/ml for 20 min did not exhibit significant alterations in cell morphology compared to both the untreated and vehicle (ethanol) controls. However, changes in the distribution of amide I, amide II and phospholipids across the cell surface were noted in the EBC treated cells, as displayed by their different cell surface colour distribution and density compared to the control groups. The strong red background (most noticeable in the EBC-1013 treated PiFM image) is a consistent signal from the mica substrate due to the approximate overlapping of the absorption peak of Si–O asymmetric stretching vibrations with the wavenumber of 1073 cm^{-1} used in the experiment. The rainbow effect seen in the alkyne EBC-1013 treated PiFM image around the edges of the imaged cells is likely due to optical interference, possibly enhanced by topographical variation.

The changes in bacterial membrane lipids and proteins after EBC treatment were further corroborated by the corresponding PiFM spectra (**Figure 4.12**). In the typical lipid range (1710-1760 cm^{-1}, corresponding to the stretching vibration of C=O in lipids), EBC-treated cells demonstrated broadened peaks and/or peak shifting when compared

to the vehicle (ethanol) treated cells, which showed a sharp peak at around 1745 cm^{-1}. These changes may be due to less uniform packing arrangements or alterations in the local environment of lipids within the bacterial membrane caused by the cell interactions with the EBCs. Other evidence supporting these lipid changes following EBC treatment is the emergence of an induced absorption band located at around 1460 cm^{-1} in all three EBC treatment groups, with a peak at this wavenumber primarily reflecting C–H bending vibrations in aliphatic components, particularly fatty acids. This band appears as a relatively flattened region in the control groups. Notably, the peak at 1772 cm^{-1} in alkyne EBC-1013 treated *E. coli* could be associated with C=O conjugated to an alkyne group. This may be a sign that the alkyne EBC-1013 had remained on the cell surface and is possible indirect evidence that it had interacted with the cell membrane. In the amide I band region (1600-1700 cm^{-1}) and amide II band region (1480-1580 cm^{-1}), the spectra of all three EBC-treated *E. coli* developed varying degrees of peak sharpening and peak position shifts compared with the spectrum of the untreated *E. coli* (which showed peaks at 1665 cm^{-1} and 1543 cm^{-1} respectively). These changes were also less prominent in the ethanol treated *E. coli* spectrum. This is indicative of induced modifications in protein conformation, especially the protein secondary structures, caused by the EBC treatment. Interestingly, treatment of EBC-1013 produced a distinct peak at 1630 cm^{-1}, which was not obvious in the spectra of the other EBC treated or control groups; this extra peak possibly corresponding to the β-sheet protein secondary structure.

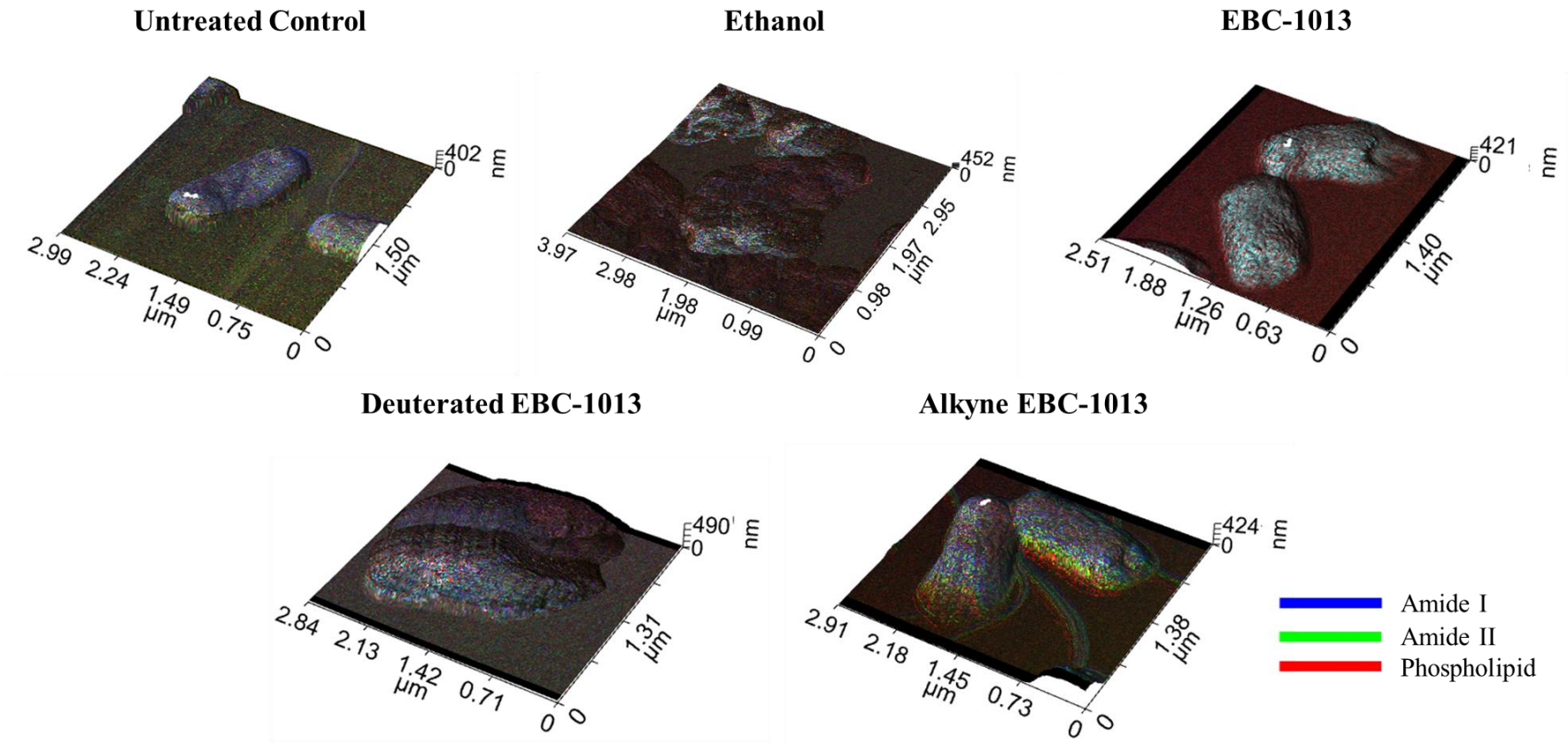

Figure 4.11 Three-dimensional PiFM spectral images of *E. coli* J53 treated with EBC-1013, deuterated EBC-1013, alkyne EBC-1013 and vehicle (ethanol) equivalent control at a concentration of 128 µg/ml for 20 min (n=3). The PiFM spectral images were mapped by IR wavenumbers at approximately 1665, 1540 and 1073 cm^{-1}, which correspond to amide I (blue), amide II (green) and the asymmetric stretching of the PO_2^- group in the phosphate of phospholipid (red) respectively. Treatment with EBCs clearly induced changes in the distribution of amide I, amide II and phospholipids across the *E. coli* cell surface.

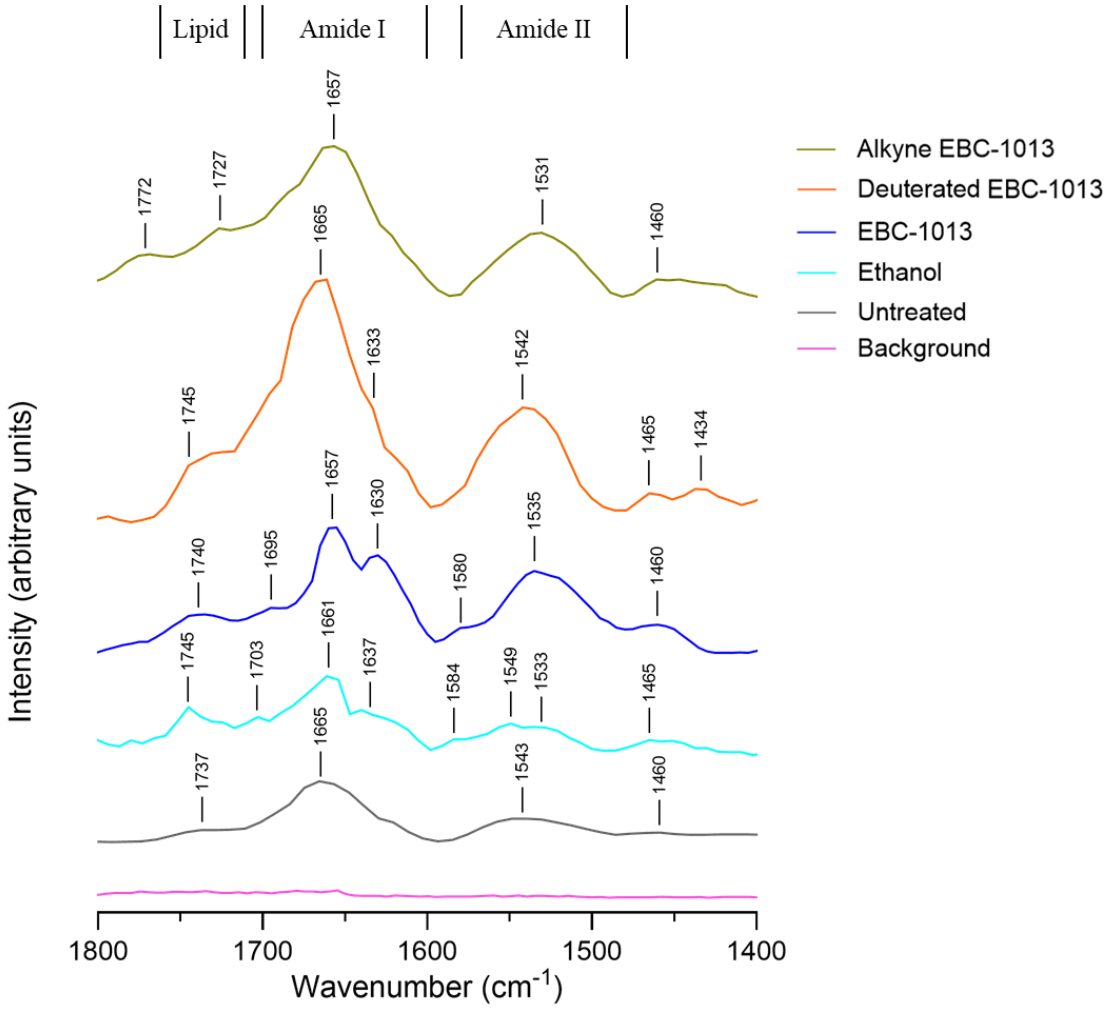

Figure 4.12 PiFM spectra (1400-1800 cm^{-1}) of *E. coli* J53 treated with EBC-1013, deuterated EBC-1013, alkyne EBC-1013 and vehicle (ethanol) equivalent control at a concentration of 128 µg/ml for 20 min (n=3). Each treatment spectrum was a mean of all the pixel locations measured in a selected region (approximately 0.01 µm^2) on the bacterial cell surface that showed consistent spectral features. Treatment with all EBCs induced various changes in peak width and position in the lipid, amide I and amide II regions of the *E. coli* PiFM spectra compared with ethanol or untreated controls, indicating alterations in the lipid and protein composition of the *E. coli* membrane.

4.4 Discussion

Gram-negative bacteria, including *E. coli*, are important MDR organisms and play a pivotal role in the worldwide challenge of antimicrobial resistance, posing serious threats to public health. These bacteria are particularly concerning because of their complex outer membrane, which acts as an effective permeability barrier that restricts the entry of many antibiotics, complicating treatment efforts against these pathogens (Choi and Lee 2019). Composed of LPS, phospholipids, and proteins, the outer membrane impedes the influx of hydrophilic drugs and can actively expel them via efflux pumps, thereby significantly diminishing antibiotic efficacy (Ghai 2023). Although effective antibiotics are available for Gram-negative bacterial infections, e.g., colistin (a last-resort option), the emergence and dissemination of resistance mechanisms such as plasmid-borne *mcr* genes (which confer colistin resistance by modifying the LPS on the bacterial outer membrane with pEtN) have greatly increased the risk of treatment failure with this antibiotic (Hassan et al. 2020b). Therefore, there is an urgent need to develop novel antimicrobial agents targeting the outer membrane as an alternative or adjuvant to colistin to combat the growing threat of MDR Gram-negative infections.

Epoxytiglianes, as outlined in **Chapter 1 Section 1.8.2** and **Chapter 4 Section 4.1.1**, have demonstrated significant potential as antimicrobial agents (Powell et al. 2022). Previous MD simulations suggested that EBC-46, EBC-1013 and EBC-147 could

quickly become closely associated with/bound to the LPS-dipalmitoylphosphatidylethanolamine (LPS-DPPE) bilayer outer membrane of the common Gram-negative pathogen *P. aeruginosa* within the first 20 ns of the simulation, with the average percentage interaction time with the outer membrane surface residues measured for EBC-46 and EBC-1013 being much longer compared to the (non-antimicrobial) control EBC-147 (Powell et al. 2022). In keeping with this finding, we showed here that EBC-1013 interacted with the normal *E. coli* outer membrane (although relatively weak when simulated alone) in a more frequent pattern than EBC-147. In addition, the observed consistent embedding of colistin within the outer membrane and the subsequent membrane destabilisation align with previous MD simulation studies, which revealed that cationic antimicrobial peptides could aggregate in the LPS headgroup region of the outer membrane and disrupt surface salt bridges, resulting in the release of calcium, leading to membrane disruption (Berglund et al. 2015; Li et al. 2020b). However, for the first time, I report the co-localisation of epoxytiglianes and colistin within the *E. coli* outer membrane when these two compounds were used in combination, with the direct molecular interactions between EBC-1013 and colistin being greater than those between EBC-147 and colistin. I speculate that this co-localisation of EBC-1013 with colistin at the *E. coli* cell surface may facilitate the penetration of colistin into the membrane, thus contributing to the colistin-induced membrane lysis.

XPS is a useful technique for chemical characterisation of bacterial cell surfaces with a

probing depth being less than 10 nm; the thickness of the Gram-negative outer membrane being reported to be around 10 nm (Owen 1992). Therefore, XPS analysis cannot extend into the interior of the cell, so is largely limited to the outer membrane layer. For *E. coli* BW25113, XPS has successfully been used to differentiate the cell surface chemical compositions of the wild-type strain and LPS mutants, based on variations in the relative concentrations of lipids, peptides and polysaccharides (Ramstedt et al. 2011). In my study, XPS effectively distinguished between untreated *E. coli* strains with or without *mcr* genes, with *mcr* carriage resulting in unique peaks in the C(1s), N(1s), O(1s) and P(2p) regions of the spectrum attributable to the pEtN addition to lipid A. However, the signals associated with pEtN modification were notably absent after treatment with colistin and/or EBC-1013, likely due to the blanketing and obscuring effects from the treatments, moving pEtN beyond the detection range of XPS. Deconvoluted XPS data also showed that 1 h treatment with EBC-1013 (either alone or in combination with colistin) significantly increased visibility of the lipid content, likely an indication of increased lipid disorganisation/disorder induced by EBC-1013. Interestingly, the antimicrobial mechanism of two monoterpenes (thymol and carvacrol) has previously been described as a gross lipid perturbation effect on the bacterial plasmic membrane, which was found to cause concentration-dependent damage to large unilamellar vesicle model membranes with different lipidic compositions (Cristani et al. 2007). Similarly, in a study applying the Langmuir monolayer technique, two pentacyclic triterpenes (ursolic acid and α-amyrin) revealed destructive activity on the *E. coli* membrane-mimicking

lipid model membranes, possibly by interfering with hydrogen bond formation between the phospholipid headgroups, as well as disorganising the packing of the phospholipid hydrophobic chains (Broniatowski et al. 2015). These observations suggest that lipid-associated effects may play an important role in terpene-mediated antimicrobial activity.

Previous literature has shown that centrifugation may damage microbial cell surfaces (Peterson et al. 2012). Hence, filtration was used in my TEM experiment to harvest colistin and/or EBC-1013-treated *mcr E. coli* to reflect the real effects from treatments. A previous study in our group has demonstrated that colistin at a sub-MIC of 2 μg/ml induced no cell membrane permeability in the tested *mcr E. coli* HRS.18, while EBC-1013 at a clinically relevant concentration of 128 μg/ml induced significant cell membrane permeability in the strain (Pritchard et al. 2025; unpublished). This result was mirrored in this study, with colistin showing no effects on the morphology of the cell membrane and EBC-1013 (both with and without colistin) causing regional and localised membrane perturbations. It should be noted that EBC-1013 at higher concentrations (256 and 512 μg/ml) could induce even more significant cell permeabilisation (Pritchard et al. 2025; unpublished). Thus, it could be reasonably inferred that the destructive effects of EBC-1013 on the bacterial cell membrane are actually concentration-dependent, e.g., more extensive membrane damage. A number of essential oil-derived compounds, including terpenes and phenylpropanoids, have been shown to exhibit bacteriostatic and bactericidal effects against *E. coli*, and were also able to cause morphological changes to the cells, with the mechanism of action

speculated to involve alterations in the membrane integrity and permeability (Nogueira et al. 2021).

mcr genes in bacterial biofilms typically confer increased resistance to colistin and are frequently found alongside other antibiotic resistance genes, making biofilm infections arising from them, very difficult to treat (Ćwiek et al. 2021; Koskeroglu et al. 2023). In my biofilm disruption assay, colistin demonstrated efficacy in disrupting colistin-sensitive *E. coli* biofilms, whereas the lipid A modification with pEtN in *mcr E. coli* biofilms rendered colistin-only treatment ineffective. EBC-1013 at 256 μg/ml has previously been reported to effectively disrupt established *mcr*-free *E. coli* IR57 biofilms, with the treated biofilms showing significantly reduced biovolume, thickness, and cell viability and increased surface roughness; furthermore, these biofilms demonstrated significant EPS matrix disruption, as evidenced by increased nanoparticle diffusion in a multiple-particle tracking assay, as well as compromised biomechanics (Powell et al. 2022). In the present study, however, a lower concentration of EBC-1013 at 128 μg/ml did not appear to significantly disrupt both the colistin-sensitive and *mcr E. coli* biofilms. Despite this, I have shown the ability of EBC-1013 to potentiate the antibiofilm activity of colistin in colistin-resistant *mcr E. coli* biofilms. I hypothesise that the observed potentiation effects here are principally related to EBC-1013-induced bacterial membrane damage and its interactions with the EPS matrix in the *mcr E. coli* biofilms. Interestingly, similar striking synergistic antibacterial activity has recently been reported with tetrandrine, a plant-derived alkaloid extract, which was

demonstrated to synergistically enhance colistin activity by inhibiting the growth of *mcr-1*-positive *E. coli* both *in vivo* and *in vitro* (Shafiq et al. 2022). These results suggest that phytochemicals such as EBC-1013 may represent an effective adjuvant to colistin that could potentially reduce colistin dosing and curb the dissemination of *mcr*-mediated colistin resistance.

Bacterial membrane integrity is essential for cellular physiology and viability, and loss of integrity compromises the membrane function as a selective barrier, resulting in uncontrolled influx or efflux of substances and cell death (Sun et al. 2022; Bramkamp and Scheffers 2023). It has been established that disruption of membrane integrity is a primary mechanism by which numerous antimicrobials of plant origin, including terpenes, exert antimicrobial effects against bacteria, especially MDR pathogens (Álvarez-Martínez et al. 2021). EBC-1013 has previously been shown to induce significant cell membrane permeability in a range of colistin-sensitive and *mcr E. coli* in a dose-dependent manner (128, 256 and 512 μg/ml) (Pritchard et al. 2025; unpublished). In keeping with this finding, EBC-1013 at the same concentrations induced increased bacterial membrane permeabilisation in the three J53 *E. coli* strains tested in our study.

To investigate whether modification of the C12/C13 ester chains of EBC-1013 with deuterium atoms or alkyne groups affected antimicrobial activity, deuterated EBC-1013 and alkyne EBC-1013 were also tested in MICs. Here, both EBC-1013 derivatives (MICs >1024 μg/ml) exhibited no improvement in direct antibacterial activity over the

parent compound EBC-1013 against *E. coli* (MICs >512 µg/ml; as determined by Pritchard et al. [2025; unpublished]). While both modified EBCs retained the ability to permeabilise the *E. coli* cell membrane, the effects showed no enhancement compared to the original EBC-1013, with the alkyne EBC-1013 demonstrating a reduced permeabilisation capacity (permeability only occurring at ≥ 256 µg/ml).

Several studies employing spectroscopic analysis have identified alkyne functional groups in phytochemical-rich extracts of microalgae, seaweed and plants showing antibacterial activity; however, no direct mechanistic link was established between the presence of alkynes and this antibacterial efficacy (Nimisha and Rani 2019; Kavisri et al. 2023; Deepak et al. 2024). In contrast, two studies on deuterated analogues of antimicrobials found that deuteration generally showed equipotent antimicrobial activity as the parent compound, but in some cases, could exhibit microorganism-specific improved efficacy, e.g., deuterated metronidazole showed better anaerobic antibacterial and anti-tubercular activity, and deuterated curcumin had better anti-fungal and anti-tubercular activity (Anjana 2022; Anjana and Kathiravan 2022). In the present study, the lack of significant changes seen in the MIC and bacterial membrane permeability assays following the incorporation of terminal alkyne groups or deuterium atoms in the molecular structure of EBC-1013 suggests that these modifications do not substantially alter the antimicrobial profile of EBC-1013 in both colistin-sensitive and *mcr E. coli*.

Knowing that deuterated EBC-1013 and alkyne EBC-1013 can induce bacterial cell

membrane permeability, I hypothesised that this was a direct result of their interactions with the cell membrane. Hence, ATR-FTIR and PiFM were conducted to examine how treatment of these EBC-1013 analogues may influence the surface chemistry of colistin-sensitive *E. coli*. A number of studies have demonstrated that ATR-FTIR is an effective tool to detect the biochemical changes (e.g., cellular components such as lipids, amide I and amide II proteins, polysaccharides and nucleic acids) in Gram-negative/Gram-positive bacteria and fungi after exposure to various antimicrobials, including nanomaterials, natural compounds, antimicrobial peptides and conventional antibiotics (Quilès et al. 2016; Pulingam et al. 2019; Tantala et al. 2019; Chen et al. 2022; Shaw et al. 2022). However, in my ATR-FTIR analysis, no clear changes in cell chemical composition were observed following treatment with any EBC compound. According to Shaw et al. (2022), ATR-FTIR data generally captures chemical information originating from both the cell membrane and intracellular components. The probing depth in ATR mode measurements is typically 1-3 μm (Chan and Kazarian 2016), while the size of a typical *E. coli* cell is 0.5 μm wide by 2 μm long (El-Hajj and Newman 2015). Therefore, ATR-FTIR can only reflect chemical information averaged over the "bulk" of a cell rather than membrane-specific information. We hypothesised that the lack of induced signal in the *E. coli* ATR-FTIR spectra following EBC treatments is due to this "averaging" effect coupled with only minor changes in cell surface chemistry caused by these EBCs used at 128 μg/ml for 1 h.

PiFM is currently a relatively new technique in the field of microbiology. Nonetheless,

its high spatial resolution (~5 nm) and low penetration depth (≤ 30 nm) (Otter et al. 2021) have enabled unprecedented nanoscale topographical and chemical characterisation of microbial cell membranes. Pioneering work by Davies-Jones et al. (2024) has demonstrated that PiFM can visualise and chemically "map" the distribution of amides, lipids, and carbohydrates across the cellular walls and membranes of bacterial (*E. coli* and *S. aureus*) and fungal (*C. albicans*) cells, highlighting its immense potential for studying the chemistry of cellular surfaces. Building on this approach, a recent study successfully employed PiFM to identify peptidoglycan cell wall destruction inflicted by vancomycin treatment (30 and 60 min) in individual *Bacillus subtilis* cells by mapping the distribution of glycan and amide signals on the bacterial surface (Ali et al. 2025). In our study, the use of PiFM has allowed us to successfully detect the chemical changes occurring in the *E. coli* cell membrane induced by EBC-1013 and its derivatives that were undetectable by the aforementioned ATR-FTIR technique, showing that all the EBC compounds can actually induce membrane lipid disorder and protein conformational change. This finding also aligns with our XPS study, which showed EBC-1013 was associated with lipid disorganisation in the outer membrane of treated *E. coli*. However, given the considerably shorter exposure time in my PiFM study (20 min) compared to the XPS study (1 h), I inferred that these EBC-induced membrane chemical changes may arise much sooner than previously anticipated. Furthermore, our results suggest that the membrane effects observed for the deuterated EBC-1013 and alkyne EBC-1013 are possibly mediated by their direct interaction with the cell membrane (as evidenced by the emergence of the peak at 1772

cm^{-1}); however, further research is warranted to confirm this finding, e.g., by using MD simulations. Finally, we recommend using PiFM over ATR-FTIR in the study of bacterial membranes due to its exceptional lateral spatial resolution, surface sensitivity and chemical specificity.

4.5 Conclusion

EBC-1013 exerts its antimicrobial activity against Gram-negative *E. coli*, in part, by directly targeting the outer membrane, resulting in lipid disorder/disorganisation and protein denaturation. Disruption of membrane integrity represents an important mechanism underlying its antimicrobial effects against planktonic *mcr E. coli*, and when combined with colistin. The binding of the lipophilic EBC-1013 to the cell membrane was evident in XPS with "masking" of the pEtN. Introduction of deuterated atoms and terminal alkyne groups into the C12/C13 ester chains does not alter either the antimicrobial efficacy or the membrane-permeabilising capacity of EBC-1013. Consistent with the parent compound, the two modified analogues also induced changes in lipid and protein compositions in the *E. coli* membrane and this demonstrates the potential of using such label-free imaging with spectral analysis to model drug/small molecule interaction with target cells.

Chapter 5

General Discussion

5.1 General discussion

The discovery of the plasmid-mediated *mcr* genes has transformed our understanding of colistin resistance in Gram-negative bacteria. Carriage of *mcr* imparts resistance to colistin through modification of lipid A in the bacterial outer membrane, which is accompanied by a spectrum of phenotypic effects. Characterising these effects provides valuable insight into the behaviour and environmental interactions of *mcr*-positive bacteria and is essential for designing effective containment and treatment strategies.

In chapters 2 and 3, I have experimentally shown that *mcr-1* and *mcr-3* plasmid carriage was associated with a fitness cost (reduced bacterial growth and gradual loss of *mcr* genes during population evolution) and altered biofilm assembly, mechanics, and stress response to colistin. Current literature on the phenotypic effects of *mcr* carriage in bacterial hosts has predominantly focused on *mcr-1*, highlighting traits such as altered motility, metabolism, virulence, and membrane morphology, integrity, and lipid organisation, as discussed in the results chapters. However, additional phenotypic effects have also been reported. By constructing an *mcr-1* deletion mutant and comparing it to the wild type strain, Li et al. (2020a) found that the expression of *mcr-1* in *E. coli* decreased cell survival under high osmotic stress conditions (e.g., 7% NaCl) and diminished resistance to hydrophobic antibiotics such as gentamicin, kanamycin, and rifampicin, due to altered membrane permeability. In another study, *mcr*-positive clinical *E. coli* isolates demonstrated reduced negative surface charge compared with

the colistin-sensitive *mcr*-free reference strain, with the degree of reduction appearing to be correlated with colistin resistance levels (Maturana et al. 2020).

Interestingly, *mcr-1* carriage has also been demonstrated to modulate microbe-host interactions and immune responses. For example, pathogenic *E. coli* harbouring *mcr-1* showed enhanced gut colonisation while maintaining intestinal microbiota composition, along with cross-resistance to microbiota- and intestinal epithelial cell-derived antimicrobial peptides, increased bacterial adhesion to intestinal eukaryotic cells, and reduced proinflammatory activity (Dalmasso et al. 2023). Similarly, human macrophages infected by *E. coli* expressing *mcr-1* exhibited attenuated inflammatory responses, with downregulated expression of proinflammatory cytokines (TNF-α, IL-12 and IL-1β) and proinflammatory pathways (NF-*κ*B, p38-MAPK and SAPK/JNK), suggesting that *mcr-1*-expressing bacteria may evade early host innate defences (Mattiuz et al. 2020). Collectively, current evidence indicates that the carriage of *mcr-1* plasmids induces intricate, multifaceted changes in bacterial physiological functions alongside conferring resistance to colistin.

Among various biological effects of *mcr* carriage, the potential fitness burden on the bacterial host is particularly important, as low fitness costs can facilitate the persistence and dissemination of *mcr* genes in bacterial populations. Within the *mcr* family, the fitness effects of *mcr-1* carriage are the most extensively studied, yet findings remain divergent. While some studies indicate a measurable fitness cost (decreased growth rate, cell viability and competitive ability), particularly with high-level *mcr-1*

expression or in specific hosts (Yang et al. 2017; Feng et al. 2022), others suggest minimal or no fitness cost, or even advantageous effects, especially in *E. coli* carrying natural, low-copy *mcr-1* plasmids (IncI2 and IncX4) (Wu et al. 2018; Yang et al. 2021; Liu et al. 2023). Thus, a tentative conclusion is that *mcr-1*-associated fitness effects are complex and context-dependent, with the magnitude of cost highly influenced by host species, plasmid type, and the level of *mcr-1* expression. In contrast to *mcr-1*, evidence on the fitness effects of other *mcr* variants remains scarce. Li et al. (2021) compared the fitness costs of *mcr-1~5* expression in *E. coli* TOP10 and found that *mcr-1* and *-2* expression led to better bacterial growth, improved cell viability and less severe membrane damage in comparison to *mcr-3*, *-4* and *-5* expression, suggesting relatively minor fitness costs associated with *mcr-1* and *-2* expression. The authors further argued that, given the high phylogenetic similarity of *mcr-6* to *mcr-1* and *-2* and of *mcr-7~10* to *mcr-3* and *-4*, the expression of these *mcr* genes may exert comparable fitness effects (Li et al. 2021). Research on the physiological impact of *mcr* expression in *E. coli* MG1655 demonstrated that both *mcr-1* and *mcr-8* suppressed bacterial growth and impaired cell viability; however, MCR-8 production induced fewer dead cells relative to MCR-1 production, indicating a lower fitness cost for *mcr-8* expression (Ullah et al. 2021). A study evaluating the fitness costs associated with *mcr-9* observed that its carriage in carbapenem-resistant *Enterobacter hormaechei* or *E. coli* did not affect bacterial growth rate, but induced overexpression of *mcr-9* in recombinant *E. coli* BL21(DE3)pLysS resulting in reduced growth and increased outer membrane permeability, a clear indication of incurred fitness cost (Wu et al. 2025). Lastly, a

plasmid-curing assay revealed that acquisition of the *mcr-10*-harbouring plasmid in *E. roggenkampii* was not associated with reduced fitness, as there were no significant differences in growth rate between the wild-type strain and the plasmid-cured mutant (Xu et al. 2021). In summary, our understanding of the fitness implications of *mcr* genes beyond *mcr-1* is currently insufficient, and further studies are required to fully elucidate their fitness costs.

Recent large-scale surveillance studies in China have shown that the prevalence of *mcr-1* in humans and food animals has reduced significantly since the ban on colistin as a feed additive in 2017 (Wang et al. 2020b; Lv et al. 2022; Zhao et al. 2022). Despite these reductions, this withdrawal policy does not appear to have been sufficient to fully eliminate *mcr*, with evidence demonstrating the continued persistence of *mcr-1*-positive strains at low levels in both animal and human populations even years after the ban (Usui et al. 2021; Zhao et al. 2022; Mei et al. 2024). Thus, understanding how *mcr*-conferred colistin resistance is maintained in bacterial populations in the absence of continuous colistin exposure is essential to help contain *mcr* dissemination. In chapter 3, by using a long-term experimental bead model mimicking bacterial population evolution, we have demonstrated that the fitness cost associated with *mcr-1* plasmid carriage can be compensated for by adaptive evolution (deletion of other costly MDR genes from the plasmid) in the absence of colistin, thereby enabling the preservation and maintenance of *mcr-1* in biofilm populations. Indeed, other compensatory mechanisms that contribute to reduced fitness costs and/or increased stability of *mcr-1*

plasmids have been previously reported. It has recently been shown that compensatory point mutations (single nucleotide polymorphisms) in the regulatory sequence immediately upstream of the *mcr-1* gene reduced its expression and alleviated associated fitness costs, while surprisingly maintaining or even increasing colistin resistance and promoting the stabilisation of *mcr-1* (Ogunlana et al. 2023). PcnR, a ProQ/FinO family protein encoded by *mcr-1*-carrying IncI2 plasmids, was found to play a key role in balancing *mcr-1* expression and the associated fitness costs through plasmid copy number repression by binding to the first stem-loop structure of the *repR* mRNA to inhibit RepA expression, and was critical for the persistence and stability of the *mcr-1* plasmid in bacterial populations (Yang et al. 2021). A plasmid-borne single-base mutation in the 5' untranslated region of the *traJ* gene, which increased plasmid conjugation transfer rates, offset the fitness cost-associated loss of *mcr-1*-bearing plasmids, rescuing them from extinction in bacterial populations (Yang et al. 2023). Additionally, in a 14-day plasmid stability test, the fitness costs initially imposed by an *mcr-1*-positive IncHI2 plasmid were largely compensated for after passage, with the potential mechanism involving compensatory mutations in the chromosomal genes of the bacterial host (e.g., molecular chaperone-encoding *dnaK*, cell division protein-encoding *cpoB* and repeat protein-encoding *rhsC*) (Ma et al. 2018). Taken together, my findings, in conjunction with existing literature, suggest that the evolutionary adaptation that compensates for the fitness costs of *mcr* plasmids arises from plasmid-host co-adaptation, and the underlying mechanism is complex, affecting various biological behaviours of both the plasmid and the bacterial host.

E. coli is the primary cause of urinary tract infections and significantly contributes to bloodstream and other extraintestinal infections in both community and hospital environments (Ramírez-Castillo et al. 2018; Wu et al. 2021a; Ibrahim et al. 2023). MDR *E. coli* strains are becoming increasingly prevalent, with resistance rates estimated to exceed 60%, making empirical treatment with first-line antibiotics difficult (Ramírez-Castillo et al. 2018; Sivarajan et al. 2025). More concerning is the emergence and widespread dissemination of *mcr* genes in MDR *E. coli* and other Gram-negative pathogens. This has rendered colistin treatment ineffective, a drug considered the last-line defence for the treatment of MDR Gram-negative infections, underscoring the urgent need for alternative therapies (Johura et al. 2020; Ejaz et al. 2021). Plant-derived compounds, especially terpenes and their derivatives, have demonstrated potent antimicrobial activity against a wide range of drug-resistant pathogenic bacteria, with cell membrane disruption representing one of the many proposed mechanisms of action (Mahizan et al. 2019). Therefore, a major focus of Chapter 4 was to explore the interactive effects of EBC-1013, a semi-synthetic epoxytigliane (diterpene ester), with the cell membrane of *mcr*-negative or -positive *E. coli* molecular models.

Previous work in our laboratory screening numerous naturally occurring and semi-synthetic EBCs for potential antimicrobial candidates has established EBC-1013 as a compound with the lead antimicrobial activity. Furthermore, a structure-activity relationship (SAR) seems to have also been established among the EBCs, with longer side ester chains connected to C12/C13 of the tigliane backbone showing greater

antimicrobial activity. MIC testing of EBC-1013, EBC-46 and EBC-147 on chronic wound and oral Gram-positive pathogens (*S. aureus* [MRSA], *S. pyogenes* and *Streptococcus mutans*) showed that EBC-1013 (with long C12/C13 side chains) was the most potent (MIC ≤ 32 μg/ml), followed by EBC-46 (≤ 512 μg/ml; medium C12/C13 side chain length), with EBC-147 being the least effective (≥ 512 μg/ml; short C12/C13 side chain) (Xue 2022). Although the direct antimicrobial activity of all three EBCs against Gram-negative bacteria (*P. aeruginosa*, *E. coli* and *A. baumannii*) was negligible (MICs > 512 μg/ml) (Powell et al. 2022), such SAR appeared to be evident in their ability to interact with the Gram-negative outer membrane. In a previous MD simulation using an LPS-DPPE bilayer mimicking the outer membrane of *P. aeruginosa*, a clear difference in interaction time with specific membrane residues for the three EBCs was observed (EBC-1013 > EBC-46 > EBC-147) (Powell et al. 2022). Similarly, in the MD simulations in this study using a model membrane mimicking the outer membrane of *E. coli*, EBC-1013 demonstrated more interactions with the membrane surface and the colistin molecule compared to EBC-147. These results are clear evidence that the structure of EBCs, particularly the C12/C13 side chain length, may significantly affect their behaviour in interacting with the bacterial cell membrane. In the context of epoxytiglianes, SARs have also been identified as crucial for anticancer activity, with the length, branching and unsaturation features of the C12 ester chain, as well as the 6,7-epoxide structural motif and position, shown to significantly influence the PKC activation efficacy of EBCs *in vitro* (Cullen et al. 2021). More broadly, the length, number, and substitutional position of ester side chains attached to

the molecular backbone markedly affects the antimicrobial activity of a diverse group of antimicrobials across different compound classes, including phytochemicals, against both bacteria and fungi (Joondan et al. 2014; Andrade et al. 2015; Song et al. 2023; Rahaman et al. 2025; Zhang et al. 2025).

Apart from the above-mentioned parameters, the nature of the ester side chain moiety also modifies the observed antimicrobial activity of an antimicrobial. A study evaluating the antibacterial properties of a set of 16 synthesised caffeic acid ester derivatives showed that compounds with alkyl side chains generally demonstrated superior *in vitro* antibacterial activity against *E. coli* compared to those with aryl side chains. Furthermore, even within alkyl substitutes, short or branched chains or the presence of heteroatoms, were all shown to reduce antibacterial activity (Araujo et al. 2019). Hence, the structural features (e.g., presence of certain functional groups or atoms) of ester side chains play a key role in tuning the efficacy of a prototypical antimicrobial. In chapter 4, deuterium atoms and alkyne bonds were introduced into the C12/C13 side chains in EBC-1013 to investigate whether these functional groups could make EBC-1013 more readily identified in PiFM and FTIR analysis. Significantly, these changes did not alter the antimicrobial profile of EBC-1013. Furthermore, the alkyne EBC-1013 showed a reduced ability to permeabilise bacterial membranes (which occurred at higher effective concentrations), which is consistent with the lack of antimicrobial activity of this functional group in the literature. Further structural modifications to EBC-1013 are required to identify a derivative with

enhanced antimicrobial activity to support the antimicrobial pipeline.

It has been widely recognised in literature that several physicochemical properties of the bacterial cell surface, including permeability, hydrophobicity, charge and rigidity, are closely linked to the structure and function of membrane lipids and proteins. For example, *E. coli* cells with defective LPS displayed enhanced outer membrane permeability and cell surface hydrophobicity (Wang et al. 2015), as well as increased susceptibility toward a series of cationic antimicrobial peptides (Ebbensgaard et al. 2018). Structural changes in the outer membrane protein A (OmpA) due to allelic variation shifted cell surface hydrophobicity and charge (zeta potential) in *E. coli* (Liao et al. 2022). Terpenes such as cinnamaldehyde have demonstrated the capacity to alter the lipid profile of the bacterial plasma membrane, leading to an increase in saturated fatty acids, consequently enhancing membrane rigidity (Di Pasqua et al. 2006). Together, these results suggest a direct correlation between microscopic alterations in bacterial membrane components and the macroscopic properties observed. In Chapter 4, by using XPS and PiFM, I have demonstrated that lipid disorder and protein conformational change are a direct consequence of EBC-1013 interacting with the cell membrane in both colistin-sensitive and *mcr E. coli*. I also confirmed the increased permeability and compromised integrity of the *E. coli* cell membrane after EBC-1013 treatment in bacterial membrane permeability assays and using TEM. Therefore, a highly likely causal and sequential relationship exists between the two findings. Indeed, lipid disorders such as lipid asymmetry disruption (e.g., mis-localisation or

accumulation of phospholipids in the outer leaflet of the *E. coli* outer membrane) have been described to result in compromised membrane integrity (May and Silhavy 2018). Ordered organisation of the outer membrane lipids and proteins across the entire bacterial surface is crucial for the maintenance of outer membrane integrity and barrier function (Benn et al. 2021).

In addition to its effects on cell membrane permeability, EBC-1013 has been demonstrated to influence other cell surface properties, i.e., surface charge and hydrophobicity. The treatment with EBC-1013 led to an increase in the negative surface charge of *E. coli* IR57 and enhanced cellular hydrophobicity among a range of *mcr E. coli* strains (Xue 2022). A more negatively charged *E. coli* cell surface is associated with higher susceptibility to colistin treatment (Maturana et al. 2020). Thus, the EBC-1013-induced surface charge alterations could be a mechanism explaining its ability to potentiate colistin activity in disrupting established *mcr E. coli* biofilms, as observed in the biofilm disruption assay, in addition to the previously discussed biofilm-associated mechanisms (matrix damage and pore formation). However, zeta potential experiments on EBC-1013 treated *mcr E. coli* are required to confirm this hypothesis. On the other hand, hydrophobic interactions between antimicrobials and the lipid-like bacterial membrane may compromise membrane permeability and induce cell death (Judge et al. 2013). Phytochemical-treated bacteria have been reported to exhibit enhanced hydrophobicity and heightened susceptibility to certain traditional antibiotics (Monte et al. 2014). This suggests that EBC-1013 may potentiate the direct

antimicrobial activity of potentially a number of antibiotics, including colistin, against *mcr E. coli*. In accord with this speculation, unpublished data have demonstrated marked synergistic effects of EBC-1013 in combination with colistin in treating a panel of planktonic *mcr* Enterobacteriaceae (fractional inhibitory concentration indices < 0.5) (Pritchard et al. 2025; unpublished). However, again, experiments are needed to screen dual combinations of EBC-1013 and other antibiotic candidates to confirm its broad antibiotic-potentiating ability.

5.2 Limitations and future work

In Chapter 2, the majority of the phenotypic characterisation experiments were performed on *E. coli* J53(pE30) and J53(pWJ1) transconjugant strains, where the plasmids had been transferred from the original host into J53. However, as discussed in the general discussion, the biological effects, especially the fitness costs conferred by *mcr* genes, are highly dependent on the host genetic background and plasmid type. Thus, additional planktonic and biofilm characterisation could be performed on the original wild-type strains E30 (*mcr-1*) and WJ1 (*mcr-3*), as well as other clinical and farm isolates of various origins, to give much deeper insights into the phenotypic effects of *mcr* carriage.

In Chapter 3, the evolutionary bead biofilm model was run for 51 days without apparent loss of *mcr-3* in the J53(pWJ1) cultures. Although a reduction in *mcr-3* was noted, it would have greatly aided in elucidating the fitness cost and the underlying

compensatory mechanism of *mcr-3* plasmid carriage in biofilm populations if it had been extended to observe *mcr-3* loss. In that case, in-depth genotypic characterisation on the *mcr-3* strain before and after evolution, similar to that done for the *mcr-1* strain, could have been performed. Future research using this evolutionary model could also investigate direct competition between *mcr-1* and *mcr-3* populations through co-inoculation of both *mcr* strains.

In Chapter 4, time constraints limited some experiments to either colistin-sensitive *mcr*-free or colistin-resistant *mcr*-positive *E. coli*, preventing the inclusion of both strains. For example, the MD simulations in this study only used a model membrane representing the *E. coli* K12 outer membrane composed of R1 core-Lipid A molecules without *mcr*-conferred lipid A modification. Similarly, the ATR-FTIR and PiFM experiments were only performed with *mcr*-negative *E. coli* CX17 and J53, respectively. Further studies on *mcr*-positive *E. coli* using these techniques remain to be undertaken to provide a better understanding of how *mcr* carriage affects EBC-1013 and/or its analogues interacting with the cell membrane. Furthermore, the use of epoxytiglianes at 128 μg/ml for 1 h in ATR-FTIR did not give positive results, with no changes in cell surface chemistry observed. If time had allowed, further studies would have tested higher concentrations and longer treatment times.

5.3 Conclusion

This study demonstrates the association of *mcr-1* and *mcr-3* plasmid carriage with

fitness costs and their ability to modify biofilm phenotypes. The *mcr-1*-harbouring plasmid is less stably maintained in bacterial populations compared to its *mcr-3* counterpart. Whilst loss of *mcr-1* in bacterial biofilm environments is evident in the absence of colistin selection, persistence of *mcr-1* plasmids occurs through compensatory adaptation. With the increasing dissemination of *mcr* genes in MDR Gram-negative bacteria, plant-derived epoxytiglianes, a novel class of antimicrobial agents, represent a promising adjuvant to colistin treatment by directly interacting with and modifying the bacterial cell membrane. Furthermore, the non-antibiotic nature of these antimicrobials, able to both target biofilm disruption and stimulate the innate immune system (Powell et al. 2022), holds considerable promise for limiting future evolution of resistance.

Appendices

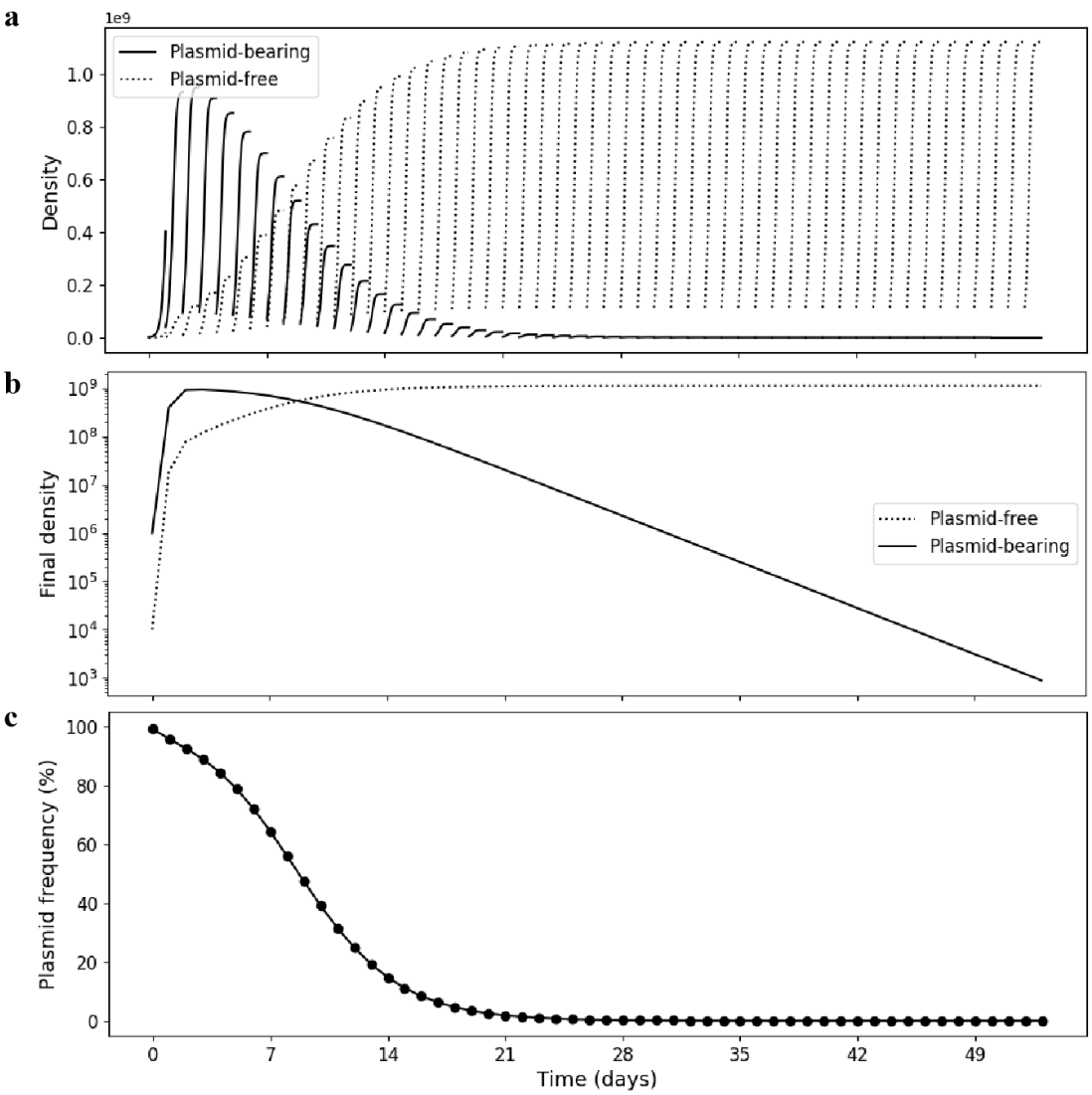

Appendix Figure 1. Numerical simulation of an evolutionary experiment in the absence of antibiotics. **a** Daily densities in a drug-free scenario, showing plasmid-free cells ($B_{ø}$, dotted line) and plasmid-bearing cells (B_p, solid line). **b** Final bacterial densities at the end of each day, illustrating changes driven by resource availability and competition. **c** Plasmid frequency in the population over time, highlighting the progressive clearance of plasmids from plasmid-bearing cells.

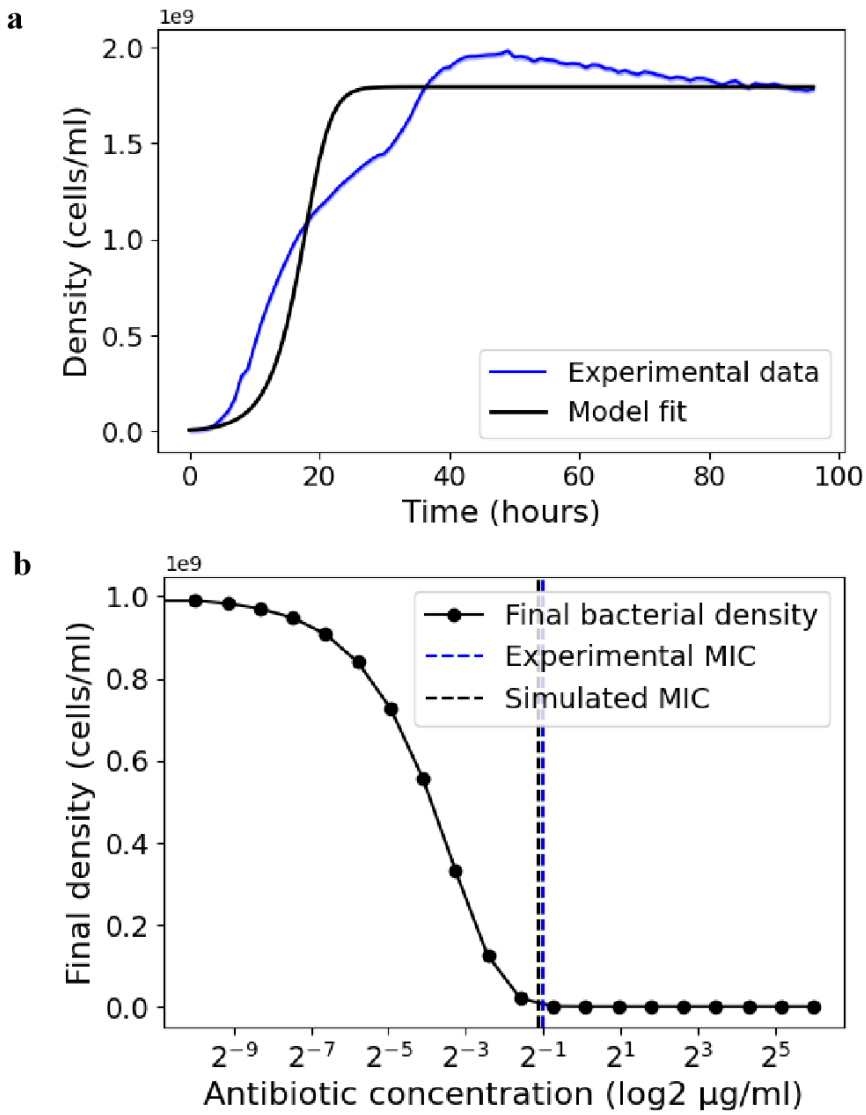

Appendix Figure 2. Example of model parameterisation. **a** Growth curve obtained experimentally, shown as a solid blue line, with shaded area representing the standard deviation. The black line corresponds to the best-fit model prediction based on Monod growth parameters. **b** Dose-response experiment showing the relationship between antibiotic concentration and final bacterial density. The black dashed line indicates the simulated MIC, while the blue dashed line marks the experimentally determined MIC.

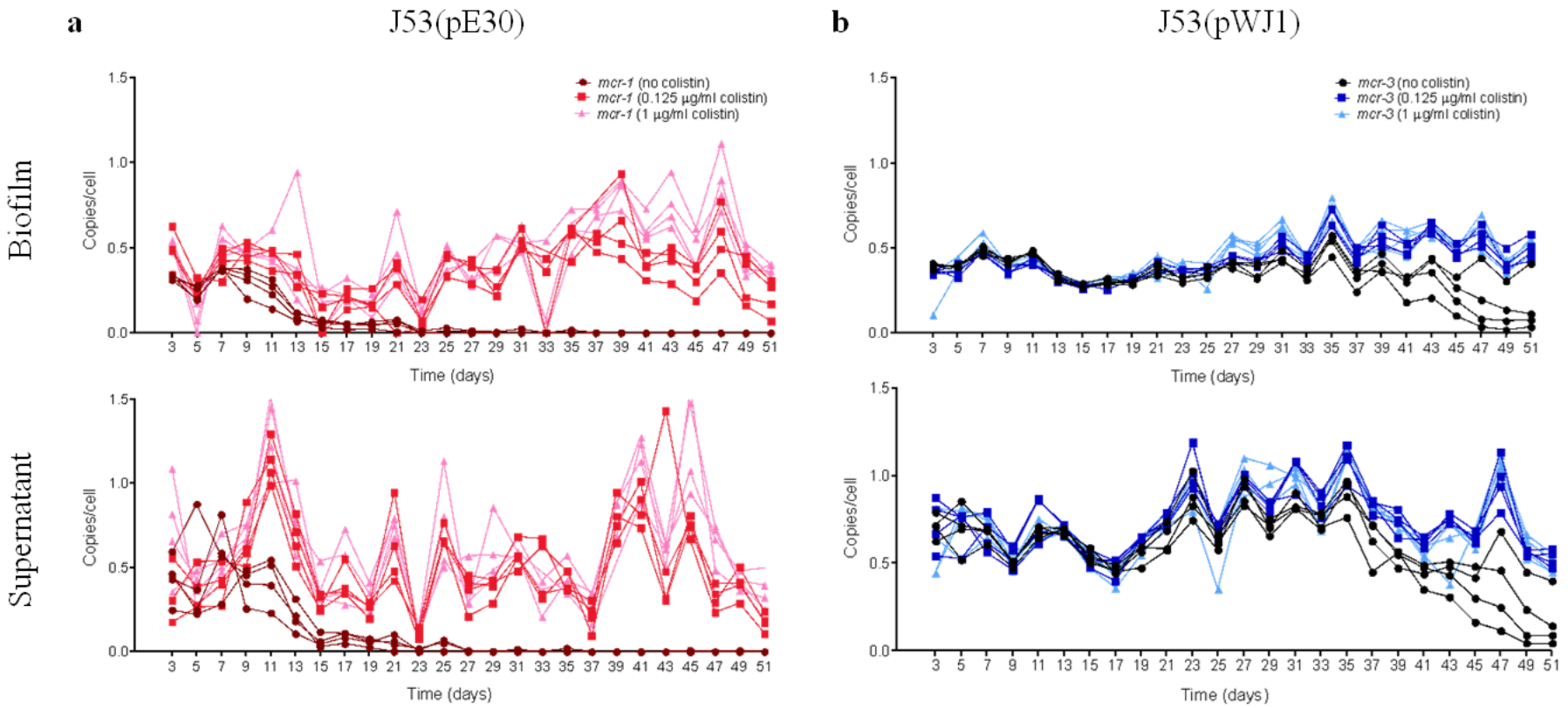

Appendix Figure 3. RT-qPCR monitoring of *mcr-1* and *mcr-3* persistence in *E. coli* J53(pE30) and J53(pWJ1), respectively, in a bead biofilm evolution model over 51 days ± colistin selective pressure (0.125 or 1 µg/ml), showing data for all 4 experimental replicates. RT-qPCR was conducted on both bead and supernatant samples to monitor *mcr* gene levels in biofilm and planktonic bacterial populations, respectively. **a** J53(pE30) *mcr-1*. **b** J53(pWJ1) *mcr-3*. Abundance of *mcr-1* and *mcr-3* was calculated as the absolute copy number of the *gene* relative to *rpoB* (representing copies/cell).

Appendix Table 1. COMSTAT analysis (Dead/Live bacterial ratio) significance table of biofilm formation assay performed on evolved *E. coli* J53(pE30) biofilm populations in the bead biofilm model (replicates 1, 2 and 3).

Time point (Day)	Colistin concentration (μg/ml)	Replicate 1 vs 2	Replicate 1 vs 3	Replicate 2 vs 3
23	0	**< 0.0001**	**< 0.0001**	> 0.9999
	0.125	**< 0.0001**	**< 0.0001**	0.9950
	1	**0.0005**	**< 0.0001**	0.7672
51	0	**< 0.0001**	**< 0.0001**	0.7303
	0.125	**0.0001**	**< 0.0001**	0.6176
	1	**< 0.0001**	**< 0.0001**	0.7260

Values in bold represent statistical significance.

Appendix Table 2. COMSTAT analysis (Biomass) significance table of biofilm formation assay performed on evolved *E. coli* J53(pE30) biofilm populations in the bead biofilm model (replicates 1, 2 and 3).

Time point (Day)	Colistin concentration (μg/ml)	Replicate 1 vs 2	Replicate 1 vs 3	Replicate 2 vs 3
23	0	0.6792	0.4304	0.0713
	0.125	**0.0192**	0.9249	**< 0.0001**
	1	0.2129	0.0776	0.7531
51	0	**0.0005**	**< 0.0001**	0.8914
	0.125	**0.0008**	**< 0.0001**	0.1074
	1	**< 0.0001**	**< 0.0001**	> 0.9999

Values in bold represent statistical significance.

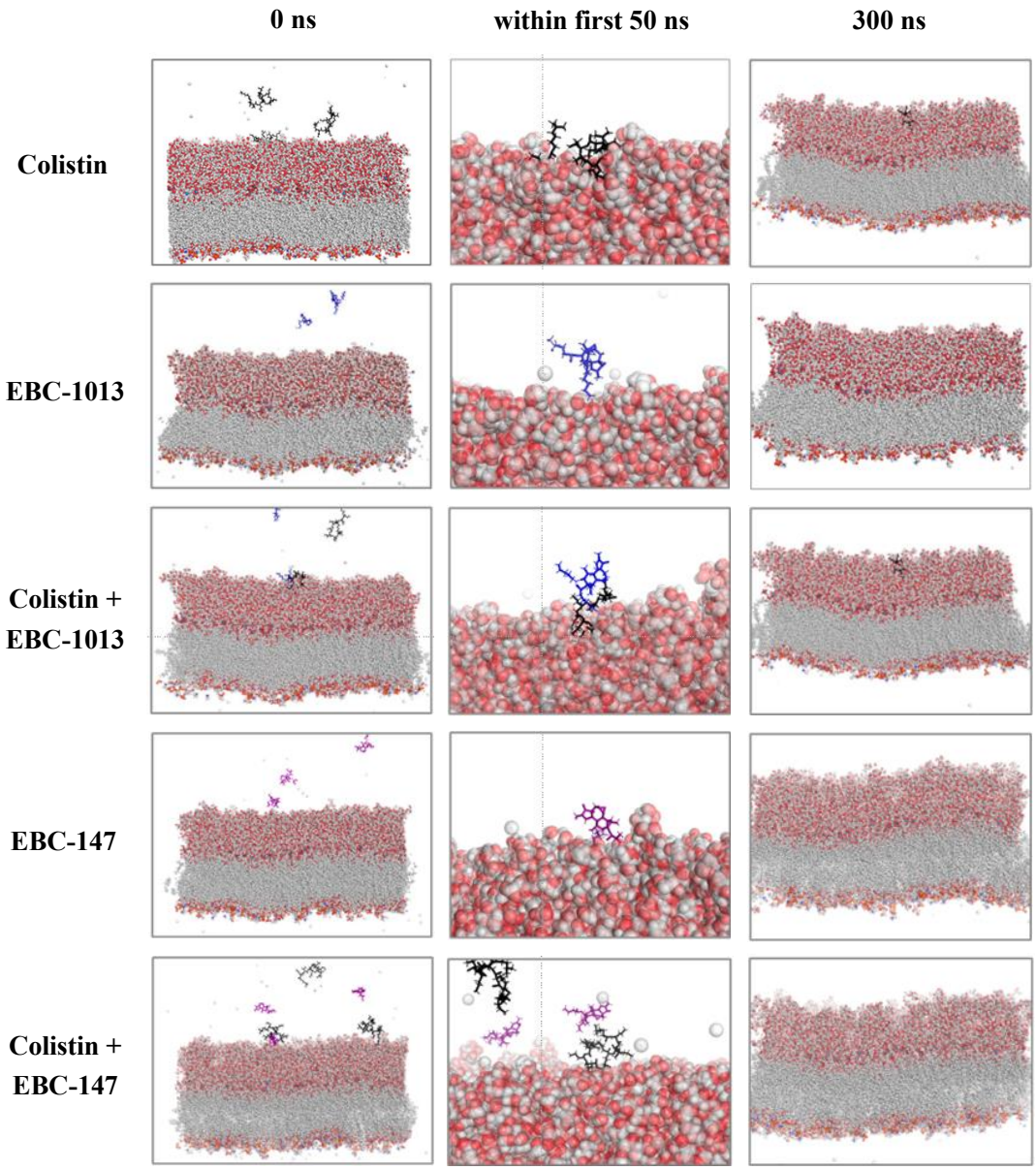

Appendix Figure 4. Images showing the beginning, middle and end point of the molecular dynamics simulations shown in Figure 4.4. Colistin, EBC-1013 and EBC-147 are shown in black, blue and purple respectively. The simulated *E. coli* membrane is shown in red and grey, and the white spheres represent circulating ions.

Appendix Table 3. Statistical significance table showing the results of CLSM COMSTAT image analysis for 18 h established *E. coli* CX-17 and CX-17(pPN16) biofilms treated with colistin, EBC-1013, their combination and the ethanol vehicle control.

Strain	Measurement	Treatment	Treatment			
			Vehicle	Colistin	EBC-1013	EBC-1013 + Colistin
CX-17	Biomass	Untreated	0.0199*	<0.0001****	0.0298*	<0.0001****
		Vehicle		<0.0001****	>0.9999	<0.0001****
		Colistin			<0.0001****	0.9989
		EBC-1013				<0.0001****
	Dead/Live bacterial ratio	Untreated	0.0072**	0.0278*	0.3246	>0.9999
		Vehicle		<0.0001****	>0.9999	0.0002***
		Colistin			<0.0001****	0.3712
		EBC-1013				0.0221*
CX-17(pPN16)	Biomass	Untreated	0.3549	0.1120	>0.9999	<0.0001****
		Vehicle		0.9956	0.9659	<0.0001****
		Colistin			0.7282	0.0053**
		EBC-1013				0.0050**
	Dead/Live bacterial ratio	Untreated	>0.9999	>0.9999	0.7433	>0.9999
		Vehicle		>0.9999	0.0043**	>0.9999
		Colistin			0.2830	>0.9999
		EBC-1013				0.9455

*P < 0.05, **P < 0.01, ***P < 0.001, ****P < 0.0001

References

Abraham, M. J., Murtola, T., Schulz, R., Páll, S., Smith, J. C., Hess, B. and Lindahl, E. 2015. GROMACS: High performance molecular simulations through multi-level parallelism from laptops to supercomputers. *SoftwareX* 1, pp. 19-25.

Abraham, N. and Kwon, D. H. 2009. A single amino acid substitution in PmrB is associated with polymyxin B resistance in clinical isolate of *Pseudomonas aeruginosa*. *FEMS microbiology letters* 298(2), pp. 249-254.

AbuOun, M. et al. 2017. *mcr-1* and *mcr-2* (*mcr-6.1*) variant genes identified in *Moraxella* species isolated from pigs in Great Britain from 2014 to 2015. *Journal of Antimicrobial Chemotherapy* 72(10), pp. 2745-2749.

Abushaheen, M. A. et al. 2020. Antimicrobial resistance, mechanisms and its clinical significance. *Dis Mon* 66(6), p. 100971. doi: 10.1016/j.disamonth.2020.100971

Adams, M. D., Nickel, G. C., Bajaksouzian, S., Lavender, H., Murthy, A. R., Jacobs, M. R. and Bonomo, R. A. 2009. Resistance to colistin in *Acinetobacter baumannii* associated with mutations in the PmrAB two-component system. *Antimicrobial agents and chemotherapy* 53(9), pp. 3628-3634.

Aghapour, Z. et al. 2019. Molecular mechanisms related to colistin resistance in Enterobacteriaceae. *Infection and drug resistance*, pp. 965-975.

Ahn, E. 2021. *Effects of the acquisition of mcr-1-harboring plasmids on virulence in enterohemorrhagic Escherichia coli.* Seoul National University Graduate School.

Al-Qadiri, H., Lin, M., Al‐Holy, M., Cavinato, A. and Rasco, B. 2008a. Detection of sublethal thermal injury in *Salmonella enterica* serotype Typhimurium and *Listeria monocytogenes* using Fourier transform infrared (FT-IR) spectroscopy (4000 to 600 cm^{-1}). *Journal of food science* 73(2), pp. M54-M61.

Al-Qadiri, H. M., Al-Alami, N. I., Al-Holy, M. A. and Rasco, B. A. 2008b. Using Fourier transform infrared (FT-IR) absorbance spectroscopy and multivariate analysis to study the effect of chlorine-induced bacterial injury in water. *Journal of agricultural and food chemistry* 56(19), pp. 8992-8997.

Al Mana, H., Johar, A. A., Kassem, I. I. and Eltai, N. O. 2022. Transmissibility and persistence of the plasmid-borne mobile colistin resistance gene, *mcr-1*, harbored in poultry-associated *E. coli*. *Antibiotics* 11(6), p. 774.

Al Musayeib, N. M., Musarat, A. and Maqsood, F. 2022. Terpenes: A Source of Novel Antimicrobials, Applications and Recent Advances. *Eco-Friendly Biobased Products Used in Microbial Diseases*, pp. 247-270.

Alder, B. J. and Wainwright, T. E. 1957. Phase transition for a hard sphere system. *The Journal of chemical physics* 27(5), p. 1208.

Aldred, K. J., Kerns, R. J. and Osheroff, N. 2014. Mechanism of quinolone action and resistance. *Biochemistry* 53(10), pp. 1565-1574.

Ali, M. et al. 2025. Subcellular nano-chemical characterization in photothermal spectroscopic imaging of antimicrobial interaction in model system *Bacillus subtilis* & vancomycin. *arXiv preprint arXiv:2505.10249*,

Allesen‐Holm, M. et al. 2006. A characterization of DNA release in *Pseudomonas aeruginosa* cultures and biofilms. *Molecular microbiology* 59(4), pp. 1114-1128.

Alonso-del Valle, A. et al. 2023. Antimicrobial resistance level and conjugation permissiveness shape plasmid distribution in clinical enterobacteria. *Proceedings of the National Academy of Sciences* 120(51), p. e2314135120.

Althunibat, O. Y. et al. 2016. Effect of Thymol and Carvacrol, the Major Components of Thymus capitatus on the Growth of *Pseudomonas aeruginosa*. *Journal of Pure & Applied Microbiology* 10(1),

Alvarez-Martinez, C. E. and Christie, P. J. 2009. Biological diversity of prokaryotic type IV secretion systems. *Microbiology and molecular biology reviews* 73(4), pp. 775-808.

Álvarez-Martínez, F. J., Barrajón-Catalán, E., Herranz-López, M. and Micol, V. 2021. Antibacterial plant compounds, extracts and essential oils: An updated review on their effects and putative mechanisms of action. *Phytomedicine* 90, p. 153626.

Alvarez-Ordóñez, A., Halisch, J. and Prieto, M. 2010. Changes in Fourier transform infrared spectra of *Salmonella enterica* serovars Typhimurium and Enteritidis after adaptation to stressful growth conditions. *International journal of food microbiology* 142(1-2), pp. 97-105.

Amaral, V. C., Santos, P. R., da Silva, A. F., dos Santos, A. R., Machinski Jr, M. and Mikcha, J. M. G. 2015. Effect of carvacrol and thymol on *Salmonella* spp. biofilms on polypropylene. *International Journal of Food Science and Technology* 50(12), pp. 2639-2643.

Anandan, A. et al. 2017. Structure of a lipid A phosphoethanolamine transferase suggests how conformational changes govern substrate binding. *Proceedings of the National Academy of Sciences* 114(9), pp. 2218-2223.

Anderson, M. S. 2000. Infrared spectroscopy with an atomic force microscope. *Applied spectroscopy* 54(3), pp. 349-352.

Andersson, D. I. and Hughes, D. 2010. Antibiotic resistance and its cost: is it possible to reverse resistance? *Nature reviews microbiology* 8(4), pp. 260-271.

Andrade, F. F., Silva, D., Rodrigues, A. and Pina-Vaz, C. 2020. Colistin update on its mechanism of action and resistance, present and future challenges. *Microorganisms* 8(11), p. 1716.

Andrade, M. et al. 2015. Fine-tuning of the hydrophobicity of caffeic acid: studies on the antimicrobial activity against *Staphylococcus aureus* and *Escherichia coli*. *RSC Advances* 5(66), pp. 53915-53925.

Angelini, P. 2024. Plant-derived antimicrobials and their crucial role in combating antimicrobial resistance. *Antibiotics* 13(8), p. 746.

Anjana, G. 2022. Synthesis and Antimicrobial Evaluation of Deuterated Analogues of Metronidazole. *Iraqi Journal of Pharmaceutical Sciences* 31(2), pp. 297-303.

Anjana, G. and Kathiravan, M. 2022. Antimicrobial activity of curcumin and deuterated curcumin.

Araujo, M. O., Freire Pessoa, H. L., Lira, A. B., Castillo, Y. P. and de Sousa, D. P. 2019. Synthesis, antibacterial evaluation, and QSAR of caffeic acid derivatives. *Journal of Chemistry* 2019(1), p. 3408315.

Arcilla, M. S., van Hattem, J. M., Matamoros, S., Melles, D. C., Penders, J., de Jong, M. D. and Schultsz, C. 2016. Dissemination of the *mcr-1* colistin resistance gene. *The Lancet Infectious Diseases* 16(2), pp. 147-149.

Ares-Arroyo, M. et al. 2022. Genomics, transcriptomics, and metabolomics reveal that minimal modifications in the host are crucial for the compensatory evolution of ColE1-like plasmids. *Msphere* 7(6), pp. e00184-00122.

Arroyo, L. A., Herrera, C. M., Fernandez, L., Hankins, J. V., Trent, M. S. and Hancock, R. E. 2011. The pmrCAB operon mediates polymyxin resistance in *Acinetobacter baumannii* ATCC 17978 and clinical isolates through phosphoethanolamine

modification of lipid A. *Antimicrobial agents and chemotherapy* 55(8), pp. 3743-3751.

Arzani, V., Soleimani, M., Fritsch, T., Jacob, U. M., Calabrese, V. and Arzani, A. 2025. Plant polyphenols, terpenes, and terpenoids in oral health. *Open Medicine* 20(1), p. 20251183.

Badar, M. S., Shamsi, S., Ahmed, J. and Alam, M. A. 2022. Molecular dynamics simulations: concept, methods, and applications.*Transdisciplinarity*. Springer, pp. 131-151.

Bader, M. W. et al. 2005. Recognition of antimicrobial peptides by a bacterial sensor kinase. *Cell* 122(3), pp. 461-472.

Baeuerlein, A., Ackermann, S. and Parlesak, A. 2009. Transepithelial activation of human leukocytes by probiotics and commensal bacteria: Role of Enterobacteriaceae‐type endotoxin. *Microbiology and immunology* 53(4), pp. 241-250.

Bagge, N., Hentzer, M., Andersen, J. B., Ciofu, O., Givskov, M. and Høiby, N. 2004. Dynamics and spatial distribution of β-lactamase expression in *Pseudomonas aeruginosa* biofilms. *Antimicrobial agents and chemotherapy* 48(4), pp. 1168-1174.

Barnett, C. M., Broit, N., Yap, P.-Y., Cullen, J. K., Parsons, P. G., Panizza, B. J. and Boyle, G. M. 2019. Optimising intratumoral treatment of head and neck squamous cell carcinoma models with the diterpene ester Tigilanol tiglate. *Investigational New Drugs* 37(1), pp. 1-8.

Baron, S., Hadjadj, L., Rolain, J.-M. and Olaitan, A. O. 2016. Molecular mechanisms of polymyxin resistance: knowns and unknowns. *International journal of antimicrobial agents* 48(6), pp. 583-591.

Barrow, K. and Kwon, D. H. 2009. Alterations in two-component regulatory systems of phoPQ and pmrAB are associated with polymyxin B resistance in clinical isolates of *Pseudomonas aeruginosa*. *Antimicrobial agents and chemotherapy* 53(12), pp. 5150-5154.

Beceiro, A. et al. 2011. Phosphoethanolamine modification of lipid A in colistin-resistant variants of *Acinetobacter baumannii* mediated by the pmrAB two-component regulatory system. *Antimicrobial agents and chemotherapy* 55(7), pp. 3370-3379.

Beceiro, A. et al. 2014. Biological cost of different mechanisms of colistin resistance and their impact on virulence in *Acinetobacter baumannii*. *Antimicrobial agents and chemotherapy* 58(1), pp. 518-526.

Belaynehe, K. M., Shin, S. W., Park, K. Y., Jang, J. Y., Won, H. G., Yoon, I. J. and Yoo, H. S. 2018. Emergence of *mcr-1* and *mcr-3* variants coding for plasmid-mediated colistin resistance in *Escherichia coli* isolates from food-producing animals in South Korea. *International Journal of Infectious Diseases* 72, pp. 22-24.

Beloin, C., Roux, A. and Ghigo, J.-M. 2008. *Escherichia coli* biofilms. *Bacterial biofilms*, pp. 249-289.

Ben Miri, Y., Nouasri, A., Herrera, M., Djenane, D. and Ariño, A. 2023. Antifungal activity of menthol, eugenol and their combination against *Aspergillus ochraceus* and *Aspergillus niger* in vitro and in stored cereals. *Foods* 12(11), p. 2108.

Benn, G. et al. 2021. Phase separation in the outer membrane of *Escherichia coli*. *Proceedings of the National Academy of Sciences* 118(44), p. e2112237118.

Benyoussef, W., Deforet, M., Monmeyran, A. and Henry, N. 2022. Flagellar motility during *E. coli* biofilm formation provides a competitive disadvantage which recedes in the presence of co-colonizers. *Frontiers in Cellular and Infection Microbiology* 12, p. 896898.

Benz, F. and Hall, A. R. 2023. Host-specific plasmid evolution explains the variable spread of clinical antibiotic-resistance plasmids. *Proceedings of the National Academy of Sciences* 120(15), p. e2212147120.

Berglund, N. A., Piggot, T. J., Jefferies, D., Sessions, R. B., Bond, P. J. and Khalid, S. 2015. Interaction of the antimicrobial peptide polymyxin B1 with both membranes of *E. coli*: a molecular dynamics study. *PLoS computational biology* 11(4), p. e1004180.

Bernier, S. P. et al. 2013. Starvation, together with the SOS response, mediates high biofilm-specific tolerance to the fluoroquinolone ofloxacin. *PLoS genetics* 9(1), p. e1003144.

Bertelloni, F., Cagnoli, G., Turchi, B. and Ebani, V. V. 2022. Low Level of Colistin Resistance and *mcr* Genes Presence in *Salmonella* spp.: Evaluation of Isolates Collected between 2000 and 2020 from Animals and Environment. *Antibiotics* 11(2), p. 272.

Bhagwat, G., O'connor, W., Grainge, I. and Palanisami, T. 2021. Understanding the fundamental basis for biofilm formation on plastic surfaces: role of conditioning films. *Frontiers in microbiology* 12, p. 687118.

Bjarnsholt, T. et al. 2005. *Pseudomonas aeruginosa* tolerance to tobramycin, hydrogen peroxide and polymorphonuclear leukocytes is quorum-sensing dependent.

Microbiology 151(2), pp. 373-383.

Björkman, J. and Andersson, D. I. 2000. The cost of antibiotic resistance from a bacterial perspective. *Drug resistance updates* 3(4), pp. 237-245.

Boags, A. T., Samsudin, F. and Khalid, S. 2019. Binding from both sides: TolR and full-length OmpA bind and maintain the local structure of the *E. coli* cell wall. *Structure* 27(4), pp. 713-724. e712.

Borowiak, M., Hammerl, J. A., Deneke, C., Fischer, J., Szabo, I. and Malorny, B. 2019. Characterization of *mcr-5*-harboring *Salmonella enterica* subsp. *enterica* serovar Typhimurium isolates from animal and food origin in Germany. *Antimicrobial agents and chemotherapy* 63(6), pp. 10.1128/aac. 00063-00019.

Borriello, G., Werner, E., Roe, F., Kim, A. M., Ehrlich, G. D. and Stewart, P. S. 2004. Oxygen limitation contributes to antibiotic tolerance of *Pseudomonas aeruginosa* in biofilms. *Antimicrobial agents and chemotherapy* 48(7), pp. 2659-2664.

Bouma, J. E. and Lenski, R. E. 1988. Evolution of a bacteria/plasmid association. *Nature* 335(6188), pp. 351-352.

Bowers, K. J. et al. eds. 2006. *Scalable algorithms for molecular dynamics simulations on commodity clusters*. *Proceedings of the 2006 ACM/IEEE Conference on Supercomputing.*

Boyle, G. M. et al. 2014. Intra-lesional injection of the novel PKC activator EBC-46 rapidly ablates tumors in mouse models. *PloS one* 9(10), p. e108887.

Bradford, P. A. 2001. Extended-spectrum β-lactamases in the 21st century: characterization, epidemiology, and detection of this important resistance threat. *Clinical microbiology reviews* 14(4), pp. 933-951.

Bramkamp, M. and Scheffers, D. J. 2023. Bacterial membrane dynamics: Compartmentalization and repair. *Molecular microbiology* 120(4), pp. 490-501.

Braun, V. 1975. Covalent lipoprotein from the outer membrane of *Escherichia coli*. *Biochimica et Biophysica Acta (BBA)-Reviews on Biomembranes* 415(3), pp. 335-377.

Bribi, N. 2018. Pharmacological activity of alkaloids: a review. *Asian J. Bot* 1(1), pp. 1-6.

Brockhurst, M. A. and Harrison, E. 2022. Ecological and evolutionary solutions to the plasmid paradox. *Trends in microbiology* 30(6), pp. 534-543.

Broniatowski, M., Mastalerz, P. and Flasiński, M. 2015. Studies of the interactions of ursane-type bioactive terpenes with the model of *Escherichia coli* inner membrane—Langmuir monolayer approach. *Biochimica et Biophysica Acta (BBA)-Biomembranes* 1848(2), pp. 469-476.

Brooks, B. R. et al. 2009. CHARMM: the biomolecular simulation program. *Journal of computational chemistry* 30(10), pp. 1545-1614.

Brown, L., Wolf, J. M., Prados-Rosales, R. and Casadevall, A. 2015. Through the wall: extracellular vesicles in Gram-positive bacteria, mycobacteria and fungi. *Nature reviews microbiology* 13(10), pp. 620-630.

Burgula, Y. et al. 2006. Detection of *Escherichia coli* O157: H7 and *Salmonella* typhimurium using filtration followed by Fourier-transform infrared spectroscopy. *Journal of food protection* 69(8), pp. 1777-1784.

Bush, K. and Jacoby, G. A. 2010. Updated functional classification of β-lactamases. *Antimicrobial agents and chemotherapy* 54(3), pp. 969-976.

Cabezón, E., Ripoll-Rozada, J., Peña, A., De La Cruz, F. and Arechaga, I. 2015. Towards an integrated model of bacterial conjugation. *FEMS microbiology reviews* 39(1), pp. 81-95.

Camilli, A. and Bassler, B. L. 2006. Bacterial small-molecule signaling pathways. *Science* 311(5764), pp. 1113-1116.

Campos, M. A., Vargas, M. A., Regueiro, V., Llompart, C. M., Albertí, S. and Bengoechea, J. A. 2004. Capsule polysaccharide mediates bacterial resistance to antimicrobial peptides. *Infection and immunity* 72(12), pp. 7107-7114.

Cannatelli, A. et al. 2013. *In vivo* emergence of colistin resistance in *Klebsiella pneumoniae* producing KPC-type carbapenemases mediated by insertional inactivation of the PhoQ/PhoP *mgrB* regulator. *Antimicrobial agents and chemotherapy* 57(11), pp. 5521-5526.

Cannatelli, A. et al. 2014a. *In vivo* evolution to colistin resistance by PmrB sensor kinase mutation in KPC-producing *Klebsiella pneumoniae* is associated with low-dosage colistin treatment. *Antimicrobial agents and chemotherapy* 58(8), pp. 4399-4403.

Cannatelli, A. et al. 2014b. MgrB inactivation is a common mechanism of colistin resistance in KPC-producing *Klebsiella pneumoniae* of clinical origin. *Antimicrobial*

agents and chemotherapy 58(10), pp. 5696-5703.

Carattoli, A. et al. 2017. Novel plasmid-mediated colistin resistance *mcr-4* gene in *Salmonella* and *Escherichia coli*, Italy 2013, Spain and Belgium, 2015 to 2016. *Eurosurveillance* 22(31), p. 30589.

Carlos, C., Maretto, D. A., Poppi, R. J., Sato, M. I. Z. and Ottoboni, L. M. 2011. Fourier transform infrared microspectroscopy as a bacterial source tracking tool to discriminate fecal *E. coli* strains. *Microchemical Journal* 99(1), pp. 15-19.

Carretto, E. et al. 2018. Detection of *mcr-4* positive *Salmonella enterica* serovar Typhimurium in clinical isolates of human origin, Italy, October to November 2016. *Eurosurveillance* 23(2), pp. 17-00821.

Casadevall, A. and Pirofski, L.-a. 2003. The damage-response framework of microbial pathogenesis. *Nature reviews microbiology* 1(1), pp. 17-24.

Catteau, L., Zhu, L., Van Bambeke, F. and Quetin-Leclercq, J. 2018. Natural and hemi-synthetic pentacyclic triterpenes as antimicrobials and resistance modifying agents against *Staphylococcus aureus*: a review. *Phytochemistry Reviews* 17, pp. 1129-1163.

Ceri, H., Olson, M. E., Stremick, C., Read, R., Morck, D. and Buret, A. 1999. The Calgary Biofilm Device: new technology for rapid determination of antibiotic susceptibilities of bacterial biofilms. *Journal of clinical microbiology* 37(6), pp. 1771-1776.

Chambers, H. F. 1999. Penicillin-binding protein-mediated resistance in pneumococci and staphylococci. *The Journal of infectious diseases* 179(Supplement_2), pp. S353-S359.

Chambers, S., Peddie, B. and Pithie, A. 2006. Ethanol disinfection of plastic-adherent micro-organisms. *Journal of Hospital Infection* 63(2), pp. 193-196.

Chan, K. A. and Kazarian, S. G. 2016. Attenuated total reflection Fourier-transform infrared (ATR-FTIR) imaging of tissues and live cells. *Chemical Society Reviews* 45(7), pp. 1850-1864.

Chandler, M., Fayet, O., Rousseau, P., Hoang, B. T. and Duval-Valentin, G. 2015. Copy-out—paste-in transposition of IS*911*: a major transposition pathway. *Mobile DNA III*, pp. 591-607.

Cheah, S.-E. et al. 2016. Polymyxin resistance in *Acinetobacter baumannii*: genetic mutations and transcriptomic changes in response to clinically relevant dosage

regimens. *Scientific reports* 6(1), p. 26233.

Chen, H. D. and Groisman, E. A. 2013. The biology of the PmrA/PmrB two-component system: the major regulator of lipopolysaccharide modifications. *Annual review of microbiology* 67, pp. 83-112.

Chen, Y., Chau, J., Yoon, J. and Hladky, J. 2022. Rapid, label-free pathogen identification system for multidrug-resistant bacterial wound infection detection on military members in the battlefield. *PloS one* 17(5), p. e0267945.

Cheng, H.-Y., Chen, Y.-F. and Peng, H.-L. 2010. Molecular characterization of the PhoPQ-PmrD-PmrAB mediated pathway regulating polymyxin B resistance in *Klebsiella pneumoniae* CG43. *Journal of biomedical science* 17(1), pp. 1-16.

Cheng, P. et al. 2021. Prevalence and characteristic of swine-origin *mcr-1*-positive *Escherichia coli* in Northeastern China. *Frontiers in microbiology* 12, p. 712707.

Cheng, Y.-H., Lin, T.-L., Lin, Y.-T. and Wang, J.-T. 2016. Amino acid substitutions of CrrB responsible for resistance to colistin through CrrC in *Klebsiella pneumoniae*. *Antimicrobial agents and chemotherapy* 60(6), pp. 3709-3716.

Chiang, W.-C., Nilsson, M., Jensen, P. Ø., Høiby, N., Nielsen, T. E., Givskov, M. and Tolker-Nielsen, T. 2013. Extracellular DNA shields against aminoglycosides in *Pseudomonas aeruginosa* biofilms. *Antimicrobial agents and chemotherapy* 57(5), pp. 2352-2361.

Choi, M.-J. and Ko, K. S. 2014. Mutant prevention concentrations of colistin for *Acinetobacter baumannii*, *Pseudomonas aeruginosa* and *Klebsiella pneumoniae* clinical isolates. *Journal of Antimicrobial Chemotherapy* 69(1), pp. 275-277.

Choi, M.-J. and Ko, K. S. 2015. Loss of hypermucoviscosity and increased fitness cost in colistin-resistant *Klebsiella pneumoniae* sequence type 23 strains. *Antimicrobial agents and chemotherapy* 59(11), pp. 6763-6773.

Choi, U. and Lee, C.-R. 2019. Antimicrobial agents that inhibit the outer membrane assembly machines of Gram-negative bacteria. *Journal of Microbiology and Biotechnology* 29(1), pp. 1-10.

Choi, Y. et al. 2020. Comparison of fitness cost and virulence in chromosome-and plasmid-mediated colistin-resistant *Escherichia coli*. *Frontiers in microbiology* 11, p. 798.

Christaki, E., Marcou, M. and Tofarides, A. 2020. Antimicrobial Resistance in Bacteria:

Mechanisms, Evolution, and Persistence. *J Mol Evol* 88(1), pp. 26-40. doi: 10.1007/s00239-019-09914-3

Ciofu, O. and Høiby, N. 2008. Cystic fibrosis—coping with resistance. *Antibiotic policies: fighting resistance*. Springer, pp. 149-174.

Ciofu, O., Tolker-Nielsen, T., Jensen, P. Ø., Wang, H. and Høiby, N. 2015. Antimicrobial resistance, respiratory tract infections and role of biofilms in lung infections in cystic fibrosis patients. *Advanced drug delivery reviews* 85, pp. 7-23.

Claverys, J.-P., Martin, B. and Polard, P. 2009. The genetic transformation machinery: composition, localization, and mechanism. *FEMS microbiology reviews* 33(3), pp. 643-656.

Clements, A. et al. 2007. Secondary acylation of *Klebsiella pneumoniae* lipopolysaccharide contributes to sensitivity to antibacterial peptides. *Journal of Biological Chemistry* 282(21), pp. 15569-15577.

Clinical and Laboratory Standards Institute. 2012. Methods for dilution antimicrobial susceptibility tests for bacteria that grow aerobically, 9th ed. Approved standard M7-A9. CLSI, Wayne, PA.

Coleman, M. L., Sullivan, M. B., Martiny, A. C., Steglich, C., Barry, K., DeLong, E. F. and Chisholm, S. W. 2006. Genomic islands and the ecology and evolution of *Prochlorococcus*. *Science* 311(5768), pp. 1768-1770.

Coloma-Rivero, R. F., Flores-Concha, M., Molina, R. E., Soto-Shara, R., Cartes, Á. and Oñate, Á. A. 2021. *Brucella* and its hidden flagellar system. *Microorganisms* 10(1), p. 83.

Cör, D., Knez, Ž. and Knez Hrnčič, M. 2018. Antitumour, antimicrobial, antioxidant and antiacetylcholinesterase effect of *Ganoderma lucidum* terpenoids and polysaccharides: A review. *Molecules* 23(3), p. 649.

Corte, L., Rellini, P., Roscini, L., Fatichenti, F. and Cardinali, G. 2010. Development of a novel, FTIR (Fourier transform infrared spectroscopy) based, yeast bioassay for toxicity testing and stress response study. *Analytica chimica acta* 659(1-2), pp. 258-265.

Cox-Georgian, D., Ramadoss, N., Dona, C. and Basu, C. 2019. Therapeutic and medicinal uses of terpenes. *Medicinal plants: from farm to pharmacy*, pp. 333-359.

Cristani, M. et al. 2007. Interaction of four monoterpenes contained in essential oils with model membranes: implications for their antibacterial activity. *Journal of*

agricultural and food chemistry 55(15), pp. 6300-6308.

Cruz, C. D., Shah, S. and Tammela, P. 2018. Defining conditions for biofilm inhibition and eradication assays for Gram-positive clinical reference strains. *BMC microbiology* 18(1), pp. 1-9.

Cullen, J. K. et al. 2021. Activation of PKC supports the anticancer activity of tigilanol tiglate and related epoxytiglianes. *Scientific reports* 11(1), p. 207.

Ćwiek, K. et al. 2021. Phenotypic and genotypic characterization of *mcr-1*-positive multidrug-resistant *Escherichia coli* ST93, ST117, ST156, ST10, and ST744 isolated from poultry in Poland. *Brazilian Journal of Microbiology* 52(3), pp. 1597-1609.

Dalmasso, G. et al. 2023. Genes *mcr* improve the intestinal fitness of pathogenic *E. coli* and balance their lifestyle to commensalism. *Microbiome* 11(1), p. 12.

Das, T., Sharma, P. K., Busscher, H. J., Van Der Mei, H. C. and Krom, B. P. 2010. Role of extracellular DNA in initial bacterial adhesion and surface aggregation. *Applied and environmental microbiology* 76(10), pp. 3405-3408.

Davies-Jones, J., Davies, P. R., Graf, A., Hewes, D., Hill, K. E. and Pascoe, M. 2024. Photoinduced force microscopy as a novel method for the study of microbial nanostructures. *Nanoscale* 16(1), pp. 223-236.

Davies, D. 2003. Understanding biofilm resistance to antibacterial agents. *Nature reviews Drug discovery* 2(2), pp. 114-122.

Davis, R. and Mauer, L. J. 2010. Fourier transform infrared (FT-IR) spectroscopy: a rapid tool for detection and analysis of foodborne pathogenic bacteria. *Current research, technology and education topics in applied microbiology and microbial biotechnology* 2, pp. 1582-1594.

Dazzi, A. and Prater, C. B. 2017. AFM-IR: Technology and applications in nanoscale infrared spectroscopy and chemical imaging. *Chemical reviews* 117(7), pp. 5146-5173.

de Beer, D., Stoodley, P. and Lewandowski, Z. 1997. Measurement of local diffusion coefficients in biofilms by microinjection and confocal microscopy. *Biotechnology and bioengineering* 53(2), pp. 151-158.

De Ridder, T. R. et al. 2021. Randomized controlled clinical study evaluating the efficacy and safety of intratumoral treatment of canine mast cell tumors with tigilanol tiglate (EBC-46). *Journal of Veterinary Internal Medicine* 35(1), pp. 415-429.

Deatherage, B. L. and Cookson, B. T. 2012. Membrane vesicle release in bacteria, eukaryotes, and archaea: a conserved yet underappreciated aspect of microbial life. *Infection and immunity* 80(6), pp. 1948-1957.

Deepak, P., Balamuralikrishnan, B., Hatamleh, A. A., Alnafisi, B. K. and Arumugam, V. A. 2024. Phenolic compound derived from *Enteromorpha intestinalis* and their bioactivity against bacterial pathogens. *Journal of King Saud University-Science* 36(8), p. 103342.

Dewan, I. and Uecker, H. 2023. A mathematician's guide to plasmids: an introduction to plasmid biology for modellers. *Microbiology* 169(7), p. 001362.

Dhaouadi, S. et al. 2023. High biofilm-forming ability and clonal dissemination among colistin-resistant *Escherichia coli* isolates recovered from cows with mastitis, diarrheic calves, and chickens with colibacillosis in Tunisia. *Life* 13(2), p. 299.

Dhekane, R., Mhade, S. and Kaushik, K. S. 2022. Adding a new dimension: Multi-level structure and organization of mixed-species *Pseudomonas aeruginosa* and *Staphylococcus aureus* biofilms in a 4-D wound microenvironment. *Biofilm* 4, p. 100087.

Di Pasqua, R., Betts, G., Hoskins, N., Edwards, M., Ercolini, D. and Mauriello, G. 2007. Membrane toxicity of antimicrobial compounds from essential oils. *Journal of agricultural and food chemistry* 55(12), pp. 4863-4870.

Di Pasqua, R., Hoskins, N., Betts, G. and Mauriello, G. 2006. Changes in membrane fatty acids composition of microbial cells induced by addiction of thymol, carvacrol, limonene, cinnamaldehyde, and eugenol in the growing media. *Journal of agricultural and food chemistry* 54(7), pp. 2745-2749.

Di Pilato, V. et al. 2016. *mcr-1.2*, a new *mcr* variant carried on a transferable plasmid from a colistin-resistant KPC carbapenemase-producing *Klebsiella pneumoniae* strain of sequence type 512. *Antimicrobial agents and chemotherapy* 60(9), pp. 5612-5615.

Diani, E., Bianco, G., Gatti, M., Gibellini, D. and Gaibani, P. 2024. Colistin: lights and shadows of an older antibiotic. *Molecules* 29(13), p. 2969.

Diene, S. M. et al. 2013. The rhizome of the multidrug-resistant *Enterobacter aerogenes* genome reveals how new "killer bugs" are created because of a sympatric lifestyle. *Molecular biology and evolution* 30(2), pp. 369-383.

Domingues, S., Harms, K., Fricke, W. F., Johnsen, P. J., Da Silva, G. J. and Nielsen, K. M. 2012. Natural transformation facilitates transfer of transposons, integrons and gene

cassettes between bacterial species. *PLoS pathogens* 8(8), p. e1002837.

Donà, V. et al. 2017. Heterogeneous genetic location of *mcr-1* in colistin-resistant *Escherichia coli* isolates from humans and retail chicken meat in Switzerland: emergence of *mcr-1*-carrying IncK2 plasmids. *Antimicrobial agents and chemotherapy* 61(11), pp. 10.1128/aac. 01245-01217.

Dong, J., Liu, L., Chen, L., Xiang, Y., Wang, Y. and Zhao, Y. 2023. The coexistence of bacterial species restructures biofilm architecture and increases tolerance to antimicrobial agents. *Microbiology Spectrum* 11(2), pp. e03581-03522.

Donlan, R. M. 2002. Biofilms: microbial life on surfaces. *Emerging infectious diseases* 8(9), p. 881.

Dorado-Morales, P., Garcillán-Barcia, M. P., Lasa, I. and Solano, C. 2021. Fitness cost evolution of natural plasmids of *Staphylococcus aureus*. *MBio* 12(1), pp. 10.1128/mbio. 03094-03020.

Doroshenko, N. et al. 2014. Extracellular DNA impedes the transport of vancomycin in *Staphylococcus epidermidis* biofilms preexposed to subinhibitory concentrations of vancomycin. *Antimicrobial agents and chemotherapy* 58(12), pp. 7273-7282.

Driffield, K., Miller, K., Bostock, J., O'neill, A. and Chopra, I. 2008. Increased mutability of *Pseudomonas aeruginosa* in biofilms. *Journal of Antimicrobial Chemotherapy* 61(5), pp. 1053-1056.

Dufrêne, Y. F., Van der Wal, A., Norde, W. and Rouxhet, P. G. 1997. X-ray photoelectron spectroscopy analysis of whole cells and isolated cell walls of Gram-positive bacteria: comparison with biochemical analysis. *Journal of bacteriology* 179(4), pp. 1023-1028.

Dunne Jr, W. M. 2002. Bacterial adhesion: seen any good biofilms lately? *Clinical microbiology reviews* 15(2), pp. 155-166.

Durante-Mangoni, E., Del Franco, M., Andini, R., Bernardo, M., Giannouli, M. and Zarrilli, R. 2015. Emergence of colistin resistance without loss of fitness and virulence after prolonged colistin administration in a patient with extensively drug-resistant *Acinetobacter baumannii*. *Diagnostic microbiology and infectious disease* 82(3), pp. 222-226.

Durão, P., Balbontín, R. and Gordo, I. 2018. Evolutionary mechanisms shaping the maintenance of antibiotic resistance. *Trends in microbiology* 26(8), pp. 677-691.

Dwyer, D. J., Collins, J. J. and Walker, G. C. 2015. Unraveling the physiological complexities of antibiotic lethality. *Annual review of pharmacology and toxicology* 55, pp. 313-332.

Eastman, P. et al. 2017. OpenMM 7: Rapid development of high performance algorithms for molecular dynamics. *PLoS computational biology* 13(7), p. e1005659.

Ebbensgaard, A., Mordhorst, H., Aarestrup, F. M. and Hansen, E. B. 2018. The role of outer membrane proteins and lipopolysaccharides for the sensitivity of *Escherichia coli* to antimicrobial peptides. *Frontiers in microbiology* 9, p. 2153.

Eed, H. R., Abdel-Kader, N. S., El Tahan, M. H., Dai, T. and Amin, R. 2016. Bioluminescence-Sensing Assay for Microbial Growth Recognition. *Journal of Sensors* 2016(1), p. 1492467.

Ejaz, H. et al. 2021. Molecular epidemiology of extensively drug-resistant *mcr* encoded colistin-resistant bacterial strains co-expressing multifarious β-lactamases. *Antibiotics* 10(4), p. 467.

El-Hajj, Z. W. and Newman, E. B. 2015. An *Escherichia coli* mutant that makes exceptionally long cells. *Journal of bacteriology* 197(8), pp. 1507-1514.

El-Sayed Ahmed, M. A. E.-G., Zhong, L.-L., Shen, C., Yang, Y., Doi, Y. and Tian, G.-B. 2020. Colistin and its role in the Era of antibiotic resistance: an extended review (2000-2019). *Emerging microbes & infections* 9(1), pp. 868-885.

El Fannassi, Y. et al. 2023. Complexation of terpenes for the production of new antimicrobial and antibiofilm molecules and their encapsulation in order to improve their activities. *Applied Sciences* 13(17), p. 9854.

Elbediwi, M. et al. 2019. Global burden of colistin-resistant bacteria: mobilized colistin resistance genes study (1980-2018). *Microorganisms* 7(10), p. 461.

Eliopoulos, G. M. and Huovinen, P. 2001. Resistance to trimethoprim-sulfamethoxazole. *Clinical infectious diseases* 32(11), pp. 1608-1614.

Ellis, C. N., Traverse, C. C., Mayo‐Smith, L., Buskirk, S. W. and Cooper, V. S. 2015. Character displacement and the evolution of niche complementarity in a model biofilm community. *Evolution* 69(2), pp. 283-293.

Enax, J., Ganss, B., Amaechi, B. T., Schulze zur Wiesche, E. and Meyer, F. 2023. The composition of the dental pellicle: an updated literature review. *Frontiers in Oral Health* 4, p. 1260442.

Erdmann, S., Tschitschko, B., Zhong, L., Raftery, M. J. and Cavicchioli, R. 2017. A plasmid from an Antarctic haloarchaeon uses specialized membrane vesicles to disseminate and infect plasmid-free cells. *Nature microbiology* 2(10), pp. 1446-1455.

Erridge, C., Bennett-Guerrero, E. and Poxton, I. R. 2002. Structure and function of lipopolysaccharides. *Microbes and infection* 4(8), pp. 837-851.

Fairley, N. et al. 2021. Systematic and collaborative approach to problem solving using X-ray photoelectron spectroscopy. *Applied Surface Science Advances* 5, p. 100112.

Falagas, M. E., Kasiakou, S. K. and Saravolatz, L. D. 2005. Colistin: the revival of polymyxins for the management of multidrug-resistant Gram-negative bacterial infections. *Clinical infectious diseases* 40(9), pp. 1333-1341.

Falagas, M. E., Rafailidis, P. I. and Matthaiou, D. K. 2010. Resistance to polymyxins: mechanisms, frequency and treatment options. *Drug resistance updates* 13(4-5), pp. 132-138.

Falgenhauer, L. et al. 2016. Colistin resistance gene *mcr-1* in extended-spectrum β-lactamase-producing and carbapenemase-producing Gram-negative bacteria in Germany. *The Lancet Infectious Diseases* 16(3), pp. 282-283.

Fang, T.-T., Li, X., Wang, Q.-S., Zhang, Z.-J., Liu, P. and Zhang, C.-C. 2012. Toxicity evaluation of CdTe quantum dots with different size on *Escherichia coli*. *Toxicology in Vitro* 26(7), pp. 1233-1239.

Feng, S. et al. 2022. MCR-1-dependent lipid remodelling compromises the viability of Gram-negative bacteria. *Emerging microbes & infections* 11(1), pp. 1236-1249.

Field, C. and Summers, D. 2011. Multicopy plasmid stability: revisiting the dimer catastrophe. *Journal of Theoretical Biology* 291, pp. 119-127.

Flemming, H.-C., Neu, T. R. and Wozniak, D. J. 2007. The EPS matrix: the "house of biofilm cells". *Journal of bacteriology* 189(22), pp. 7945-7947.

Flemming, H.-C. and Wingender, J. 2010. The biofilm matrix. *Nature reviews microbiology* 8(9), pp. 623-633.

Flensburg, J. and Sköld, O. 1987. Massive overproduction of dihydrofolate reductase in bacteria as a response to the use of trimethoprim. *European Journal of Biochemistry* 162(3), pp. 473-476.

Formosa, C., Herold, M., Vidaillac, C., Duval, R. and Dague, E. 2015. Unravelling of a mechanism of resistance to colistin in *Klebsiella pneumoniae* using atomic force microscopy. *Journal of Antimicrobial Chemotherapy* 70(8), pp. 2261-2270.

Foti, J. J., Devadoss, B., Winkler, J. A., Collins, J. J. and Walker, G. C. 2012. Oxidation of the guanine nucleotide pool underlies cell death by bactericidal antibiotics. *Science* 336(6079), pp. 315-319.

Frantz, R. et al. 2023. A single residue within the MCR-1 protein confers anticipatory resilience. *Microbiology Spectrum* 11(3), pp. e03592-03522.

Fux, C., Wilson, S. and Stoodley, P. 2004. Detachment characteristics and oxacillin resistance of *Staphyloccocus aureus* biofilm emboli in an in vitro catheter infection model. Am Soc Microbiol.

Gaibani, P., Lombardo, D., Lewis, R. E., Mercuri, M., Bonora, S., Landini, M. P. and Ambretti, S. 2014. *In vitro* activity and post-antibiotic effects of colistin in combination with other antimicrobials against colistin-resistant KPC-producing *Klebsiella pneumoniae* bloodstream isolates. *Journal of Antimicrobial Chemotherapy* 69(7), pp. 1856-1865.

Gallily, R., Yekhtin, Z. and Hanuš, L. O. 2018. The anti-inflammatory properties of terpenoids from cannabis. *Cannabis and cannabinoid research* 3(1), pp. 282-290.

Gao, R. et al. 2016. Dissemination and mechanism for the MCR-1 colistin resistance. *PLoS pathogens* 12(11), p. e1005957.

Garrett, T. R., Bhakoo, M. and Zhang, Z. 2008. Bacterial adhesion and biofilms on surfaces. *Progress in natural science* 18(9), pp. 1049-1056.

Gaudin, M., Gauliard, E., Schouten, S., Houel‐Renault, L., Lenormand, P., Marguet, E. and Forterre, P. 2013. Hyperthermophilic archaea produce membrane vesicles that can transfer DNA. *Environmental microbiology reports* 5(1), pp. 109-116.

Gentry, Z. O. et al. 2025. Synthesis and preclinical evaluation of tigilanol tiglate analogs as latency-reversing agents for the eradication of HIV. *Science Advances* 11(4), p. eads1911.

Ghai, I. 2023. A barrier to entry: examining the bacterial outer membrane and antibiotic resistance. *Applied Sciences* 13(7), p. 4238.

Gloag, E. S. et al. 2013. Self-organization of bacterial biofilms is facilitated by extracellular DNA. *Proceedings of the National Academy of Sciences* 110(28), pp.

11541-11546.

Godlewska, K., Ronga, D. and Michalak, I. 2021. Plant extracts-importance in sustainable agriculture. *Italian Journal of Agronomy* 16(2), p. 1851.

Goeders, N. and Van Melderen, L. 2014. Toxin-antitoxin systems as multilevel interaction systems. *Toxins* 6(1), pp. 304-324.

Gogry, F. A., Siddiqui, M. T., Sultan, I. and Haq, Q. M. R. 2021. Current update on intrinsic and acquired colistin resistance mechanisms in bacteria. *Frontiers in medicine* 8, p. 677720.

Goldstein, B. P. 2014. Resistance to rifampicin: a review. *The Journal of antibiotics* 67(9), pp. 625-630.

Grant, E. L., Wallace, H. M., Trueman, S. J., Reddell, P. W. and Ogbourne, S. M. 2017. Floral and reproductive biology of the medicinally significant rainforest tree, *Fontainea picrosperma* (Euphorbiaceae). *Industrial Crops and Products* 108, pp. 416-422.

Grindley, N. D. 2007. The Movement of Tn*3*-Like Elements: Transposition and Cointegrate Resolution. *Mobile DNA II*, pp. 272-302.

Guimarães, A. C., Meireles, L. M., Lemos, M. F., Guimarães, M. C. C., Endringer, D. C., Fronza, M. and Scherer, R. 2019. Antibacterial activity of terpenes and terpenoids present in essential oils. *Molecules* 24(13), p. 2471.

Gunn, J. S. 2001. Bacterial modification of LPS and resistance to antimicrobial peptides. *Journal of endotoxin research* 7(1), pp. 57-62.

Gunn, J. S. 2008. The *Salmonella* PmrAB regulon: lipopolysaccharide modifications, antimicrobial peptide resistance and more. *Trends in microbiology* 16(6), pp. 284-290.

Gunn, J. S., Lim, K. B., Krueger, J., Kim, K., Guo, L., Hackett, M. and Miller, S. I. 1998. PmrA-PmrB-regulated genes necessary for 4-aminoarabinose lipid A modification and polymyxin resistance. *Molecular microbiology* 27(6), pp. 1171-1182.

Gunn, J. S. and Miller, S. I. 1996. PhoP-PhoQ activates transcription of *pmrAB*, encoding a two-component regulatory system involved in *Salmonella typhimurium* antimicrobial peptide resistance. *Journal of bacteriology* 178(23), pp. 6857-6864.

Gunn, J. S. and Richards, S. M. 2007. Recognition and integration of multiple environmental signals by the bacterial sensor kinase PhoQ. *Cell host & microbe* 1(3), pp. 163-165.

Gunn, J. S., Ryan, S. S., Van Velkinburgh, J. C., Ernst, R. K. and Miller, S. I. 2000. Genetic and functional analysis of a PmrA-PmrB-regulated locus necessary for lipopolysaccharide modification, antimicrobial peptide resistance, and oral virulence of *Salmonella enterica* serovar typhimurium. *Infection and immunity* 68(11), pp. 6139-6146.

Hadjadj, L., Baron, S. A., Olaitan, A. O., Morand, S. and Rolain, J.-M. 2019. Co-occurrence of variants of *mcr-3* and *mcr-8* genes in a *Klebsiella pneumoniae* isolate from Laos. *Frontiers in microbiology* 10, p. 2720.

Haiko, J. and Westerlund-Wikström, B. 2013. The role of the bacterial flagellum in adhesion and virulence. *Biology* 2(4), pp. 1242-1267.

Hall-Stoodley, L. and Stoodley, P. 2002. Developmental regulation of microbial biofilms. *Current opinion in biotechnology* 13(3), pp. 228-233.

Hamadi, F., Latrache, H., Zahir, H., Elghmari, A., Timinouni, M. and Ellouali, M. 2008. The relation between *Escherichia coli* surface functional groups' composition and their physicochemical properties. *Brazilian Journal of Microbiology* 39, pp. 10-15.

Hamel, M., Rolain, J.-M. and Baron, S. A. 2021. The history of colistin resistance mechanisms in bacteria: progress and challenges. *Microorganisms* 9(2), p. 442.

Hammel, E., Steiner, M., Marvan, C., Marvan, M., Retzlaff, K., Bergholz, W. and Jacquine, A. 2024. CO2 Back-Radiation Sensitivity Studies under Laboratory and Field Conditions. *Atmospheric and Climate Sciences* 14(4), pp. 407-428.

Hammerl, J. A. et al. 2018. *mcr-5* and a novel *mcr-5.2* variant in *Escherichia coli* isolates from food and food-producing animals, Germany, 2010 to 2017. *Journal of Antimicrobial Chemotherapy* 73(5), pp. 1433-1435.

Hammiche, A., Pollock, H., Reading, M., Claybourn, M., Turner, P. and Jewkes, K. 1999. Photothermal FT-IR spectroscopy: A step towards FT-IR microscopy at a resolution better than the diffraction limit. *Applied spectroscopy* 53(7), pp. 810-815.

Han, J., Liu, X., Zhang, L., Quinn, R. J. and Feng, Y. 2022. Anti-mycobacterial natural products and mechanisms of action. *Natural product reports* 39(1), pp. 77-89.

Hanberger, H., Nilsson, L., Kihlström, E. and Maller, R. 1990. Postantibiotic effect of beta-lactam antibiotics on *Escherichia coli* evaluated by bioluminescence assay of bacterial ATP. *Antimicrobial agents and chemotherapy* 34(1), pp. 102-106.

Hancock, R., Siehnel, R. and Martin, N. 1990. Outer membrane proteins of *Pseudomonas*. *Molecular microbiology* 4(7), pp. 1069-1075.

Harder, E. et al. 2016. OPLS3: a force field providing broad coverage of drug-like small molecules and proteins. *Journal of chemical theory and computation* 12(1), pp. 281-296.

Harrison, E., Dytham, C., Hall, J. P., Guymer, D., Spiers, A. J., Paterson, S. and Brockhurst, M. A. 2016. Rapid compensatory evolution promotes the survival of conjugative plasmids. *Mobile genetic elements* 6(3), pp. 2034-2039.

Hasman, H. et al. 2015. Detection of *mcr-1* encoding plasmid-mediated colistin-resistant *Escherichia coli* isolates from human bloodstream infection and imported chicken meat, Denmark 2015. *Eurosurveillance* 20(49), p. 30085.

Hassan, J., Eddine, R. Z., Mann, D., Li, S., Deng, X., Saoud, I. P. and Kassem, I. I. 2020a. The mobile colistin resistance gene, *mcr-1.1*, is carried on IncX4 plasmids in multidrug resistant *E. coli* isolated from rainbow trout aquaculture. *Microorganisms* 8(11), p. 1636.

Hassan, J., El-Gemayel, L., Bashour, I. and Kassem, I. I. 2020b. On the edge of a precipice: The global emergence and dissemination of plasmid-borne *mcr* genes that confer resistance to colistin, a last-resort antibiotic. *Antibiotics and antimicrobial resistance genes in the environment*. Elsevier, pp. 155-182.

Hausner, M. and Wuertz, S. 1999. High rates of conjugation in bacterial biofilms as determined by quantitative in situ analysis. *Applied and environmental microbiology* 65(8), pp. 3710-3713.

Hazan, R. et al. 2016. Auto poisoning of the respiratory chain by a quorum-sensing-regulated molecule favors biofilm formation and antibiotic tolerance. *Current Biology* 26(2), pp. 195-206.

Helander, I. M. et al. 1996. Characterization of Lipopolysaccharides of polymyxin-resistant and polymyxin-sensitive *Klebsiella pneumoniae* O3. *European Journal of Biochemistry* 237(1), pp. 272-278.

Helm, D., Labischinski, H., Schallehn, G. and Naumann, D. 1991. Classification and identification of bacteria by Fourier-transform infrared spectroscopy. *Microbiology* 137(1), pp. 69-79.

Hengzhuang, W., Ciofu, O., Yang, L., Wu, H., Song, Z., Oliver, A. and Høiby, N. 2013. High β-lactamase levels change the pharmacodynamics of β-lactam antibiotics in

Pseudomonas aeruginosa biofilms. *Antimicrobial agents and chemotherapy* 57(1), pp. 196-204.

Henriksen, N. N. et al. 2022. Biofilm cultivation facilitates coexistence and adaptive evolution in an industrial bacterial community. *npj Biofilms and Microbiomes* 8(1), p. 59.

Hernández-Beltrán, J. C. R., San Millán, A., Fuentes-Hernández, A. and Peña-Miller, R. 2021. Mathematical models of plasmid population dynamics. *Frontiers in microbiology* 12, p. 606396.

Hernando-Amado, S., Sanz-García, F., Blanco, P. and Martinez, J. L. 2017. Fitness costs associated with the acquisition of antibiotic resistance. *Essays in biochemistry* 61(1), pp. 37-48.

Herrera, C. M., Hankins, J. V. and Trent, M. S. 2010. Activation of PmrA inhibits LpxT-dependent phosphorylation of lipid A promoting resistance to antimicrobial peptides. *Molecular microbiology* 76(6), pp. 1444-1460.

Herten, M., Bisdas, T., Knaack, D., Becker, K., Osada, N., Torsello, G. B. and Idelevich, E. A. 2017. Rapid *in vitro* quantification of *S. aureus* biofilms on vascular graft surfaces. *Frontiers in microbiology* 8, p. 2333.

Heydorn, A., Nielsen, A. T., Hentzer, M., Sternberg, C., Givskov, M., Ersbøll, B. K. and Molin, S. 2000. Quantification of biofilm structures by the novel computer program COMSTAT. *Microbiology* 146(10), pp. 2395-2407.

Hinchliffe, P. et al. 2017. Insights into the mechanistic basis of plasmid-mediated colistin resistance from crystal structures of the catalytic domain of MCR-1. *Scientific reports* 7(1), pp. 1-10.

Hiramatsu, K. et al. 2013. Genomic basis for methicillin resistance in *Staphylococcus aureus*. *Infection & chemotherapy* 45(2), pp. 117-136.

Hollingsworth, S. A. and Dror, R. O. 2018. Molecular dynamics simulation for all. *Neuron* 99(6), pp. 1129-1143.

Honore, P. M., Jacobs, R., Joannes-Boyau, O., Boer, W., De Waele, E., Van Gorp, V. and Spapen, H. D. 2013. Continuous renal replacement therapy allows higher colistin dosing without increasing toxicity. *Journal of Translational Internal Medicine* 1(1), pp. 6-8.

Horvat, M., Pannuri, A., Romeo, T., Dogsa, I. and Stopar, D. 2019. Viscoelastic

response of *Escherichia coli* biofilms to genetically altered expression of extracellular matrix components. *Soft Matter* 15(25), pp. 5042-5051.

Hu, C., Guo, J., Qu, J. and Hu, X. 2007. Photocatalytic degradation of pathogenic bacteria with AgI/TiO2 under visible light irradiation. *Langmuir* 23(9), pp. 4982-4987.

Hu, M., Guo, J., Cheng, Q., Yang, Z., Chan, E. W. C., Chen, S. and Hao, Q. 2016. Crystal structure of *Escherichia coli* originated MCR-1, a phosphoethanolamine transferase for colistin resistance. *Scientific reports* 6(1), p. 38793.

Huang, J., Li, C., Song, J., Velkov, T., Wang, L., Zhu, Y. and Li, J. 2020. Regulating polymyxin resistance in Gram-negative bacteria: roles of two-component systems PhoPQ and PmrAB. *Future microbiology* 15(6), pp. 445-459.

Huang, J. et al. 2017. CHARMM36m: an improved force field for folded and intrinsically disordered proteins. *Nature methods* 14(1), pp. 71-73.

Hung, C. et al. 2013. *Escherichia coli* biofilms have an organized and complex extracellular matrix structure. *MBio* 4(5), pp. 10.1128/mbio. 00645-00613.

Hussein, N. H., Al-Kadmy, I. M. S., Taha, B. M. and Hussein, J. D. 2021. Mobilized colistin resistance (*mcr*) genes from 1 to 10: a comprehensive review. *Mol Biol Rep* 48(3), pp. 2897-2907. doi: 10.1007/s11033-021-06307-y

Huynh, R. and McPhee, J. B. 2021. A mutation in the promoter of the *pmrD* gene of *Shigella flexneri* abrogates functional PhoPQ-PmrD-PmrAB signaling and polymyxin B resistance. *bioRxiv*, p. 2021.2007. 2026.453917.

Ibrahim, D. R., Dodd, C. E., Stekel, D. J., Meshioye, R. T., Diggle, M., Lister, M. and Hobman, J. L. 2023. Multidrug-resistant ESBL-producing *E. coli* in clinical samples from the UK. *Antibiotics* 12(1), p. 169.

Imlay, J. A. 2013. The molecular mechanisms and physiological consequences of oxidative stress: lessons from a model bacterium. *Nature reviews microbiology* 11(7), pp. 443-454.

Irrgang, A. et al. 2016. Prevalence of *mcr-1* in *E. coli* from livestock and food in Germany, 2010-2015. *PloS one* 11(7), p. e0159863.

Jacoby, G. A. and Han, P. 1996. Detection of extended-spectrum beta-lactamases in clinical isolates of *Klebsiella pneumoniae* and *Escherichia coli*. *Journal of clinical microbiology* 34(4), pp. 908-911.

Jahng, J. et al. 2014. Gradient and scattering forces in photoinduced force microscopy. *Physical Review B* 90(15), p. 155417.

Jahng, J. et al. 2015. Ultrafast pump-probe force microscopy with nanoscale resolution. *Applied physics letters* 106(8),

Jahng, J., Kim, B., Lee, E. S. and Potma, E. O. 2016. Quantitative analysis of sideband coupling in photoinduced force microscopy. *Physical Review B* 94(19), p. 195407.

Jahng, J., Potma, E. O. and Lee, E. S. 2018. Tip-enhanced thermal expansion force for nanoscale chemical imaging and spectroscopy in photoinduced force microscopy. *Analytical chemistry* 90(18), pp. 11054-11061.

Jahng, J., Potma, E. O. and Lee, E. S. 2019. Nanoscale spectroscopic origins of photoinduced tip–sample force in the midinfrared. *Proceedings of the National Academy of Sciences* 116(52), pp. 26359-26366.

Jakubovics, N., Shields, R., Rajarajan, N. and Burgess, J. 2013. Life after death: the critical role of extracellular DNA in microbial biofilms. *Letters in applied microbiology* 57(6), pp. 467-475.

Jamal, M. et al. 2018. Bacterial biofilm and associated infections. *J Chin Med Assoc* 81(1), pp. 7-11. doi: 10.1016/j.jcma.2017.07.012

Jayol, A., Nordmann, P., Brink, A. and Poirel, L. 2015. Heteroresistance to colistin in *Klebsiella pneumoniae* associated with alterations in the PhoPQ regulatory system. *Antimicrobial agents and chemotherapy* 59(5), pp. 2780-2784.

Jayol, A., Poirel, L., Brink, A., Villegas, M.-V., Yilmaz, M. and Nordmann, P. 2014. Resistance to colistin associated with a single amino acid change in protein PmrB among *Klebsiella pneumoniae* isolates of worldwide origin. *Antimicrobial agents and chemotherapy* 58(8), pp. 4762-4766.

Jensen, P. Ø. et al. 2014. Formation of hydroxyl radicals contributes to the bactericidal activity of ciprofloxacin against *Pseudomonas aeruginosa* biofilms. *Pathogens and disease* 70(3), pp. 440-443.

Ji, X. et al. 2019. Dissemination of extended-spectrum β-lactamase-producing *Escherichia coli* carrying *mcr-1* among multiple environmental sources in rural China and associated risk to human health. *Environmental pollution* 251, pp. 619-627.

Jiang, L., Cai, W., Tang, F., Wang, Z. and Liu, Y. 2021. Characterization of fitness cost caused by tigecycline-resistance gene *tet* (X6) in different host bacteria. *Antibiotics*

10(10), p. 1172.

Jiang, W., Yang, K., Vachet, R. W. and Xing, B. 2010. Interaction between oxide nanoparticles and biomolecules of the bacterial cell envelope as examined by infrared spectroscopy. *Langmuir* 26(23), pp. 18071-18077.

Jo, S., Kim, T., Iyer, V. G. and Im, W. 2008. CHARMM-GUI: a web-based graphical user interface for CHARMM. *Journal of computational chemistry* 29(11), pp. 1859-1865.

Johnson, L., Horsman, S. R., Charron-Mazenod, L., Turnbull, A. L., Mulcahy, H., Surette, M. G. and Lewenza, S. 2013. Extracellular DNA-induced antimicrobial peptide resistance in *Salmonella enterica* serovar Typhimurium. *BMC microbiology* 13, pp. 1-8.

Johnston, C., Martin, B., Fichant, G., Polard, P. and Claverys, J.-P. 2014. Bacterial transformation: distribution, shared mechanisms and divergent control. *Nature reviews microbiology* 12(3), pp. 181-196.

Johura, F.-T. et al. 2020. Colistin-resistant *Escherichia coli* carrying *mcr-1* in food, water, hand rinse, and healthy human gut in Bangladesh. *Gut pathogens* 12(1), p. 5.

Jones, J. W., Shaffer, S. A., Ernst, R. K., Goodlett, D. R. and Tureček, F. 2008. Determination of pyrophosphorylated forms of lipid A in Gram-negative bacteria using a multivaried mass spectrometric approach. *Proceedings of the National Academy of Sciences* 105(35), pp. 12742-12747.

Jones, P. D., Campbell, J. E., Brown, G., Johannes, C. M. and Reddell, P. 2021. Recurrence-free interval 12 months after local treatment of mast cell tumors in dogs using intratumoral injection of tigilanol tiglate. *Journal of Veterinary Internal Medicine* 35(1), pp. 451-455.

Joondan, N., Jhaumeer-Laulloo, S. and Caumul, P. 2014. A study of the antibacterial activity of l-Phenylalanine and l-Tyrosine esters in relation to their CMCs and their interactions with 1, 2-dipalmitoyl-sn-glycero-3-phosphocholine, DPPC as model membrane. *Microbiological Research* 169(9-10), pp. 675-685.

Jørgensen, K. M., Wassermann, T., Jensen, P. Ø., Hengzuang, W., Molin, S., Høiby, N. and Ciofu, O. 2013. Sublethal ciprofloxacin treatment leads to rapid development of high-level ciprofloxacin resistance during long-term experimental evolution of *Pseudomonas aeruginosa*. *Antimicrobial agents and chemotherapy* 57(9), pp. 4215-4221.

Judge, V. et al. 2013. Synthesis, antimycobacterial, antiviral, antimicrobial activity and QSAR studies of N2-acyl isonicotinic acid hydrazide derivatives. *Medicinal Chemistry* 9(1), pp. 53-76.

Juhas, M., Crook, D. W. and Hood, D. W. 2008. Type IV secretion systems: tools of bacterial horizontal gene transfer and virulence. *Cellular microbiology* 10(12), pp. 2377-2386.

Kabanov, D. and Prokhorenko, I. 2010. Structural analysis of lipopolysaccharides from Gram-negative bacteria. *Biochemistry (Moscow)* 75, pp. 383-404.

Kamio, Y. and Nikaido, H. 1976. Outer membrane of *Salmonella typhimurium*: accessibility of phospholipid head groups to phospholipase c and cyanogen bromide activated dextran in the external medium. *Biochemistry* 15(12), pp. 2561-2570.

Kang, K. N., Klein, D. R., Kazi, M. I., Guérin, F., Cattoir, V., Brodbelt, J. S. and Boll, J. M. 2019. Colistin heteroresistance in *Enterobacter cloacae* is regulated by PhoPQ-dependent 4-amino-4-deoxy-L-arabinose addition to lipid A. *Molecular microbiology* 111(6), pp. 1604-1616.

Kaplan, J. B., Velliyagounder, K., Ragunath, C., Rohde, H., Mack, D., Knobloch, J. K.-M. and Ramasubbu, N. 2004. Genes involved in the synthesis and degradation of matrix polysaccharide in *Actinobacillus actinomycetemcomitans* and *Actinobacillus pleuropneumoniae* biofilms. *Journal of bacteriology* 186(24), pp. 8213-8220.

Kassen, R. 2009. Toward a general theory of adaptive radiation: insights from microbial experimental evolution. *Annals of the New York Academy of Sciences* 1168(1), pp. 3-22.

Kato, A., Chen, H. D., Latifi, T. and Groisman, E. A. 2012. Reciprocal control between a bacterium's regulatory system and the modification status of its lipopolysaccharide. *Molecular cell* 47(6), pp. 897-908.

Kato, A. and Groisman, E. A. 2004. Connecting two-component regulatory systems by a protein that protects a response regulator from dephosphorylation by its cognate sensor. *Genes & development* 18(18), pp. 2302-2313.

Kato, A., Tanabe, H. and Utsumi, R. 1999. Molecular characterization of the PhoP-PhoQ two-component system in *Escherichia coli* K-12: identification of extracellular Mg^{2+}-responsive promoters. *Journal of bacteriology* 181(17), pp. 5516-5520.

Kavisri, M., Abraham, M., Prabakaran, G., Elangovan, M. and Moovendhan, M. 2023. Phytochemistry, bioactive potential and chemical characterization of metabolites from

marine microalgae (*Spirulina platensis*) biomass. *Biomass Conversion and Biorefinery* 13(11), pp. 10147-10154.

Kawasaki, K., China, K. and Nishijima, M. 2007. Release of the lipopolysaccharide deacylase PagL from latency compensates for a lack of lipopolysaccharide aminoarabinose modification-dependent resistance to the antimicrobial peptide polymyxin B in *Salmonella enterica*. *Journal of bacteriology* 189(13), pp. 4911-4919.

Kehrenberg, C., Schwarz, S., Jacobsen, L., Hansen, L. H. and Vester, B. 2005. A new mechanism for chloramphenicol, florfenicol and clindamycin resistance: methylation of 23S ribosomal RNA at A2503. *Molecular microbiology* 57(4), pp. 1064-1073.

Kempf, I. et al. 2013. What do we know about resistance to colistin in Enterobacteriaceae in avian and pig production in Europe? *International journal of antimicrobial agents* 42(5), pp. 379-383.

Kenner, B. A., Riddle, J. W., Rockwood, S. W. and Bordner, R. H. 1958. Bacterial Identification by Infrared Spectrophotometry II: Effect of Instrumental and Environmental Variables. *Journal of bacteriology* 75(1), pp. 16-20.

Keren, I., Shah, D., Spoering, A., Kaldalu, N. and Lewis, K. 2004. Specialized persister cells and the mechanism of multidrug tolerance in *Escherichia coli*. *Journal of bacteriology* 186(24), pp. 8172-8180.

Khameneh, B., Eskin, N. M., Iranshahy, M. and Fazly Bazzaz, B. S. 2021. Phytochemicals: a promising weapon in the arsenal against antibiotic-resistant bacteria. *Antibiotics* 10(9), p. 1044.

Kieffer, N., Nordmann, P. and Poirel, L. 2017. *Moraxella* species as potential sources of MCR-like polymyxin resistance determinants. *Antimicrobial agents and chemotherapy* 61(6), pp. 10.1128/aac. 00129-00117.

Kim, J., Hwang, B. K., Choi, H., Wang, Y., Choi, S. H., Ryu, S. and Jeon, B. 2019. Characterization of *mcr-1*-harboring plasmids from pan drug-resistant *Escherichia coli* strains isolated from retail raw chicken in South Korea. *Microorganisms* 7(9), p. 344.

Kim, J. H., Lee, J., Park, J. and Gho, Y. S. eds. 2015. *Gram-negative and Gram-positive bacterial extracellular vesicles*. *Seminars in cell & developmental biology.* Elsevier.

Kim, S. Y., Choi, H. J. and Ko, K. S. 2014. Differential expression of two-component systems, *pmrAB* and *phoPQ*, with different growth phases of *Klebsiella pneumoniae* in the presence or absence of colistin. *Current microbiology* 69, pp. 37-41.

Kiss, J., Nagy, Z., Tóth, G., Kiss, G. B., Jakab, J., Chandler, M. and Olasz, F. 2007. Transposition and target specificity of the typical IS*30* family element IS*1655* from *Neisseria meningitidis*. *Molecular microbiology* 63(6), pp. 1731-1747.

Kiwi, J. and Nadtochenko, V. 2005. Evidence for the mechanism of photocatalytic degradation of the bacterial wall membrane at the TiO_2 interface by ATR-FTIR and laser kinetic spectroscopy. *Langmuir* 21(10), pp. 4631-4641.

Knoll, B. and Keilmann, F. 1999. Near-field probing of vibrational absorption for chemical microscopy. *Nature* 399(6732), pp. 134-137.

Kohanski, M. A., Dwyer, D. J., Hayete, B., Lawrence, C. A. and Collins, J. J. 2007. A common mechanism of cellular death induced by bactericidal antibiotics. *Cell* 130(5), pp. 797-810.

Koskeroglu, K., Barel, M., Hizlisoy, H. and Yildirim, Y. 2023. Biofilm formation and antibiotic resistance profiles of water-borne pathogens. *Research in Microbiology* 174(5), p. 104056.

Kotra, L. P., Golemi, D., Amro, N. A., Liu, G.-Y. and Mobashery, S. 1999. Dynamics of the lipopolysaccharide assembly on the surface of *Escherichia coli*. *Journal of the American Chemical Society* 121(38), pp. 8707-8711.

Król, J. E., Wojtowicz, A. J., Rogers, L. M., Heuer, H., Smalla, K., Krone, S. M. and Top, E. M. 2013. Invasion of *E. coli* biofilms by antibiotic resistance plasmids. *Plasmid* 70(1), pp. 110-119.

Krüger, N. J. and Stingl, K. 2011. Two steps away from novelty–principles of bacterial DNA uptake. *Molecular microbiology* 80(4), pp. 860-867.

Kumarasamy, K. K. et al. 2010. Emergence of a new antibiotic resistance mechanism in India, Pakistan, and the UK: a molecular, biological, and epidemiological study. *The Lancet Infectious Diseases* 10(9), pp. 597-602.

Landman, D., Georgescu, C., Martin, D. A. and Quale, J. 2008. Polymyxins revisited. *Clinical microbiology reviews* 21(3), pp. 449-465.

Leclercq, R. 2002. Mechanisms of resistance to macrolides and lincosamides: nature of the resistance elements and their clinical implications. *Clinical infectious diseases* 34(4), pp. 482-492.

Lee, J.-Y. and Ko, K. S. 2014. Mutations and expression of PmrAB and PhoPQ related with colistin resistance in *Pseudomonas aeruginosa* clinical isolates. *Diagnostic*

microbiology and infectious disease 78(3), pp. 271-276.

Lee, S. Y. 1996. High cell-density culture of *Escherichia coli*. *Trends in biotechnology* 14(3), pp. 98-105.

Leefmann, T., Heim, C., Lausmaa, J., Sjövall, P., Ionescu, D., Reitner, J. and Thiel, V. 2015. An imaging mass spectrometry study on the formation of conditioning films and biofilms in the subsurface (Äspö Hard Rock Laboratory, SE Sweden). *Geomicrobiology Journal* 32(3-4), pp. 197-206.

Lenz, A. P., Williamson, K. S., Pitts, B., Stewart, P. S. and Franklin, M. J. 2008. Localized gene expression in *Pseudomonas aeruginosa* biofilms. *Applied and environmental microbiology* 74(14), pp. 4463-4471.

Leone, L., Loring, J., Sjöberg, S., Persson, P. and Shchukarev, A. 2006. Surface characterization of the Gram-positive bacteria *Bacillus subtilis*-an XPS study. *Surface and Interface Analysis: An International Journal devoted to the development and application of techniques for the analysis of surfaces, interfaces and thin films* 38(4), pp. 202-205.

Lesho, E. et al. 2013. Emergence of colistin-resistance in extremely drug-resistant *Acinetobacter baumannii* containing a novel *pmrCAB* operon during colistin therapy of wound infections. *The Journal of infectious diseases* 208(7), pp. 1142-1151.

Levine, S., Stevenson, H. J., Chambers, L. A. and Kenner, B. A. 1953. Infrared spectrophotometry of enteric bacteria. *Journal of bacteriology* 65(1), pp. 10-15.

Lewenza, S. 2013. Extracellular DNA-induced antimicrobial peptide resistance mechanisms in *Pseudomonas aeruginosa*. *Frontiers in microbiology* 4, p. 21.

Lewis, K. 2007. Persister cells, dormancy and infectious disease. *Nature reviews microbiology* 5(1), pp. 48-56.

Li, A. et al. 2016. Complete sequences of *mcr-1*-harboring plasmids from extended-spectrum-β-lactamase- and carbapenemase-producing *Enterobacteriaceae*. *Antimicrobial agents and chemotherapy* 60(7), pp. 4351-4354.

Li, B. et al. 2020a. Colistin resistance gene *mcr-1* mediates cell permeability and resistance to hydrophobic antibiotics. *Frontiers in microbiology* 10, p. 3015.

Li, G., Li, X., Wu, Y., Xu, J. and He, F. 2022. Genomic Insights into the Colistin Resistant *mcr*-Carrying *Escherichia coli* Strains in a Tertiary Hospital in China. *Antibiotics* 11(11), p. 1522.

Li, J., Beuerman, R. and Verma, C. S. 2020b. Dissecting the molecular mechanism of colistin resistance in *mcr-1* bacteria. *Journal of chemical information and modeling* 60(10), pp. 4975-4984.

Li, J., Nation, R. L., Turnidge, J. D., Milne, R. W., Coulthard, K., Rayner, C. R. and Paterson, D. L. 2006. Colistin: the re-emerging antibiotic for multidrug-resistant Gram-negative bacterial infections. *The Lancet Infectious Diseases* 6(9), pp. 589-601.

Li, M. 2023. *Assessment of the global impact of MCR-1/MCR-3 mediated colistin resistance.* Cardiff University.

Li, R., Chen, K., Chan, E. W.-C. and Chen, S. 2019. Characterization of the stability and dynamics of Tn*6330* in an *Escherichia coli* strain by nanopore long reads. *Journal of Antimicrobial Chemotherapy* 74(7), pp. 1807-1811.

Li, R., Xie, M., Lv, J., Wai-Chi Chan, E. and Chen, S. 2017a. Complete genetic analysis of plasmids carrying *mcr-1* and other resistance genes in an *Escherichia coli* isolate of animal origin. *Journal of Antimicrobial Chemotherapy* 72(3), pp. 696-699.

Li, R. et al. 2017b. Genetic characterization of *mcr-1*-bearing plasmids to depict molecular mechanisms underlying dissemination of the colistin resistance determinant. *Journal of Antimicrobial Chemotherapy* 72(2), pp. 393-401.

Li, R. et al. 2018. Genetic basis of chromosomally-encoded *mcr-1* gene. *International journal of antimicrobial agents* 51(4), pp. 578-585.

Li, W. et al. 2021. MCR expression conferring varied fitness costs on host bacteria and affecting bacteria virulence. *Antibiotics* 10(7), p. 872.

Liao, C., Santoscoy, M. C., Craft, J., Anderson, C., Soupir, M. L. and Jarboe, L. R. 2022. Allelic variation of *Escherichia coli* outer membrane protein A: Impact on cell surface properties, stress tolerance and allele distribution. *PloS one* 17(10), p. e0276046.

Lim, L. M. et al. 2010. Resurgence of colistin: a review of resistance, toxicity, pharmacodynamics, and dosing. *Pharmacotherapy: The Journal of Human Pharmacology and Drug Therapy* 30(12), pp. 1279-1291.

Lima, T., Loureiro, D., Henriques, A., Ramos, F., Pomba, C., Domingues, S. and da Silva, G. J. 2022. Occurrence and biological cost of *mcr-1*-carrying plasmids co-harbouring beta-lactamase resistance genes in zoonotic pathogens from intensive animal production. *Antibiotics* 11(10), p. 1356.

Lima, W. G., Alves, M. C., Cruz, W. S. and Paiva, M. C. 2018. Chromosomally encoded and plasmid-mediated polymyxins resistance in *Acinetobacter baumannii*: a huge public health threat. *European journal of clinical microbiology & infectious diseases* 37, pp. 1009-1019.

Lin, M.-F., Lin, Y.-Y. and Lan, C.-Y. 2017. Contribution of EmrAB efflux pumps to colistin resistance in *Acinetobacter baumannii*. *Journal of Microbiology* 55, pp. 130-136.

Lin, M., Al-Holy, M., Al-Qadiri, H., Kang, D.-H., Cavinato, A. G., Huang, Y. and Rasco, B. A. 2004. Discrimination of intact and injured *Listeria monocytogenes* by Fourier transform infrared spectroscopy and principal component analysis. *Journal of agricultural and food chemistry* 52(19), pp. 5769-5772.

Lin, Y. et al. 2020. Genomic features of an *Escherichia coli* ST156 strain harboring chromosome-located *mcr-1* and plasmid-mediated *bla*$_{\text{NDM-5}}$. *Infection, Genetics and Evolution* 85, p. 104499.

Ling, Z. et al. 2017. Chromosome-mediated *mcr-3* variants in *Aeromonas veronii* from chicken meat. *Antimicrobial agents and chemotherapy* 61(11), pp. e01272-01217.

Ling, Z., Yin, W., Shen, Z., Wang, Y., Shen, J. and Walsh, T. R. 2020. Epidemiology of mobile colistin resistance genes *mcr-1* to *mcr-9*. *Journal of Antimicrobial Chemotherapy* 75(11), pp. 3087-3095.

Lippa, A. M. and Goulian, M. 2009. Feedback inhibition in the PhoQ/PhoP signaling system by a membrane peptide. *PLoS genetics* 5(12), p. e1000788.

Liu, J.-H., Liu, Y.-Y., Shen, Y.-B., Yang, J., Walsh, T. R., Wang, Y. and Shen, J. 2024a. Plasmid-mediated colistin-resistance genes: *mcr*. *Trends in microbiology* 32(4), pp. 365-378.

Liu, Y.-Y. et al. 2016. Emergence of plasmid-mediated colistin resistance mechanism MCR-1 in animals and human beings in China: a microbiological and molecular biological study. *The Lancet Infectious Diseases* 16(2), pp. 161-168.

Liu, Y.-Y., Zhu, X.-Q., Nang, S. C., Xun, H., Lv, L., Yang, J. and Liu, J.-H. 2023. Greater Invasion and Persistence of *mcr-1*-Bearing Plasmids in *Escherichia coli* than in *Klebsiella pneumoniae*. *Microbiology Spectrum* 11(2), pp. e03223-03222.

Liu, Y.-Y. et al. 2020. Metabolic perturbations caused by the over-expression of *mcr-1* in *Escherichia coli*. *Frontiers in microbiology* 11, p. 588658.

Liu, Z. et al. 2024b. Adaptive evolution of plasmid and chromosome contributes to the fitness of a *bla*$_{NDM}$-bearing cointegrate plasmid in *Escherichia coli*. *The ISME Journal* 18(1), p. wrae037.

Liu, Z. et al. 2021. Genetic features of plasmid- and chromosome-mediated *mcr-1* in *Escherichia coli* isolates from animal organs with lesions. *Frontiers in microbiology* 12, p. 707332.

Liu, Z. et al. 2011. The alteration of cell membrane of sulfate reducing bacteria in the presence of Mn (II) and Cd (II). *Minerals Engineering* 24(8), pp. 839-844.

Liu, Z., Zhao, Q., Xu, C. and Song, H. 2024c. Compensatory evolution of chromosomes and plasmids counteracts the plasmid fitness cost. *Ecology and Evolution* 14(8), p. e70121.

Llobet, E., Tomas, J. M. and Bengoechea, J. A. 2008. Capsule polysaccharide is a bacterial decoy for antimicrobial peptides. *Microbiology* 154(12), pp. 3877-3886.

Lobritz, M. A. et al. 2015. Antibiotic efficacy is linked to bacterial cellular respiration. *Proceedings of the National Academy of Sciences* 112(27), pp. 8173-8180.

Loftie-Eaton, W. et al. 2016. Evolutionary paths that expand plasmid host-range: implications for spread of antibiotic resistance. *Molecular biology and evolution* 33(4), pp. 885-897.

López-Camacho, E. et al. 2014. Genomic analysis of the emergence and evolution of multidrug resistance during a *Klebsiella pneumoniae* outbreak including carbapenem and colistin resistance. *Journal of Antimicrobial Chemotherapy* 69(3), pp. 632-636.

Lorin-Latxague, C. and Melin, A. M. 2005. Radical induced damage of *Micrococcus luteus* bacteria monitored using FT-IR spectroscopy. *Spectroscopy* 19(1), pp. 17-26.

Lu, X. et al. 2017. MCR-1.6, a new MCR variant carried by an IncP plasmid in a colistin-resistant *Salmonella enterica* serovar Typhimurium isolate from a healthy individual. *Antimicrobial agents and chemotherapy* 61(5), pp. e02632-02616.

Lu, Y., Liu, J.-H., Yue, C., Bergen, P. J., Wu, R., Li, J. and Liu, Y.-Y. 2022. Overexpression of *mcr-1* disrupts cell envelope synthesis and causes the dysregulation of carbon metabolism, redox balance and nucleic acids. *International journal of antimicrobial agents* 60(3), p. 106643.

Luo, S.-C., Lou, Y.-C., Rajasekaran, M., Chang, Y.-W., Hsiao, C.-D. and Chen, C. 2013. Structural basis of a physical blockage mechanism for the interaction of response

regulator PmrA with connector protein PmrD from *Klebsiella pneumoniae*. *Journal of Biological Chemistry* 288(35), pp. 25551-25561.

Lv, Z. et al. 2022. Prevalence and risk factors of *mcr-1*-positive volunteers after colistin banning as animal growth promoter in China: a community-based case-control study. *Clinical Microbiology and Infection* 28(2), pp. 267-272.

Lynch, D. J., Fountain, T. L., Mazurkiewicz, J. E. and Banas, J. A. 2007. Glucan-binding proteins are essential for shaping *Streptococcus mutans* biofilm architecture. *FEMS microbiology letters* 268(2), pp. 158-165.

Lyon, G. J. and Muir, T. W. 2003. Chemical signaling among bacteria and its inhibition. *Chemistry & biology* 10(11), pp. 1007-1021.

Ma, K., Feng, Y. and Zong, Z. 2018. Fitness cost of a *mcr-1*-carrying IncHI2 plasmid. *PloS one* 13(12), p. e0209706.

Ma, W., Jiang, X., Dou, Y., Zhang, Z., Li, J., Yuan, B. and Yang, K. 2021. Biophysical impact of lipid A modification caused by mobile colistin resistance gene on bacterial outer membranes. *The Journal of Physical Chemistry Letters* 12(48), pp. 11629-11635.

Madsen, J. S., Burmølle, M., Hansen, L. H. and Sørensen, S. J. 2012. The interconnection between biofilm formation and horizontal gene transfer. *FEMS Immunology & Medical Microbiology* 65(2), pp. 183-195.

Mah, T.-F. 2012a. Biofilm-specific antibiotic resistance. *Future microbiology* 7(9), pp. 1061-1072.

Mah, T.-F. 2012b. Regulating antibiotic tolerance within biofilm microcolonies. *Journal of bacteriology* 194(18), pp. 4791-4792.

Mah, T.-F., Pitts, B., Pellock, B., Walker, G. C., Stewart, P. S. and O'Toole, G. A. 2003. A genetic basis for *Pseudomonas aeruginosa* biofilm antibiotic resistance. *Nature* 426(6964), pp. 306-310.

Mahajan, A. et al. 2009. An investigation of the expression and adhesin function of H7 flagella in the interaction of *Escherichia coli* O157: H7 with bovine intestinal epithelium. *Cellular microbiology* 11(1), pp. 121-137.

Mahizan, N. A. et al. 2019. Terpene derivatives as a potential agent against antimicrobial resistance (AMR) pathogens. *Molecules* 24(14), p. 2631.

Marchal, K. et al. 2004. *In silico* identification and experimental validation of PmrAB

targets in *Salmonella typhimurium* by regulatory motif detection. *Genome biology* 5, pp. 1-20.

Mariey, L., Signolle, J., Amiel, C. and Travert, J. 2001. Discrimination, classification, identification of microorganisms using FTIR spectroscopy and chemometrics. *Vibrational spectroscopy* 26(2), pp. 151-159.

Marinelli, L., Di Stefano, A. and Cacciatore, I. 2018. Carvacrol and its derivatives as antibacterial agents. *Phytochemistry Reviews* 17, pp. 903-921.

Marquis, R. E., Mayzel, K. and Carstensen, E. L. 1976. Cation exchange in cell walls of Gram-positive bacteria. *Canadian journal of microbiology* 22(7), pp. 975-982.

Matamoros, S. et al. 2017. Global phylogenetic analysis of *Escherichia coli* and plasmids carrying the *mcr-1* gene indicates bacterial diversity but plasmid restriction. *Scientific reports* 7(1), p. 15364.

Mattiuz, G. et al. 2020. *mcr-1* gene expression modulates the inflammatory response of human macrophages to *Escherichia coli*. *Infection and immunity* 88(8), pp. 10.1128/iai. 00018-00020.

Maturana, P., Martinez, M., Faccone, D., Semorile, L., Maffia, P. C. and Hollmann, A. 2020. New insights into novel *Escherichia coli* colistin-resistant strains isolated from Argentina. *European Biophysics Journal* 49(3), pp. 307-313.

May, K. L. and Silhavy, T. J. 2018. The *Escherichia coli* phospholipase PldA regulates outer membrane homeostasis via lipid signaling. *MBio* 9(2), pp. 10.1128/mbio. 00379-00318.

Mayo, S. L., Olafson, B. D. and Goddard, W. A. 1990. DREIDING: a generic force field for molecular simulations. *Journal of Physical chemistry* 94(26), pp. 8897-8909.

McCammon, J. A., Gelin, B. R. and Karplus, M. 1977. Dynamics of folded proteins. *Nature* 267(5612), pp. 585-590.

McConville, T. H. et al. 2020. CrrB positively regulates high-level polymyxin resistance and virulence in *Klebsiella pneumoniae*. *Cell reports* 33(4), p. 108313.

McLean, D. T., Lundy, F. T. and Timson, D. J. 2013. IQ-motif peptides as novel anti-microbial agents. *Biochimie* 95(4), pp. 875-880.

Mei, C.-Y. et al. 2024. Low prevalence of *mcr-1* in *Escherichia coli* from food-producing animals and food products in China. *BMC Veterinary Research* 20(1), p. 40.

Melnyk, A. H., Wong, A. and Kassen, R. 2015. The fitness costs of antibiotic resistance mutations. *Evolutionary applications* 8(3), pp. 273-283.

Metzger, G. A. et al. 2022. Biofilms preserve the transmissibility of a multi-drug resistance plasmid. *npj Biofilms and Microbiomes* 8(1), p. 95.

Millan, A. S., Peña-Miller, R., Toll-Riera, M., Halbert, Z., McLean, A., Cooper, B. and MacLean, R. 2014. Positive selection and compensatory adaptation interact to stabilize non-transmissible plasmids. *Nature communications* 5(1), p. 5208.

Miller, A. K. et al. 2011. PhoQ mutations promote lipid A modification and polymyxin resistance of *Pseudomonas aeruginosa* found in colistin-treated cystic fibrosis patients. *Antimicrobial agents and chemotherapy* 55(12), pp. 5761-5769.

Miller, M. B. and Bassler, B. L. 2001. Quorum sensing in bacteria. *Annual Reviews in Microbiology* 55(1), pp. 165-199.

Miller, S. I., Kukral, A. M. and Mekalanos, J. J. 1989. A two-component regulatory system (*phoP phoQ*) controls *Salmonella typhimurium* virulence. *Proceedings of the National Academy of Sciences* 86(13), pp. 5054-5058.

Mishra, A., Tabassum, N., Aggarwal, A., Kim, Y.-M. and Khan, F. 2024. Artificial intelligence-driven analysis of antimicrobial-resistant and biofilm-forming pathogens on biotic and abiotic surfaces. *Antibiotics* 13(8), p. 788.

Mitrophanov, A. Y., Jewett, M. W., Hadley, T. J. and Groisman, E. A. 2008. Evolution and dynamics of regulatory architectures controlling polymyxin B resistance in enteric bacteria. *PLoS genetics* 4(10), p. e1000233.

Mmatli, M., Mbelle, N. M. and Sekyere, J. O. 2022. Global epidemiology and genetic environment of *mcr* genes: a One Health systematic review of current and emerging trends. *medRxiv*, p. 2022.2002. 2028.22271560.

Modi, S. R., Lee, H. H., Spina, C. S. and Collins, J. J. 2013. Antibiotic treatment expands the resistance reservoir and ecological network of the phage metagenome. *Nature* 499(7457), pp. 219-222.

Moellering Jr, R. C. 2012. MRSA: the first half century. *Journal of Antimicrobial Chemotherapy* 67(1), pp. 4-11.

Moffatt, J. H., Harper, M., Adler, B., Nation, R. L., Li, J. and Boyce, J. D. 2011. Insertion sequence IS*Aba11* is involved in colistin resistance and loss of

lipopolysaccharide in *Acinetobacter baumannii*. *Antimicrobial agents and chemotherapy* 55(6), pp. 3022-3024.

Moffatt, J. H. et al. 2010. Colistin resistance in *Acinetobacter baumannii* is mediated by complete loss of lipopolysaccharide production. *Antimicrobial agents and chemotherapy* 54(12), pp. 4971-4977.

Mohapatra, S. S., Dwibedy, S. K. and Padhy, I. 2021. Polymyxins, the last-resort antibiotics: Mode of action, resistance emergence, and potential solutions. *Journal of Biosciences* 46(3), p. 85.

Molin, S. and Tolker-Nielsen, T. 2003. Gene transfer occurs with enhanced efficiency in biofilms and induces enhanced stabilisation of the biofilm structure. *Current opinion in biotechnology* 14(3), pp. 255-261.

Monte, J., Abreu, A. C., Borges, A., Simões, L. C. and Simões, M. 2014. Antimicrobial activity of selected phytochemicals against *Escherichia coli* and *Staphylococcus aureus* and their biofilms. *Pathogens* 3(2), pp. 473-498.

Moon, K. and Gottesman, S. 2009. A PhoQ/P-regulated small RNA regulates sensitivity of *Escherichia coli* to antimicrobial peptides. *Molecular microbiology* 74(6), pp. 1314-1330.

Moosavian, M., Emam, N., Pletzer, D. and Savari, M. 2020. Rough-type and loss of the LPS due to *lpx* genes deletions are associated with colistin resistance in multidrug-resistant clinical *Escherichia coli* isolates not harbouring *mcr* genes. *PloS one* 15(5), p. e0233518.

Morales, G. et al. 2010. Resistance to linezolid is mediated by the *cfr* gene in the first report of an outbreak of linezolid-resistant *Staphylococcus aureus*. *Clinical infectious diseases* 50(6), pp. 821-825.

Moses, R. L. et al. 2020. Novel epoxy-tiglianes stimulate skin keratinocyte wound healing responses and re-epithelialization via protein kinase C activation. *Biochem Pharmacol* 178, p. 114048. doi: 10.1016/j.bcp.2020.114048

Moses, R. L., Prescott, T. A., Mas-Claret, E., Steadman, R., Moseley, R. and Sloan, A. J. 2023. Evidence for natural products as alternative wound-healing therapies. *Biomolecules* 13(3), p. 444.

Moskowitz, S. M. et al. 2012. PmrB mutations promote polymyxin resistance of *Pseudomonas aeruginosa* isolated from colistin-treated cystic fibrosis patients. *Antimicrobial agents and chemotherapy* 56(2), pp. 1019-1030.

Mulcahy, H., Charron-Mazenod, L. and Lewenza, S. 2008. Extracellular DNA chelates cations and induces antibiotic resistance in *Pseudomonas aeruginosa* biofilms. *PLoS pathogens* 4(11), p. e1000213.

Mulyaningsih, S., Sporer, F., Zimmermann, S., Reichling, J. and Wink, M. 2010. Synergistic properties of the terpenoids aromadendrene and 1, 8-cineole from the essential oil of *Eucalyptus globulus* against antibiotic-susceptible and antibiotic-resistant pathogens. *Phytomedicine* 17(13), pp. 1061-1066.

Murdick, R. A., Morrison, W., Nowak, D., Albrecht, T. R., Jahng, J. and Park, S. 2017. Photoinduced force microscopy: A technique for hyperspectral nanochemical mapping. *Japanese Journal of Applied Physics* 56(8S1), p. 08LA04.

Murray, S. R., Ernst, R. K., Bermudes, D., Miller, S. I. and Low, K. B. 2007. pmrA (Con) confers *pmrHFIJKL*-dependent EGTA and polymyxin resistance on *msbB Salmonella* by decorating lipid A with phosphoethanolamine. *Journal of bacteriology* 189(14), pp. 5161-5169.

Nadell, C. D., Xavier, J. B. and Foster, K. R. 2008. The sociobiology of biofilms. *FEMS microbiology reviews* 33(1), pp. 206-224.

Nadtochenko, V., Rincon, A., Stanca, S. and Kiwi, J. 2005. Dynamics of *E. coli* membrane cell peroxidation during TiO_2 photocatalysis studied by ATR-FTIR spectroscopy and AFM microscopy. *Journal of Photochemistry and Photobiology A: Chemistry* 169(2), pp. 131-137.

Nang, S. C., Li, J. and Velkov, T. 2019. The rise and spread of *mcr* plasmid-mediated polymyxin resistance. *Critical reviews in microbiology* 45(2), pp. 131-161.

Nang, S. C. et al. 2018. Fitness cost of *mcr-1*-mediated polymyxin resistance in *Klebsiella pneumoniae*. *Journal of Antimicrobial Chemotherapy* 73(6), pp. 1604-1610.

Naumann, D. 2000. Infrared spectroscopy in microbiology. *Encyclopedia of analytical chemistry* 102, p. 131.

Naumann, D., Helm, D. and Labischinski, H. 1991. Microbiological characterizations by FT-IR spectroscopy. *Nature* 351(6321), pp. 81-82.

Nazzaro, F., Fratianni, F., De Martino, L., Coppola, R. and De Feo, V. 2013. Effect of essential oils on pathogenic bacteria. *Pharmaceuticals* 6(12), pp. 1451-1474.

Needham, B. D. and Trent, M. S. 2013. Fortifying the barrier: the impact of lipid A

remodelling on bacterial pathogenesis. *Nature reviews microbiology* 11(7), pp. 467-481.

Neuhaus, F. C. and Baddiley, J. 2003. A continuum of anionic charge: structures and functions of D-alanyl-teichoic acids in Gram-positive bacteria. *Microbiology and molecular biology reviews* 67(4), pp. 686-723.

Neves, M. M. et al. 2024. Perspectives of FTIR as Promising Tool for Pathogen Diagnosis, Sanitary and Welfare Monitoring in Animal Experimentation Models: A Review Based on Pertinent Literature. *Microorganisms* 12(4), p. 833.

Nguyen, N. T. et al. 2016. Use of colistin and other critical antimicrobials on pig and chicken farms in southern Vietnam and its association with resistance in commensal *Escherichia coli* bacteria. *Applied and environmental microbiology* 82(13), pp. 3727-3735.

Nikaido, H. 2003. Molecular basis of bacterial outer membrane permeability revisited. *Microbiology and molecular biology reviews* 67(4), pp. 593-656.

Nikaido, H. and Pagès, J.-M. 2012. Broad-specificity efflux pumps and their role in multidrug resistance of Gram-negative bacteria. *FEMS microbiology reviews* 36(2), pp. 340-363.

Nimisha, S. and Rani, K. B. 2019. Antibacterial activity and phytochemical screening of ethanolic leaf, stem and flower extract of *Aerva lanata*. *Journal of Applied and Natural Science* 11(2), p. 455.

Nogueira, J. O. e. et al. 2021. Mechanism of action of various terpenes and phenylpropanoids against *Escherichia coli* and *Staphylococcus aureus*. *FEMS microbiology letters* 368(9), p. fnab052.

Nordmann, P., Jayol, A. and Poirel, L. 2016. Rapid detection of polymyxin resistance in *Enterobacteriaceae*. *Emerging infectious diseases* 22(6), p. 1038.

Noreen, A. et al. 2022. Investigating the Role of Antibiotics on Induction, Inhibition and Eradication of Biofilms of Poultry Associated *Escherichia coli* Isolated from Retail Chicken Meat. *Antibiotics* 11(11), p. 1663.

Novick, R. P., Christie, G. E. and Penadés, J. R. 2010. The phage-related chromosomal islands of Gram-positive bacteria. *Nature reviews microbiology* 8(8), pp. 541-551.

Nowak, D. et al. 2016. Nanoscale chemical imaging by photoinduced force microscopy. *Science Advances* 2(3), p. e1501571.

Nwodo, U. U., Green, E. and Okoh, A. I. 2012. Bacterial exopolysaccharides: functionality and prospects. *International journal of molecular sciences* 13(11), pp. 14002-14015.

Nydegger, M. W., Rock, W. and Cheatum, C. M. 2011. 2D IR spectroscopy of the C–D stretching vibration of the deuterated formic acid dimer. *Physical Chemistry Chemical Physics* 13(13), pp. 6098-6104.

O'Rourke, D., FitzGerald, C. E., Traverse, C. C. and Cooper, V. S. 2015. There and back again: consequences of biofilm specialization under selection for dispersal. *Frontiers in genetics* 6, p. 18.

Oakley, J. L. et al. 2021. Phenotypic and genotypic adaptations in *Pseudomonas aeruginosa* biofilms following long-term exposure to an alginate oligomer therapy. *Msphere* 6(1), pp. e01216-01220.

Ogunlana, L., Kaur, D., Shaw, L. P., Jangir, P., Walsh, T., Uphoff, S. and MacLean, R. 2023. Regulatory fine-tuning of *mcr-1* increases bacterial fitness and stabilises antibiotic resistance in agricultural settings. *The ISME Journal* 17(11), pp. 2058-2069.

Ojeda, J. J., Romero-González, M. E., Bachmann, R. T., Edyvean, R. G. and Banwart, S. A. 2008. Characterization of the cell surface and cell wall chemistry of drinking water bacteria by combining XPS, FTIR spectroscopy, modeling, and potentiometric titrations. *Langmuir* 24(8), pp. 4032-4040.

Olaitan, A. O. et al. 2014a. Worldwide emergence of colistin resistance in *Klebsiella pneumoniae* from healthy humans and patients in Lao PDR, Thailand, Israel, Nigeria and France owing to inactivation of the PhoP/PhoQ regulator *mgrB*: an epidemiological and molecular study. *International journal of antimicrobial agents* 44(6), pp. 500-507.

Olaitan, A. O., Morand, S. and Rolain, J.-M. 2014b. Mechanisms of polymyxin resistance: acquired and intrinsic resistance in bacteria. *Frontiers in microbiology* 5, p. 643.

Olaitan, A. O. et al. 2015. Clonal transmission of a colistin-resistant *Escherichia coli* from a domesticated pig to a human in Laos. *Journal of Antimicrobial Chemotherapy* 70(12), pp. 3402-3404.

Organization, W. H. 2014. *Antimicrobial resistance: global report on surveillance*. World Health Organization.

Otter, L. M. et al. 2021. Nanoscale chemical imaging by photo-induced force microscopy: technical aspects and application to the geosciences. *Geostandards and*

Geoanalytical Research 45(1), pp. 5-27.

Owen, P. 1992. The Gram-negative outer membrane: structure, biochemistry and vaccine potential. *Biochemical Society transactions* 20(1), pp. 1-6.

Padilla, E., Llobet, E., Doménech-Sánchez, A., Martínez-Martínez, L., Bengoechea, J. A. and Albertí, S. 2010. *Klebsiella pneumoniae* AcrAB efflux pump contributes to antimicrobial resistance and virulence. *Antimicrobial agents and chemotherapy* 54(1), pp. 177-183.

Palmer, J., Flint, S. and Brooks, J. 2007. Bacterial cell attachment, the beginning of a biofilm. *Journal of Industrial Microbiology and Biotechnology* 34(9), pp. 577-588.

Pamp, S. J., Gjermansen, M., Johansen, H. K. and Tolker-Nielsen, T. 2008. Tolerance to the antimicrobial peptide colistin in *Pseudomonas aeruginosa* biofilms is linked to metabolically active cells, and depends on the *pmr* and *mexAB-oprM* genes. *Molecular microbiology* 68(1), pp. 223-240.

Panizza, B. J., de Souza, P., Cooper, A., Roohullah, A., Karapetis, C. S. and Lickliter, J. D. 2019. Phase I dose-escalation study to determine the safety, tolerability, preliminary efficacy and pharmacokinetics of an intratumoral injection of tigilanol tiglate (EBC-46). *EBioMedicine* 50, pp. 433-441.

Park, Y. K., Choi, J. Y., Shin, D. and Ko, K. S. 2011. Correlation between overexpression and amino acid substitution of the PmrAB locus and colistin resistance in *Acinetobacter baumannii*. *International journal of antimicrobial agents* 37(6), pp. 525-530.

Paterson, D. L. and Harris, P. N. 2016. Colistin resistance: a major breach in our last line of defence. *The Lancet. Infectious diseases* 16(2), pp. 132-133.

Paul, S. 1999. Bacteria in biology, biotechnology and medicine. Biddle Ltd.

Paulander, W., Pennhag, A., Andersson, D. I. and Maisnier-Patin, S. 2007. *Caenorhabditis elegans* as a model to determine fitness of antibiotic-resistant *Salmonella enterica* serovar typhimurium. *Antimicrobial agents and chemotherapy* 51(2), pp. 766-769.

Paveenkittiporn, W., Kamjumphol, W., Ungcharoen, R. and Kerdsin, A. 2021. Whole-genome sequencing of clinically isolated carbapenem-resistant Enterobacterales harboring *mcr* genes in Thailand, 2016–2019. *Frontiers in microbiology* 11, p. 586368.

Percival, S. L., Hill, K. E., Williams, D. W., Hooper, S. J., Thomas, D. W. and Costerton,

J. W. 2012. A review of the scientific evidence for biofilms in wounds. *Wound repair and regeneration* 20(5), pp. 647-657.

Perez, J. C. and Groisman, E. A. 2007. Acid pH activation of the PmrA/PmrB two-component regulatory system of *Salmonella enterica*. *Molecular microbiology* 63(1), pp. 283-293.

Perni, S., Preedy, E. C. and Prokopovich, P. 2014. Success and failure of colloidal approaches in adhesion of microorganisms to surfaces. *Advances in Colloid and Interface Science* 206, pp. 265-274.

Perveen, S., Al-Taweel, A. M. and Blumenberg, M. 2021. *Terpenes and Terpenoids: Recent Advances*. IntechOpen.

Peterson, B. W., Sharma, P. K., van der Mei, H. C. and Busscher, H. J. 2012. Bacterial cell surface damage due to centrifugal compaction. *Applied and environmental microbiology* 78(1), pp. 120-125.

Pham Thanh, D. et al. 2016. Inducible colistin resistance via a disrupted plasmid-borne *mcr-1* gene in a 2008 Vietnamese *Shigella sonnei* isolate. *Journal of Antimicrobial Chemotherapy* 71(8), pp. 2314-2317.

Phillips, J. C. et al. 2005. Scalable molecular dynamics with NAMD. *Journal of computational chemistry* 26(16), pp. 1781-1802.

Picquart, M., Haro-Poniatowski, E., Morhange, J., Jouanne, M. and Kanehisa, M. 2000. Low frequency vibrations and structural characterization of a murine IgG2a monoclonal antibody studied by Raman and IR spectroscopies. *Biopolymers: Original Research on Biomolecules* 53(4), pp. 342-349.

Piddock, L. J. 2006a. Clinically relevant chromosomally encoded multidrug resistance efflux pumps in bacteria. *Clinical microbiology reviews* 19(2), pp. 382-402.

Piddock, L. J. 2006b. Multidrug-resistance efflux pumps — not just for resistance. *Nature reviews microbiology* 4(8), pp. 629-636.

Podstawka-Proniewicz, E., Piergies, N., Skołuba, D., Kafarski, P., Kim, Y. and Proniewicz, L. M. 2011. Vibrational characterization of L-leucine phosphonate analogues: FT-IR, FT-Raman, and SERS spectroscopy studies and DFT calculations. *The Journal of Physical Chemistry A* 115(40), pp. 11067-11078.

Pogozheva, I. D. et al. 2022. Comparative molecular dynamics simulation studies of realistic eukaryotic, prokaryotic, and archaeal membranes. *Journal of chemical*

information and modeling 62(4), pp. 1036-1051.

Poirel, L., Jayol, A., Bontron, S., Villegas, M.-V., Ozdamar, M., Türkoglu, S. and Nordmann, P. 2015. The *mgrB* gene as a key target for acquired resistance to colistin in *Klebsiella pneumoniae*. *Journal of Antimicrobial Chemotherapy* 70(1), pp. 75-80.

Poirel, L., Jayol, A. and Nordmann, P. 2017a. Polymyxins: antibacterial activity, susceptibility testing, and resistance mechanisms encoded by plasmids or chromosomes. *Clinical microbiology reviews* 30(2), pp. 557-596.

Poirel, L., Kieffer, N., Brink, A., Coetze, J., Jayol, A. and Nordmann, P. 2016. Genetic features of MCR-1-producing colistin-resistant *Escherichia coli* isolates in South Africa. *Antimicrobial agents and chemotherapy* 60(7), pp. 4394-4397.

Poirel, L., Kieffer, N., Fernandez-Garayzabal, J. F., Vela, A. I., Larpin, Y. and Nordmann, P. 2017b. MCR-2-mediated plasmid-borne polymyxin resistance most likely originates from *Moraxella pluranimalium*. *Journal of Antimicrobial Chemotherapy* 72(10), pp. 2947-2949.

Poirel, L., Kieffer, N. and Nordmann, P. 2017c. *In vitro* study of IS*Apl1*-mediated mobilization of the colistin resistance gene *mcr-1*. *Antimicrobial agents and chemotherapy* 61(7), pp. 10.1128/aac. 00127-00117.

Poltak, S. R. and Cooper, V. S. 2011. Ecological succession in long-term experimentally evolved biofilms produces synergistic communities. *The ISME Journal* 5(3), pp. 369-378.

Poole, K. 2005. Efflux-mediated antimicrobial resistance. *Journal of Antimicrobial Chemotherapy* 56(1), pp. 20-51.

Pope, C. F., McHugh, T. D. and Gillespie, S. H. 2010. Methods to determine fitness in bacteria. *Antibiotic Resistance Protocols: Second Edition*, pp. 113-121.

Porse, A., Schønning, K., Munck, C. and Sommer, M. O. 2016. Survival and evolution of a large multidrug resistance plasmid in new clinical bacterial hosts. *Molecular biology and evolution* 33(11), pp. 2860-2873.

Potma, E. O., Jahng, J., Ladani, F. T. and Khan, R. M. 2015. Nanoscopic imaging with optical forces. *SPIE Newsroom*, pp. 1-3.

Powell, L. C. et al. 2022. Topical, immunomodulatory epoxy-tiglianes induce biofilm disruption and healing in acute and chronic skin wounds. *Science translational medicine* 14(662), p. eabn3758.

Pozzi, E. A., Sonntag, M. D., Jiang, N., Klingsporn, J. M., Hersam, M. C. and Van Duyne, R. P. 2013. Tip-enhanced Raman imaging: an emergent tool for probing biology at the nanoscale. *ACS nano* 7(2), pp. 885-888.

Prost, L. R. and Miller, S. I. 2008. The Salmonellae PhoQ sensor: mechanisms of detection of phagosome signals. *Cellular microbiology* 10(3), pp. 576-582.

Pulingam, T., Thong, K. L., Ali, M. E., Appaturi, J. N., Dinshaw, I. J., Ong, Z. Y. and Leo, B. F. 2019. Graphene oxide exhibits differential mechanistic action towards Gram-positive and Gram-negative bacteria. *Colloids and surfaces B: Biointerfaces* 181, pp. 6-15.

Putman, M., van Veen, H. W. and Konings, W. N. 2000. Molecular properties of bacterial multidrug transporters. *Microbiology and molecular biology reviews* 64(4), pp. 672-693.

Quan, J. et al. 2017. Prevalence of *mcr-1* in *Escherichia coli* and *Klebsiella pneumoniae* recovered from bloodstream infections in China: a multicentre longitudinal study. *The Lancet Infectious Diseases* 17(4), pp. 400-410.

Quilès, F., Saadi, S., Francius, G., Bacharouche, J. and Humbert, F. 2016. In situ and real time investigation of the evolution of a *Pseudomonas fluorescens* nascent biofilm in the presence of an antimicrobial peptide. *Biochimica et Biophysica Acta (BBA)-Biomembranes* 1858(1), pp. 75-84.

Rabin, N., Zheng, Y., Opoku-Temeng, C., Du, Y., Bonsu, E. and Sintim, H. O. 2015. Biofilm formation mechanisms and targets for developing antibiofilm agents. *Future medicinal chemistry* 7(4), pp. 493-512.

Raetz, C. R., Reynolds, C. M., Trent, M. S. and Bishop, R. E. 2007. Lipid A modification systems in Gram-negative bacteria. *Annu. Rev. Biochem.* 76(1), pp. 295-329.

Raetz, C. R. and Whitfield, C. 2002. Lipopolysaccharide endotoxins. *Annual review of biochemistry* 71(1), pp. 635-700.

Rahaman, M. L. et al. 2025. Efficient synthesis of mannopyranoside-based fatty acyl esters: Effects of acyl groups on antimicrobial potential. *Medicinal Chemistry* 21(5), pp. 385-402.

Rainey, P. B. and Travisano, M. 1998. Adaptive radiation in a heterogeneous environment. *Nature* 394(6688), pp. 69-72.

Rajapaksa, I., Uenal, K. and Wickramasinghe, H. K. 2010. Image force microscopy of molecular resonance: A microscope principle. *Applied physics letters* 97(7),

Rajer, F. and Sandegren, L. 2022. The role of antibiotic resistance genes in the fitness cost of multiresistance plasmids. *MBio* 13(1), pp. e03552-03521.

Ramírez-Castillo, F. Y., Moreno-Flores, A. C., Avelar-González, F. J., Márquez-Díaz, F., Harel, J. and Guerrero-Barrera, A. L. 2018. An evaluation of multidrug-resistant *Escherichia coli* isolates in urinary tract infections from Aguascalientes, Mexico: cross-sectional study. *Annals of clinical microbiology and antimicrobials* 17(1), p. 34.

Ramirez, M. S. and Tolmasky, M. E. 2010. Aminoglycoside modifying enzymes. *Drug resistance updates* 13(6), pp. 151-171.

Ramstedt, M., Nakao, R., Wai, S. N., Uhlin, B. E. and Boily, J.-F. 2011. Monitoring surface chemical changes in the bacterial cell wall: multivariate analysis of cryo-X-ray photoelectron spectroscopy data. *Journal of Biological Chemistry* 286(14), pp. 12389-12396.

Rathinam, P., Vijay Kumar, H. and Viswanathan, P. 2017. Eugenol exhibits anti-virulence properties by competitively binding to quorum sensing receptors. *Biofouling* 33(8), pp. 624-639.

Reddell, P. et al. 2021. Wound formation, wound size, and progression of wound healing after intratumoral treatment of mast cell tumors in dogs with tigilanol tiglate. *Journal of Veterinary Internal Medicine* 35(1), pp. 430-441.

Reed, M. D., Stern, R. C., O'Riordan, M. A. and Blumer, J. L. 2001. The pharmacokinetics of colistin in patients with cystic fibrosis. *The Journal of Clinical Pharmacology* 41(6), pp. 645-654.

Reisner, A. et al. 2014. Type 1 fimbriae contribute to catheter-associated urinary tract infections caused by *Escherichia coli*. *Journal of bacteriology* 196(5), pp. 931-939.

Reynolds, C. M., Kalb, S. R., Cotter, R. J. and Raetz, C. R. 2005. A phosphoethanolamine transferase specific for the outer 3-deoxy-D-manno-octulosonic acid residue of *Escherichia coli* lipopolysaccharide: identification of the *eptB* gene and Ca^{2+} hypersensitivity of an *eptB* deletion mutant. *Journal of Biological Chemistry* 280(22), pp. 21202-21211.

Reynolds, C. M., Ribeiro, A. A., McGrath, S. C., Cotter, R. J., Raetz, C. R. and Trent, M. S. 2006. An outer membrane enzyme encoded by *Salmonella typhimurium lpxR* that

removes the 3'-acyloxyacyl moiety of lipid A. *Journal of Biological Chemistry* 281(31), pp. 21974-21987.

Reynolds, E. S. 1963. The use of lead citrate at high pH as an electron-opaque stain in electron microscopy. *The Journal of cell biology* 17(1), p. 208.

Rezzonico, F. and Duffy, B. 2008. Lack of genomic evidence of AI-2 receptors suggests a non-quorum sensing role for *luxS* in most bacteria. *BMC microbiology* 8(1), pp. 1-19.

Rhouma, M., Beaudry, F., Theriault, W. and Letellier, A. 2016. Colistin in pig production: chemistry, mechanism of antibacterial action, microbial resistance emergence, and one health perspectives. *Frontiers in microbiology* 7, p. 1789.

Riddle, J. W., Kabler, P. W., Kenner, B. A., Bordner, R. H., Rockwood, S. W. and Stevenson, H. J. 1956. Bacterial identification by infrared spectrophotometry. *Journal of bacteriology* 72(5), pp. 593-603.

Riding, M. J., Martin, F. L., Trevisan, J., Llabjani, V., Patel, I. I., Jones, K. C. and Semple, K. T. 2012. Concentration-dependent effects of carbon nanoparticles in Gram-negative bacteria determined by infrared spectroscopy with multivariate analysis. *Environmental pollution* 163, pp. 226-234.

Roberts, A. P. and Mullany, P. 2010. Oral biofilms: a reservoir of transferable, bacterial, antimicrobial resistance. *Expert review of anti-infective therapy* 8(12), pp. 1441-1450.

Robustelli, P., Piana, S. and Shaw, D. E. 2018. Developing a molecular dynamics force field for both folded and disordered protein states. *Proceedings of the National Academy of Sciences* 115(21), pp. E4758-E4766.

Rodríguez-Beltrán, J., DelaFuente, J., León-Sampedro, R., MacLean, R. C. and San Millán, Á. 2021. Beyond horizontal gene transfer: the role of plasmids in bacterial evolution. *Nature reviews microbiology* 19(6), pp. 347-359.

Roland, K. L., Martin, L. E., Esther, C. R. and Spitznagel, J. K. 1993. Spontaneous *pmrA* mutants of *Salmonella typhimurium* LT2 define a new two-component regulatory system with a possible role in virulence. *Journal of bacteriology* 175(13), pp. 4154-4164.

Rubin, E. J., Herrera, C. M., Crofts, A. A. and Trent, M. S. 2015. PmrD is required for modifications to *Escherichia coli* endotoxin that promote antimicrobial resistance. *Antimicrobial agents and chemotherapy* 59(4), pp. 2051-2061.

Salminen, A., Lehtonen, M., Suuronen, T., Kaarniranta, K. and Huuskonen, J. 2008.

Terpenoids: natural inhibitors of NF-κB signaling with anti-inflammatory and anticancer potential. *Cellular and Molecular Life Sciences* 65, pp. 2979-2999.

San Millan, A. 2018. Evolution of plasmid-mediated antibiotic resistance in the clinical context. *Trends in microbiology* 26(12), pp. 978-985.

San Millan, A. and MacLean, R. C. 2017. Fitness costs of plasmids: a limit to plasmid transmission. *Microbiology Spectrum* 5(5), pp. 10.1128/microbiolspec. mtbp-0016-2017.

San Millan, A., Toll-Riera, M., Qi, Q. and MacLean, R. C. 2015. Interactions between horizontally acquired genes create a fitness cost in *Pseudomonas aeruginosa*. *Nature communications* 6(1), p. 6845.

Santos-Lopez, A., Marshall, C. W., Scribner, M. R., Snyder, D. J. and Cooper, V. S. 2019. Evolutionary pathways to antibiotic resistance are dependent upon environmental structure and bacterial lifestyle. *Elife* 8, p. e47612.

Savage, V. J., Chopra, I. and O'Neill, A. J. 2013. *Staphylococcus aureus* biofilms promote horizontal transfer of antibiotic resistance. *Antimicrobial agents and chemotherapy* 57(4), pp. 1968-1970.

Schwarz, S., Cloeckaert, A. and Roberts, M. C. 2005. Mechanisms and spread of bacterial resistance to antimicrobial agents. *Antimicrobial resistance in bacteria of animal origin*, pp. 73-98.

Schwarz, S. and Johnson, A. P. 2016. Transferable resistance to colistin: a new but old threat. *Journal of Antimicrobial Chemotherapy* 71(8), pp. 2066-2070.

Schwarz, S., Kehrenberg, C., Doublet, B. and Cloeckaert, A. 2004. Molecular basis of bacterial resistance to chloramphenicol and florfenicol. *FEMS microbiology reviews* 28(5), pp. 519-542.

Schwechheimer, C. and Kuehn, M. J. 2015. Outer-membrane vesicles from Gram-negative bacteria: biogenesis and functions. *Nature reviews microbiology* 13(10), pp. 605-619.

Scott, J. R. and Barnett, T. C. 2006. Surface proteins of Gram-positive bacteria and how they get there. *Annu. Rev. Microbiol.* 60, pp. 397-423.

Serra, D. O. and Hengge, R. 2021. Bacterial multicellularity: the biology of *Escherichia coli* building large-scale biofilm communities. *Annual review of microbiology* 75(1), pp. 269-290.

Shafiq, M. et al. 2022. Synergistic activity of Tetrandrine and Colistin against *mcr-1*-Harboring *Escherichia coli*. *Antibiotics* 11(10), p. 1346.

Shaner, S. E. and Stone, K. L. 2023. Determination of stretching frequencies by isotopic substitution using infrared spectroscopy: an upper-level undergraduate experiment for an in-person or online laboratory. *Journal of Chemical Education* 100(6), pp. 2347-2352.

Sharma, G., Sharma, S., Sharma, P., Chandola, D., Dang, S., Gupta, S. and Gabrani, R. 2016. *Escherichia coli* biofilm: development and therapeutic strategies. *J Appl Microbiol* 121(2), pp. 309-319. doi: 10.1111/jam.13078

Sharma, P., Vaiwala, R., Gopinath, A. K., Chockalingam, R. and Ayappa, K. G. 2024. Structure of the bacterial cell envelope and interactions with antimicrobials: insights from molecular dynamics simulations. *Langmuir* 40(15), pp. 7791-7811.

Shaw, Z. et al. 2022. Illuminating the biochemical interaction of antimicrobial few-layer black phosphorus with microbial cells using synchrotron macro-ATR-FTIR. *Journal of Materials Chemistry B* 10(37), pp. 7527-7539.

Shchukarev, A., Gojkovic, Z., Funk, C. and Ramstedt, M. 2020. Cryo-XPS analysis reveals surface composition of microalgae. *Applied Surface Science* 526, p. 146538.

Shen, Y. et al. 2019. Integrated aquaculture contributes to the transfer of *mcr-1* between animals and humans via the aquaculture supply chain. *Environment international* 130, p. 104708.

Shen, Y. et al. 2018a. Prevalence and genetic analysis of *mcr-3*-positive *Aeromonas* species from humans, retail meat, and environmental water samples. *Antimicrobial agents and chemotherapy* 62(9), pp. e00404-00418.

Shen, Y., Zhang, R., Schwarz, S., Wu, C., Shen, J., Walsh, T. R. and Wang, Y. 2020. Farm animals and aquaculture: significant reservoirs of mobile colistin resistance genes. *Environmental microbiology* 22(7), pp. 2469-2484.

Shen, Z. et al. 2018b. Emerging carriage of NDM-5 and MCR-1 in *Escherichia coli* from healthy people in multiple regions in China: a cross sectional observational study. *EClinicalMedicine* 6, pp. 11-20.

Shen, Z., Wang, Y., Shen, Y., Shen, J. and Wu, C. 2016. Early emergence of *mcr-1* in *Escherichia coli* from food-producing animals. *The Lancet Infectious Diseases* 16(3), p. 293.

Sia, C. M. et al. 2020. The characterization of mobile colistin resistance (*mcr*) genes among 33000 *Salmonella enterica* genomes from routine public health surveillance in England. *Microbial Genomics* 6(2),

Sifat, A. A., Jahng, J. and Potma, E. O. 2022. Photo-induced force microscopy (PiFM)–principles and implementations. *Chemical Society Reviews* 51(11), pp. 4208-4222.

Silhavy, T. J., Kahne, D. and Walker, S. 2010. The bacterial cell envelope. *Cold Spring Harb Perspect Biol* 2(5), p. a000414. doi: 10.1101/cshperspect.a000414

Simpson, B. W. and Trent, M. S. 2019. Pushing the envelope: LPS modifications and their consequences. *Nature reviews microbiology* 17(7), pp. 403-416.

Sinha, A., Nyongesa, S., Viau, C., Gruenheid, S., Veyrier, F. J. and Le Moual, H. 2019. PmrC (EptA) and CptA negatively affect outer membrane vesicle production in *Citrobacter rodentium*. *Journal of bacteriology* 201(7), pp. 10.1128/jb. 00454-00418.

Siri, M., Vázquez-Dávila, M., Sotelo Guzman, C. and Bidan, C. M. 2024. Nutrient availability influences *E. coli* biofilm properties and the structure of purified curli amyloid fibers. *npj Biofilms and Microbiomes* 10(1), pp. 1-12.

Sivarajan, V. et al. 2025. Prevalence and genomic insights of carbapenem resistant and ESBL producing Multidrug resistant *Escherichia coli* in urinary tract infections. *Scientific reports* 15(1), p. 2541.

Smelikova, E., Tkadlec, J. and Krutova, M. 2022. How to: screening for *mcr*-mediated resistance to colistin. *Clinical Microbiology and Infection* 28(1), pp. 43-50.

Snesrud, E., He, S., Chandler, M., Dekker, J. P., Hickman, A. B., McGann, P. and Dyda, F. 2016. A model for transposition of the colistin resistance gene *mcr-1* by IS*Apl1*. *Antimicrobial agents and chemotherapy* 60(11), pp. 6973-6976.

Snesrud, E., McGann, P. and Chandler, M. 2018. The birth and demise of the IS*Apl1*-*mcr-1*-IS*Apl1* composite transposon: the vehicle for transferable colistin resistance. *MBio* 9(1), pp. 10.1128/mbio. 02381-02317.

Snesrud, E. et al. 2017. Analysis of serial isolates of *mcr-1*-positive *Escherichia coli* reveals a highly active IS*Apl1* transposon. *Antimicrobial agents and chemotherapy* 61(5), pp. 10.1128/aac. 00056-00017.

Soler, N. and Forterre, P. 2020. Vesiduction: the fourth way of HGT. *Environmental microbiology* 22(7), pp. 2457-2460.

Soncini, F. C. and Groisman, E. A. 1996. Two-component regulatory systems can interact to process multiple environmental signals. *Journal of bacteriology* 178(23), pp. 6796-6801.

Song, W., Xin, J., Yu, C., Xia, C. and Pan, Y. 2023. Alkyl ferulic acid esters: Evaluating their structure and antibacterial properties. *Frontiers in microbiology* 14, p. 1135308.

Sota, M., Yano, H., M Hughes, J., Daughdrill, G. W., Abdo, Z., Forney, L. J. and Top, E. M. 2010. Shifts in the host range of a promiscuous plasmid through parallel evolution of its replication initiation protein. *The ISME Journal* 4(12), pp. 1568-1580.

Spiers, A. J. 2014. A mechanistic explanation linking adaptive mutation, niche change, and fitness advantage for the wrinkly spreader. *International journal of evolutionary biology* 2014,

Spinosa, M. R., Progida, C., Tala, A., Cogli, L., Alifano, P. and Bucci, C. 2007. The *Neisseria meningitidis* capsule is important for intracellular survival in human cells. *Infection and immunity* 75(7), pp. 3594-3603.

Sprenger, D. and Anderson, O. 1991. Deconvolution of XPS spectra. *Fresenius' journal of analytical chemistry* 341, pp. 116-120.

Srinivasan, V. B. and Rajamohan, G. 2013. KpnEF, a new member of the *Klebsiella pneumoniae* cell envelope stress response regulon, is an SMR-type efflux pump involved in broad-spectrum antimicrobial resistance. *Antimicrobial agents and chemotherapy* 57(9), pp. 4449-4462.

Stalder, T., Rogers, L. M., Renfrow, C., Yano, H., Smith, Z. and Top, E. M. 2017. Emerging patterns of plasmid-host coevolution that stabilize antibiotic resistance. *Scientific reports* 7(1), p. 4853.

Steenackers, H. P., Parijs, I., Foster, K. R. and Vanderleyden, J. 2016. Experimental evolution in biofilm populations. *FEMS microbiology reviews* 40(3), pp. 373-397.

Stefaniuk, E. M. and Tyski, S. 2019. Colistin resistance in Enterobacterales strains – a current view. *Polish journal of microbiology* 68(4), p. 417.

Stewart, P. S. and Franklin, M. J. 2008. Physiological heterogeneity in biofilms. *Nature reviews microbiology* 6(3), pp. 199-210.

Stöckle, R. M., Suh, Y. D., Deckert, V. and Zenobi, R. 2000. Nanoscale chemical analysis by tip-enhanced Raman spectroscopy. *Chemical Physics Letters* 318(1-3), pp.

131-136.

Stojanoski, V., Sankaran, B., Prasad, B. V., Poirel, L., Nordmann, P. and Palzkill, T. 2016. Structure of the catalytic domain of the colistin resistance enzyme MCR-1. *BMC biology* 14, pp. 1-10.

Storm, D. R., Rosenthal, K. S. and Swanson, P. E. 1977. Polymyxin and related peptide antibiotics. *Annual review of biochemistry* 46(1), pp. 723-763.

Sturød, K., Salvadori, G., Junges, R. and Petersen, F. 2018. Antibiotics alter the window of competence for natural transformation in streptococci. *Molecular oral microbiology* 33(5), pp. 378-387.

Sulian, O. et al. 2020. Co-production of MCR-1 and NDM-1 by *Escherichia coli* sequence type 31 isolated from a newborn in Moscow, Russia. *International Journal of Infectious Diseases* 101, pp. 4-5.

Sultan, I., Ali, A., Gogry, F. A., Rather, I. A., Sabir, J. S. and Haq, Q. M. 2020. Bacterial isolates harboring antibiotics and heavy-metal resistance genes co-existing with mobile genetic elements in natural aquatic water bodies. *Saudi Journal of Biological Sciences* 27(10), pp. 2660-2668.

Sun, J. et al. 2018. Co-occurrence of *mcr-1* in the chromosome and on an IncHI2 plasmid: persistence of colistin resistance in *Escherichia coli*. *International journal of antimicrobial agents* 51(6), pp. 842-847.

Sun, J., Rutherford, S. T., Silhavy, T. J. and Huang, K. C. 2022. Physical properties of the bacterial outer membrane. *Nature reviews microbiology* 20(4), pp. 236-248.

Sun, S., Negrea, A., Rhen, M. and Andersson, D. I. 2009. Genetic analysis of colistin resistance in *Salmonella enterica* serovar Typhimurium. *Antimicrobial agents and chemotherapy* 53(6), pp. 2298-2305.

Szabó, M., Kiss, J., Nagy, Z., Chandler, M. and Olasz, F. 2008. Sub-terminal sequences modulating IS*30* transposition *in vivo* and *in vitro*. *Journal of molecular biology* 375(2), pp. 337-352.

Takahashi, Y. et al. 2015. Modulation of primary cell function of host *Pseudomonas* bacteria by the conjugative plasmid pCAR1. *Environmental microbiology* 17(1), pp. 134-155.

Tamagnone, M., Ambrosio, A., Chaudhary, K., Jauregui, L. A., Kim, P., Wilson, W. L. and Capasso, F. 2018. Ultra-confined mid-infrared resonant phonon polaritons in van

der Waals nanostructures. *Science Advances* 4(6), p. eaat7189.

Tamayo, R., Choudhury, B., Septer, A., Merighi, M., Carlson, R. and Gunn, J. 2005a. Identification of *cptA*, a PmrA-regulated locus required for phosphoethanolamine modification of the *Salmonella enterica* serovar typhimurium lipopolysaccharide core. *Journal of bacteriology* 187(10), pp. 3391-3399.

Tamayo, R., Prouty, A. M. and Gunn, J. S. 2005b. Identification and functional analysis of *Salmonella enterica* serovar Typhimurium PmrA-regulated genes. *FEMS Immunology & Medical Microbiology* 43(2), pp. 249-258.

Tamayo, R., Ryan, S. S., McCoy, A. J. and Gunn, J. S. 2002. Identification and genetic characterization of PmrA-regulated genes and genes involved in polymyxin B resistance in *Salmonella enterica* serovar Typhimurium. *Infection and immunity* 70(12), pp. 6770-6778.

Tantala, J., Thumanu, K. and Rachtanapun, C. 2019. An assessment of antibacterial mode of action of chitosan on *Listeria innocua* cells using real-time HATR-FTIR spectroscopy. *International journal of biological macromolecules* 135, pp. 386-393.

Tarabai, H. et al. 2019. Plasmid-mediated *mcr-1* colistin resistance in *Escherichia coli* from a black kite in Russia. *Antimicrobial agents and chemotherapy* 63(9), pp. 10.1128/aac. 01266-01219.

Tegetmeyer, H. E., Jones, S. C., Langford, P. R. and Baltes, N. 2008. IS*Apl1*, a novel insertion element of *Actinobacillus pleuropneumoniae*, prevents ApxIV-based serological detection of serotype 7 strain AP76. *Veterinary microbiology* 128(3-4), pp. 342-353.

Teo, J. W., Kalisvar, M., Venkatachalam, I., Ng, O. T., Lin, R. T. and Octavia, S. 2018. *mcr-3* and *mcr-4* variants in carbapenemase-producing clinical *Enterobacteriaceae* do not confer phenotypic polymyxin resistance. *Journal of clinical microbiology* 56(3), pp. e01562-01517.

Tietgen, M., Semmler, T., Riedel-Christ, S., Kempf, V. A., Molinaro, A., Ewers, C. and Göttig, S. 2018. Impact of the colistin resistance gene *mcr-1* on bacterial fitness. *International journal of antimicrobial agents* 51(4), pp. 554-561.

Toffolatti, S. L., Maddalena, G., Passera, A., Casati, P., Bianco, P. A. and Quaglino, F. 2021. Role of terpenes in plant defense to biotic stress. *Biocontrol agents and secondary metabolites*. Elsevier, pp. 401-417.

Touzé, T., Tran, A. X., Hankins, J. V., Mengin-Lecreulx, D. and Trent, M. S. 2008.

Periplasmic phosphorylation of lipid A is linked to the synthesis of undecaprenyl phosphate. *Molecular microbiology* 67(2), pp. 264-277.

Tran, A. X. et al. 2005. Resistance to the antimicrobial peptide polymyxin requires myristoylation of *Escherichia coli* and *Salmonella typhimurium* lipid A. *Journal of Biological Chemistry* 280(31), pp. 28186-28194.

Traverse, C. C., Mayo-Smith, L. M., Poltak, S. R. and Cooper, V. S. 2013. Tangled bank of experimentally evolved *Burkholderia* biofilms reflects selection during chronic infections. *Proceedings of the National Academy of Sciences* 110(3), pp. E250-E259.

Trent, M. S., Pabich, W., Raetz, C. R. and Miller, S. I. 2001a. A PhoP/PhoQ-induced Lipase (PagL) That Catalyzes 3-O-Deacylation of Lipid A Precursors in Membranes of *Salmonella typhimurium*. *Journal of Biological Chemistry* 276(12), pp. 9083-9092.

Trent, M. S., Ribeiro, A. A., Lin, S., Cotter, R. J. and Raetz, C. R. 2001b. An inner membrane enzyme in *Salmonella* and *Escherichia coli* that transfers 4-amino-4-deoxy-L-arabinose to Lipid A: Induction in polymyxin-resistant mutants and role of a novel lipid-linked donor. *Journal of Biological Chemistry* 276(46), pp. 43122-43131.

Ullah, S. et al. 2021. Characterization of NMCR-2, a new non-mobile colistin resistance enzyme: implications for an MCR-8 ancestor. *Environmental microbiology* 23(2), pp. 844-860.

Upadhyay, H. C., Dwivedi, G. R., Roy, S., Sharma, A., Darokar, M. P. and Srivastava, S. K. 2014. Phytol derivatives as drug resistance reversal agents. *ChemMedChem* 9(8), pp. 1860-1868.

Usui, M., Nozawa, Y., Fukuda, A., Sato, T., Yamada, M., Makita, K. and Tamura, Y. 2021. Decreased colistin resistance and *mcr-1* prevalence in pig-derived *Escherichia coli* in Japan after banning colistin as a feed additive. *Journal of Global Antimicrobial Resistance* 24, pp. 383-386.

Vaara, M. 1992. Agents that increase the permeability of the outer membrane. *Microbiological reviews* 56(3), pp. 395-411.

van Hoek, A. H., Mevius, D., Guerra, B., Mullany, P., Roberts, A. P. and Aarts, H. J. 2011. Acquired antibiotic resistance genes: an overview. *Front Microbiol* 2, p. 203. doi: 10.3389/fmicb.2011.00203

van Merode, A. E., van der Mei, H. C., Busscher, H. J. and Krom, B. P. 2006. Influence of culture heterogeneity in cell surface charge on adhesion and biofilm formation by *Enterococcus faecalis*. *Journal of bacteriology* 188(7), pp. 2421-2426.

Velkov, T., Thompson, P. E., Nation, R. L. and Li, J. 2010. Structure−activity relationships of polymyxin antibiotics. *Journal of medicinal chemistry* 53(5), pp. 1898-1916.

Véscovi, E. G., Soncini, F. C. and Groisman, E. A. 1996. Mg^{2+} as an extracellular signal: environmental regulation of Salmonella virulence. *Cell* 84(1), pp. 165-174.

Vogeleer, P., Tremblay, Y. D., Mafu, A. A., Jacques, M. and Harel, J. 2014. Life on the outside: role of biofilms in environmental persistence of Shiga-toxin producing *Escherichia coli*. *Frontiers in microbiology* 5, p. 317.

Vollmer, W., Blanot, D. and de Pedro, M. A. 2008. Peptidoglycan structure and architecture. *FEMS Microbiol Rev* 32(2), pp. 149-167. doi: 10.1111/j.1574-6976.2007.00094.x

Vorregaard, M. 2008. *Comstat2 - a modern 3D image analysis environment for biofilms.* Technical University of Denmark, DTU, DK-2800 Kgs. Lyngby, Denmark.

Walsh, T. R. and Wu, Y. 2016. China bans colistin as a feed additive for animals. *The Lancet Infectious Diseases* 16(10), p. 1102.

Walters III, M. C., Roe, F., Bugnicourt, A., Franklin, M. J. and Stewart, P. S. 2003. Contributions of antibiotic penetration, oxygen limitation, and low metabolic activity to tolerance of *Pseudomonas aeruginosa* biofilms to ciprofloxacin and tobramycin. *Antimicrobial agents and chemotherapy* 47(1), pp. 317-323.

Wang, C.-Y., Chen, Y.-W. and Hou, C.-Y. 2019a. Antioxidant and antibacterial activity of seven predominant terpenoids. *International Journal of food properties* 22(1), pp. 230-238.

Wang, C., Feng, Y., Liu, L., Wei, L., Kang, M. and Zong, Z. 2020a. Identification of novel mobile colistin resistance gene *mcr-10*. *Emerging microbes & infections* 9(1), pp. 508-516.

Wang, L., Jakob, D. S., Wang, H., Apostolos, A., Pires, M. M. and Xu, X. G. 2019b. Generalized heterodyne configurations for photoinduced force microscopy. *Analytical chemistry* 91(20), pp. 13251-13259.

Wang, Q. et al. 2017a. Expanding landscapes of the diversified *mcr-1*-bearing plasmid reservoirs. *Microbiome* 5, pp. 1-9.

Wang, R. et al. 2018a. The prevalence of colistin resistance in *Escherichia coli* and

Klebsiella pneumoniae isolated from food animals in China: coexistence of *mcr-1* and *bla*$_{NDM}$ with low fitness cost. *International journal of antimicrobial agents* 51(5), pp. 739-744.

Wang, X., Wang, W., Liu, P., Wang, p. and Zhang, L. 2011. Photocatalytic degradation of *E. coli* membrane cell in the presence of ZnO nanowires. *Journal of Wuhan University of Technology-Mater. Sci. Ed.* 26, pp. 222-225.

Wang, X. et al. 2018b. Emergence of a novel mobile colistin resistance gene, *mcr-8*, in NDM-producing *Klebsiella pneumoniae*. *Emerging microbes & infections* 7(1), pp. 1-9.

Wang, Y. et al. 2020b. Changes in colistin resistance and *mcr-1* abundance in *Escherichia coli* of animal and human origins following the ban of colistin-positive additives in China: an epidemiological comparative study. *The Lancet Infectious Diseases* 20(10), pp. 1161-1171.

Wang, Y. et al. 2017b. Comprehensive resistome analysis reveals the prevalence of NDM and MCR-1 in Chinese poultry production. *Nature microbiology* 2(4), pp. 1-7.

Wang, Z., Wang, J., Ren, G., Li, Y. and Wang, X. 2015. Influence of core oligosaccharide of lipopolysaccharide to outer membrane behavior of *Escherichia coli*. *Marine drugs* 13(6), pp. 3325-3339.

Wanty, C. et al. 2013. The structure of the neisserial lipooligosaccharide phosphoethanolamine transferase A (LptA) required for resistance to polymyxin. *Journal of molecular biology* 425(18), pp. 3389-3402.

Wei, H., Yang, X.-Y., Van der Mei, H. C. and Busscher, H. J. 2021. X-Ray photoelectron spectroscopy on microbial cell surfaces: a forgotten method for the characterization of microorganisms encapsulated with surface-engineered shells. *Frontiers in Chemistry* 9, p. 666159.

Wei, P. et al. 2018. Substrate analog interaction with MCR-1 offers insight into the rising threat of the plasmid-mediated transferable colistin resistance. *The FASEB Journal* 32(2), pp. 1085-1098.

Wein, T., Hülter, N. F., Mizrahi, I. and Dagan, T. 2019. Emergence of plasmid stability under non-selective conditions maintains antibiotic resistance. *Nature communications* 10(1), p. 2595.

Weston-Green, K., Clunas, H. and Jimenez Naranjo, C. 2021. A review of the potential use of pinene and linalool as terpene-based medicines for brain health: discovering

novel therapeutics in the flavours and fragrances of cannabis. *Frontiers in psychiatry* 12, p. 583211.

Whittaker, P., Mossoba, M., Al-Khaldi, S., Fry, F., Dunkel, V., Tall, B. and Yurawecz, M. 2003. Identification of foodborne bacteria by infrared spectroscopy using cellular fatty acid methyl esters. *Journal of microbiological methods* 55(3), pp. 709-716.

Wick, R. R., Judd, L. M., Gorrie, C. L. and Holt, K. E. 2017. Unicycler: resolving bacterial genome assemblies from short and long sequencing reads. *PLoS computational biology* 13(6), p. e1005595.

Wickramasinghe, H. K. and Park, S. 2015. Force detection of IR response at sub-10 nm resolution. *SPIE Newsroom* 2015, pp. 1-3.

Williamson, K. S., Richards, L. A., Perez-Osorio, A. C., Pitts, B., McInnerney, K., Stewart, P. S. and Franklin, M. J. 2012. Heterogeneity in *Pseudomonas aeruginosa* biofilms includes expression of ribosome hibernation factors in the antibiotic-tolerant subpopulation and hypoxia-induced stress response in the metabolically active population. *Journal of bacteriology* 194(8), pp. 2062-2073.

Winder, C. L. and Goodacre, R. 2004. Comparison of diffuse-reflectance absorbance and attenuated total reflectance FT-IR for the discrimination of bacteria. *Analyst* 129(11), pp. 1118-1122.

Winfield, M. D., Latifi, T. and Groisman, E. A. 2005. Transcriptional regulation of the 4-amino-4-deoxy-L-arabinose biosynthetic genes in *Yersinia pestis*. *Journal of Biological Chemistry* 280(15), pp. 14765-14772.

Wongsuvan, G., Wuthiekanun, V., Hinjoy, S., Day, N. P. and Limmathurotsakul, D. 2018. Antibiotic use in poultry: a survey of eight farms in Thailand. *Bulletin of the World Health Organization* 96(2), p. 94.

Wood, T. K. 2009. Insights on *Escherichia coli* biofilm formation and inhibition from whole-transcriptome profiling. *Environ Microbiol* 11(1), pp. 1-15. doi: 10.1111/j.1462-2920.2008.01768.x

Wood, T. K. 2017. Strategies for combating persister cell and biofilm infections. *Microbial biotechnology* 10(5), pp. 1054-1056.

Wozniak, R. A. and Waldor, M. K. 2010. Integrative and conjugative elements: mosaic mobile genetic elements enabling dynamic lateral gene flow. *Nature reviews microbiology* 8(8), pp. 552-563.

Wright, M. S. et al. 2015. Genomic and transcriptomic analyses of colistin-resistant clinical isolates of *Klebsiella pneumoniae* reveal multiple pathways of resistance. *Antimicrobial agents and chemotherapy* 59(1), pp. 536-543.

Wu, D., Ding, Y., Yao, K., Gao, W. and Wang, Y. 2021a. Antimicrobial resistance analysis of clinical *Escherichia coli* isolates in neonatal ward. *Frontiers in pediatrics* 9, p. 670470.

Wu, J., Dong, X., Zhang, L., Lin, Y. and Yang, K. 2021b. Reversing antibiotic resistance caused by mobile resistance genes of high fitness cost. *Msphere* 6(3), pp. 10.1128/msphere. 00356-00321.

Wu, J. et al. 2025. Insertion sequences in *mgrB* and mutations in two-component system genes confer high polymyxin resistance to carbapenem-resistant *Enterobacter cloacae* complex strains. *Frontiers in microbiology* 16, p. 1553148.

Wu, R. et al. 2018. Fitness advantage of *mcr-1*-bearing IncI2 and IncX4 plasmids *in vitro*. *Frontiers in microbiology* 9, p. 331.

Xu, K. D., Stewart, P. S., Xia, F., Huang, C.-T. and McFeters, G. A. 1998. Spatial physiological heterogeneity in *Pseudomonas aeruginosa* biofilm is determined by oxygen availability. *Applied and environmental microbiology* 64(10), pp. 4035-4039.

Xu, T. et al. 2022a. Frequent convergence of *mcr-9* and carbapenemase genes in *Enterobacter cloacae* complex driven by epidemic plasmids and host incompatibility. *Emerging microbes & infections* 11(1), pp. 1959-1972.

Xu, T., Xue, C.-X., Huang, J., Wu, J., Chen, R. and Zhou, K. 2022b. Emergence of an epidemic hypervirulent clone of *Enterobacter hormaechei* coproducing *mcr-9* and carbapenemases. *The Lancet Microbe* 3(7), pp. e474-e475.

Xu, T., Zhang, C., Ji, Y., Song, J., Liu, Y., Guo, Y. and Zhou, K. 2021. Identification of *mcr-10* carried by self-transmissible plasmids and chromosome in *Enterobacter roggenkampii* strains isolated from hospital sewage water. *Environmental pollution* 268, p. 115706.

Xu, Y., Lin, J., Cui, T., Srinivas, S. and Feng, Y. 2018a. Mechanistic insights into transferable polymyxin resistance among gut bacteria. *Journal of Biological Chemistry* 293(12), pp. 4350-4365.

Xu, Y., Wei, W., Lei, S., Lin, J., Srinivas, S. and Feng, Y. 2018b. An evolutionarily conserved mechanism for intrinsic and transferable polymyxin resistance. *MBio* 9(2), pp. 10.1128/mbio. 02317-02317.

Xue, W. 2022. *Epoxy-tiglianes for the treatment of chronic wounds, multi-drug resistant bacteria and oral infections.* Cardiff University.

Xue, W. et al. 2023. Defining *in vitro* topical antimicrobial and antibiofilm activity of epoxy-tigliane structures against oral pathogens. *Journal of Oral Microbiology* 15(1), p. 2241326.

Yadav, M. K., Chae, S.-W., Im, G. J., Chung, J.-W. and Song, J.-J. 2015. Eugenol: a phyto-compound effective against methicillin-resistant and methicillin-sensitive *Staphylococcus aureus* clinical strain biofilms. *PloS one* 10(3), p. e0119564.

Yan, A., Guan, Z. and Raetz, C. R. 2007. An undecaprenyl phosphate-aminoarabinose flippase required for polymyxin resistance in *Escherichia coli*. *Journal of Biological Chemistry* 282(49), pp. 36077-36089.

Yang, J. et al. 2021. A ProQ/FinO family protein involved in plasmid copy number control favours fitness of bacteria carrying *mcr-1*-bearing IncI2 plasmids. *Nucleic acids research* 49(7), pp. 3981-3996.

Yang, J. et al. 2023. The evolution of infectious transmission promotes the persistence of *mcr-1* plasmids. *MBio* 14(4), pp. e00442-00423.

Yang, Q. et al. 2017. Balancing *mcr-1* expression and bacterial survival is a delicate equilibrium between essential cellular defence mechanisms. *Nature communications* 8(1), p. 2054.

Yang, Q. E. et al. 2020. Compensatory mutations modulate the competitiveness and dynamics of plasmid-mediated colistin resistance in *Escherichia coli* clones. *ISME J* 14(3), pp. 861-865. doi: 10.1038/s41396-019-0578-6

Yang, Y.-Q., Li, Y.-X., Lei, C.-W., Zhang, A.-Y. and Wang, H.-N. 2018. Novel plasmid-mediated colistin resistance gene *mcr-7.1* in *Klebsiella pneumoniae*. *Journal of Antimicrobial Chemotherapy* 73(7), pp. 1791-1795.

Yang, Y. et al. 2016. Proteins dominate in the surface layers formed on materials exposed to extracellular polymeric substances from bacterial cultures. *Biofouling* 32(1), pp. 95-108.

Yano, H. et al. 2016. Evolved plasmid-host interactions reduce plasmid interference cost. *Molecular microbiology* 101(5), pp. 743-756.

Yin, W. et al. 2017. Novel plasmid-mediated colistin resistance gene *mcr-3* in

Escherichia coli. *MBio* 8(3), pp. e00543-00517.

Yong, D., Toleman, M. A., Giske, C. G., Cho, H. S., Sundman, K., Lee, K. and Walsh, T. R. 2009. Characterization of a new metallo-β-lactamase gene, *bla*$_{NDM-1}$, and a novel erythromycin esterase gene carried on a unique genetic structure in *Klebsiella pneumoniae* sequence type 14 from India. *Antimicrobial agents and chemotherapy* 53(12), pp. 5046-5054.

Yu, Z., Qin, W., Lin, J., Fang, S. and Qiu, J. 2015. Antibacterial mechanisms of polymyxin and bacterial resistance. *Biomed Res Int* 2015(679109),

Zahrl, D., Wagner, M., Bischof, K. and Koraimann, G. n. 2006. Expression and assembly of a functional type IV secretion system elicit extracytoplasmic and cytoplasmic stress responses in *Escherichia coli*. *Journal of bacteriology* 188(18), pp. 6611-6621.

Zajac, M. et al. 2019. Occurrence and characterization of *mcr-1*-positive *Escherichia coli* isolated from food-producing animals in Poland, 2011–2016. *Frontiers in microbiology* 10, p. 1753.

Zapun, A., Contreras-Martel, C. and Vernet, T. 2008. Penicillin-binding proteins and β-lactam resistance. *FEMS microbiology reviews* 32(2), pp. 361-385.

Zhang, H., Hou, M., Xu, Y., Srinivas, S., Huang, M., Liu, L. and Feng, Y. 2019a. Action and mechanism of the colistin resistance enzyme MCR-4. *Communications biology* 2(1), p. 36.

Zhang, J.-F. et al. 2022. A trade-off for maintenance of multidrug-resistant IncHI2 plasmids in *Salmonella enterica* serovar Typhimurium through adaptive evolution. *Msystems* 7(5), pp. e00248-00222.

Zhang, P., Bai, L., Li, Y., Wang, Z. and Li, R. 2019b. Loss of *mcr* Genes Mediated by Plasmid Elimination and IS*Apl1*. *Antimicrobial agents and chemotherapy* 63(9), pp. 10.1128/aac. 01002-01019.

Zhang, S. et al. 2021a. Updates on the global dissemination of colistin-resistant *Escherichia coli*: An emerging threat to public health. *Science of The Total Environment* 799, p. 149280.

Zhang, X. and Bishop, P. L. 2003. Biodegradability of biofilm extracellular polymeric substances. *Chemosphere* 50(1), pp. 63-69.

Zhang, X., Bishop, P. L. and Kupferle, M. J. 1998. Measurement of polysaccharides

and proteins in biofilm extracellular polymers. *Water science and technology* 37(4-5), pp. 345-348.

Zhang, Y., Liu, X., Jiang, P., Li, W. and Wang, Y. 2015. Mechanism and antibacterial activity of cinnamaldehyde against *Escherichia coli* and *Staphylococcus aureu*s. *Mod. Food Sci. Technol* 31, pp. 31-35.

Zhang, Y., Liu, Y., Luo, J., Jie, J., Deng, X. and Song, L. 2021b. The herbal compound thymol targets multiple *Salmonella* Typhimurium virulence factors for Lon protease degradation. *Frontiers in Pharmacology* 12, p. 674955.

Zhang, Z., Lin, Q., Huang, Z., Xu, D. and Ren, K. 2025. Recent advances in sugar-fatty acid esters and their analogs: antimicrobial properties, structural-functional relationships and potential mechanisms. *Critical Reviews in Food Science and Nutrition*, pp. 1-21.

Zhao, F., Feng, Y., Lü, X., McNally, A. and Zong, Z. 2017. IncP plasmid carrying colistin resistance gene *mcr-1* in *Klebsiella pneumoniae* from hospital sewage. *Antimicrobial agents and chemotherapy* 61(2), pp. 10.1128/aac. 02229-02216.

Zhao, Q., Li, Y., Tian, Y., Shen, Y., Wang, S. and Zhang, Y. 2022. Clinical impact of colistin banning in food animal on *mcr-1*-positive Enterobacteriaceae in patients from Beijing, China, 2009–2019: a long-term longitudinal observational study. *Frontiers in microbiology* 13, p. 826624.

Zheng, B. et al. 2017. Complete genome sequencing and genomic characterization of two *Escherichia coli* strains co-producing MCR-1 and NDM-1 from bloodstream infection. *Scientific reports* 7(1), p. 17885.

Zhou, F. and Pichersky, E. 2020. More is better: the diversity of terpene metabolism in plants. *Current opinion in plant biology* 55, pp. 1-10.

Zhou, K. et al. 2018. Silent transmission of an IS*1294b*-deactivated *mcr-1* gene with inducible colistin resistance. *International journal of antimicrobial agents* 51(6), pp. 822-828.

Zhou, Y. et al. 2022. A one-health sampling strategy to explore the dissemination and relationship between colistin resistance in human, animal, and environmental sectors in Laos. *Engineering* 15, pp. 45-56.

Zurfluh, K., Nüesch-Inderbinen, M., Klumpp, J., Poirel, L., Nordmann, P. and Stephan, R. 2017. Key features of *mcr-1*-bearing plasmids from *Escherichia coli* isolated from humans and food. *Antimicrobial Resistance & Infection Control* 6(1), pp. 1-6.

Zurfluh, K., Tasara, T., Poirel, L., Nordmann, P. and Stephan, R. 2016. Draft genome sequence of *Escherichia coli* S51, a chicken isolate harboring a chromosomally encoded *mcr-1* gene. *Genome announcements* 4(4), pp. 10.1128/genomea. 00796-00716.

Zwanzig, M., Harrison, E., Brockhurst, M. A., Hall, J. P., Berendonk, T. U. and Berger, U. 2019. Mobile compensatory mutations promote plasmid survival. *Msystems* 4(1), pp. 10.1128/msystems. 00186-00118.